CHEMICAL AND PHYSICAL CHARACTERIZATION OF CLAY BODIES.

DEBBIE MARIE KAVANAGH

THESIS FOR THE DEGREE OF DOCTOR OF PHILOSOPHY

THE UNIVERSITY OF ASTON IN BIRMINGHAM.

November 2001.

To my mom. Who is everything a daughter could ever wish for.

Also, in loving memory of my dad.

James Anthony Kavanagh

1938 – 1988.

THESIS SUMMARY.

Suitable methods for the assessment of the effect of freeze-thaw action upon ceramic tiles have been determined. The results obtained have been shown to be reproducible with some work in this area still warranted. The analysis of Whichford Potteries clays *via* a variety of analytical techniques has shown them to be a complex mix of both clay and non-clay minerals. ^{57}Fe Mössbauer spectroscopy has highlighted the presence of both small and large particle α-Fe_2O_3, removable *via* acid washing.

^{19}F MAS NMR has demonstrated that the raw Whichford Pottery clays examined have negligible fluorine content. This is unlikely to be detrimental to ceramic wares during the heating process. A unique technique was used for the identification of fluorine in solid-state systems.

The exchange of various cations into Wyoming Bentonite clay by microwave methodology did not show the appearance of five co-ordinate aluminium when examined by ^{27}Al MAS NMR. The appearance of Q_0 silicate was linked to an increase in the amount of tetrahedrally bound aluminium in the silicate framework. This is formed as a result of the heating process.

The analysis of two Chinese clays and two Chinese clay raw materials has highlighted a possible link between the two. These have also been shown to be a mix of both clay and non-clay minerals.

Layered double hydroxides formed by conventional and microwave methods exhibited interesting characteristics. The main differences between the samples examined were not found to be solely attributable to the differences between microwave and conventional methods but more attributable to different experimental conditions used.

KEYWORDS

Freeze-thaw, ^{19}F MAS NMR, Microwave methodology, Cation exchange, Five co-ordinate aluminium, Wyoming Bentonite.

ACKNOWLEDGEMENTS.

Special thanks go to the late Professor W.R. McWhinnie for his continued support and encouragement throughout the course of my PhD. Many thanks also go to Dr D Miller and Professor F J Berry (Open University) without whom the finalisation of this thesis would not have been possible.

Thankyou also to my step-dad, Raymond Armstrong for all his support. Also to Mr Simon Hawley, Mrs S Bastock and Mr N Bastock, Mrs R Gee and Mr M Gee and Miss F Morris and all my friends for their continual encouragement.

Thanks also to;

Mr J Keeling and Mr J Atkinson (Whichford Potteries) for their support.

Dr Pari Monsef-Mirazi for her friendly advice and encouragement.
Dr Mike Perry (Aston University) for endless help with MAS NMR.
Dr Sayeed (Aston University) for advice regarding XPS.
Dr P Tack (Aston University) for invaluable advice regarding gas analysis.
Mrs D Ingram-Hall (Aston University)

Dr P Purnell (Wolverhampton University) for assistance with Ultrasonic analysis and Three Point Flexural testing.
Mr C Thompson (Aston University) for advice regarding TGA/DTA analyses.

Dr G Rowbotham (Keele University) for XRD and XRF analyses.
Dr N Coleman (Imperial College) for advice on nitrogen sorption isotherms.
Mr J Duggins (Aston University) SEM
Mr J Coundon and Mr P Hands (Birmingham University) preparation of thin sections.
Mr I Ayub and Professor F Berry (Open University) for invaluable help with ^{57}Fe Mössbauer spectroscopy.

Financial support for this work by Whichford Potteries and the EPSRC is gratefully acknowledged.

LIST OF FIGURES (page number)

LIST OF TABLES (page number)

CHAPTER ONE

1.0 INTRODUCTION.

1.1 AIMS AND OBJECTIVES.

The aims and objectives of the work reported in this thesis can be summarised as follows.

- Physical and chemical analysis of raw and fired clay bodies to gain a better understanding of their composition.

- Assessment of the action of frost upon terracotta bodies using a number of chemical and engineering techniques so that the most appropriate techniques for identifying the early stages of frost damage can be identified.

- Analysis of gases emitted as a result of the microwave pyrolysis of raw materials.

- The determination of the changes that occur in clay bodies as a result of heat treatment emulating the firing process.

- The achievement of microwave-enhanced cation exchange in smectite clays.

- The achievement of microwave assisted layered double hydroxide formation and subsequent exchange.

- The analysis of some Chinese clays.

The original aims of the work reported here are primarily based on rough guidelines set out by Whichford Potteries, Warwickshire, which were to gain a better understanding of clay body composition and the action of frost upon ceramic wares.

Due to its being only a small cottage industry, Whichfords' consumption of raw materials is low using only six tonnes per month. They do not have privately owned

clay pit resources so raw materials are purchased externally. The company sometimes is required to alter raw material suppliers, who offer clays of different composition and type. Thus inconsistency in final clay body composition and product properties is common. It is of paramount importance to a high quality producer that each new formulation offers properties comparable to previous ones. Previously, problems have been solved over time using empirical formulae, however, due to the market place now offering cheaper alternatives time is no longer the main factor if Whichford are to maintain their position in the competitive field. Scientific techniques have been used to investigate new materials.

Furthermore, Whichford Potteries have identified recently the action of frost on their products is a matter of increasing importance. It is essential that Whichford have a basic and informed understanding of the action of frost so they can offer guarantees on products to the consumer.

More recently work has been published which demonstrates the use of microwave-enhanced chemistry principally for the exchange of anionic and cationic species in clay and clay like materials in conjunction with the formation of layered double hydroxides. This is also examined in this thesis. The thesis also reports on the application of a variety of analytical techniques for the analysis of Chinese clay bodies

1.2 THE NATURE OF CLAY AND CERAMICS.

Clay is the most basic, and undoubtedly the oldest, ceramic raw material. Clays are formed as a result of geological processes occurring over thousands of years and are essentially alumino-silicates combined with a host of other important mineral components. The exact composition of a clay body is dependant upon the time of formation and subsequent weathering and aging processes.[1] Clays are rarely 'pure' and are often a mix of many different minerals; this is particularly true for the 'potters' clay

All clays share the same basic chemical and physical properties. The definition as a fine-grained rock which, when suitably treated, becomes plastic when wet, hard when dried, and upon firing is converted to a solid rock-like mass describes most.[2] Since early times these properties have been recognised and it is these that make clay particularly valuable in the ceramics industry.

The term ceramics is derived from the Greek word *keramikos*, which when literally translated means *earthen*, it is therefore fair to say that ceramics can be determined as any article made from naturally occurring earths.[3] This, highlights the relationship to clay minerals.

The application of X-ray diffraction during the 1920s' to clay mineral analysis led to an enormous increase in knowledge surrounding clay mineral composition. It provided enhanced information regarding both structure and properties, showing how relatively small alterations in structure can dramatically influence chemical and physical properties.

More recent work concerning clay morphology has included industrial applications of clays, e.g. in catalysis, paint and paper coatings.

---

[1] Grim, R.E., *Clay Mineralogy*, McGraw-Hill, New York, **1953.**
[2] The Royal Society, *Clay Minerals: Their Structure Behaviour and use,* University Press, Cambridge, **1984.**
[3] Grimshaw, R.W., *The Chemistry and physics of clays and allied ceramic materials,* Fourth Edition, **1971.**

1.3 STRUCTURAL PROPERTIES OF CLAYS.

Clays share a common morphology, the basic structural unit that combines to form the layer lattice silicates[4] being the $(SiO_4)^{4-}$ tetrahedron (Figure 1).

Figure 1 : $(SiO_4)^{4-}$ Tetrahedron

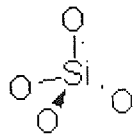

When three oxygen atoms of every tetrahedron are linked, through condensation reactions, a continuous sheet-like structure is formed which is capable of infinite extension in two directions, thus giving a plate-like structure. As a consequence of this structure one oxygen of each tetrahedron is capable of bearing a residual charge thus leaving it free to be balanced by external cations. Usually, it is found that the silica units arrange themselves in hexagonal (twelve membered) rings (Figure. 2), each surrounded by six similar rings so that bonding involves the silica tetrahedra, which share three corners. The structure is such that the single oxygen atom of each tetrahedron now lies perpendicular to the plane, orientated in the same spatial direction. The layer composition can be represented as $(Si_2O_5^{2-})_n$.

Figure 2 : Sheet Silicate $(Si_2O_5^{2-})_n$

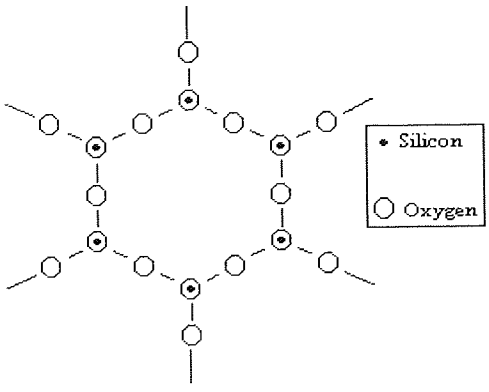

Neutrality of the silicate layer is maintained by condensing one $Si(O, OH)_4$ tetrahedral layer with layers of $M_{2-3}(OH)_6$ octahedra where M_{2-3} is a divalent or trivalent metal ion, usually Mg^{2+} or Al^{3+} respectively. The condensation of one octahedral and one tetrahedral layer gives rise to a 1:1 layer where the exposed surface of the octahedral sheet consists of OH groups (Figure 3). This has the general formula $M_{2-3}Si_2O_5(OH)_4$. Similarly, if both sides of the octahedral sheet are linked to tetrahedral sheets then it is termed a 2:1 condensation unit, giving rise to the general formula $M_{2-3}Si_4O_{10}(OH)_2$ (Figure 4).

Figure 3 : 1:1 Layer Unit.

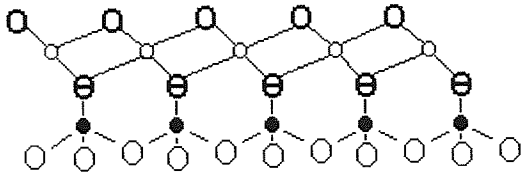

Figure 4 : 2:1 Layer Unit

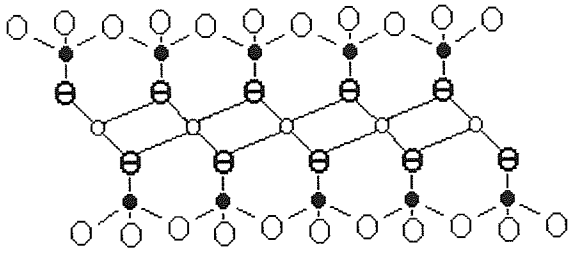

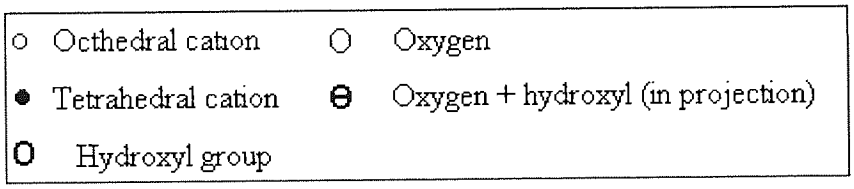

The layered structure of clays shows them as belonging to the family of phyllosilicates (literal meaning: a layer silicate).

Further to this there is also the possibility, within these structures, of isomorphous substitution of Si^{4+} by other positively charged ions of similar shape and size, but of lower valency. This results in the clay structure having an overall residual negative charge. Charge balancing occurs through interlayer cations, hydrated cations or co-ordination of the hydroxyl groups on the octahedral layer. This is primarily dependent upon the type of clay mineral concerned.

---

[4] Grimshaw, R.W., and Harland, C.E., *Ion-Exchange: Introduction to theory and practice,* The Royal Society, Mongraphs for Teachers No.29, **1975.**

The amount, as well as the type, of isomorphous substitution will affect the overall properties of the clay, for example the ability to swell in aqueous media.

Although there are many similarities between clay minerals there are also differences that lead to subdivision into several main groups. The most important groupings are the kandites (kaolinite group), illites (mica group), smectites (montmorillonite group) and of lesser significance chlorites and vermiculites (Figure 5). Talc and pyrophyllite are also important clay minerals, being the most basic 2:1 type clays.

Each group has a characteristic basal spacing (distance between layers); approximately 7Å, 10Å, 15Å and 14Å respectively; which changes when introduced into an aqueous environment or due to cation exchange.

Figure 5 : Representation of the principal clay minerals.[5]

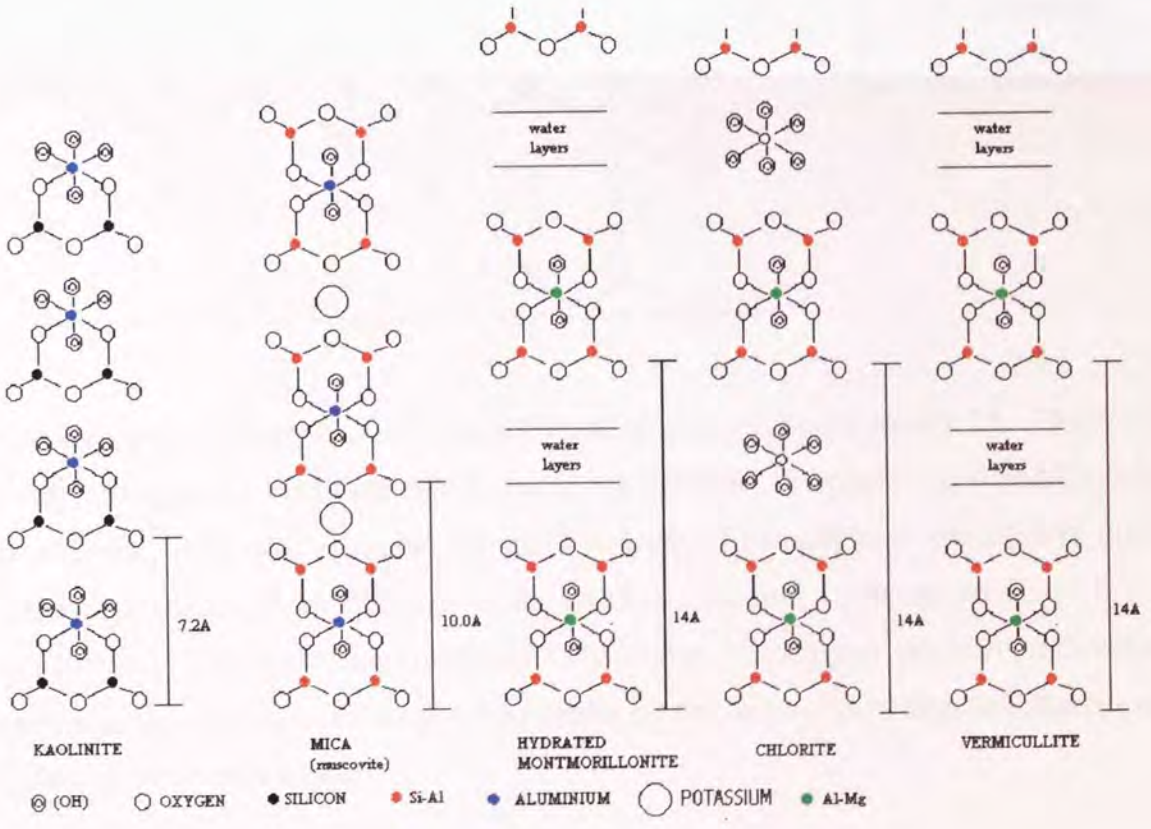

[5] Millot. G., *Geology of Clay;* Chapman and Hall, **1970.**

1.3.1 THE KANDITES/KAOLINITES.

Like all clay minerals kaolin is a phyllosilicate; the structure was first established by Gruner (1932) and further revised by Brindley and Robinson (1946)[5]. Figure 6 shows a diagrammatic representation of the kaolin 1:1 type mineral structure. Kaolin has the general formula $(OH)_4Al_2Si_2O_5$ and theoretically is electrically neutral.

Figure 6 : Diagrammatic representation of kaolinite.

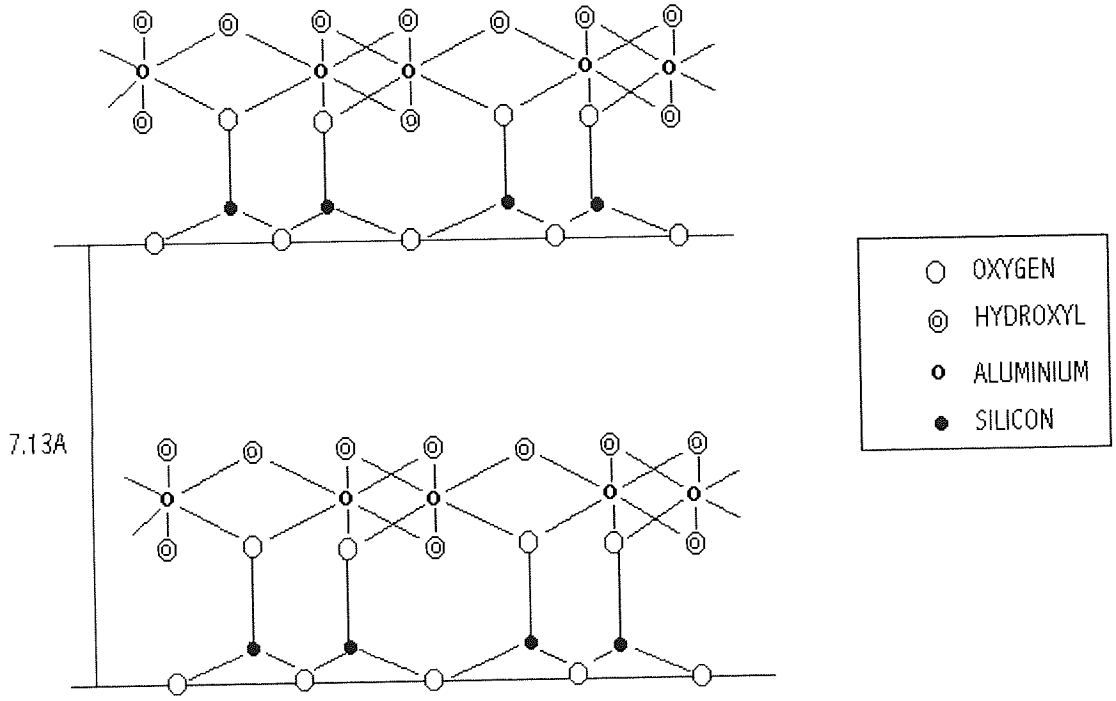

The layers are regularly stacked giving a basal spacing of approximately 7Å. This value rarely differs as the layers are tightly bound and therefore insertion of an organic moiety is difficult. This also accounts for the low level of isomorphous substitution found within the kaolin group reflected in its low C.E.C.(cation exchange capacity) in the range 3 to 15 millequivalents (meq) per 100g of clay. Binding or substitution therefore occurs predominantly at the edge of the kaolin crystal; any residual negative charges are balanced by counter cations.

Under suitable conditions it is possible for a single water layer to be located between the kaolin layers, thus forming halloysite. This increases the basal spacing to 10Å and gives the general formula $Al_2Si_2O_5(OH)_4.2H_2O$. The insertion of water into the

structural unit causes halloysite to have much weaker bonding forces than kaolinite. Due to kaolin's being able to exhibit several spatial stacking arrangements there are several minerals within the kaolin group. They share general chemical composition, namely $Al_2Si_2O_5(OH)_4$, but differ in properties; some well-recognised species are nacrite, dickite, kaolinite and livesite.

In the majority of British fireclays and ballclays used within the ceramics industry kaolin is the predominant clay mineral; usually it is imperfectly crystalline with some disorder in the stacking units.

1.3.2 TALC AND PYROPHYLLITE

Ideally talc and pyrophyllite consist of electrically neutral 2:1 layers, talc is trioctahedral, $Mg_6Si_8O_{20}(OH)_4$ and pyrophyllite is dioctahedral , $Al_4Si_8O_{20}(OH)_4$. The terms dioctahedral and trioctahedral describe the nature of the interaction between the octahedral and tetrahedral sheet in 2:1 layer silicates. In trioctahedral minerals all of the available sites in the octahedral sheet are full, so there are three octahedra within each hexagonal ring of the tetrahedra. For a dioctahedral mineral only two-thirds of the available sites on the octahedral sheet are filled.

The layers in talc are weakly bonded by Van Der Waals forces and ionic attraction. Talc undergoes very little isomorphous substitution; there is little or no replacement of Si^{4+} with Al^{3+} of Fe^{3+} ions. For talc the dominant octahedral cation is Mg^{2+}. Conversely, pyrophyllite, which shows very little variation in basal spacing does exhibit extensive isomorphous substitution and thus a wide range of Si^{4+}/R^{3+} ratios. The dominant octahedral cation in pyrophyllite is Al^{3+}.

1.3.3 THE SMECTITE/MONTMORILLONITE GROUP.

Smectites/montmorillonites are of the 2:1 layer type structure and exhibit a chemical composition similar to that of micas, differing predominantly in their weaker bonding forces, thus exhibiting less rigidity.

Structurally, the smectites are of similar structure to talc and pyrophyllite except for the presence of additional water, and have the general formula $Al_2O_34SiO_2.H_2O + xH_2O$. These smectites exhibit a range of basal spacing from 10Å – 20Å as a result of hydration and isomorphous substitution of the species, with a typical spacing of *ca*14Å.

Lattice substitutions occur predominantly in the octahedral layer, usually of Al^{3+} by Mg^{2+} and result in a residual negative charge over the structure. Electrical neutrality is restored by inserting charge balancing cations in the interlayer, usually Na^+ or Ca^{2+}. These cations are usually easily exchangeable and therefore smectites have a C.E.C of 80 –150 meq per 100g of clay. As a consequence a wide range of minerals exist that may be included in the smectite group which are related by common structure and chemical composition. Of these montmorillonite is derived from pyrophyllite through the replacement of aluminium by magnesium cations in the ratio 5:1, charge balanced by sodium, thus giving the formula:

$$Na^+_{0.33}(Al^{3+}_{1.67}Mg^{2+}_{0.33})Si^{4+}_4O^{2-}_{10}(OH)^-_2$$

The Na^+ ion position is outside the lattice therefore rendering it easily exchangeable. Figure 7 shows a diagrammatic representation of the structure of montmorillonite.

Figure 7 : Proposed structure for Montmorillonite.

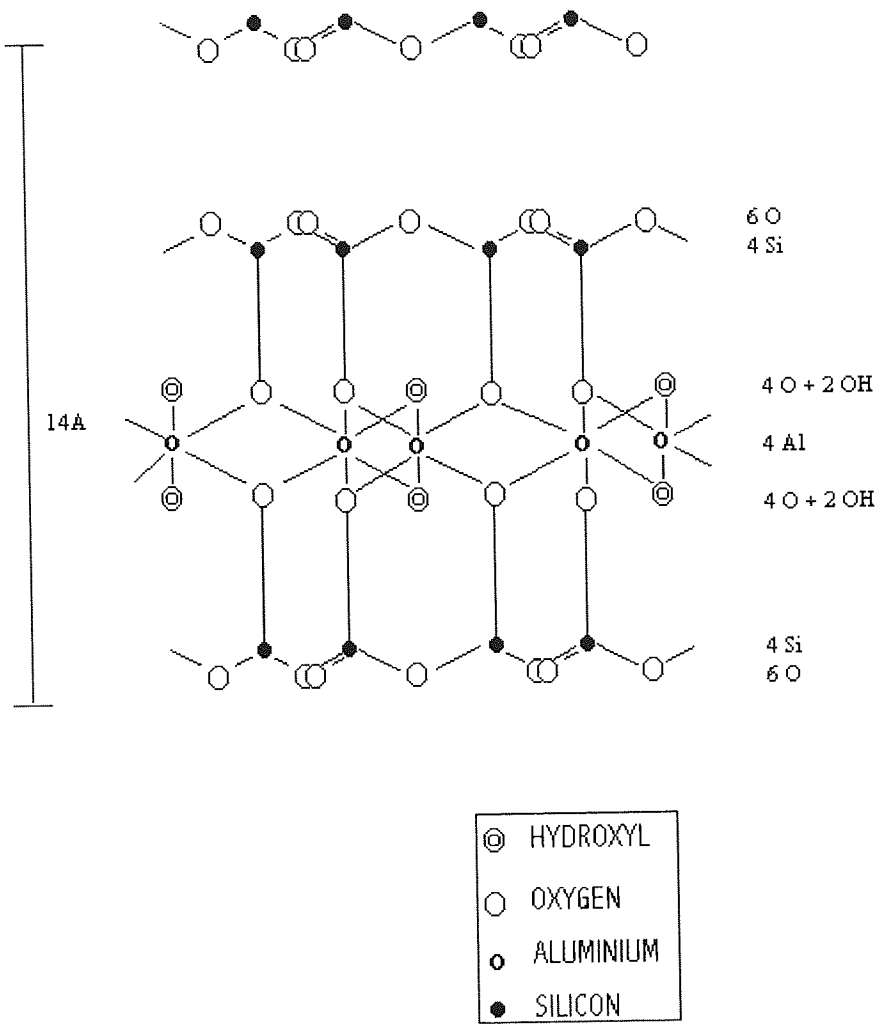

Within montmorillonite the unit layers are held together by weak intermolecular Van der Waals forces, thus water can readily force the unit layers apart so swelling in aqueous media occurs.

The term smectites is the alternative phrase used to describe this type of clay; other members of the group are nontronite, beidellite, hectorite and saponite. The latter two are trioctahedral [6]smectites based on talc rather than pyrophyllite.

---

[6] Trioctahedral meaning that all octahedral lattice site are filled and isomorphous substitution in the tetrahedral sheet of Al^{3+} for Si^{4+} has occurred.

The chemical forms of all smectites are similar to either talc or pyrophyllite differing only in substitutions in the octahedral or tetrahedral sites by ions of lower valency therefore resulting in charge balancing by interlayer cations. For montmorillonite and hectorite substitution occurs predominantly in the octahedral sheet whilst for beidellite and saponite it is in the tetrahedral sheet. It is possible to achieve both types of substitution and for both a series can be attained.[7]

Figure 8 : Dioctahedral 'monmorillonite-beidellite-nontronite' series.

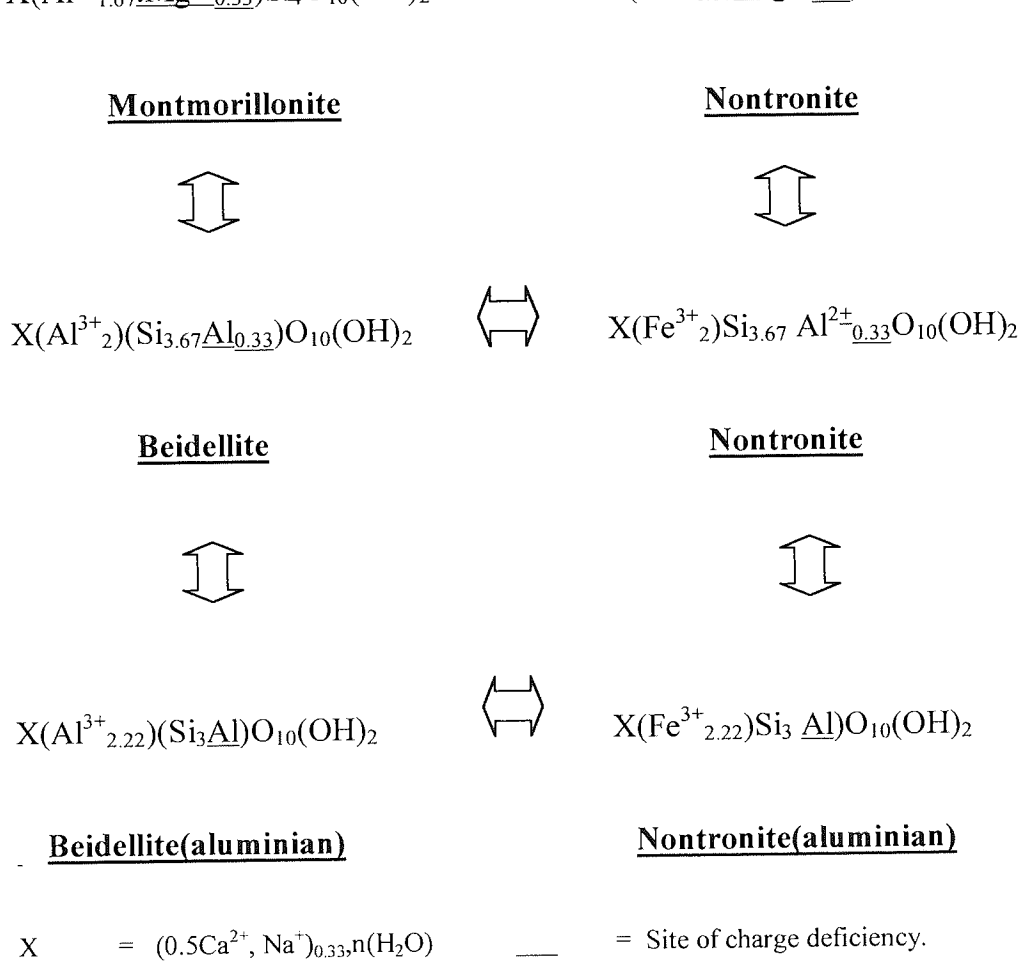

[7] Michael. P., *Studies of Clay Minerals and their decomposition products,* PhD Thesis, Aston University, 1989.

1.3.4 THE MICA GROUP.

Structurally, micas are regarded as a natural follow-on from montmorillonites and hence show similarities to both pyrophyllite and talc. Differences manifest themselves in that micas can undergo numerous isomorphous substitutions. Therefore, chemically they are a far more complex group of minerals. The extent of substitution results in micas having a greater charge deficiency and for that reason interlayer cations are often held more strongly by bonds more similar to ionic than to Van der Waals forces. Unlike montmorillonite-type minerals micas do not undergo expansion by water, whilst cation exchange will only occur as a result of decomposition.

Depending on the actual type of substitution occurring the mica group can be subdivided into dioctahedral or trioctahedral minerals. Muscovite mica (Figure 9) is the true dioctahedral mica, where the interlayer cation is predominantly K^+ or Na^+, with the formula $KAl_2(Si_3Al)O_{10}(OH)_2$ and an interlayer distance of approximately 10Å. The sodium equivalent is paragonite where K^+ is substituted for Na^+. Due to size differences sodium ions are not held as tightly as potassium ions and their decomposition is easier.

Figure 9 : Muscovite Mica

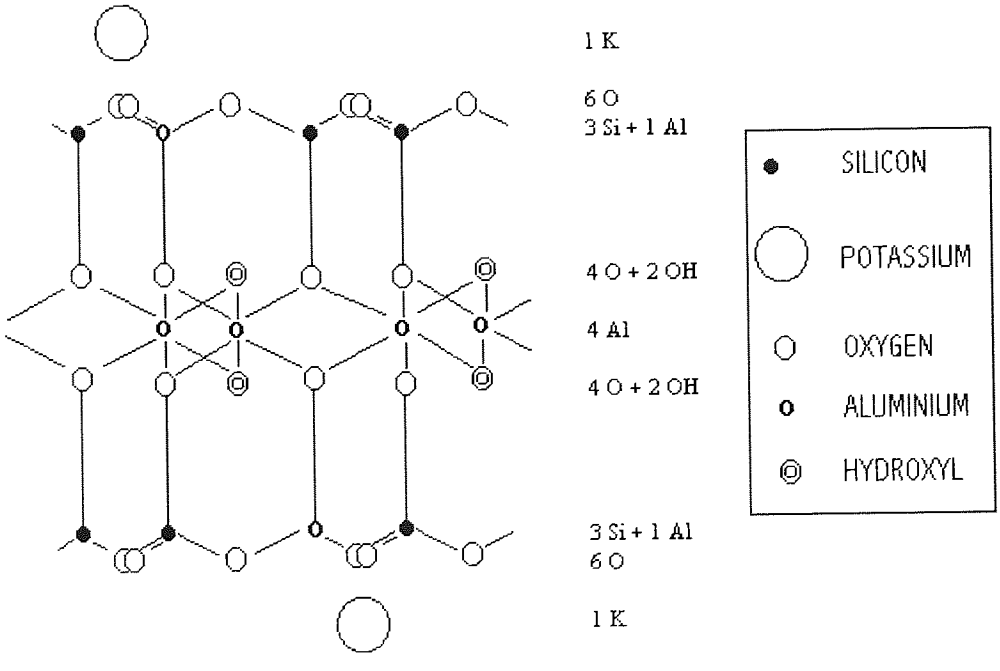

A further typical dioctahedral mica is margarite, $Ca^{2+}Al_2(Si_2Al_2)^{2-}O_{10}(OH)_2$, otherwise known as brittle dioctahedral calcium mica, as it does not undergo easy cleaving. Often magnesium is observed in place of calcium. It is possible for Li^+ to substitute into the octahedral sheet thus producing a mix of both di- and tri-octahedral minerals. Trioctahedral micas include, phlogopite, $KMg_3(Si_3Al)O_{10}(OH)_2$ and annite, $KFe_3^{II}(Si_3Al)O_{10}(OH)_2$.

1.3.5 THE ILLITES.

Illites are considered as being fine-grained micas, where a deficiency in potassium is compensated by the inclusion of water. Due to this deficiency layers are no longer as tightly bound and hence expansion characteristics are dependent upon the degree of hydration; for this reason they are often termed hydrous micas and have a basal spacing of *ca*10Å. It has been suggested that the hydroxonium ion may replace K^+ ions in muscovite thus providing illite with a lower alkali and hence higher water content. A partial replacement of Al^{3+} octahedral ions by Mg^{2+} and $Fe^{2+/3+}$ is possible and often observed.

The true composition of hydrous micas is unknown and as yet full elucidation has not been possible, primarily due to the finely ground samples being contaminated with a multitude of impurities. Isolation of larger flakes has led to a general formula of;

$$K_xAl_2(Si_{4-x}Al_x)O_{10}(OH)_2; \qquad 0.5 < x < 0.75$$

For illites the total iron content is less than one cation per four octahedral sites and this is what distinguishes illites from glauconites, an important member of the group that exhibit more iron than illite. There are possibilities for a wide range of illite minerals with a decreasing alkali content and increasing water content; there would also be a tendency for the silica : alumina ratio to extend beyond 2:1, corresponding to ideal muscovite.

1.3.6 THE CHLORITES.

Chlorites form a plate-like class of minerals that are similar to mica, but much softer and of different composition. Essentially they are hydrated silicates of magnesium and aluminium with a proportion of either ferrous or ferric iron. They are minerals of small particle size and usually greenish in colour.

Structurally they are essentially 2:1 layers with a further octahedral layer situated in the interlayer region, they can therefore be considered as 2:1:1 layered structures. Essentially they are based on talc, $Mg_3Si_4O_{10}$ but with a brucite layer, $Mg(OH)_2$ between each talc layer. The talc layers have a residual negative charge due to isomorphous substitution of silicon by aluminium in the tetrahedral layers and magnesium for aluminium or ferrous ions in the octahedral layers. This is balanced by the intercalation of a brucite layer, which carries a residual positive charge. It is therefore reasonable to suggest that bonding between the layers is partly ionic.

A typical chlorite is pennite, of formula:

$$(Mg_2(Al,Fe^{III})(OH)_6)^+(Mg_3(Al.Si_3)O_{10}(OH)_2)^-$$

Brucite layer Talc layer

Most chlorites are trioctahedral and of the talc structure, however there are some of the pyrophyllite structure. Due to the absence of exchangeable cations, exchange capacity is low, only 10 – 40meq per 100g of clay. Typically, they exhibit a basal spacing of *ca*14Å which, unlike the smectite group, is fixed.

1.3.7 THE VERMICULITES.

This distinct group of minerals are characterised by their large mica-like flakes. They are trioctahedral with a 2:1 layer structure that is not electrically neutral and have a cation exchange capacity of 100-150meq per 100g of clay. Characteristically they exhibit a basal spacing of 14Å which upon heating reduces through a two-fold process to 9Å The heating of vermiculites causes up to a 100 fold increase in the magnitude of

the spacing. The resultant products are used in the ceramics industry as thermal insulators.

The average molecular formula of vermiculite has been determined as $22MgO.5Al_2O_3.Fe_2O_3.22SiO_24H_2O$, although some of the magnesium is present as an exchangeable base situated between the electrically imbalanced talc layers. Structurally, similarities to chlorite are observed where hydroxyl or water molecules take the place of the brucite layers, thus they display extensive hydration.

1.4 THE PROPERTIES OF CLAYS.

All clays share the same basic chemical and physical properties. It is their plasticity when wet that makes them of particular value to the ceramics industry, a unique property not exhibited by any other material. In addition to this, clays also exhibit the ability to swell in aqueous media thus demonstrating the aptitude to undergo cation exchange with many simple or complex organic ions. Upon heating, clays loose free and bound water and this is accompanied by observable changes in structure.

These unique properties exhibited by smectite clays are a result of small particle size, variations in internal structure, variation of exchangeable cation with the ability to undergo exchange and the ability to interact with organic and inorganic molecules.

Those properties examined in further detail are of particular interest to the scope of the work reported in this thesis.

1.4.1 CATION EXCHANGE CAPACITY.

Due to the isomorphous substitution of high valence cations by ones of lower valency (i.e. Si^{4+} replaced by Al^{3+}) the clay structure becomes negatively charged and hence all clay minerals adsorb positive cations to maintain electrical neutrality. Although these cations do not affect the structure of the clay mineral they do have a great influence on the properties of the clay and due to being held by only weak electrostatic forces they are easily replaced by ions of a similar nature in the presence of polar reagents such as water, which act to solvate the interlayer cations. The ability of clays to undergo exchange of one cation for another is known as cation exchange capacity (C.E.C.) with the amount of cation adsorbed being very small and being expressed as milliquivalents (meq) of ions adsorbed per 100g of clay.

Not all clay minerals exhibit the same cation exchange capacities with a range of values existing for each specific group of minerals. The ability of a clay to undergo exchange depends upon a number of variants, most importantly, the concentration of exchange solution being used in concurrence with the size and valencies of the cations in

question. Cation exchange in clays is a stoichiometric reaction, so as the concentration of exchanging cation increases easier exchange will occur. Some of the most commonly exchanged cations are Ca^{2+}, Li^{+}, Na^{+}, K^{+}, Mg^{2+} and H^{+} for which an order of preferred adsorption can be determined in which the divalent ions are favoured over the monovalent ions.

$$H^{+} > Mg^{2+} > Ca^{2+} > Li^{+} > Na^{+} > K^{+}$$

The ease of replacement of an ion will also depend upon the ions filling the remaining sites. For example, as the amount of exchangeable calcium ions on the clay is reduced the remaining ions become more tenaciously held, conversely sodium ions become easier to remove as the degree of saturation of sodium ions reduces.

There is no doubt that isomorphous substitution is the main cause of cation exchange in montmorillonites with the extent to which it occurs resulting in a high cation exchange capacity of 70 – 150meq/100g. In contrast the kaolin clays exhibit unsatisfied valency bonds at the outer edges of the clay lattice so allowing combination with further ions to occur. Due to these outer charges being both positive and negative, valencies are satisfied by both anions and cations, hence kaolins show a relatively high anion exchange capacity and a much lower cation exchange capacity in the region of 3 – 6 meq/100g.

The ease of replacement of cations in montmorillonite by other cationic species in combination with the ability to swell in aqueous environments has led to the modification of clays by pillaring and the formation of alternative types of clay structure.

The cation exchange capacity of a clay is vitally important to a ceramicist as it dictates not only typical characteristics but is also indicative of the type of minerals likely to be found.

1.4.2 HYDRATION AND DEHYDRATION

All clay minerals show a great affinity for water causing them to swell up to 100% of their natural size, for example smectites minerals can show lattice expansion from 10Å to 19.5Å upon immersion in liquid water. It is the weak electrostatic and Van der Waals forces between layers that allow the ease of insertion of water molecules.

The degree of swelling of all clay minerals is dependent upon a number of factors these being: type and amount of clay mineral, the particle shape and size and most crucially the exchangeable ions associated within the interstitial layers, in particular their size and valency. It is important to realize here that the silicate layer itself does not play an important role in either the hydration or dehydration of clay species.

Of all the clay minerals the smectite group exhibit the greatest ability to swell, this is especially prevalent if the interlayer cation is small and monovalent, such as Li^+ or Na^+, due to water molecules arranging themselves around interlayer cations and in effect co-ordinating with them. For monovalent ions in particular this tends to reinforce a rigid structure of water layers completely dissociated from the silicate surface. It has been suggested that the water molecules adopt an ice- like structure.[3]

The mechanism associated with hydration of smectite minerals is unclear and seems primarily dependent upon the size and valency of the interlayer cation. Ca^{2+} montmorillonite exhibits the formation of both mono- and di-molecular sheets in the interlayer region with a non-uniform increase in basal spacing. In contrast Na^+ intercalated smectites demonstrate a stepwise expansion up to 20Å consisting of various ordered crystalline states, the sudden jump to 40Å is followed by a smooth increase. The common factor linking all these is that the first water layer is always uniformly formed adopting a rigid appearance regardless of cation type.

The monovalent cations such as Na^+ and Li^+ demonstrate unlimited swelling capabilities whilst, conversely, divalent cations act as a bridge between the charged silicate sheets. The swelling of clay minerals by either water or organic moieties is characteristic of the type of clay mineral involved as often aids in identification *via* techniques such as X-ray powder diffraction. The ability of all clay minerals to swell in

aqueous media is an essential component of ion exchange reactions. The process of hydration is reversible and upon dehydration normality should be achieved. However, drying of a swollen hydrated mass often results in disruption of the lattice due to unsymmetrical drying.

The heating of clay minerals also causes structural and interlamellar changes. Clays undergo two main processes that of dehydration where the absorbed or loosely bound water is lost and that of dehydroxylation involving the loss of chemically bound water in the form of hydroxyl groups. Both involve the application of a heating process but to different extremes.

Free water removal begins at approximately 110°C and extends up to 200°C giving a collapsed dehydrated structure. The nature of dehydration depends somewhat on the clay mineral structure but more importantly on the interlayer cation. Literature reports[8] that, for Na^{+}, low temperature water is lost in a single step whilst for Ca^{2+} two steps are observed. This can be studied by the application of thermal gravimetric and differential thermal analysis and has been included in the present work. Any loosely bound water is lost at slightly higher temperatures of approximately 200 – 300°C.

The detailed behaviour during the loss of lattice water can be used to characterise specific minerals, due primarily to their different crystalline structures and chemical compositions. Dehydroxylation can occur in the wide range of 200 – 800°C, depending upon the mineral type and this induces structural changes in the silicate layer to form other silicate analogues.

The method of dehydration is reversible. Any smectite mineral subjected to heating up to 200°C will undergo complete rehydration in liquid water. After further heating to 500 – 700°C rehydration will still occur. The process, however, may differ due to the occurrence of structural changes during the heating process. Clays heated above 700°C are almost impossible to rehydrate due to the many structural changes which lead to conversion into other silicates and the complete destruction of the clay structure.

1.5 POTTERS CLAY AND THE CERAMIC COUNTERPARTS.

The potters' clay is invariably a complex mix of the 'pure' clay minerals discussed above. It is often the nature and amount of impurities in a clay that determines the uses to which the clay can be put. The current expansion in the field of ceramics has meant that the 'Potters' clay is the most basic and important of earthenware raw materials.

The variety in ceramic products is enormous. Subdivision into those used at room temperature and those at elevated temperatures reduces the range. For the purpose of discussion here it is ceramics used at room temperature and below that are of specific interest. In particular terracotta vessels for the housing of plants in an external environment is of special interest.

Typically a ceramic material is considered as any of a number of hard, brittle, heat and corrosion resistant materials made by shaping and firing a non-metallic material, such as clay, at a high temperature.[9] It is the features of heat and corrosion resistance that producers of high quality ceramic wares aim to fulfil; it is when there is a breakdown in one or both of these areas that problems begin to manifest themselves. One widespread concern is the action of frost upon terracotta clay bodies as it is often expensive and difficult to rectify. An average clay body can be exposed to between 40 and 200 freeze thaw cycles per year, depending upon its geographical location. The need, therefore, to gain an understanding of the damage that occurs, is of importance.

1.5.1 RESISTANCE TO FREEZING AND THAWING, THE MAJOR FACTORS[10]

There are generally considered to be three main factors involved in the examination of the action of freeze thaw cycling upon ceramic materials. These are air entrainment or air trapped in voids within the structure, water content and volume stability. These factors influence the degree of expansion that results from water freezing. It is therefore an adverse change in any of these properties that affects the overall strength and

---

[8] Brindley, G.W., and Brown, G., *Crystal structures of clay minerals and their X-ray identification*, Mineralogical Society of London, **1984.**

[9] http://www.neutron.anl.gov/ceramics.htm

[10] http://www.ceaspub.eas.asu.edu/concrete/hardened-concrete/img001.jpg

durability of a ceramic material. For the purpose of discussion here, durability is defined as the resistance to freezing and thawing, to cracking and hence an overall resistance to internal change.

Invariably, over time, ceramic materials like most others show a reduction in durability. That is most likely to originate from internal or external cracks. The ease with which water can now access the body is increased and hence prolonged damage can begin. Harm does not only arise from the 9% expansion of water as it freezes and the position of the freezing, but also as a direct result of increased load. Deformations of this type allow the leaching of sulfates from soil into the clay body, thus resulting in further expansion and deterioration. It is therefore of prime importance to the ceramics industry to determine the action of freeze-thaw cycling to identify procedures to enhance quality of product, and enable improved product guarantees to be offered.

1.5.2 THE IMPORTANCE OF FREEZE/THAW.

Climatic conditions often demand that outdoor ceramic materials must be able to survive the natural stresses of freeze-thaw. Porous ceramics absorb water which freezing temperatures cause to expand thus eventually causing the matrix to break down and crumble Some literature reports suggest that if the possible level of adsorption is below a certain amount then a fired ceramic product will be suitable for outdoor use[11]. However, it is also claimed[11] that any fired clay that exhibits greater than zero percent absorption is susceptible to freeze-thaw damage. Certainly this is found to occur for most ceramic materials. There is therefore a need for a better understanding of frost action.

It is possible to replicate the action of freeze-thaw by following a process of soaking a sample of known mass of fired clay in water until a constant weight is obtained. The procedure of freezing at –15°C followed by thawing under hot water over a period of time is used to simulate the natural process. Within the scope of present work it is the action of freeze-thaw cycling upon ceramic bodies that is of interest. Macro-

[11] http://digitalfire.com/education/clay/outdoor.htm

deformations and micro-deformations can be determined *via* the application of a number of analytical techniques.

There is currently very little scientific literature on research of this type. *Maciulaitis*[12] discusses the frost resistance and long service life of ceramic façade products. This work looks primarily at the action of unilateral and multilateral freeze methods which are now accepted as an essential feature of frost testing and is characteristic to the type of failure observed in practice. There were few conclusions reached of relevance to the research undertaken here, the only analogies that can be made are to concrete structures. *Challis*[13] discussed frost failure and resistance of porous building materials, and is currently studying the ice/water system within brick structures and its relationship to the failure process. Ultrasound is documented to be the best method for the determination of the action of frost[13] as it allows the early detection of frost failure before it becomes clearly visible. Specimens are deemed as frost resistant if no visual damage is observed and no conditional change is found in comparison with the initial condition.

Because of time constraints, laboratory simulation of frost tests must involve rates much faster than those which occur in practice.

---

[12] Maciulaitis Romuldas, *Zi Int.*, **1994,** 47, 313 – 322.

[13] http://www.ceramres.co.uk/ptp/1997_projects/molearyp.htm

1.6 MODIFIED CLAY STRUCTURES.

1.6.1 LAYERED DOUBLE HYDROXIDES.

Layered double hydroxides (LDH's) are a synthetic class of layered materials similar to clays and are often described as "anionic clays" or "anti-clays" of the 2:1 type clay minerals. Structurally LDH's consist of positively charged brucite ($Mg(OH)_2$) -like layers where partial substitution of M^{II} cations by M^{III} cations has occurred[14] thus resulting in positively charged layers that are balanced *via* anions in the interlayer region, typically CO_3^{2-}, NO_3^-, SO_4^{2-}, OH^- and Cl^-.[14,15,16.] Water molecules also occupy the gallery region, held by hydrogen bonds to both the layers and anions.

Layered double hydroxides generally show reluctance to anion exchange. Often carbonate which is tenaciously held and thus difficult to remove, is the preferred anion. However, the anion exchange capacity of LDH's is greater than the cation exchange capacity of clays, with the range of 2.4 – 4.1meq/g and 0.7 – 1.0meq/g respectively. An order of anion preference for LDH's has been determined.[16]

$$CO_3^{2-} >> SO_4^{2-} >> OH^- > F^- > Cl^- > Br^- > NO_3^- > I^-$$

A number of LDH's have been synthesised with a variety of different anions whose size will cause a change in basal spacing and hence gallery height. These are often tailored towards a specific function. Literature reports show LDH's to exhibit properties similar to clay minerals with applications as pharmaceuticals, catalysts, adsorbents and anion scavengers.[14,15,16.]

Conventionally LDH's are synthesised *via* a method of co-precipitation, where metal nitrates and precipitants are added together slowly and at fixed pH under stirring. The resultant layered double hydroxide has a general formula:

---

[14] Ulibarri, M.A., Labajos, F.M., Rives, V., Trujillano, R., Kagunya, W., and Jones, W., *Inorg. Chem.* **1994,** 33, 2592.
[15] Taehyun, K., Tsigdinos, G.A., and Pinnavaia, T.J., *J. Am. Chem. Soc.*, **1988,** 110, 3653.
[16] Carlino, S., "Chemistry between the sheets", *Chemistry in Britian,* **Sept 1997,** 59 .

$[M^{II}_{1-x}\ M^{III}_{x}\ (OH)_2]\ [A^{n-}]_{x/n.y}H_2O$. Where M^{II} and M^{III} are metal cations occupying octahedral positions and A is the gallery anion. Figure 10 provides a diagrammatic representation of a typical layered double hydroxide, where the interlayer cation is in conjunction with water molecules.

Figure 10 : Diagrammatic representation of a layered double hydroxide.

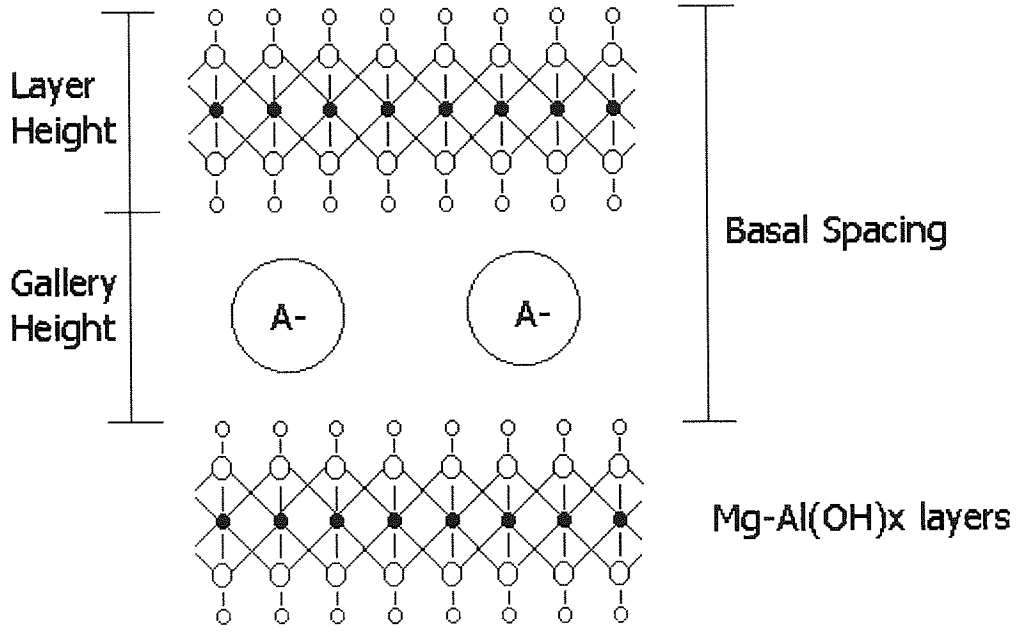

More recent reports have suggested that the synthesis of layered double hydroxides *via* use of microwave irradiation[17,18] produces materials which exhibit enhanced crystallinity, whilst the reaction time is reduced considerably. Enhancement of crystallinity is said to be dependent upon the nature of the trivalent cation. Work on the synthesis of layered double hydroxides *via* microwave methodology is described herein.

---

[17] Prévot.V., Casal, B., and Ruiz-Hitzky.E., *"Intracrystalline alkylation of Benzoate ions into layered double hydroxides"*,. In press.
[18] Kannan, S., and Jasra.R.V., *"Microwave assisted rapid crystallization of Mg-M(III) hydrotalcite where M(III) = Al, Fe and Cr."*, In press.

1.7 MICROWAVE ENHANCED CHEMISTRY.

The use of microwave ovens as a laboratory tool has long since been established, with reports of the potential use of microwaves for chemical synthesis dating back to the early 1980s.[19] Only recently has their full potential begun to be explored.[19] Early reports on the use of microwave irradiation primarily focused on analytical sample preparation.[19,20] More recently rapid growth expansion has led to the chemical applications of microwaves being extended to all areas, often replacing conventional thermal methods and increasing laboratory productivity.[20]

The benefits of microwave heating over conventional methods are well documented and include reaction rate enhancment,[19,20,21,22,23,24] one-pot synthesis,[23,25] reactant selectivity,[22,23] reduction in the production of waste solvents[23,26] and in some instances solvent-less reactions[23]. Microwave-driven chemistry has found applications in many fields of synthetic chemistry. A great deal of literature exists demonstrating its importance in organic synthesis,[20,22,23,26,27,28,29] pharmaceuticals,[22,23,26] polymerisation,[19,24,26,27] inorganic co-ordination chemistry,[26] intercalation chemistry,[19,26,30] formation of zeolites,[26] and, most significantly, the sintering of ceramic materials.[19, 21,23,27,31]

The attention that has been paid to microwave-enhanced chemistry over the last 10 –15 years has meant that the scope and limitations have been well established.

---

[19] Whittaker, A.G., and Mingos, D.M.P., *Journal of Microwave Power and Electromagnetic Energy,* **1994,** 29, 195 – 219.
[20] Ferguson, D.R., *"The basics of microwave heating for organic synthesis"*, **Oct 2000,** 69.
[21] Gabriel, C., Gabriel, S., Grant, E.H., Halstead, B.S.J. and Mingos, M.P., *Chemical Society Reviews,* **1998**, 27, 213 – 223.
[22] Laurent, R., Laporterie, A., Dubac, J., Berlan, J., Lefeuvre, S. and Audhuy, M., *Journal of Organic Chemistry,* **1992**, 56, 7099 –7102.
[23] Whittaker, G., *The New Scientist,* **Feb 1998**, 34 –37.
[24] Baghurst, D.R. and Mingos, M.P., *Journal of the Chemical Society., Chemical Communications,* **1992**, 674 – 677.
[25] Varma, R.S. and Kumar, D., *Tetrahedron Letters,* **1999**, 40, 7665 – 7669.
[26] Galema, S.A., *Chemical Society Reviews,* **1997**, 26, 233 – 238.
[27] Thostenson, E.T. and Chou, T.W., *Composites part A: Applied Science and Manufacturing,* **1999,** 30, 1055 – 1071.
[28] Gedye, R.N., Smith, F.E. and Westaway, K.C., *Canadian Journal of Chemistry,* **1988**, 66, 17 –26.
[29] Gedye, R.N., Rank, W. and Westaway, K., *Canadian Journal of Chemistry,* **1991**, 69, 706 – 711.
[30] Ashcroft, R.C., Bond, S.P., Beever, M.S., Lawrence, M.A.M., Gelder, A., McWhinnie, W.R. and Berry, F.J., *Polyhedron,* **1992**, 11, 1001 – 1006.
[31] Pelesko, J.A., *IMA Journal of Applied Mathematics,* **2000**, 64, 39 – 50.

1.7.1. MICROWAVE DIELECTRIC HEATING[21,24,26]

The use of microwave ovens as a laboratory tool in both solvent (homogenous) and solid (heterogeneous) based reactions is well known.

Microwave dielectric heating involves the conversion of electromagnetic energy through molecular interactions into thermal energy, making microwave heating a far superior method to conventional heating. Heat transfer occurs when energy is emitted by convection, conduction and radiation from the materials surface. This means in conventional heating there is often a trade off between processing time and product quality, a phenonomen not observed with microwave irradiation where enhanced reaction rates often lead to superior quality products.

Workers in the field postulate both thermal and athermal (non-thermal) effects of microwave heating. The existence of a thermal effect is widely accepted as a source of reactant activation and rate enhancement. The existence of an athermal 'microwave effect' is still under debate.

The mechanism associated with the microwave heating of dielectric materials involves both conduction and dipolar polarisation.

1.7.1.2 CONDUCTION[20,23]

When microwave energy impinges on a conductor or semiconductor electrons or ions in the material experience an extremely high voltage causing them to migrate in the direction of the electric field. During migration energy transfers from the electric field to the reaction system due to ionic interactions, thus causing a current to pass through the material and so heating it up.

Ionic conduction increases with temperature allowing ionic solutions to become stronger absorbers as they heat up.

1.7.1.3 DIPOLAR POLARISATION[20,21,26]

A dielectric material is one that has permanent or induced dipoles that can act as capacitors when placed between two electrodes. Polarisation of the charges occurs when an electric field is applied to the material. The force exerted upon charged particles causes them to rotate which in turn causes further polarisation of the already polar molecules.

Using microwave irradiation, the applied field rapidly changes direction at a rate of approximately 2.4×10^9 cycles per second. The molecules are unable to respond immediately to the changing field. This results in friction and thermal energy that causes heating of the material.

Microwave-enhanced reactions *via* dipolar rotation and/or ionic conduction allow the efficient transfer of energy directly to the reactants, causing rapid and uniform heating.

1.7.2 THE NATURE OF MICROWAVE ACTIVATION.

Microwave activation is dependent upon a number of variables. These include the nature of reagents, the dielectric constant of the material/complex, and the reaction conditions, e.g. solvent or dry. The most studied area of microwave activation is the superheating of solvents in homogeneous reactions.[22,23,24] Superheating occurs as microwaves heat the solvent in a reaction vessel directly, thus allowing the entire bulk to reach a higher temperature before cavitation and hence boiling occurs. Conversely a bunsen burner only heats the edges of a flask and so essentially heats the solvent through the walls of the vessel. Heating *via* conventional methods is a much slower process.

Baghurst and Mingos[24] in 1992 demonstrated this phenonomen, showing how the increase above normal boiling point can be up to 26°C. Table one shows the increase in boiling temperature for a variety of solvents commonly used in microwave-enhanced reactions.

Table 1 : Increases in boiling temperatures under microwave irradiation.[24]

SOLVENT TYPE	NORMAL BOILING POINT	ELEVATED BOILING POINT	INCREASE
WATER	100°C	104°C	4°C
ETHANOL	79°C	103°C	24°C
METHANOL	65°C	84°C	19°C
ACETONITRILE	81°C	107°C	26°C

Work described in this thesis makes use of microwave irradiation using a 2.45GHz oven. Reactions were performed in a Teflon vessel in an aqueous environment.

Most chemists have now adopted this explanation of faster reactions under microwave irradiation. Reactions performed in a sealed Teflon vessel have shown further rate enhancement, due to build up of pressure with its impact on temperature.

Literature[24] shows that the most likely cause of boiling is nucleate boiling. This is reflected in a dramatic increase in temperatures. Nucleate boiling relies on the existence of scratches/cavities on the vessel surface at which bubbles can form. Vapour embryos exist inside the cavities trapped by a layer of superheated liquid and when temperature of the surrounding liquid is equal to that of the vapour, bubble formation occurs. Once the forces holding the bubble in place are overcome boiling occurs.

In summary, when exposed to microwave irradiation solvents are heated above their normal boiling temperature. This phenonomen is known as superheating. The process of superheating is responsible for the increased reaction rates observed during microwave heating of homogeneous systems.

1.7.3 THE MICROWAVE EFFECT.

Microwave irradiation has been used extensively over recent years and in many facets of chemistry. Particular interest has been observed in organic synthesis with relation to pharmaceutical production. The sintering of ceramics has also been of importance.

From the early days of microwave-enhanced chemistry there has been much debate as to the exact nature of microwave activation and the rate enhancements associated with

it. Early work by *Baghurst and Mingos*[24] provided an explanation, by demonstrating the superheating of solvents in homogeneous reactions. Conversely, *Laurent et al.*[22] reported that rate enhancements observed under homogeneous conditions were independent of heating method; providing that temperature and pressure remain constant. *Laurent* further suggested that lack of experimental control resulted in misleading conclusions. *Gabriel et al.* [21] carried out more detailed reaction rate measurements and established, that in general, chemical reactions under microwave conditions are governed by the same fundamental principles of thermodynamics and kinetics as reactions occurring under conventional conditions.

Although the phenomenon of superheating has been generally accepted, some chemists believe that microwaves do more than apply heat in a different way and began to examine the possibility of the radiation affecting molecules in other ways.

Rate enhancement in heterogeneous catalysis is thought to be a result of the formation of 'hot spots' at the catalyst surface. *Laurent et al.*[22] reported reactions performed under heterogeneous conditions with the use of a clay catalyst showed markedly enhanced reaction rates. *Wroe* writes of having 'proven' the existence of a microwave effect when performing experiments with microwaves in the sintering of ceramic materials. *Wroe* formulated the theory that microwaves lower the energy barriers that ions must overcome. *Wroe* suggests that the microwave electric field helps to 'pick them up' and 'shunt' them along.

Generally there is still much disagreement as to what confers to a microwave effect. Often the accumulation of reproducible results in this area is hampered by difficulties associated with the rapid and reliable measurement of temperature within the microwave cavity. Many would agree that the main problem occurs due to differences in experimental conditions resulting from imprecise monitoring and improper controls.[22,23]

It is fair to say that rate enhancements observed as a result of microwave irradiation are fundamentally thermal in nature that is the kinetic energy of the system is increased or redistributed. Enhancements of reaction rate are therefore a result of three important factors:

- The superheating of solvents above their normal boiling point; superheating occurs prior to bubble formation and hence boiling, so boiling is suppressed.

- The effects of increased pressure when reactions are performed inside closed vessels hence causing a further increase in temperature.

- Formation of 'hot spots' due to dielectric relaxation on the molecular scale, similar in some ways to ultrasonic cavitation.

The attempts made to identify a non-thermal microwave effect appear now to be based on a disagreement as to what having a microwave effect actually means. This has led to the conclusion that rate enhancement is predominantly attributable to thermal effects.

1.7.4 MICROWAVE ENHANCED CERAMIC AND CLAY MATERIALS.

Over recent years microwave processing of ceramic materials has reached a high degree of maturity and has become what can be termed as an intense activity. Early work[19] in the area involved the removal of water from solid systems and was in effect used as a highly effective drying mechanism. More recently, microwave-enhanced ceramic chemistry has expanded into many facets including zeolite formation,[26] calcination,[26] pyrolysis of ceramic polymers,[27] intercalation,[30] and sintering of ceramic particles.[19,23,26,27,31] Reports on such work has highlighted enhanced processing times, increased crystallinity combined with fine grain size and increased densities.

Of late, a great deal of attention has been focused on ceramic processing with the aim of reducing processing time and enhancing product qualities. Many ceramics such as MgO are good microwave receptors, whilst others such as Al_2O_3 are poor up to a critical temperature. Above this temperature, dielectric loss increases and the material couples with microwave irradiation. This often causes difficulties, as heating to the critical temperature can be slow. For this reason poor receptors are often doped with materials such as zirconia.

In non-uniform electromagnetic fields the local temperature can vary within the material and so create 'hot-spots'. These sites will reach their critical temperature before the

remainder of the material and so will heat even more rapidly. This can lead to localized thermal runaway causing stresses and possible fracture.

A large amount of work has been performed on ceramics in the area of sintering.[19,23,26,27,31] The high pressure compression of powdered ceramics, followed by sintering together of particles can produce materials of desirable porosity, increased mechanical properties, finer and/or more uniform grain size, combined with improved uniformity of ceramic microstructure.

Work described in this thesis has utilised microwave heating as a tool for the exchange of Na^+ into Wyoming Bentonite clays to produce mono-ionic species for use in subsequent exchange reactions with other cations, in an aqueous environment. The use of microwave heating in ion exchange experiments can lead to significant timesavings whilst also being of greater convenience. *Monsef-Mirazi et al*[32] report successful exchange of quaternary ammonium salts into smectite clay in five minutes by use of microwave irradiation. *Bond et al*[33]also demonstrate the complete exchange of Lithium cations with Laponite RD (sodium form) in five minutes in the microwave oven. By contrast a minimum of one week was required for conventional preparations reported by *Posner and Quirk.*[34]

Microwave irradiation has also been used for the formation of layered double hydroxides and subsequent ion exchange reactions.[32] Anion exchange of both nitrate and carbonate into preformed layered double hydroxides has been achieved *via* microwave irradiation in under ten minutes. A very recent report concerns the formation of layered double hydroxides using microwave heating[35] *Kannan and Jasra*[18] report the formation of well-ordered and crystalline materials in under 12 minutes, compared to typical digestion times of twenty-five hours. An investigation into the formation of layered double hydroxides by use of microwave irradiation is included in this thesis.

---

[32] Monsef-Mirazi, P., Kavanagh,D.M., Bodman, S., Lange, S, and McWhinnie, W.R., *Journal of Microwave Power and Electromagnetic Energy,* **1999**, 34, 216 – 220.
[33] Bond,S.P., Gelder, A., Homer, J., McWhinnie, W.R. and Perry, M.C., *Journal of Materials Chemistry,* **1991**, 1, 327 – 330.
[34] Posner, A.N. and Quirk, J.P., *Proceedings of the Royal Society of London Seris A,* **1964**, 278, 35 – 56.

Closely linked to this work is the pyrolysis of clay minerals so as to determine their organic content. Early work began with the use of zeolites and other catalyst beds[19] under pyrolysis conditions as close to conventional methods is possible. Here pyrolysis has been used to determine the organic content of clay bodies used in the production of ceramic materials.

In summary it can be concluded that microwave irradiation is a suitable technique for the preparation and subsequent exchange of both cationic and anionic species into clay minerals, in particular the smectite family of clays. This technique offers significant savings in time, greater convenience and enhanced material properties.[36]

---

[35] Zapata, B., Bosch, P., Fetter. G., Valenzuela, M.A., Navarette, J. and Lara, V.H., *International Journal of InorganicMaterials,* **2001,** 3, 23 –29.

CHAPTER TWO

2.0 MATERIALS AND METHODS

2.1 CHEMICALS AND PHYSICAL TECHNIQUES.

2.1.1 STARTING MATERIALS AND CHEMICALS.

Ceramic raw materials, obtained as individual clays and mixed clay bodies were received from Whichford Potteries, Warwickshire. These were used as received and pre-treated to form mono-ionic species, using an aqueous sodium chloride solution. Freeze-thaw ceramic tiles, received from Whichford Potteries were used as obtained and had been subjected to varying amounts of freeze-thaw treatment.

Standards for gas analysis of Whichford clays were obtained from Speciality Gases Limited, Birmingham and used as received.

Wyoming Bentonite clay was received from AKZO Nobel and was pre-treated with an aqueous sodium chloride solution to form a mono-ionic species used in subsequent exchange reactions.

Chinese clays were obtained from potteries in the regions of Yixing, Wuxi and Jingdezhen in South China and were used as obtained.

All other chemicals were received from Aldrich and were used as received unless otherwise stated in methodology.

2.1.2 SCANNING ELECTRON MICROSCOPY.

Freeze/thaw ceramic tiles were examined with a Cambridge S90 scanning electron microscope (SEM). Sections of tile millimetres in diameter are mounted in araldite and polished to a high surface smoothness. Prior to analysis the samples were carbon coated to prevent electron repulsion inside the chamber and silver tracked to produce a conductive line between the sample and the instrument.

Sections were observed at various resolutions from 1mm to 50μm for the whole of the portion. It is important to appreciate that the area observed is only a small section of a larger tile and therefore may not provide a representative view.

2.1.3 MERCURY INTRUSION POROSIMETRY.

Mercury Intrusion Porosimetry has long been used as an experimental technique for the characterisation of pore and void structure. The data provide information on pore size distributions that are directly affected by pore shape.

The methodology involves mercury being forced into the pores of a sample which has previously been broken into segments of a few millimetres in dimension. The mercury is forced by means of applied pressure and a change in electrical capacitance indicates the amount of mercury used. Multiplying by a calibration factor converts capacitance to volume and the statistical data produced can be represented graphically to allow easier interpretation.

Samples were analysed on a Micrometrics Pore Sizer 9310.

2.1.4 NITROGEN SORPTION TECHNIQUES

Adsorption of gas occurs when gas molecules impinging on a surface remain for the time on the surface. If a graph of amount adsorbed (V) is plotted against adsorption pressure (P) or relative pressure (P/Po) then an adsorption isotherm is obtained. The shapes of isotherms obtained are dependant upon pore structure. The majority of isotherms can be grouped into five types.

2.1.4.1 CLASSIFICATIONS OF ISOTHERM TYPE.

- Key to graph notations.

- P/P_o = Relative pressure
- P_o = Saturated vapour pressure
- n_a = Amount of gas adsorbed
- n_m = Monolayer capacity

TYPE I THE LANGMUIR ISOTHERM

Relates to microporous solids.

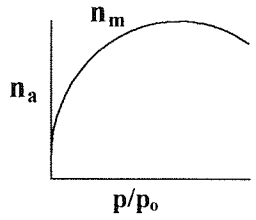

Micropores are considered to be < 20Å.

Type I isotherms are reversible and the rate of adsorption as a function of relative pressure is initially high. An interaction potential exists between the solid and adsorbable gas. The width of a micropore is only a few molecular diameters therefore there is an enhanced interaction between the adsorbable gas and the solid. It is generally accepted that the shape of the isotherm is characteristic of micropore filling.

TYPE II

Relates to Non-porous or macroporous solids (significant interaction between gas and surface).

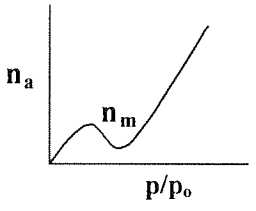

Macropores are considered to be < 500Å.

The initial uptake of gas is high as the most 'active' sites become filled. The 'knee' corresponds with the formation of a monolayer. The more pronounced this knee becomes the higher the interaction between the adsorbate and adsorbent.

TYPE III

Non porous or macroporous solids (little interaction between gas and surface).

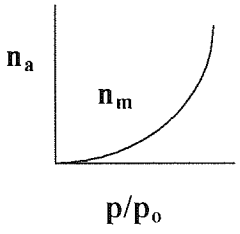

A low initial rate of adsorption due to the affinity between adsorbate and adsorbent being weaker than the affinity between the adsorbate molecules. The rate of adsorption as a function of relative pressure increases as more gas is adsorbed.

TYPE IV

Mesoporous solids (significant interaction between gas and surface).

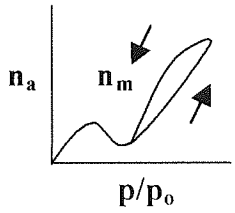

20Å < Mesopores < 500Å.

The characteristic feature of a type IV isotherm is the hysteresis loop. The desorption branch follows a different path to the adsorption path. The hysteresis is attributed to capillary cracks from which the adsorbate molecules do not desorb as rapidly as they adsorb due to a lowering of vapour over the concave meniscus formed by the condensed liquid in the pores.

TYPE V

Mesoporous solids (little interaction between gas and solid).

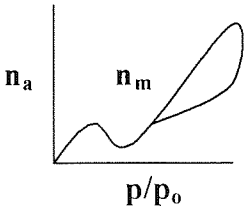

Exhibits the same characteristics as type IV isotherm except there is low interaction between surface and gas.

Samples of a few millimetres in dimension were analysed on a Quantachrome Autosorb Automated Gas Sorption system and the corresponding isotherms for each sample were produced. It is assumed that any microcracks will behave in the same manner as pores and therefore differences should be observable.

These measurements were performed at Imperial College, London.

2.1.5 ULTRASONIC TECHNIQUES.

Ultrasonic phenonoma are observed by passing a wave through a sample and noting the time (μsec) it takes for the wave to travel across the sample. Providing the width of the sample is known (mm), it is possible to convert this time into velocity (mmμsec). It is assumed that any deformities in the sample as a result of frost action will act to hinder the passage of the wave through the sample therefore take longer and have a slower velocity.

This technique does not require a specific sample size providing that the whole of the transducer is covered by sample. Sets of six samples were tested on Pundit Ultrasonic apparatus and time was converted to velocity by use of $V = d/t$.

2.1.6 THREE POINT FLEXURAL TESTING.

Samples of approximately 90mm x 30mm in dimension were tested on a Hounsfield load cell 2500N machine, for flexural strength. The instrumentation acts by applying a force to the centre of the ceramic sample that is supported at either end by two small prongs.

2.1.7 THIN SECTION.

Thin slices of tile are removed from a larger sample and mounted on a microscope slide. The sample is then impregnated with dye that highlights all pores and voids within the sample. This allows observation of any microcracks or deformations occurring as a result of frost action. The identification of mineral inclusion can assist in determination of chemical composition

Work was performed using Logitech systems LP50 within the Department of Earth Sciences, Birmingham University.

2.1.8 X-RAY PHOTOELECTRON SPECTROSCOPY (XPS).

XPS provides a broad spectrum analysis of the surface composition of the clays. In XPS the sample is irradiated with X-rays which produce photo electrons from core levels in atoms near to the surface. Measurement of the binding energies associated with these electrons allows the identification of elements present in the near surface region, hence providing an indication of chemical composition.

X-ray photoelectron spectra were recorded with a Fison VG Escalab 200D spectrometer using a MgK - α source and a 20 eV analyser using 5 scans on samples, of approximately 0.5cm^2 dimension.

2.1.9 X-RAY POWDER DIFFRACTION (XRD).

XRD reveals the interlayer distance (basal spacing) of the potters' clay in question. X-ray powder patterns provide a 'fingerprint' that may used, by reference to literature, for the identification of clay minerals.

The X-radiation most commonly used is that of copper. When the incident beam strikes a powder sample diffraction occurs in every possible orientation of 2θ, routinely this is over a range of 5 to 70 degrees. The diffracted beam is detected by means of a moveable detector such as a Geiger counter, which is connected to a chart recorder.

XRD was performed on a number of samples on a Phillips PW1710 based diffractometer using a Cu tube anode, monochromator and step type scanning. Data collection was carried out at the Department of Earth Sciences, Keele University.

2.1.10 THERMAL GRAVIMETRIC ANALYSIS (TGA) AND DIFFERENTIAL THERMAL ANALYSIS (DTA).

Both TGA and DTA were used to give an indication of the thermal stability of a material in addition to providing information relating to structural changes that occur during heating.

Both TGA and DTA were performed simultaneously on an PL Thermal Sciences STA 1500 analyser using approximately 45mg of finely ground sample under air, heated to 1000°C at a rate of 20°C/min, with data sampling at 0.5 s intervals.

2.1.11 X-RAY FLUORESENCE (XRF)

Elemental analysis of the clay samples under investigation was carried out *via* XRF by fusion of dry powdered specimens. XRF provides analysis of the bulk of the material unlike XPS, which only examines the surface. Both the major elements and a number of the trace elements can be rapidly and routinely analysed by XRF.

The principles of XRF involve re-excitation elements present in the sample to produce their own characteristic radiation. This emitted fluorescence radiation is dispersed by diffraction on suitable crystals so that the characteristic lines of elements can be recorded by use of a scintillation or gas flow detector.

Data was collected within the Department of Earth Sciences, Keele University.

2.1.12 ^{57}Fe MÖSSBAUER SPECTROSCOPY.

Mössbauer Spectroscopy is one of the best techniques for determining the oxidation state of iron within a sample, and its local environment.

Mössbauer Spectroscopy involves measuring the resonant gamma rays emitted when an atom in its excited state decays back to its ground state. In order to determine ^{57}Fe a ^{57}Co source is used; this absorbs an electron to produce ^{57}Fe in its excited state, which will decay back to its ground state emitting gamma rays. It is necessary to modify the

gamma rays prior to plotting gamma ray counts against velocity and a spectrum being produced, a calibration spectrum is therefore run before collection of the sample spectrum.

Data collection was carried out on a microprocessor controlled spectrometer in the Department of Chemistry at The Open University, Milton Keynes.

2.1.13 USE OF MICROWAVE IRRADITATION.

Microwave irradiation was used as a means of enhancing reaction rate and was carried out using a CEM MDS 81 microwave oven and Teflon reaction vessels. Microwave power and irradiation time are program controlled and all Teflon vessels have inbuilt pressure seals that will split to release pressure in the case of excess build up.

Pressures and temperatures did not exceed 200 psi and 200°C.

2.1.14 GAS CHROMATAOGRAPHY.

The technique was used to analyse the gaseous emissions from microwave pyrolysis.of Whichford clay bodies. The gases collected were measured against standard samples of known composition using helium as a carrier gas. Performed on a Sigma 2B GC Perkin-Elmer GC.

2.1.15 MAGNETIC SUSCEPTIBILITY.

The technique was used to distinguish between diamagnetic and paramagnetic species by measuring weight changes of a sample in a magnetic field. When placed in a magnetic field diamagnetic species are repelled, however, paramagnetic species are attracted. Results are presented as mass susceptibility (χ_g), which is converted to molar susceptibility (χ_m) when multiplied by relative molecular mass.

The data were recorded using a Sherwood Scientific, Magnetic Susceptibility Balance.

2.1.16 NUCLEAR MAGNETIC RESONANCE SPECTROSCOPY.

NMR will provide information regarding the environment of NMR active nuclei.

All MAS NMR spectra were recorded with a Bruker AC-300 instrument. All samples used solid state techniques of magic angle spinning and the same contact time was used for all samples although the number of scans varied

Table 2 : Data relating to nuclei examined

NUCLEI	NATURAL ABUNDANCE	SPIN	OBSERVATION FREQUENCIES	STANDARD
^{27}Al	100%	5/2	78.2MHz	aluminium sulphate(aq)
^{29}Si	4.7%	1/2	59.6MHz	tetra-methyl silane
^{19}F	100%	1/2	282.2MHz	Sodium fluoride (aq)
^{6}Li	7.5%	1	44.2MHz	Lithium chloride (aq)

2.1.16.1 CHARACTERIZATION OF ^{29}Si MAS NMR SPECTRA.

The ^{29}Si nucleus is probably the most characterized nucleus in clay chemistry. Being a spin I=½ nucleus spectral acquisition is relatively straightforward although its low abundance (4.7%) means that experiment time is often long. The application of magic angle spinning techniques means that linewidths can be significantly reduced except when large quantities of paramagnetic impurities are present as this causes loss of resolution due to large dipolar interactions and overall magnetic susceptibility of the sample.

The ^{29}Si chemical isomer shift is strongly affected by the chemical environment of the nucleus. For tetrahedral silicon there is a good correlation between the isomer shift, the degree of polymerisation and with the number of next nearest neighbour Al atoms (figure 11). As the shielding of the silicon nucleus is decreased due to decreasing polymerization the isomer shift becomes less negative with respect to TMS, and hence the number of next nearest neighbour Al atoms increases. It is noted that paramagnetic impurities within the samples examined herein, do not cause shifts in resonant peaks but will cause broadening and loss of resonance.

Figure 11 : Isomer shift ranges for ^{29}Si as a function of number of next nearest neighbour Al atoms.

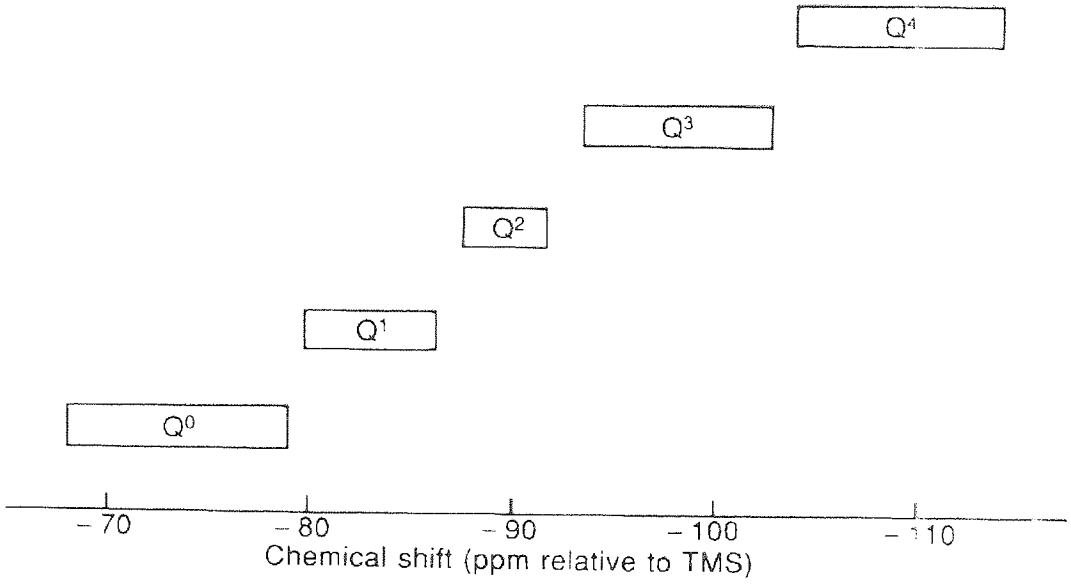

Isomer shift is also affected by bond angle of Si-O-T (where T = Al or Si). Often disorder of silicon in the plane can occur this results from slightly differing bond angles in the SiO_4 tetrahedra. These should result in a number of separate resonances, however due to isomer shifts being so close together and the nature of MAS NMR often broad resonances are observed.

2.1.16.2 CHARACTERIZATION OF ^{27}Al MAS NMR SPECTRA

The principles behind ^{27}Al MAS NMR spectroscopy in clay mineralogy allow us to distinguish between aluminium in an octahedral and tetrahedral environment. As shown in table 2, ^{27}Al is a quadrupolar nucleus with a spin I =5/2, the quadrupole interaction causes a large number of spinning side bands and often smearing of the resonant peak in to the spinning side bands. The application of magic angle spinning techniques causes a reduction in the quadrupolar contribution to the linewidth by approximately 80%, therefore distortions are still observed.

The positions of ^{27}Al resonances are strongly influenced by co-ordination number (as shown in figure 12) and it is therefore easy to distinguish between tetrahedrally and octahedrally bound Al.

Figure 12 : Relationship between chemical shift and co-ordination number for ^{27}Al.

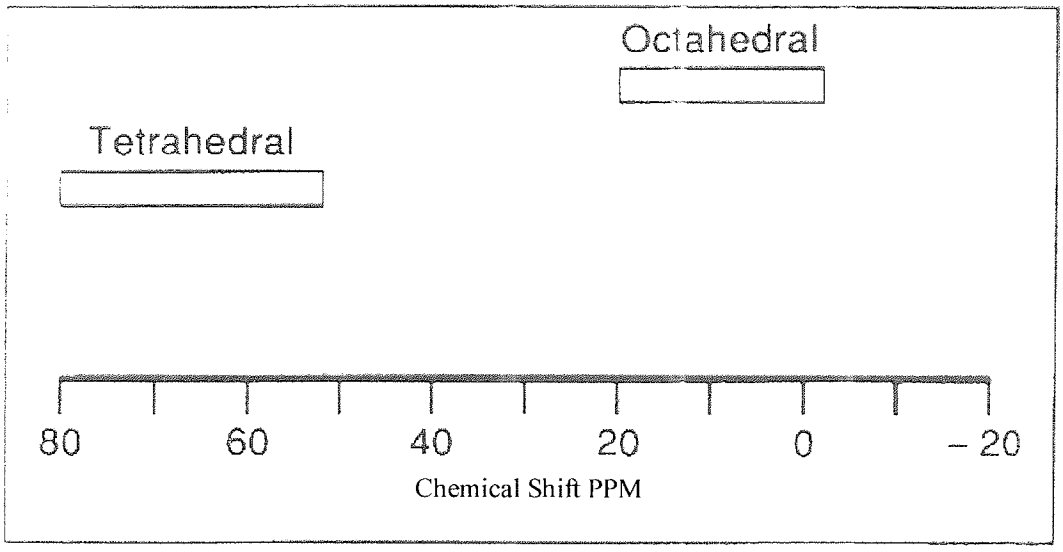

2.1.16.3 CHARACTERIZATION OF ^{19}F MAS NMR SPECTRA.

^{19}Fluorine is an ideal nucleus for nuclear magnetic resonance since its 100% natural abundance and spin ½ make it identical to the proton.

The identification of fluorine in solid-state systems using MAS NMR techniques is difficult. The resonance peaks obtained from such experiments are broad as a result of large gyromagnetic ratios that result in strong dipole-dipole couplings. The large chemical shift anisotropies of fluorine also mean that spectra often exhibit large spinning side bands resulting in loss of intensity of the resonant peak. Due to the proximity of ^{19}F and ^{1}H resonance frequencies the decoupling of highly protonated systems is also difficult.

Fortunately, clay systems have a relatively low abundance of free protons and therefore decoupling is not required. This combined with the high sensitivity of the nuclei means that adequate spectra of fluorine in solid state systems can be obtained.

Chemical shifts are measured relative to trichlorofluoromethane ($CFCl_3$) in order to allow the assignment of the peaks comparative to those quoted in the literature.

2.1.16.4 CHARACTERIZATION OF ^{6}Li MAS NMR SPECTRA.

Conventionally ^{7}Li is the nucleus examined in lithium MAS NMR, however the much lower quadrupole moment of ^{6}Li (-8×10^{-32} e m^2 and -4.5×10^{-30}, respectively) makes it a much better nucleus to examine.

The large quadrupole moment of the ^{7}Li nucleus (-4.5×10^{-30}) combined with its quadrupole nuclear spin of $^{3}/_{2}$ does make it a problematic nucleus as exhibited by noisy spectra that are difficult to interpret.

The spectra obtained can provide information regarding the environment and the symmetry of the nucleus being examined.

2.1.17 INFRA RED SPECTROSCOPY.

Infra red spectroscopy indicates the presence and nature of functional groups. Infra red spectra were recorded using a BIO-RAD Fts40A and were recorded over the range 4000 – 500cm^{-1} using KBr discs.

2.2 EXPERIMENTAL METHODS.

Whichford Potteries' clays are the raw material constituents of the clay bodies. They are a mix of a number of natural clay minerals and originate from a number of areas across the British Isles. Wyoming Bentonite is a naturally occurring clay composed of approximately 85% montmorillonite and has a cation exchange capacity of 70meq100g^{-1}.

The modification of Whichford raw clays has been carried out using sodium salts in an aqueous solution *via* both conventional and microwave methods. Additional modification of natural clay, Wyoming Bentonite; was performed using sodium, lithium, potassium and copper salts in aqueous solution *via* microwave methodology. Subsequent calcination of both Whichford clays and Wyoming Bentonite in air have been performed. Prior to modification the clays were pre-treated to remove impurities

by washing in distilled water and shaking overnight. The suspended clay solution was decanted off and dried overnight in an oven at 80°C.

Freeze-thaw treatment of tiles of dimensions 115mm x 120mm x 18mm was performed at Whichford Potteries, the process used was adapted from the German DIN52252 part 1 test for bricks. Samples were subjected to various numbers of freeze-thaw cycles; comparison to a control allowed the action of frost to be determined. Investigations was performed into redox processes occurring during firing used raw clay bodies supplied by Whichford Potteries.

2.2.1 PREPARATION OF FREEZE-THAW TILES.

The objective of producing these tiles was to determine the action of frost upon terracotta clay bodies. In order to allow reproducible testing, tiles were of uniform size and were a blend of two or more clays. Tiles were fired to normal temperature (~1000 – 1100°C) in a kiln before treatment. Each set consists of six tiles that had been subjected to varying numbers of freeze-thaw cycles.

The method used involved soaking a sample of known mass of fired clay in water. This was then weighed at regular intervals until a constant weight is obtained. It is assumed at this stage that complete adsorption has occurred. The samples were then subjected to freezing at –15°C in air and thawed naturally overnight by submerging in hot tap water. Samples are assessed for frost damage by comparison to a control.

2.2.2 REDOX INVESTIGATIONS OF WHICHFORD CLAYS.

Often ceramic materials when fired can exhibit a phenomenon known as 'black heart' caused by reductive processes occurring during the firing process. Black hearting is a problem experienced commonly in the ceramics industry. The objective has been to produce a firing process to lessen/eliminate the degree of black hearting that occurs in Whichford clays.

Discs of Whichford clay (current formulae and new formulae) of dimension 4.8cm x 4.8cm x 0.8cm were dried at room temperature for a week. This eliminates residual

water, avoiding fracturing during the initial heating. The dried discs were evenly stacked in a furnace and heat was applied in stages over a 27 hour time period. Upon cooling, the samples were examined for any signs of black heart, fracturing or size reduction as a result of the heating process.

2.2.3 TREATMENT OF WHICHFORD AND WYOMING BENTONITE CLAYS.

All raw clays were treated to remove impurities before use in further reactions. Raw clay (12g) was suspended in distilled water (350cm^3) and stirred overnight *via* mechanical methods. After stirring, impurities settle out and clay suspension is removed by decantation. Centrifugation separates clay and aqueous components. Any liquor is decanted off whilst the residual wet clay is dried overnight at 80°C. The resultant white material is ground for further use in exchange and calcination experiments.

2.2.4 CATION EXCHANGE *VIA* SHAKER METHODOLOGY.

Pre-treated Whichford clays (5g) were suspended in aqueous sodium chloride solution (150ml) and stirred for three days on a mechanical shaker. Subsequent filtration under vacuum followed by washing with deionised water resulted in a clay slurry. The resultant white slurry was dried overnight at 85°C and ground for further use. Exchange liquor was stored and tested titrametrically for the presence of Ca^{2+} ions.

2.3 MICROWAVE METHODOLOGY

2.3.1 EQUIPMENT.

All microwave irradiation was carried out using a CEM MDS 81 microwave oven; reactants were sealed in a Teflon vessel, whose operating limits are:

- Pressure 200 psi
- Temperature 200°C
- Sample Volume 50 mL

2.3.2 PREPARATION OF MONO-IONIC SODIUM WYOMING BENTONITE.

The use of microwave irradiation to enhance ion-exchange in clays has been studied extensively at Aston.[33]

Prior to microwave exchange Wyoming Bentonite is a mixed ion clay, intercalated with both Na^+ and Ca^{2+}. The objective is to produce a mono-ionic species for subsequent exchange with other ions.

When exchanging ions it is important to consider the cation exchange capacity of the clay, in order to ensure an excess of exchanging ions, allowing full exchange to occur. Wyoming Bentonite has a cation exchange capacity of $70meq100g^{-1}$ clay.

Pre-treated Wyoming Bentonite (0.5g) was suspended in an aqueous solution of sodium chloride (15 mL) in a tightly sealed Teflon vessel. Microwave energy, was applied at 100% power in 30 second increments such that the total irradiation time is 10 minutes. The reaction vessel is allowed to cool fully between each 30 second burst of energy so as to avoid excess pressure build up. The contents of the vessel are filtered under vacuum and washed with distilled water. The resultant white slurry was dried overnight at 85°C and ground for further use.

Mono-ionic Wyoming Bentonite was used in further exchange reactions using aqueous solutions of potassium chloride, lithium chloride and copper nitrate (15 mL). These yielded two white products and a green product respectively. All washings from copper exchange were colourless, showing that all copper had been taken up and that none was leached during washing.

Mono-ionic sodium Whichford clays were also produced using the microwave enhanced method outlined above.

2.3.3 MICROWAVE ENHANCED PYROLYSIS.

Pyrolysis of ceramic polymers has been detailed within literature reports.[27]

Microwave pyrolysis of clays (Whichford and Wyoming Bentonite) has been carried out to determine organic content. Reactions are performed in a silica microwave vessel that has been coated internally in metal oxide, an excellent microwave receptor.

Clay (3g) was transferred to a microwave vessel of known mass. A small microwave condenser, of known mass, was packed with dry ice and fitted to the microwave vessel. The equipment was transferred to a CEM MDS 81 microwave oven and purged with nitrogen. Microwave energy, was applied at 100% power for ten minutes. Nitrogen purging continued throughout the experiment. The reaction vessel was allowed to cool. Any organic constituents trapped within the condensor were removed by washing with organic solvents such as methanol and dichloromethane. The solvent was allowed to evaporate off in a fume hood, and residual tar was analysed for organic functional groups *via* infra-red and ^{13}C NMR.

2.3.4 GAS ANALYSIS *VIA* MICROWAVE ENHANCED PYROLYSIS.

This form of investigation was carried out to determine the type and quantity of gases emitted by Whichford clay blends and raw materials during the firing process. Gases were emitted during microwave pyrolysis of the clays and captured in a gas-bag. Analysis was *via* gas chromatography against known standards.

Clay (3g) was transferred to a silica microwave vessel; the condenser was packed with solid carbon dioxide. The vessels were transferred to a CEM MDS 81 microwave oven and the system was purged with nitrogen. Gases were emitted from the system to the gas-bag. Gas collection commenced one minute after starting pyrolysis. Excess nitrogen was diverted through a bubbler. The gas-bag was evacuated prior to collection thus expelling any oxygen. Microwave irradiation was applied at 100% power for 10 minutes.

Figure 13 : Diagrammatic representation of gas collection *via* microwave pyrolysis.

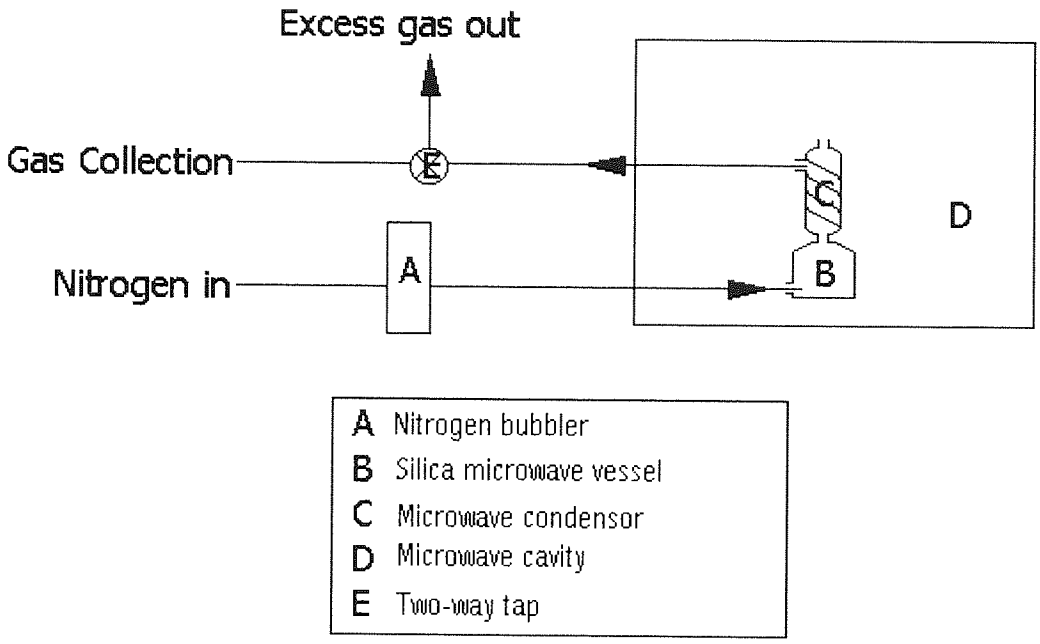

2.4 MICROWAVE FORMATION OF 2:1 TYPE LAYERED DOUBLE HYDROXIDES.

The formation of layered double hydroxides, *via* conventional methods, is well documented in the literature.[14,15,16] More recent reports have suggested the synthesis of layered double hydroxides *via* microwave irradiation.[17,18] Workers in the field have reported highly crystalline materials produced in significantly reduced reaction times.

The synthesis of layered double hydroxides using microwave irradiation, reported herein is based on work published by *Drezdon*[37], *Prévot* [17] and *Kannan* [18].

Terephthalic acid (8.4g) was added to 50% sodium hydroxide (35.9g) in deionized water (100 mL) and stirred. Magnesium nitrate (32.0g) and aluminium nitrate (23.4g) were added to deionized water (100 mL) and stirred. The resultant solutions were added together simultaneously and stirred for two minutes. A portion (50 mL) of the resultant white slurry was transferred to a 250 mL beaker. Microwave irradiation, was applied at 100% for a total of ten minutes in 2.5 minute increments. The resulting

[37] Drezdon, M.A., *Inorganic chemistry,* **1988,** 27, 4628 – 4632.

material was filtered and dried at 85°C overnight. The white product formed was ground for subsequent use in microwave enhanced exchange reactions.

A further reaction was carried out replacing aluminium nitrate by chromium (25.0g).

Subsequent microwave-enhanced ion exchange reactions were carried out using the magnesium/aluminium terephthalate layered double hydroxide (0.5g) with varying concentrations of aqueous sodium fluoride solutions (15 mL). The method was followed as described previously. The extent of exchange was examined *via* ^{19}F MAS NMR spectroscopy.

2.4.1 BENCH TOP PREPARATION OF LAYERED DOUBLE HYDROXIDES.

A one litre four necked round bottomed flask equipped with a reflux condenser, mechanical stirrer, thermometer, subaseal and nitrogen flow was charged with terephthalic acid (26.62g, 016mol) and deionised water (320mL) and stirred. A 50% NaOH solution was then added, slowly, by cannula from a 250mL round bottomed flask into the reaction vessel. Upon complete addition of the NaOH the reaction mixture is allowed to stir and cool back to room temperature.

A separately prepared solution containing $Mg(NO_3)_2.6H_2O$ (82.02g, 0.32mol) and $Al(NO_3)_3.9H_2O$ (60.0g, 0.16mol) and deionised water (256mL) was added dropwise *via* cannulation over a 90 minute time period to the stirring reaction mixture.

Once addition was complete the resultant mixture was heated to 73°C and digested whilst being left to stir overnight for 18hours. Upon cooling, the product, a white slurry, was filtered by vacuum and repeatedly washed with fresh deionised water. The product, now a thick white slurry, was dried at 120°C under vacuum to yield a chalky white clay like material.

2.5 CALCINATION REACTIONS.

Calcination reactions were performed on all clay samples to track the changes that occur during the firing process. The effect of interlayer cation on the appearance of five co-

ordinate aluminium and Q_0 silicate during the firing process, was examined by ^{27}Al and ^{29}Si MAS NMR.

Clays (Whichford and Wyoming Bentonite) were subjected to heating over the range 500°C – 1000°C. At each stage the temperature was held for one hour before the sample was removed. Analysis was primarily by MAS NMR and infra-red spectroscopy.

CHAPTER THREE

3.0 THE ACTION OF FROST UPON CERAMIC BODIES.

3.1 FREEZE-THAW TILE CHARACTERISATION.

Initially, freeze-thaw treated tiles were examined using elemental analysis (EDAX) techniques. This was used as a means of identifying mineral inclusions within the clay samples. Progression in this area led to the application of Scanning Electron Microscopy (SEM) in an attempt to identify any cracks or deformations resulting from frost action.

An important part of SEM sample preparation relies on the grinding of ceramic samples to a high surface smoothness. Recent reports[38] have shown how different types of cracks may be produced as a result of the grinding process. The determination of these is therefore important when examining for frost attack.

Further information regarding the effect of freeze-thaw treatment upon the clay tiles was gained by the utilisation of a number of analytical techniques, including Mercury Intrusion Porosimetry (MIP), Gas (N_2) Sorption techniques, Ultrasonic analysis, Three Point Flexural Testing and LECO analysis. The results from these tests are discussed later in detail.

A selection of samples provided by Whichford Potteries were examined.

Table 3 : Samples chosen for SEM analysis.

TILE IDENIFICATION	FREEZE-THAW CYCLES.
Whichford Original	106
Stoke Red	35
T2C.7	75

For each experimental tile there was a corresponding control tile that had not been exposed to freeze-thaw treatment. Experimental tiles were produced at Whichford Potteries and not all freeze-thaw tiles were subjected to identical numbers of freeze-

[38] Maksoud, T.M.A., Mokbel, A.A. and Morgan, J.E., *Journal of Materials Processing Technology*

thaw cycles. These tiles were chosen since Whichford Original is the potteries standard formulation, Stoke Red was a formulation currently under investigation and T2C.7/8 (T2C.8 is the control to T2C.7) is thought to be a fragile fired ceramic sample.

3.1.1 ANALYSIS OF WHICHFORD ORIGINAL 106 CYCLES AND CONTROL.

The investigations upon Whichford clay bodies began with determination of elemental composition of the clays *via* SEM and elemental analysis techniques (EDAX). Primarily the objective was to identify and quantify inclusions of iron oxides within the samples; in addition to this a brief overview of total elemental composition of each Whichford sample was gained. Iron being a paramagnetic species causes adverse effects in MAS NMR spectroscopy, a technique of major importance in later work. Large quantities of iron will render MAS NMR spectra almost indecipherable, due to the broadening of resonant peaks and the appearance of large spinning side bands.

The images provided by elemental analysis of samples identified large inclusions of iron shown as white particles (figure 14). Due to each photograph only providing a partial view of the whole sample it is not possible to quantify the amount of iron present. It can, however, be concluded that for each sample iron appears in significant quantities.

Figure 14 : Inclusion of iron within the clay matrix, shown as a white particle.

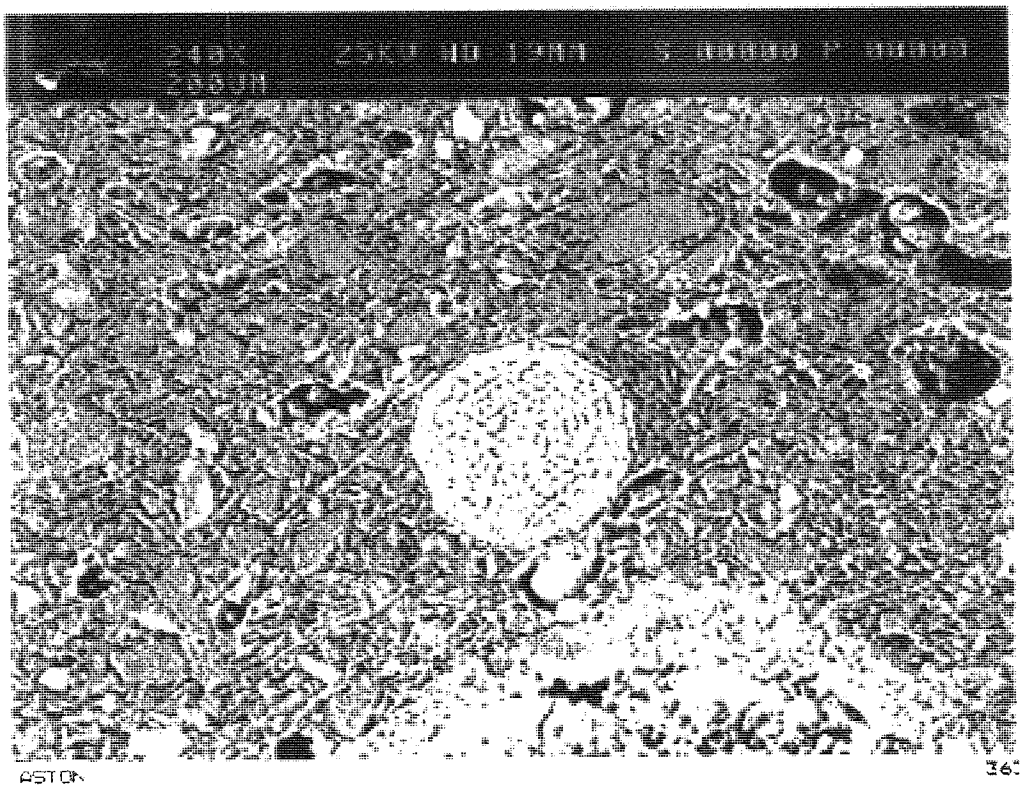

In addition to iron, silica was easily identified as dark particles in the matrix, as shown in figure 15.

Figure 15 : Inclusion of silica within the clay matrix, shown as a dark particle.

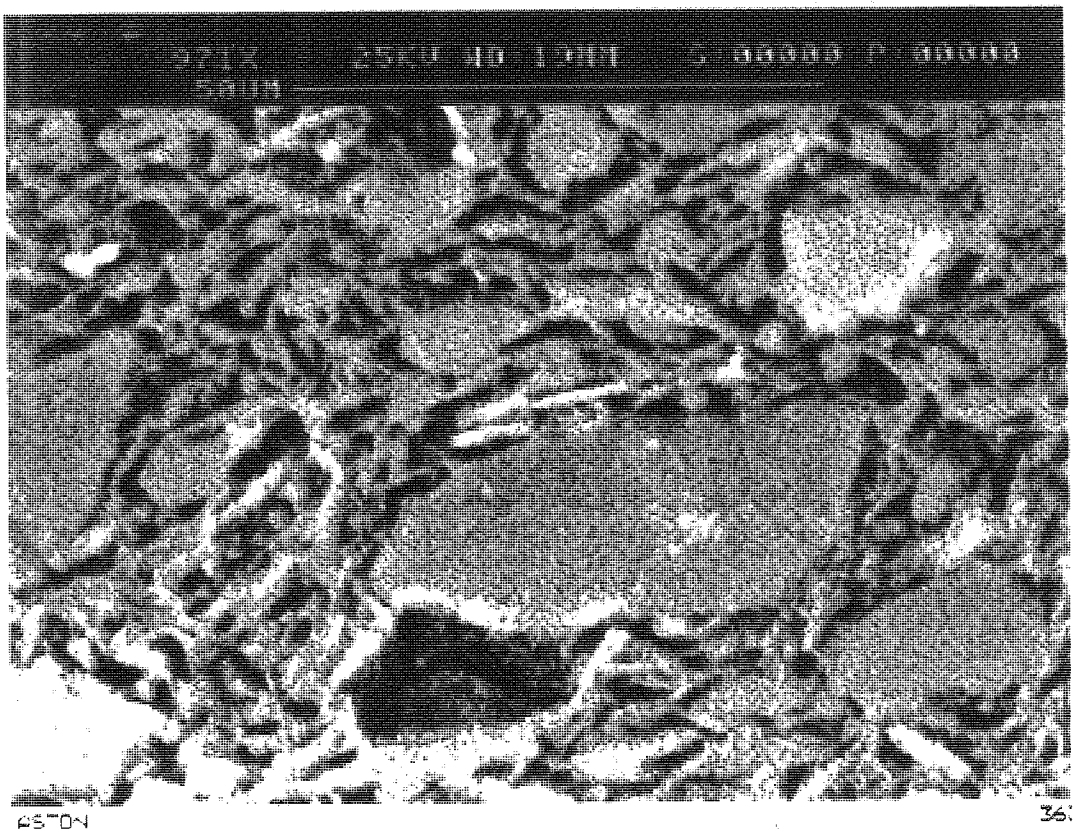

Oxygen, calcium and aluminium were also identified in large amounts with the appearance of calcium suggesting the appearance of an important smectite type mineral.

The work using SEM progressed onto attempting to assess the effect that the freeze-thaw treatment had upon the Whichford clay bodies. Initial work in this area used gold sputter coating of samples to induce conductivity within samples. The results were inconclusive and the images lacked clarity with problems stemming from uneven surfaces and high porosity of the sample. It was therefore decided that an alternative method of sample preparation would be required in order to allow SEM to be a suitable technique. Further work therefore used samples mounted in araldite, ground by a diamond wheel to produce a flat surface and thus analysed *via* SEM. It is the images captured from samples obtained by this preparation method that will be discussed here.

The sections of Whichford original experimental and control tiles studied by SEM were representative of the tile as a whole. These were examined at varying magnifications. Examples of the images captured of Whichford original control and experimental tiles

are shown in figures 16 and 17. All sample structures were clearly discernible at x132 magnification, showing well-defined inclusions of iron and silica. Pores appeared as abundant black spots of varying size.

Figure 16 : SEM image of Whichford Original control tile.

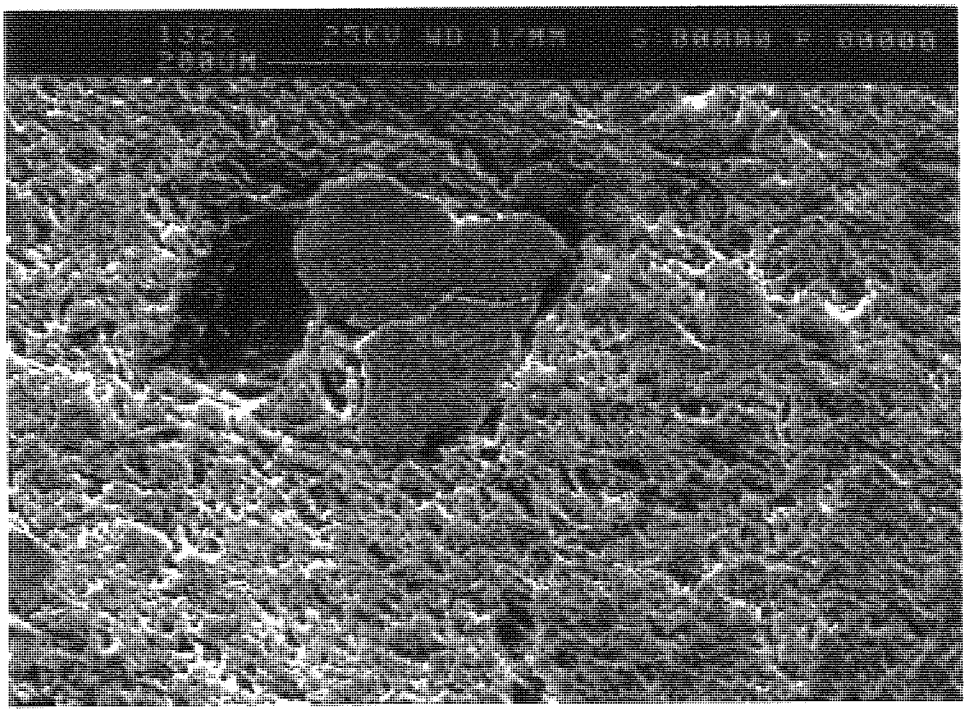

Figure 17 : SEM image of Whichford Original experimental tile 106 cycles.

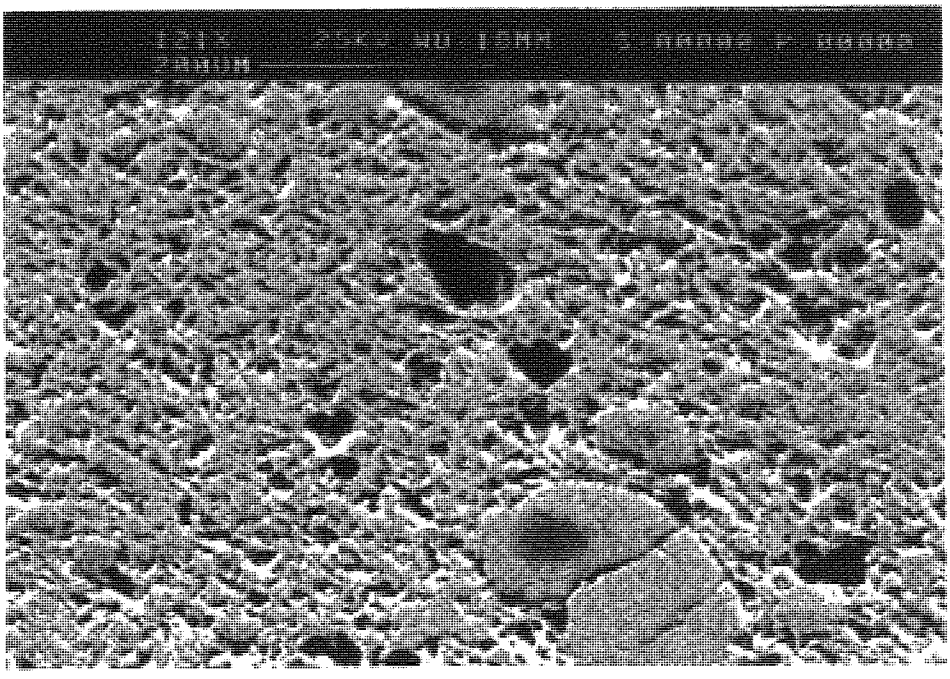

The close scrutiny of the SEM images of Whichford original control and experimental tiles (figures 16 and 17) highlighted very small differences in surface morphology. They showed a number of inclusions of silica and iron some of which appeared to show small surface cracks. It is concluded that because this phenomenon was observed in both experimental and control tiles the surface cracks cannot be solely attributed to the action of frost upon the clay body. Cracks can be attributed to the grinding process used in sample preparation.

The images captured do not show any sign of the presence of cracks or deformations occurring as a result of the action of frost upon the Whichford original clay bodies

In summary, SEM suggests that the action of frost upon the Whichford original samples has been insignificant; it may be that deformations are too small to be identified *via* this technique. It is the author's opinion that if significant pore deformation or micro-cracking were occurring then it would be easily identified by this method. Literature reports of frost resistance in concrete unambiguously claim that micro-cracking can be observed *via* this same microscope methodology as shown in figure 18.[39]

[39] Ed. Setzer, M.J. and Auberg, R., *Frost Resistance of Concrete, Proceedings of the International Rilem Workshop 34,* Chapman and Hall, **1997.**

Figure : 18 Propagation of a microcrack throughout a calcareous aggregate, after freeze-thaw cycling.[38]

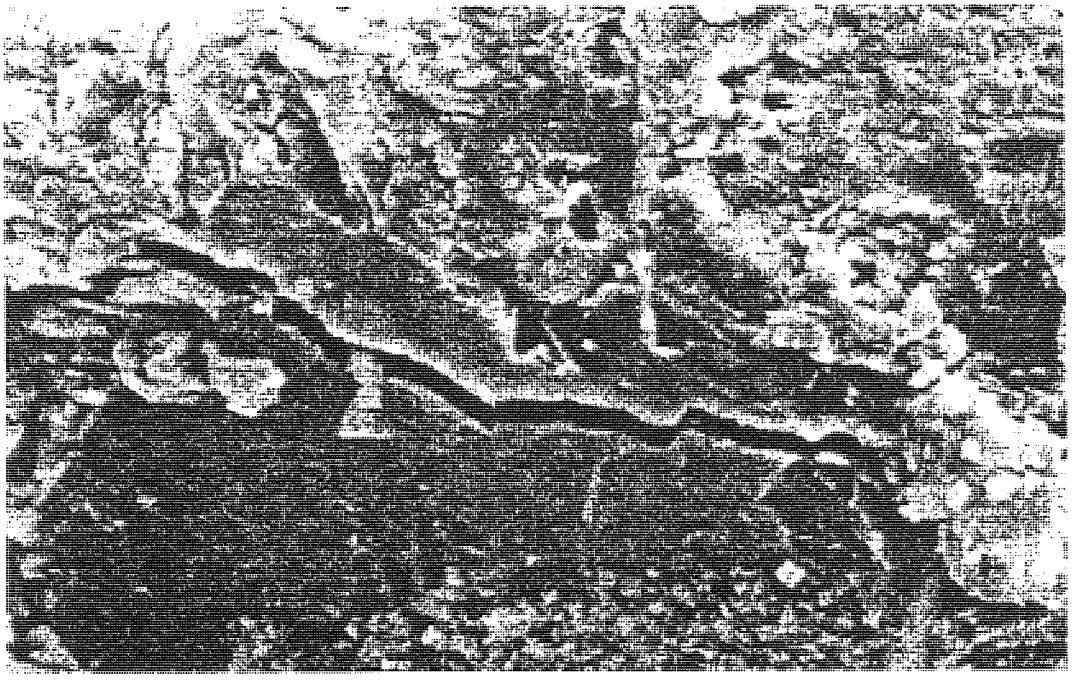

Further analysis of the Whichford original clay systems involved the utilisation of gas (nitrogen) sorption techniques. These were performed at Imperial College London by Dr N Coleman and are appropriate for pore sizes in the range 0.002μm – 0.4μm.

Gas sorption works on the principle that the amount of gas adsorbed by a sample depends upon the nature of the adsorbent and the pressure at which adsorption takes place. A mass increase of sample or a decrease of gas volume from the system can be used to determine the actual amount of gas adsorbed.

In general adsorption processes can be either chemical or physical depending upon the nature of the forces involved. In this work, only physical forces are considered as the adsorption processes involved allowed easy removal of the gas from the solid system. This is far more difficult to achieve for a chemical process.

Physisorption will occur when the gas comes into contact with the surface and does not rely on any chemical interactions. The resulting data gave rise to an adsorption isotherm, which is collected by measuring the amount of gas adsorped onto a surface at equilibrium as a function of relative pressure, P/P_o. Where P_o the saturated vapour

pressure, is plotted against n_a (the amount of gas adsorbed), the incline of the curve can be used to determine the specific surface of the solid. This is performed by deducing the monolayer capacity from the isotherm, n_m, defined by the amount of adsorbate required to cover the adsorbent with a monolayer of molecules. Usually a second layer is forming before the first one is complete but n_m is determined irrespective of this.

The shape of the isotherm will fit into one of five categories, dependent upon the nature of the adsorption process (see chapter two). The shape of the isotherm depends upon specific surface of the powder and pore structure. It is considered that if pore deformations or micro-cracks are present then they will act in the same manner as regular pores and adsorb gas.

The data presented in figures 19 and 20 for Whichford original control and experimental tiles exhibit non-typical type III isotherms. It is difficult to assign the isotherms exactly to a definite type as the shapes are not consistent with any reported within the literature.[40,41] It is also difficult therefore to explain fully the effects that appear to be occurring. However, the general shape of the curve suggests type III that usually arise when there is a low initial rate of adsorption due to the occurrence of very little interaction between the solid and the adsorpable gas. The rate of adsorption as a function of relative pressure increases, as more gas is adsorped, due to the interaction of previously adsorped gas with the adsorping gas being greater than between the adsorped gas and the exposed surface. This therefore suggests that the pores in the Whichford original samples are very small and that the gas may have difficulty penetrating them so resulting in attraction between the gaseous layers that form rather than the solid and the gas.

---

[40] Allen, T., *Particle size measurement, Volume 2, Fifth Edition,* Chapman and Hall, **1997.**
[41] Gregg, S. J., and Sing, K. S. W., *Adsorption surface area and porosity,* ACADEMIC PRESS London and New York, **1967.**

Figure : 19 Gas Sorption isotherm Whichford original control.

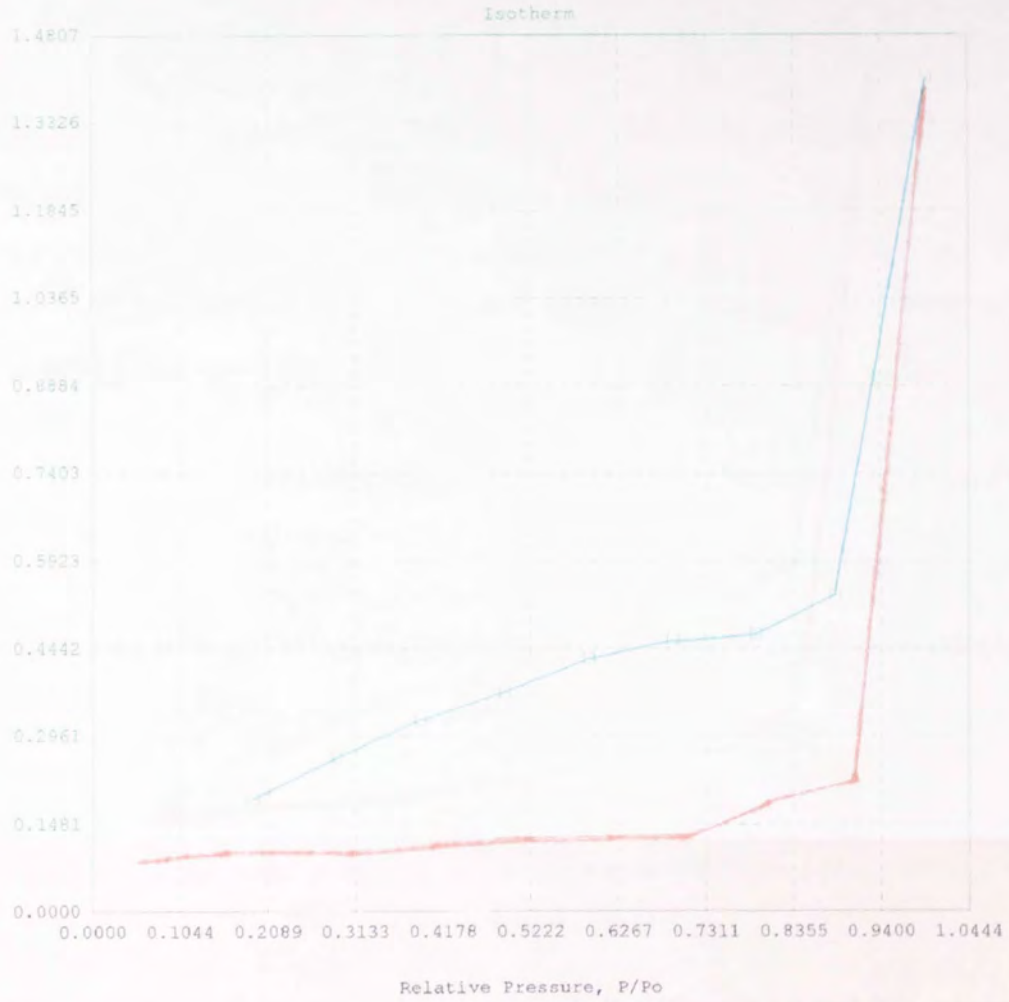

Red Line – Adsorption isotherm

Blue Line – Desorption isotherm

Figure 20 : Gas Sorption isotherm Whichford original experimental (106 cycles).

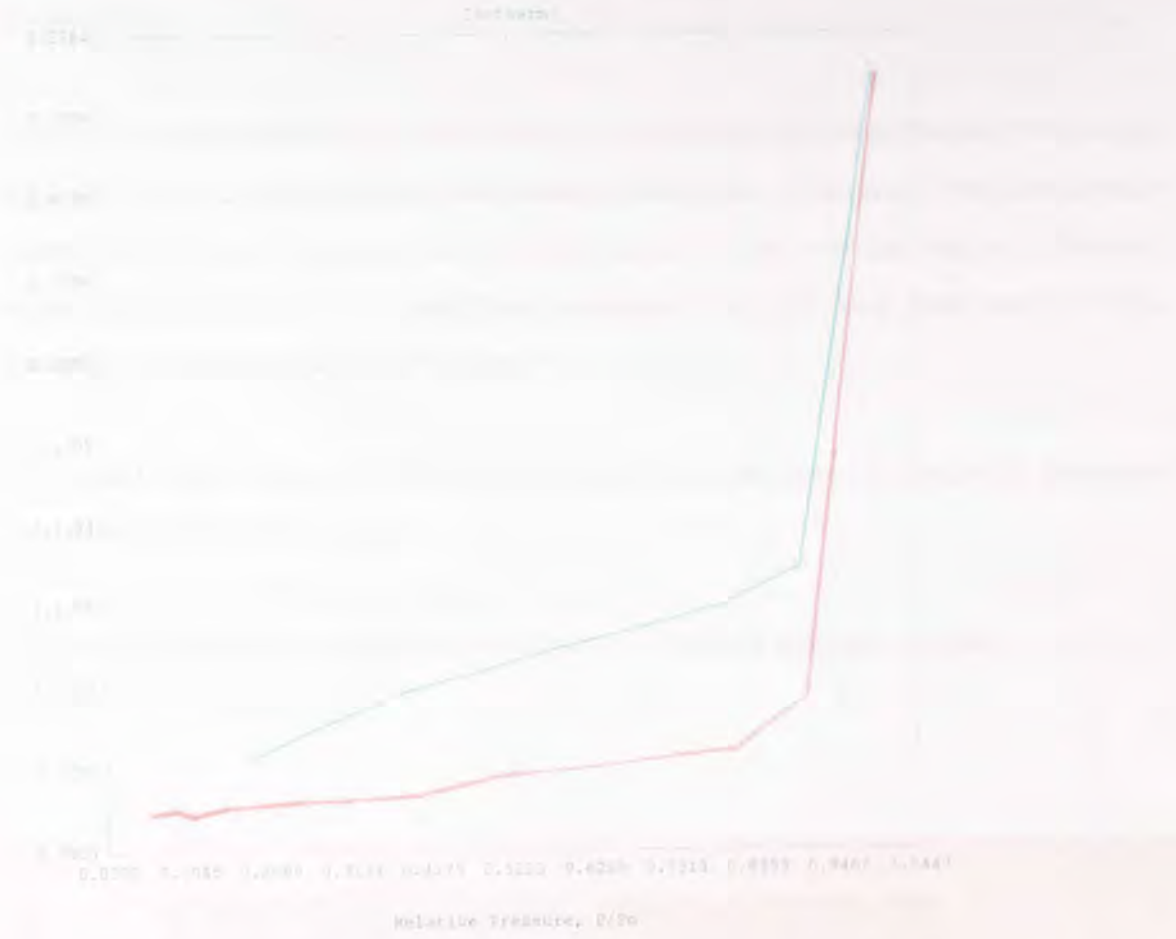

The data shown for the Whichford original tiles (figures 19 and 20), suggest very little difference between control and experimental samples. This suggests that the action of frost has been minimal. It was anticipated that any deformations, as a result of frost action, would act in a similar manner to pores and uptake gas. Therefore, an increased rate of adsorption should be observed for experimental samples. Reproduction of results did not yield any fresh data, providing further evidence to suggest there is little difference between Whichford original control and freeze-thaw samples. It may be that any deformations present as a result of freeze-thaw are too small to be identified *via* this method.

The data presented thus far on Whichford original control and experimental tiles has shown there to be very little difference between the samples. SEM has shown to be of limited use although elemental analysis did provide useful information. The gas sorption data previously shown conforms to SEM data to suggest frost action has been

minimal. The lack of consistency of gas sorption data with that shown in the literature has made interpretation very difficult and repetition of experiments did not provide fresh results.

Mercury intrusion porosimetry and nitrogen porosimetry are complementary techniques with the former covering a much wider range, 0.002μm – 1,000μm. Often considerable agreement is found between the two techniques in the overlap region. Mercury intrusion porosimetry is an analytical technique that has long been used for the investigation of pore and void structure.

The initial data obtained for Whichford Original tiles as shown in figure 21, presented an interesting set of data points.

Figure 21 : Mercury Intrusion Porosimetry for Whichford Original samples.

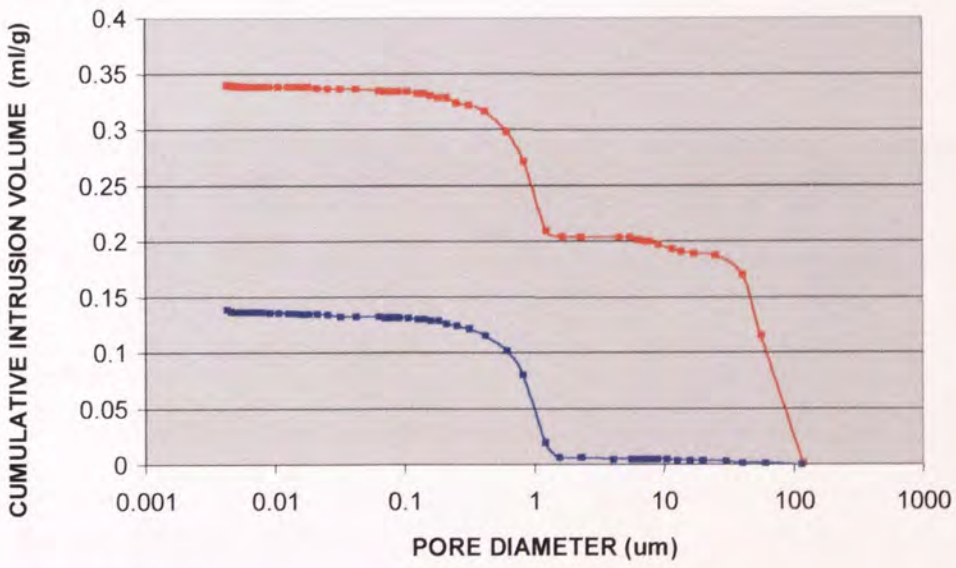

Red line Whichford Original experimental tile 106 cycles.

Blue line Whichford Original control.

The latter sections of both graphs shown in figure 21, are very similar, the steep incline at ~1μm shows that there is a predominance of pores in this region. The overall shape of the curve for Whichford original control tile is further indicative of a narrow pore

size distribution.[39] The data presented for Whichford original experimental tile was far more interesting in addition to the steep incline at ~1μm another is observed in the early part of the curve at ~100μm (figure 21 red line). This suggested the appearance of more pore like structures such as cracks that could appear as a result of the action of freeze thaw treatment. Cracks would appear from frost action due to there not being enough room for the water to expand into thus causing strain on the clay structure and hence cracking or pore deformations occur. Nevertheless it was expected that pores or cracks of this magnitude would be observable visually. No such damage was detected. This set of experiments was therefore repeated in an attempt to verify the results found.

The new data acquired did not fit in with those obtained previously. As shown in figure 22, the fresh results suggest there is very little difference between the control and experimental tiles. Both Whichford original control and experimental tiles are shown to have a narrow pore size distribution as dictated by the shape of the curve with the majority of the pores having a pore size of 1μm.

Figure 22 : Mercury Intrusion Porosimetry for Whichford Original samples. Run two.

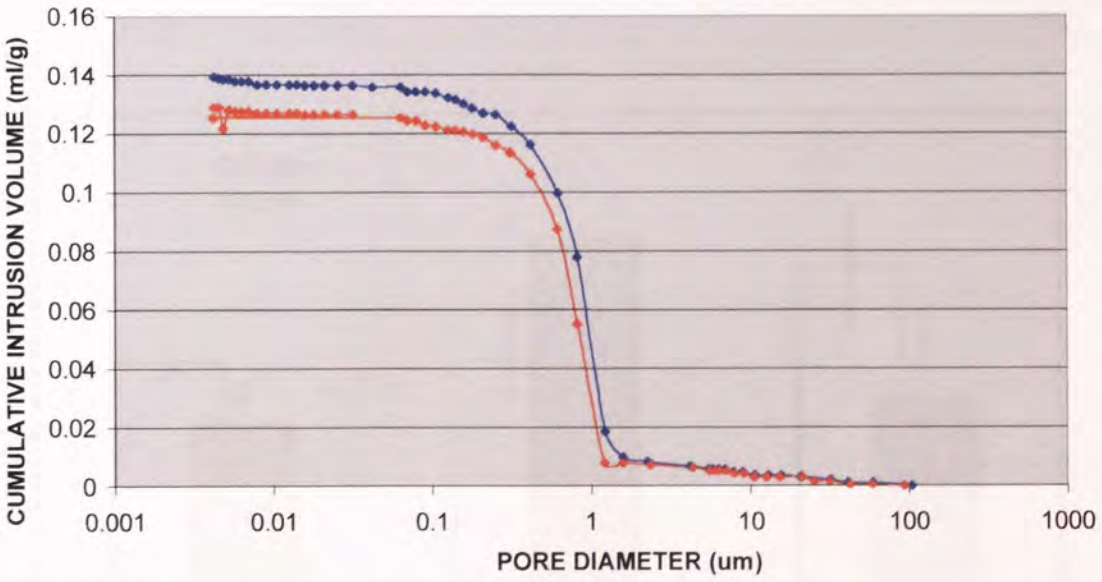

Blue line Whichford Original control.

Red line Whichford Original experimental tile 106 cycles.

It can be noted that there are small differences in cumulative intrusion volume between the two samples shown in figure 22, this would suggest that freeze-thaw treatment has had an effect upon the Whichford original samples, however these differences are of such a small amount it is unfair to say that they are significant. Up to this point it is fair to say that the action of frost upon the clay systems may have been shown to be minimal by MIP techniques.

The use of Three Point Flexural Testing to determine the effect of frost action upon Whichford clay bodies provided some very interesting and potentially important data. This is a technique that is most commonly used in Civil Engineering and involves applying a force to a sample and measuring its breaking strength. The relevance here is the assumption that any pores or deformations present as a result of frost action would act to weaken the material and hence lower its resistance to force.

Tiles of approximately 90mm x 30mm were tested in sets of six samples. Data obtained were analysed statistically to determine any significant differences. Figure 23 shows the data presented as histograms, with errors being equal to standard deviations.

Figure 23 : Data obtained from Three Point Flexural testing.

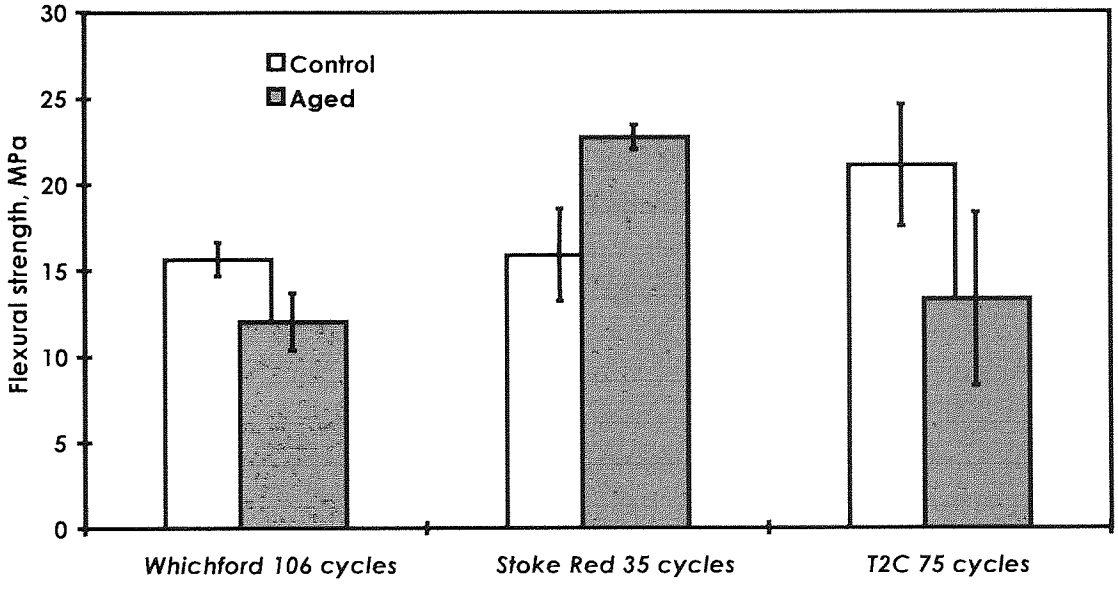

Superficially it appears that the action of freeze-thaw upon the Whichford original tiles has been detrimental thus weakening the material, as indicated by the lower flexural strength of the Whichford experimental tile when compared to the control tile. Further analysis of the data by the application of a statistical analysis of variants provides a different picture. The results obtained tell us that when tested to a 99% confidence limit the differences being observed for the Whichford original samples are not significant. This therefore means that the action of freeze-thaw upon the tiles has been very small and that in fact the two sets of data can be considered as coming from the same group.

In summary data has so far shown a minimal effect upon Whichford clay materials as a result of freeze-thaw treatment and hence frost action. The ease of use of Three Point Flexural testing along with the testing of results against statistical variants makes it an ideal technique for analysis of this type. Later work looks at the other tiles under analysis and it is here that Three Point Flexural testing produces some interesting results.

The use of ultrasonic analysis provided data consistent with that obtained from Three Point Flexural testing. Ultrasonic analysis worked on the principle that any deformations present as a result of frost action would act to hinder the passage of the wave through the sample, thus reducing its velocity. In this technique the sample width is measured in mm and the time the wave takes to travel through the sample is measured in μs, hence the velocity is given in units of $mm\mu s^{-1}$.

Samples were tested in sets of six and the results are presented as histograms as shown in figure 24.

Figure 24 : Results from Ultrasonic testing of freeze-thaw tiles.

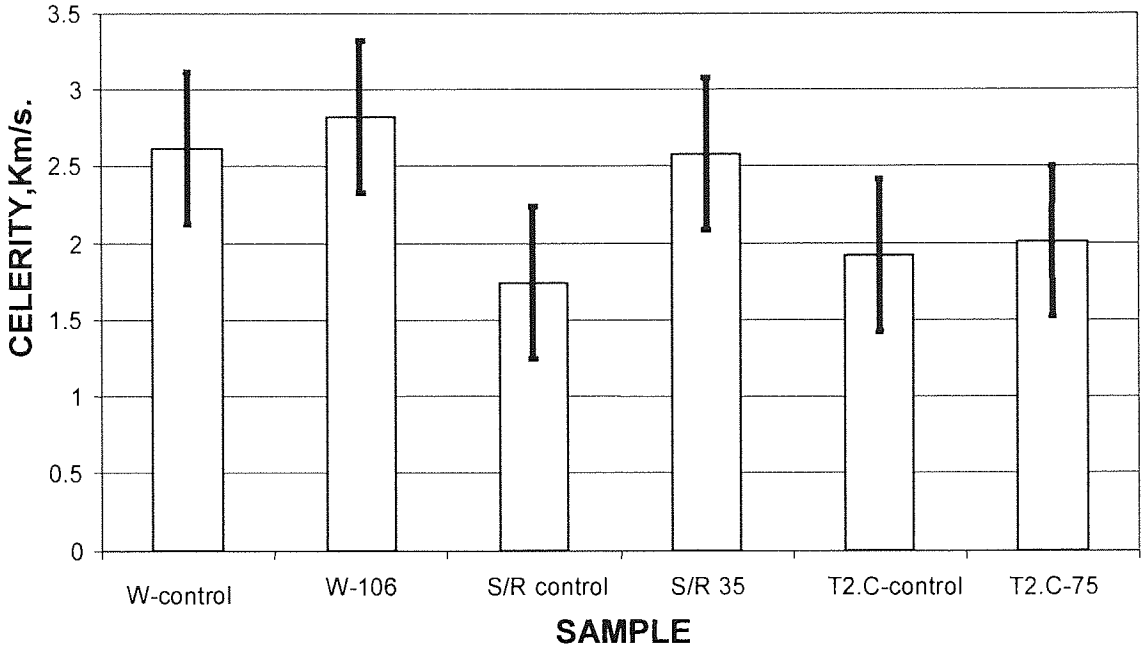

Again, visual interpretation of the graphical data suggests that the action of freeze-thaw has had very little effect upon the Whichford original samples and in fact it appears that Whichford original experimental tile is actually more compounded than its control counterpart as shown by the slightly increased velocity at which the wave travelled through the sample.

Further analysis of this data using a 95% confidence limit provides information that links in with Three Point Flexural testing. The data showed that the results obtained were not statistically significant and therefore the phenonomen that it seemed was being observed visually is not demonstrable. It can therefore be said that the two sets of data for Whichford original control come from the same group and the action of frost upon these tiles has been minimal.

Thus far it has been shown that the action of frost upon Whichford original samples has not been detrimental and that damage to the clay bodies may only have been minimal. The analysis of Whichford original clays *via* thin section showed the presence of mineral inclusions within the clay bodies that may play an important role in frost

resistance. It was also assumed that the presence of any cracks or deformations of significant size would be observed *via* this method.

The thin sections were prepared at Birmingham University by the Geological Sciences department. Analysis was performed at Aston University, within the Department of Civil Engineering using petrographic techniques.

The Whichford original samples examined showed varying amounts inclusions of bronze coloured minerals. These appeared bronze under both plane and polarised light and were thought to make up approximately 2% of the whole matrix. Analysis had already shown that next to silicon and aluminium, iron containing materials were the next most predominant species, it was therefore assumed due to the frequency of these bronze inclusions they were a type of iron complex. There are a number of possibilities for inclusions fitting this description, namely pyrite (FeS_2) or pyrrohotite ($Fe_{1-x}S$). There is the possibility of their being a mixture of the two, due to differing extents of oxidation during the firing process. LECO sulfur analysis will provide information regarding the amount of sulfur present. If this value is low then the inclusions are attributable to hematite or some other iron oxide derivative.

It was clearly observed when looking at the Whichford Original thin sections that the bronze inclusions observed correlated with many of them de-bonding, this appeared more prevalent around the larger bronze inclusions and where it had occurred the bronze inclusions had tended to fall apart. De-bonding was seen as the breaking away of the bronze inclusions from the matrix. It was therefore assumed that this could be related to the freeze thaw process.

The experimental sample appeared to exhibit far more strain than the control sample with the bronze inclusions appearing to be closer together.

LECO sulfur analysis was performed at ROTECH laboratories, West Midlands and was used to determine the amount of sulfur within the Whichford Original samples so the exact nature of the bronze inclusions could be determined. The percentage sulfur in each Whichford original sample is summarised in table 4.

Table 4 : Percentage sulfur in Whichford original freeze-thaw treated samples.

SAMPLE	% SULFUR
Whichford original control	0.19
Whichford original 106 cycles	0.10

The results shown in table 4 clearly show there is not enough sulfur present in the samples for the bronze inclusions to be an iron sulfide. It can therefore be concluded that the inclusions observed belong to the family of iron oxides probably hematite.

3.1.2 CONCLUSIONS ON THE FREEZE-THAW ANALYSIS OF WHICHFORD ORIGINAL SAMPLES.

The analysis performed on Whichford original control and experimental tiles (106 cycles) has shown overall that the action of frost appears to have been minimal.

SEM analysis was of limited use and the images captured (figures 16 & 17) did not show any differences between experimental and control tiles. The small surface cracks observed in elemental inclusions were thought to be as a result of the grinding process used in sample preparation. It is to be noted that samples are ground by hand and therefore although care is taken during preparation it is not possible to grind each sample to the same extent.

SEM elemental analysis was useful in identifying elemental inclusions of iron (figure 15) and silicon (figure 16) further analysis showed that in addition to aluminium these were the main three components of the clay.

It is clear at this stage that SEM is not a viable technique for the analysis of Whichford original samples.

The unexpected results from gas (N_2) sorption techniques made the analysis of data very difficult. The results presented in figures 19 and 20 did not correspond with literature data[39,40] therefore making interpretation of results complicated. The general shape of the isotherm suggested a type III interaction between the solid and the gas. This occurs

when there is a greater affinity between gas molecules than there is between the solid and adsorpable gas. This suggested that the pores in the Whichford original samples were very small and therefore the gas had difficulty penetrating them. The lack of apparent differences between control and experimental tiles suggested that the action of frost had been minimal. It can be concluded thus far that gas sorption did not provide any additional data bearing on the effect of freeze-thaw treatment upon the Whichford original tiles.

Mercury Intrusion Porosimetry of Whichford original samples initially produced some very interesting data (figure 21). It can be seen that the latter half of both graphs are very similar with an obvious predominance of pores in the ~1μm region. In addition to this data Whichford original experimental tile showed a large number of pores in the ~100μm region. This suggested the appearance of additional pore like structures possibly as cracks or pore deformations that would occur as a result of frost action.

Repetition of this set of experiments did not show the same phenomenon. Fresh data showed both Whichford original control and experimental samples to have a narrow pore size distribution, as indicated by the shape of the curve, with the majority of pores existing at ~1μm.

Small differences in cumulative intrusion volume may suggest a minimal effect resulting from frost action, however differences are so small it is unfair to say conclusively.

The use of Three Point Flexural testing to detect deformations present as a result of frost action relied on any cracks or deformations present acting to weaken the material hence having a lower breaking strength.

Figure 23 shows the data gained represented as a histogram this suggests that for Whichford Original samples the action of freeze-thaw has been detrimental, as shown by the lower flexural strength. The statistical analysis of variants upon this data to a 99% confidence limit showed the figures not to be statistically significant and that the action of freeze-thaw had been minimal. Further testing using Ultrasonic techniques

provided information that conformed with that obtained from Three Point Flexural testing, as shown in figure 24.

Thin section analysis demonstrated the presence of bronze coloured inclusions initially considered to belong to the family of iron sulfides. Analysis *via* LECO sulfur techniques showed the levels of sulfur in Whichford original clays to be very low, it was therefore determined that these inclusions belonged to the family of iron oxides, possibly hematite. It is assumed that these inclusions may be related to the freeze-thaw process as many were observed associated with de-bonding and where this had occurred there had been breakdown of the bronze inclusion. This was especially prevalent in Whichford original samples around larger particles. Whichford experimental sample appeared to show more strain than its control with the bronze inclusions being much closer together.

In summary, analysis of Whichford original control and experimental tiles by the techniques discussed has shown that the action of freeze-thaw has been minimal.

3.2 ANALYSIS OF STOKE RED CONTROL AND EXPERIMENTAL TILES.

The Stoke Red samples examined were Stoke Red control and Stoke Red experimental 35 cycles.

The results obtained from SEM elemental analysis confirmed the presence of iron and silica (figures 14 and 15) with oxygen, calcium and aluminium also being identified.

Figures 25 and 26 are examples of the images captured by SEM analysis of Stoke Red samples. The photographs provide a representative view of the whole sample and tiles were examined over the intensity range 100μm – 2mm

Figure 25 : SEM image of Stoke Red control tile.

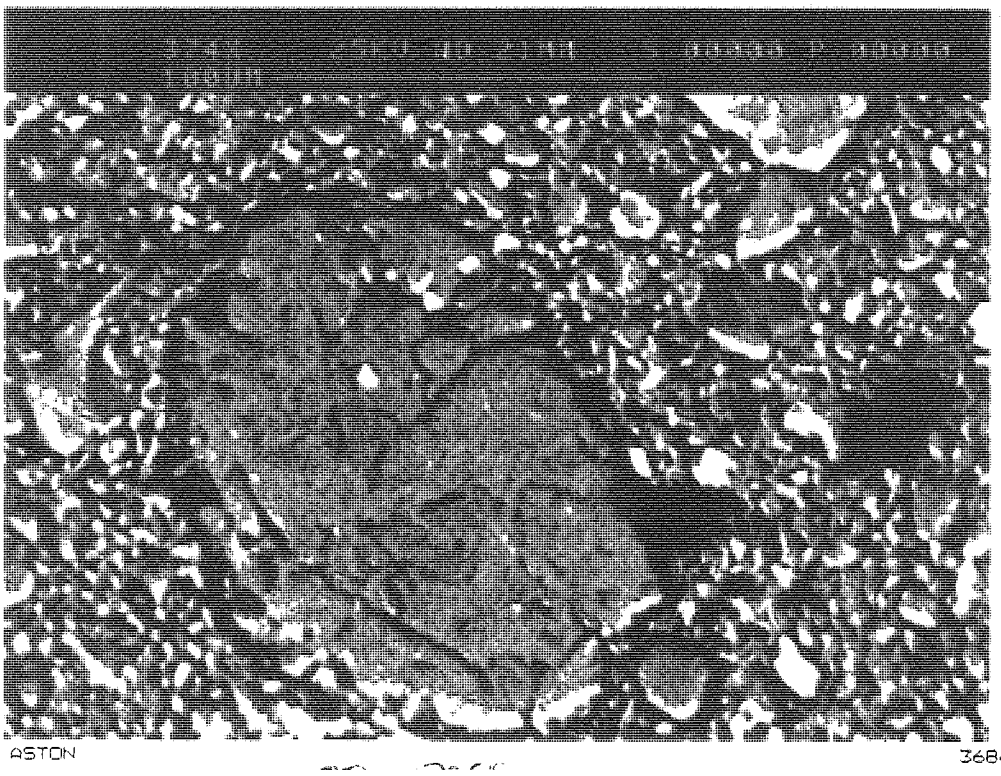

Figure 26 : SEM image of Stoke Red experimental tile (35 cycles.)

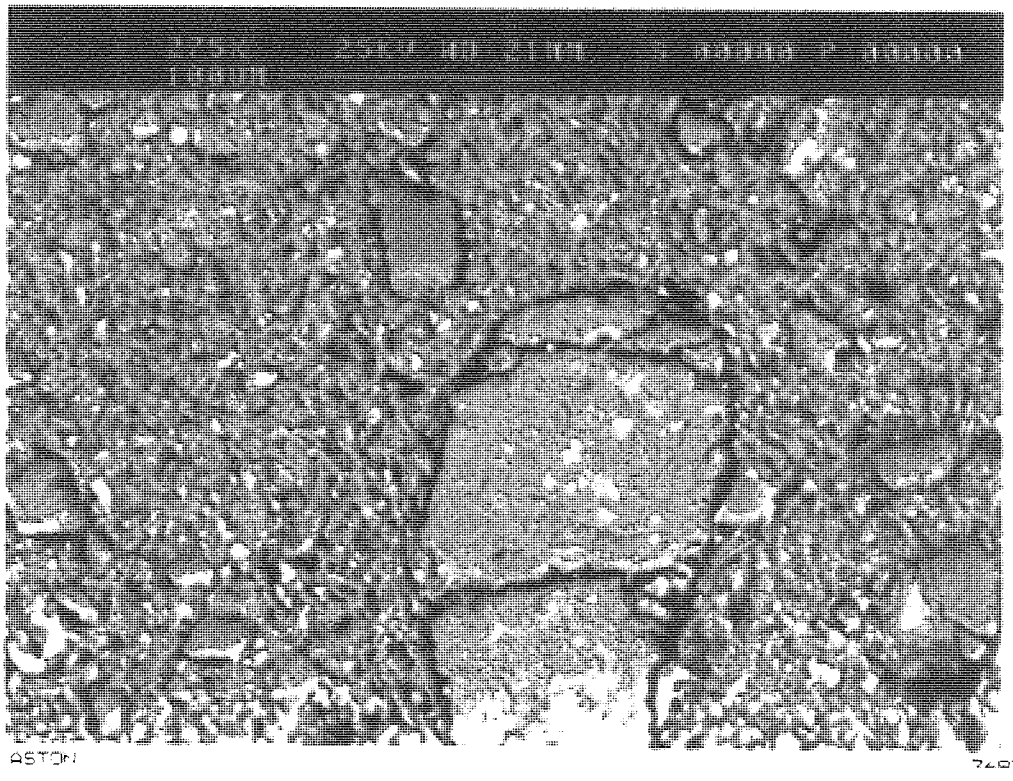

As shown with Whichford original tiles SEM appears of limited of use for analysis of this type. The images captured of Stoke Red experimental and control tiles appear very similar with no apparent differences detected. Again it can be seen how inclusions of iron and silica within the matrix exhibit small surface cracks. This phenonomen is observed in both the control and experimental tiles and therefore cannot be solely attributed to the action of frost upon the clay body. Cracks are further attributed to the grinding process used in sample preparations.

It is therefore concluded that SEM analysis of Stoke Red samples has shown the effect of freeze-thaw cycling to be minimal.

Gas sorption isotherms for Stoke Red control and experimental (figures 27 and 28) provided data that suggested type III adsorption processes to be occurring. The lack of conformity of experimental data obtained with that shown in the literature, made interpretation of the data difficult and therefore a full explanation of the effects occurring cannot be given.

The isotherms shown in figure 27 and 28 for Stoke Red samples show non-typical type III isotherms indicative of non-porous or macroporous solids where there is very little interaction between the solid surface and the adsorpable gas. Ideally the adsorption pathway would be equal to that of the desorption pathway with an increase in adsorption being observed after the formation of the initial monolayer due to an enhanced interaction between gas molecules. The small hysteresis effect observed on the Stoke Red isotherms is usually indicative of small capillary cracks from which the adsorbate molecules do not desorb as quickly as they adsorb due to a lowering of vapour pressure and hence the formation of a meniscus over the liquid in the pores. The appearance of this hysteresis effect would therefore suggest that freeze-thaw action has had a detrimental effect resulting in the formation of small capillary cracks, however this effect is observed on both experimental and control tiles and is therefore unlikely to be as a result of frost action. It is possible that these small deformations are present both before and after freeze-thaw treatment showing that frost action has had a negligible effect.

Figure 27 : Gas Sorption isotherm for Stoke Red control.

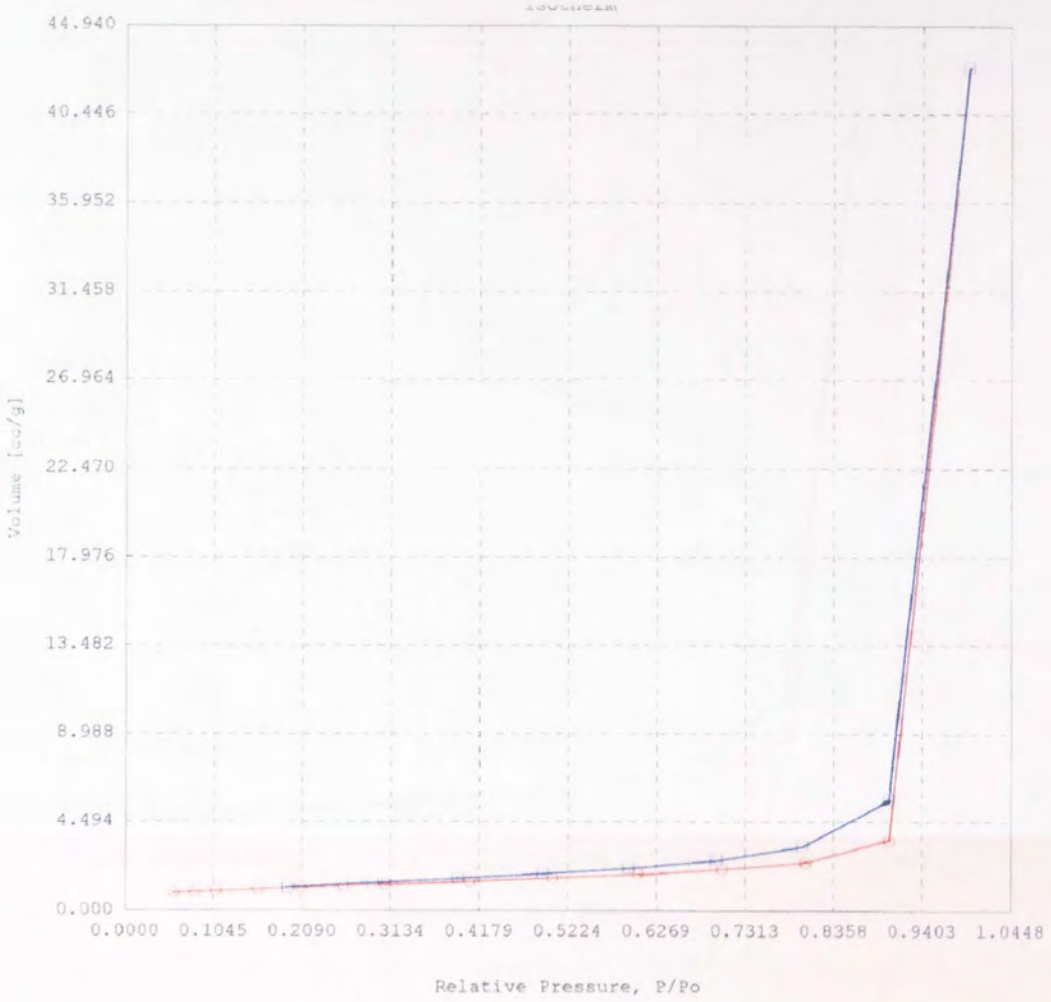

Red Line – Adsorption Isotherm

Blue Line – Desorption Isotherm

Figure 28 : Gas Sorption isotherm for Stoke Red experimental (35 cycles).

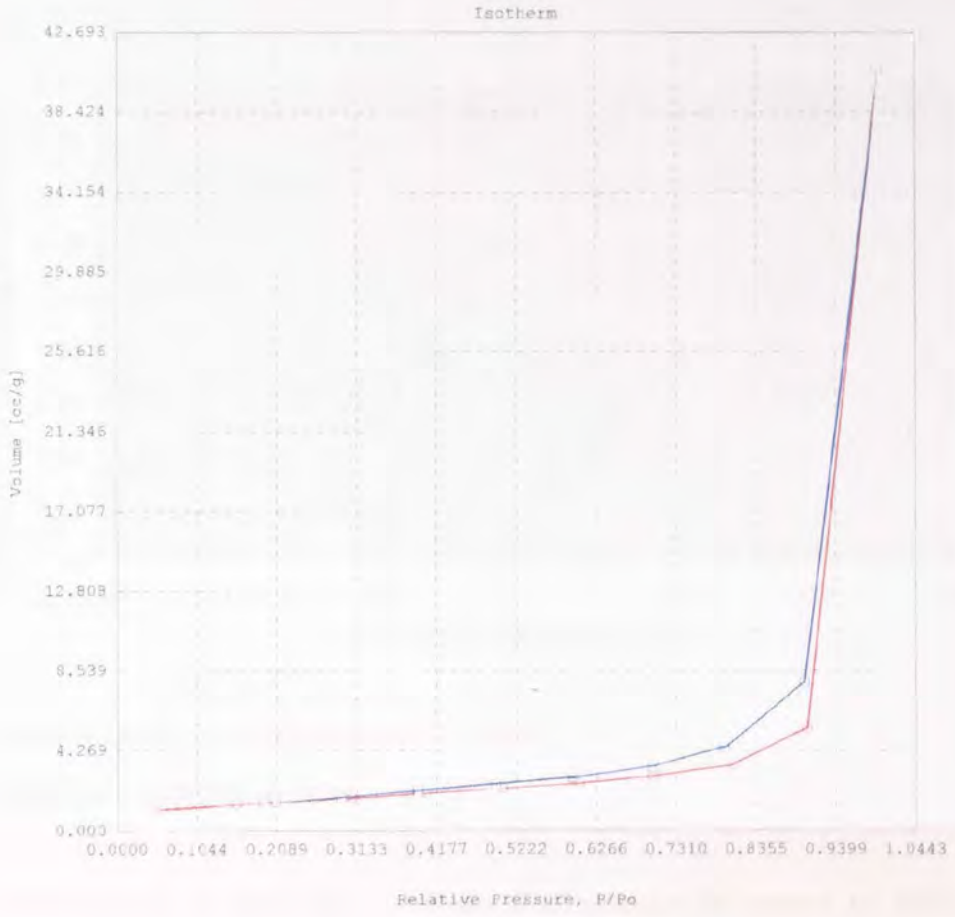

Further repetition of results did not yield any additional data, providing further evidence to suggest there is little difference between control and freeze-thaw samples. It may be that the deformations present are too small to be identified *via* this method. At this stage gas sorption analysis appears to be in agreement with SEM in suggesting that the action of frost upon Stoke Red samples has been minimal.

Mercury intrusion porosimetry a complimentary technique to gas sorption analysis has shown (figure 29) that both Stoke Red control and experimental samples have a narrow pore size distribution as dictated by the overall shape of the curve.[39] The steep incline in the curve at ~0.1μm is indicative of a predominance of pores within this region, a ten-fold decrease when compared to Whichford original samples as shown in figure 22.

Figure : 29 Mercury Intrusion Porosimetry for Stoke Red control and 35 cycles.

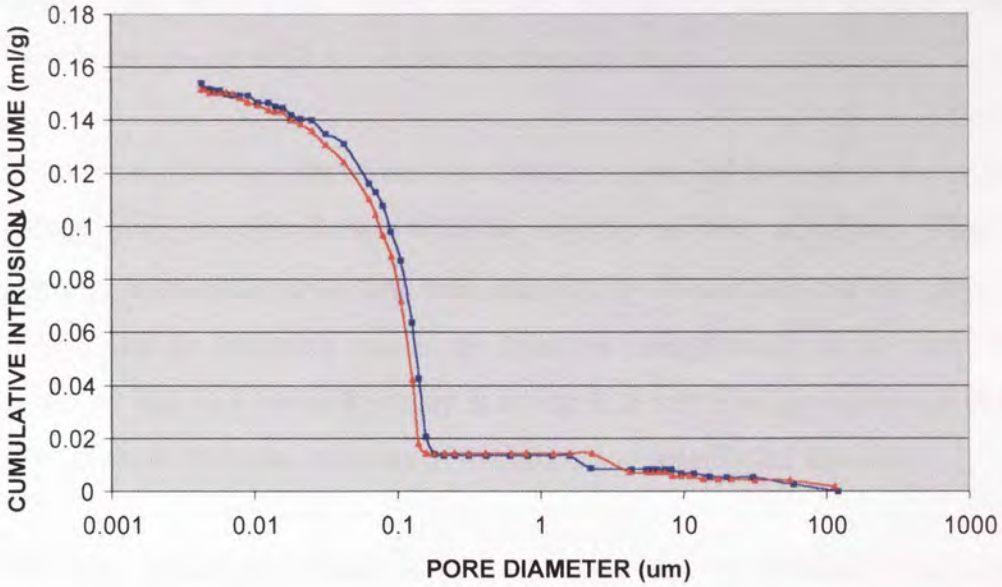

Red line Stoke Red experimental 35 cycles.

Blue line Stoke Red control.

The decrease in pore size of Stoke Red samples compared to Whichford original samples suggests that in the event of frost action the Whichford samples would show a greater resilience as there is more space into which the water can expand upon freezing. Data so far has not shown this theory to hold true. There are no observable differences in cumulative intrusion volume for Stoke Red samples.

Repetition of experiments on a number of occasions did not yield any further information it can therefore be concluded thus far that the action of freeze-thaw upon Stoke Red tiles has been minimal.

In contrast to this, interpretation of the data from Three Point Flexural testing provided some very interesting data. It can be seen from figure 23 how the action of freeze-thaw upon the Stoke Red samples appears to have acted to make the clay structure stronger. The statistical analysis of the variants of these data verifies the visual interpretation of data that the action of freeze-thaw has acted to intensify the clay and hence make it stronger. Three Point Flexural testing of Whichford original samples has already shown

how the action of frost has been minimal. It is therefore reasonable to suggest that a threshold region exists, where up to a certain number of freeze-thaw cycles strengthening of the clay system occurs, once this threshold is surpassed weakening will begin. Data so far, from Stoke Red and Whichford original samples suggests this to exist in the region of 35 to 106 freeze-thaw cycles.

In addition, Mercury Intrusion Porosimetry (figure 29) has shown Stoke Red to have a narrow pore size distribution with the majority of pores at 0.1μm. This considerably lower pore entry diameter than that exhibited by Whichford original clays (1μm) could indeed play an important role in the apparent strengthening of the Stoke Red material. It can be said that Stoke Red clay is acting in a very similar manner to concrete where over time the hydrous elements of the mix act to solidify the material.

The data provided by analysis of Stoke Red tiles by Ultrasonic techniques were in agreement with that obtained from Three Point Flexural testing.

The visual interpretation of the graphical data (figure 24) again suggests that the action of freeze-thaw treatment upon Stoke Red tiles has acted to further bond the clay together so making the passage of the wave easier, yielding a higher velocity.

The statistical analysis of the variants of these data to a 95% confidence limit shows the data presented to be statistically significant therefore showing the results for Stoke Red experimental and control to be from two separate groups, hence showing the action of freeze-thaw processing to have had an effect upon the Stoke Red clay tiles. It is again assumed that this apparent strengthening could be related to the lower pore entry diameter of Stoke Red samples, whilst suggesting that a threshold region may exist. It is assumed that because this phenonomen has only been observed in Stoke Red and Whichford original tiles that the threshold will exist between the two freeze-thaw extremes demonstrated thus far, so in the region of 35 and 106 cycles.

The data presented thus far for Stoke Red tiles has shown an apparent strengthening of the material as a result of frost action, it was therefore assumed at this stage that if the bronze inclusions identified by thin section were playing an important role then obvious differences between Stoke Red and Whichford original would be observed.

Thin section analysis of Stoke Red control and experimental tiles showed quartz to make up ~10-20% of the matrix as a whole whilst the bronze inclusions noted earlier (page 67) contributed to ~5-10%. The Stoke Red samples examined showed there to be very little de-bonding associated with the bronze inclusions, with those in the experimental tile taking on an octahedral shape, possibly suggesting a stronger appearance. Both samples appeared to have a much denser matrix as indicated by an apparent smaller porosity and evident packing of the matrix. This is consistent with the data from Three Point Flexural tests and Ultrasonic analysis. Samples appeared to have a lower porosity with smaller sized pores as evident in Mercury Intrusion Porosimetry.

The LECO sulfur analysis of Stoke Red clays again, like Whichford clays (table 4) showed there to be very low levels of sulfur within the clay as shown in table 5.

Table 5 : Percentage sulfur in Stoke Red freeze-thaw treated samples.

SAMPLE	% SULFUR
Stoke Red Control	0.011
Stoke Red 35 Cycles	0.036

Such low levels of sulfur show that the bronze inclusions present cannot belong to the family of iron sulfides. It can therefore be concluded that the inclusions observed belong to the family of iron oxides probably hematite.

3.2.1 CONCLUSIONS ON FREEZE-THAW ANALYSIS OF STOKE RED SAMPLES

As shown for Whichford original tiles the application of SEM and Gas Sorption techniques to Stoke Red tiles was of limited use, the images and data obtained showed there to be very little difference between control and experimental tiles. The small hysteresis effect observed on Stoke Red patterns (figures 27 and 28) suggested the presence of small capillary cracks, which may suggest an adverse effect resulting from frost action. However, the appearance of a small hysteresis on both control and experimental tiles suggests that any small cracks appearing will be as a result of the preparation process and not due to freeze-thaw.

Mercury Intrusion Porosimetry data became important later in the proceedings when examining results from Three Point Flexural testing and Ultrasonic analysis. It was shown by MIP that Stoke Red exhibits a predominance of pores in the region of ~0.1μm, a ten-fold decrease when compared to Whichford original samples. It was further exhibited by Three Point Flexural testing and Ultrasonic analysis, when tested to a 95% confidence limit, that the action of freeze-thaw upon Stoke Red samples had acted to compound the clay and make it stronger. It was therefore assumed that this strengthening could be related to the lower pore diameter of Stoke Red as it is harder for the pores to be penetrated. In addition it was assumed that a threshold region exists up to which strengthening of the clay body occurs and once this is surpassed the body weakens. At this stage it is assumed that this occurs in the region of 35 and 106 cycles, as these are the limits of the Stoke Red and Whichford original tiles examined thus far. The examination of slides produced by thin section, linked in with this data show that Stoke Red appears to have an overall denser matrix of smaller pore size, whilst any bronze inclusions observed were intact with no de-bonding occurring. LECO sulfur analysis suggests these bronze inclusions to members of the iron oxide family probably hematite.

In summary, so far it has been seen how freeze-thaw analysis upon Stoke Red tiles has acted to compound the clay and make it stronger. The most appropriate techniques for analysis of this type are Three Point Flexural testing and Ultrasonic analysis, whilst Mercury Intrusion Porosimetry is informative on providing pore size distribution information. Thin section analysis has also shown to have its merits.

3.3 ANALYSIS OF T2C.7 AND T2.C8 EXPERIMENTAL AND CONTROL TILES.

The last set of samples to be examined in this manner was T2C.7 experimental tile subjected to 75 freeze-thaw cycles and T2C.8 control tile. These were tiles considered by Whichford Potteries to be of weak nature and so were additionally analysed. As with both Whichford original and Stoke Red tiles, the analysis of these samples *via* SEM was of limited use. The images captured (figures 30 and 31) showed very little differences. Inclusions of iron and silica were clearly observed and although the tiles

were examined at varying resolutions there was nothing to suggest that the action of freeze-thaw had been detrimental.

Figure 30 : SEM analysis of T2C.7, 75 cycle experimental tile.

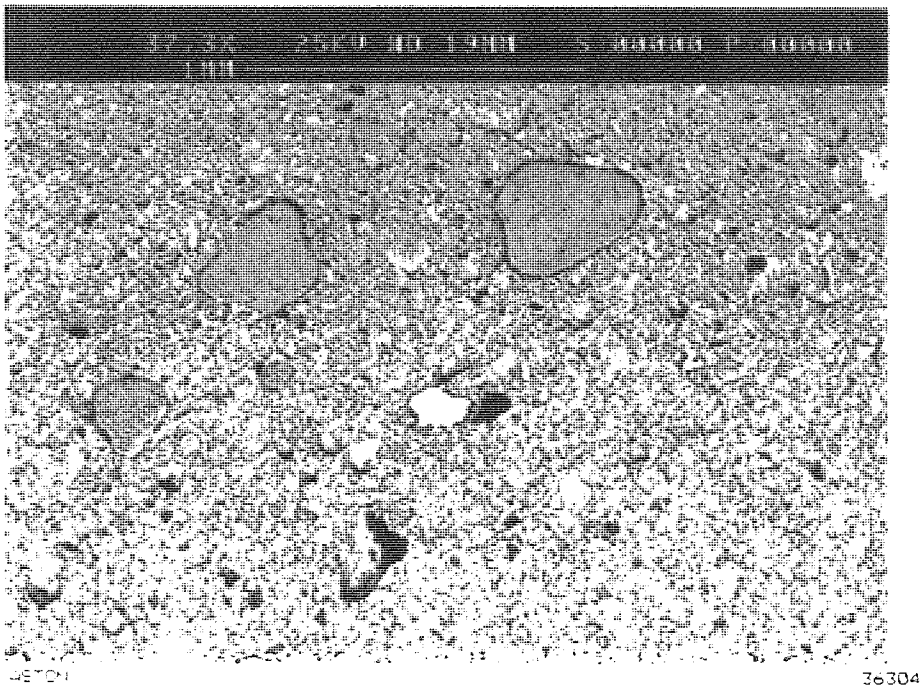

Figure 31 : SEM analysis of T2C.8 control tile.

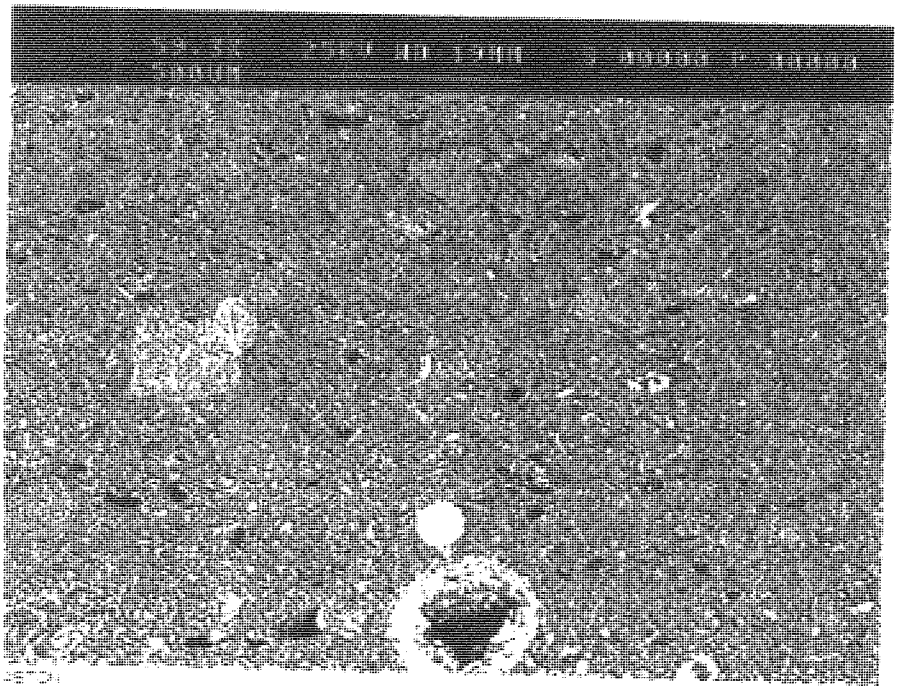

The results obtained from Gas Sorption analysis were the most spurious out of all the samples examined thus far. The isotherms obtained (figures 32 and 33) were the most inconsistent not showing any correlation with those printed in the literature.[39] This therefore resulted in an inability to identify the exact processes occurring and the type of adsorption process being observed.

Figure 32 : Gas Sorption isotherm for T2C.7, experimental tile.

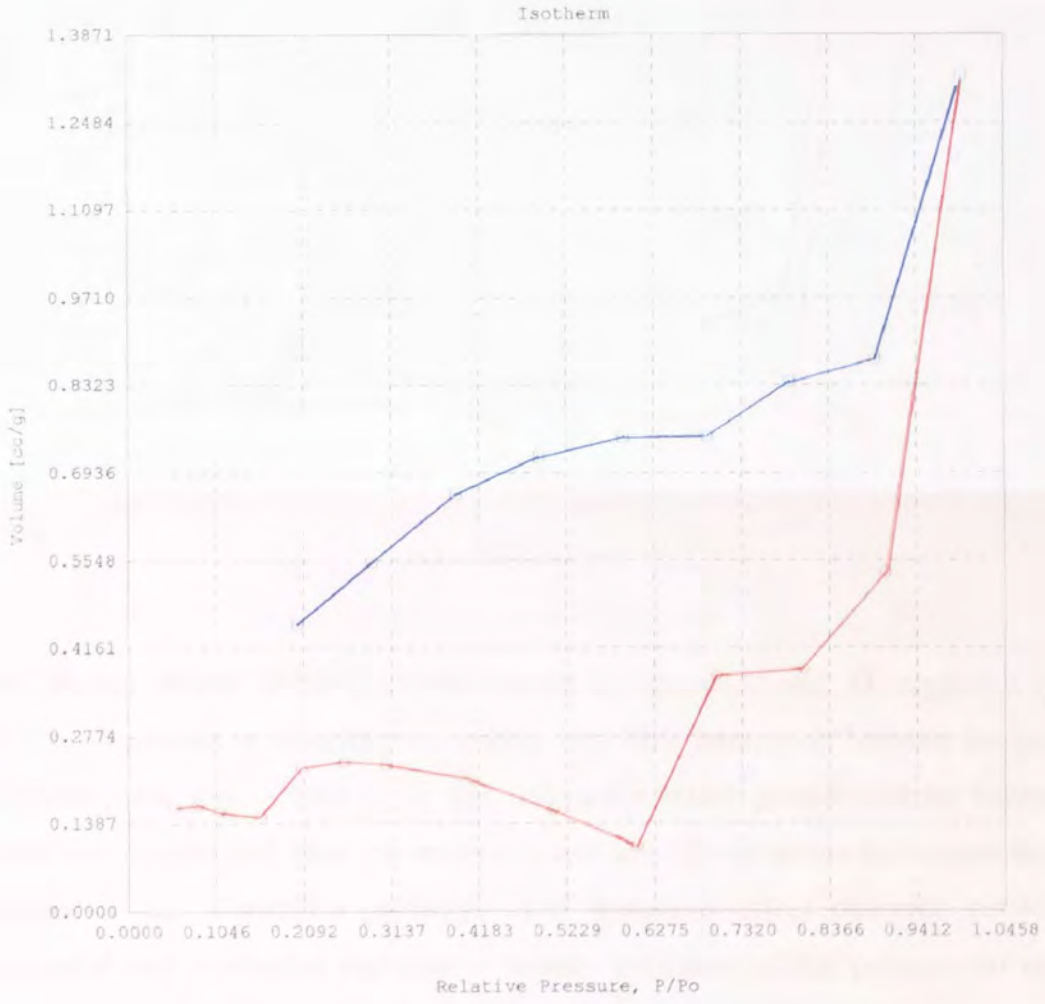

Figure 33 : Gas Sorption isotherm for T2C.8 control.

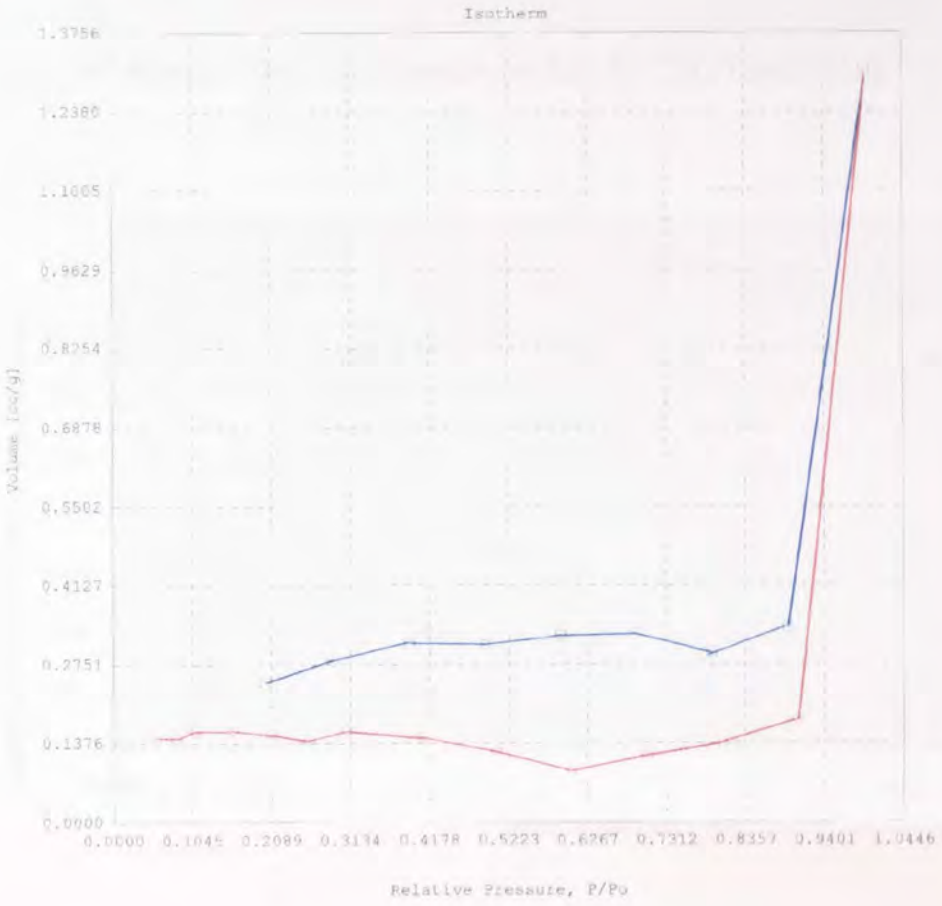

The general shapes of the isotherms shown in figures 32 and 33 suggest a type III adsorption process is occurring suggesting very little interaction between the solid and the adsorpable gas. There is in this instance a much greater affinity between the monolayer formed and other gas molecules and it is this attraction that causes the initial increase in the adsorption pathway. The hysteresis effect observed between the adsorption and desorption pathway is usually indicative of the presence of capillary cracks from which the gas molecules cannot desorb as quickly. The appearance of this phenomenon in both control and experimental tiles does not show this theory to hold true and is therefore difficult to explain. Any cracks appearing in the tiles must have been formed as a part of the manufacturing process. It is concluded at this stage that Gas Sorption is not a valid technique for analysis of this type as the results obtained have been difficult to interpret and not consistent with those shown in the literature.[39]

Mercury Intrusion Porosimetry provided very similar results for T2C.7 and T2C.8 (figure 34) as were shown for Whichford original tiles (figure 22).

Figure 34 : Mercury Intrusion Porosimetry data for T2C.7 and T2C.8.

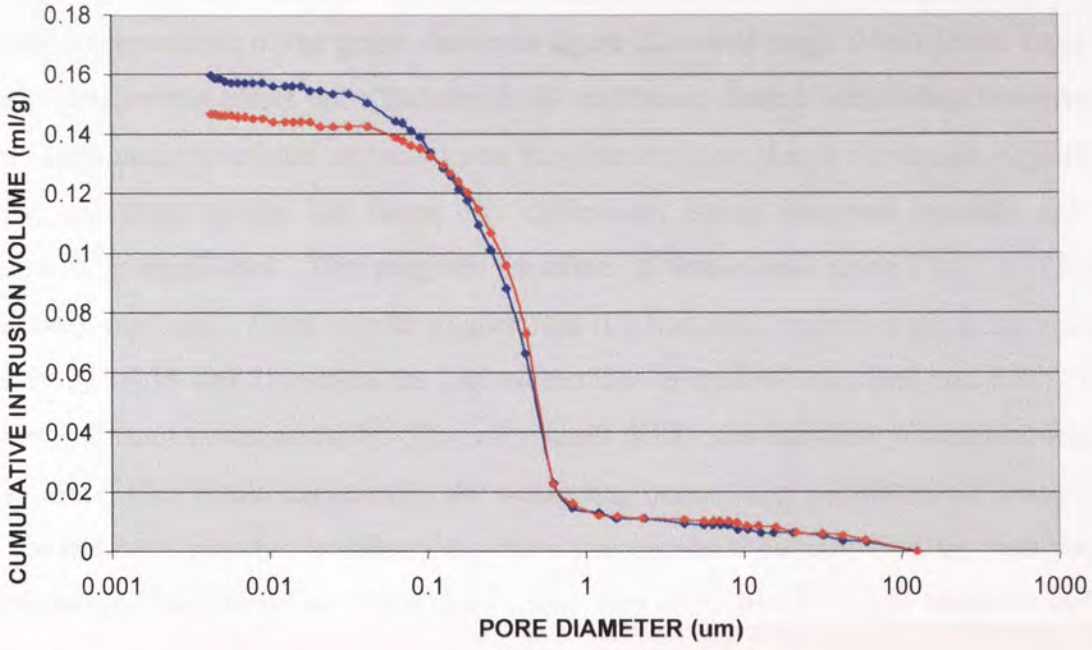

Red Line T2C.7 Experimental freeze-thaw tile, 75 cycles.

Blue Line T2C.8 Freeze-thaw control tile.

The shape of the curve is indicative of a narrow pore size distribution.[39]

It is observed from this graph that the majority of pores for T2C.7 and T2C.8 samples have a diameter of ~1μm with a much smaller amount at either end of the scale. This is identical to that observed for Whichford original tiles (figure 22) with pores being ten times bigger than those observed for Stoke Red (figure 29). Although there is a small difference between the amounts of mercury uptake, results from only one set of data points cannot be seen as significant. Repetition of this set of experiments yielded identical data, therefore, it can be concluded that the effects of freeze-thaw have been minimal and so it is assumed that frost treatment has not had a significant effect upon the clay system.

Mercury intrusion porosimetry does of course have its limitations; very tiny micro-cracks would not be observed *via* this method. This would also suggest why differences are not being observed by Gas Sorption techniques as MIP covers a wider pore range.

As shown in figure 23 the results obtained from Three Point flexural testing of T2C.7 and T2C.8 were consistent with those obtained from Whichford original tiles. The visual interpretation of the graph shown in figure 22 would suggest that freeze-thaw has had a detrimental effect upon the clay body and hence caused weakening, however the statistical analysis of the variants upon this data tells us that the two sets of data are from the same group and hence the differences being observed visually are not statistically significant. This suggests the effect of freeze-thaw upon T2C.7 and T2C.8 has been minimal. These results suggest that if a threshold region exists in now lies in the range of 35 and 75 cycles, the highest number of cycles Stoke Red and T2C.7 have been subjected to respectively. The very small difference between Whichford original and T2C.7 tiles would suggest that the weakening occurs after this threshold is minimal. It has not been possible to determine where this threshold actually lies, the best way of determining this would be to run tests using tiles of different cycles, however lack of experimental tiles did not permit this.

The results obtained from Ultrasonic testing of T2C.7 and T2C.8 were shown to be consistent with those obtained from Three Point Flexural testing. Again the visual interpretation of the data showed that frost action had acted to slightly compound the clay, however statistical analysis of the variants of this data shows it not to be statistically significant. This therefore suggests that the action of frost has been minimal.

The interpretation of thin section results from T2C.7 and T2C.8 show this to be the weakest sample although this has not been observed by the corresponding data. The control sample showed to have a high porosity, which from MIP is known to be ~1μm. There were a number of holes evident in the sample, which appeared in trains in a preferred orientation. This suggests a fairly weak material with a low resistance to strain. The bronze inclusions observed are plentiful, although in general de-bonding has not occurred.

In the T2C.7 experimental sample it appears that de-bonding has occurred around all of the bronze inclusions with it appearing to be the larger the particle the more likely it is to have undergone de-bonding. This suggests this to be a weaker species than its corresponding control, which if visual interpretation of Three Point Flexural testing is believed is true.

LECO sulfur analysis has shown very low levels of sulfur in T2C.7 and T2C.8 samples, as shown in table 6. This is therefore in agreement with the other data obtained suggesting the bronze inclusions to be a member of the iron oxide family, probably hematite.

Table 6 : Percentage sulfur in T2C.7 and T2C.8 samples.

SAMPLE	% SULFUR
T2C.7 75 Cycles	0.005
T2C.8 Control	0.013

3.4 CONCLUSIONS ON FREEZE THAW TREATMENT OF WHICHFORD ORIGINAL, STOKE RED AND T2C.7/8 TILES.

The samples chosen for analysis were subjected to various levels of freeze-thaw treatment and those samples examined were,

- Whichford Original control and 106 cycle experimental tiles.
- Stoke Red control and 35 cycle experimental tiles.
- T2C.8 control and T2C.7 75 cycle control tiles.

SEM elemental analysis *via* EDAX techniques were performed on all clays and identified inclusions of iron (figure 15) and silicon (figure 16) within the matrix. In addition to this oxygen, calcium and aluminium were also identified in large amounts. It was not possible to quantify the amounts present as the images captured, only provide a representative view of the whole sample. It can be concluded that iron, silicon and

aluminium are present in significant quantities being the three largest components of the matrix.

The sections of tile analysed *via* SEM at various intensities of 100μm – 2mm did not provide information to suggest that freeze-thaw treatment had been detrimental. Inclusions of iron and silicon containing materials were clearly discernable at all magnifications although there was not any evidence of micro-cracking or pore deformations resulting from freeze-thaw treatment. The appearance of small surface cracks on the inclusions of iron and silicon containing materials were determined to be as a result of the preparation process as these were observed in both control and experimental tiles for all samples.(figures 16, 17, 25, 26, 30 and 31)

In conclusion it is reasonable to suggest that SEM is not a viable technique for analysis of this type with very little effects of freeze-thaw being observed on any of the tiles examined.

The further analysis *via* Gas Sorption techniques produced isotherms for all samples examined that were not consistent with those shown in the literature. In general they all suggest an unusual type III isotherm that is usually observed for non-porous or macroporous solids. These types of isotherms arise when there is little interaction between the solid and the adsorpable gas. This is also indicative of samples with small pore sizes.

It is usual in these types of isotherms that the desorption pathway will be equal to the adsorption pathway, however a hysteresis effect is observed for all samples, this is particularly prevalent in Whichford original and T2C samples. Such effects are usually observed as a result of capillary cracks within the samples, which causes slower desorption of gas, however this is observed in both control and experimental tiles therefore suggesting very small pores or cracks probably present during the manufacturing process.

It is interesting at this stage to note how the hysteresis phenonomen is particularly prevalent in Whichford original and T2C samples, with a lesser effect being observed for Stoke Red that is later shown to be compounded as a result of frost action. This

could be a very weak but early indication of Stoke Red being a stronger clay system after freeze-thaw treatment.

As a stand alone technique Gas Sorption did not provide any additional information to suggest that the action of freeze-thaw has been detrimental and it can be seen to be consistent with SEM analysis.

The complementary technique of MIP provided pore size distributions for all samples. The initial results shown in figure 21 for Whichford original samples suggested a detrimental effect as a result of freeze-thaw. This data was non-reproducible and therefore discounted. Figure 22 shows Whichford original to have a predominance of pores in the ~1μm region as shown by the steep incline in the curve. Identical data are observed for T2C.7 and T2C.8 (figure 34) whereas Stoke Red (figure 29) shows a ten fold decrease exhibiting a predominance of pores in the ~0.1μm region. All samples show a much smaller number of pores at either end of the pore size scale. The small differences in observed in cumulative intrusion volume may suggest a minimal effect resulting from frost action. However, due to such small differences it is unfair to say conclusively that the discrepancies in cumulative intrusion volume, are a result of frost action. Again there is a striking connection between Whichford original and T2C.7/8 samples with Stoke Red showing contrasting results.

The results from Three Point Flexural testing and Ultrasonic analysis provided some very interesting data. Visual interpretation of both sets of data, as shown in figures 23 and 24 shows that freeze-thaw treatment has had an effect upon the samples.

Three Point Flexural testing suggests that for Whichford original and T2C.7/8 tiles the action of freeze-thaw has acted to weaken the clay system where as for Stoke Red the opposite effect is observed with an apparent strengthening of the clay system. The statistical analysis of the variants of this data at a 99% confidence limit shows that the differences observed for Whichford original and T2C are not significant and therefore do not hold true. Conversely, analysis of the Stoke Red data shows to be statistically significant showing that the action of freeze-thaw has acted to compound the clay thus making it stronger.

Results from Ultrasonic analysis when tested to a 95% confidence limit provided data that were consistent with those from Three Point Flexural testing. It was therefore assumed that a threshold region exists, an area in which strengthening of the clay body occurs, once this threshold limit is surpassed weakening will begin. It is assumed from the data presented herein that this threshold region exists between 35 and 75 freeze-thaw cycles. It has not been possible to determine exactly where this threshold lies due to lack of experimental samples. It has also been assumed that the apparent weakening that occurs after this region is slow due to lack of differences between T2C and Whichford original samples.

It is also worth noting that Stoke Red has a much smaller pore size distribution than Whichford original and T2C samples this suggests that the pores may be more difficult to penetrate thus providing a protection mechanism.

The bronze inclusions observed in all samples examined were thought to be related to the freeze-thaw process. For Whichford original and T2C samples the bronze inclusions contributed to ~5-10% of the matrix as a whole. It was seen that de-bonding had occurred around the majority of these inclusions especially those of larger size. Whichford original experimental sample appeared to show more strain than the control sample whilst T2C appeared to be the weakest tile with holes and de-bonding clearly evident. The Stoke Red tile exhibited very little de-bonding around the bronze inclusions with a denser matrix as indicated by the obvious small porosity and close packing.

LECO sulfur analysis showed low levels of sulfur for all samples therefore showing the bronze inclusions not to belong to the family of iron sulfides as initially determined but rather associated with the iron oxides, probably hematite.

CHAPTER FOUR

4.0 PHYSICAL AND CHEMICAL ANALYSIS OF WHICHFORD CLAYS.

Of the objectives set by Whichford Potteries one has been to characterise existing and replacement clay bodies. The aim is to identify similarities and differences and to determine if both clay bodies possess the same important features.

The samples chosen for analysis were non-fired clay bodies consistent with those used to assess the action of freeze-thaw. These were Whichford original clay and Whichford T2.C clay. The original clay is considered in its fired and non-fired states whilst T2.C clay is assessed in its non-fired state only.

4.1 ANALYSIS OF FIRED WHICHFORD ORIGINAL CLAY

A number of analytical techniques have been used in assessing the characteristics of the Whichford clays. The use of XRD to reveal interlayer distance (basal spacing) has aided in the characterisation of the clay minerals. This technique has been useful to some extent in revealing uniformity in structure, as sharp peaks often indicate well-ordered crystalline materials. The XRD pattern shown in figure 35 for fired Whichford original clay exhibits sharp narrow peaks indicative of a well-ordered crystalline material.

Figure 35 : XRD pattern for fired Whichford Original clay.

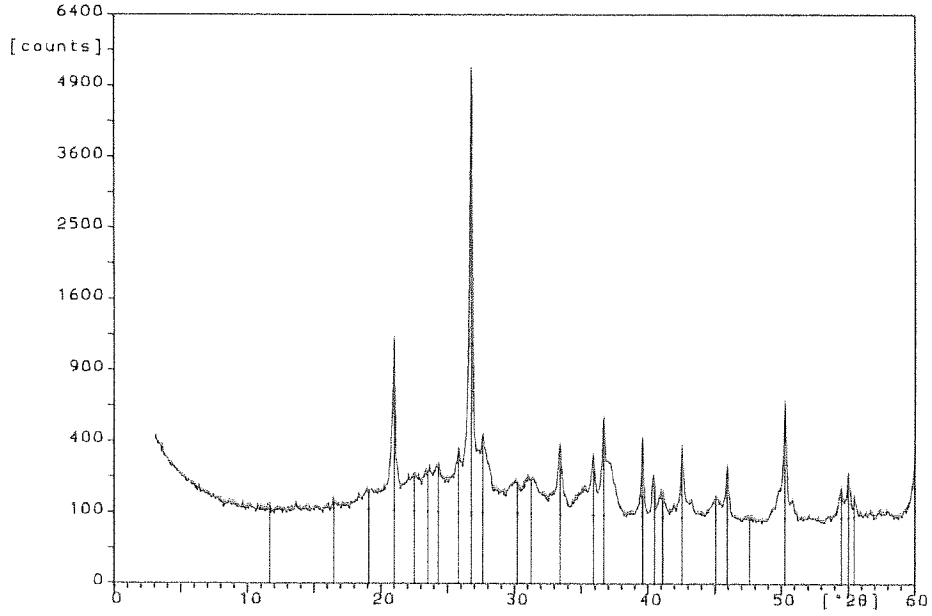

Table 7 : Interpretation of XRD pattern for fired Whichford Original clay.

2θ	d values (Å)	Assignment	Comment
20.97 26.74	4.23 3.33	SiO_2	Very sharp peaks indicative of a well-ordered and crystalline material, probably attributable to quartz. There is no indication of other polymorphs of silica.[43]
11.61 24.28	7.61 3.66	Kaolinite	Indicative of the presence of clay mineral kaolinite Very small, broad peaks suggesting lattice disorder.[43]

The results obtained from the interpretation of figure 35 correspond closely to those stated in the literature[42,43,44] although d(measured) is dependent upon experimental conditions and so a small margin of error will exist.

The results obtained show Whichford original fired clay to be a mix of both clay and non-clay minerals, kaolinite and quartz respectively.

---

[42] Moore, D.M., and Reynolds, R.C., *X-Ray Diffraction and the identification and analysis of clay minerals,* Oxford University Press, **1989**.
[43] Ed. Van Olphen, H., and Fripiat, J.J., *Data handbook for clay and other non-metallic minerals,* Pergamon Press, **1979**.
[44] Berry, L.G., and Thompson, R.M., *X-Ray powder data for ore minerals,* The Geological Society of America, Memoir 85, **1962**.

No further polymorphs of silica were observed nor did the results indicate the presence of iron within the sample. ^{57}Fe Mössbauer spectroscopy results will reveal further information regards the nature of any iron within the clay samples (see later).

Infra red analysis can be used in conjunction with XRD to aid in the identification of chemical composition. Infra red analysis leads to the determination of the functional groups within the clay bodies, which in turn leads to identification of clay mineral types. The interpretation of the spectrum for fired Whichford original clay (figure 36) was made by reference to literature material[45,46,47,48,49] and *via* comparison with spectra of 'pure' clay minerals.

Figure 36 : Infra red spectrum of fired Whichford Original clay.

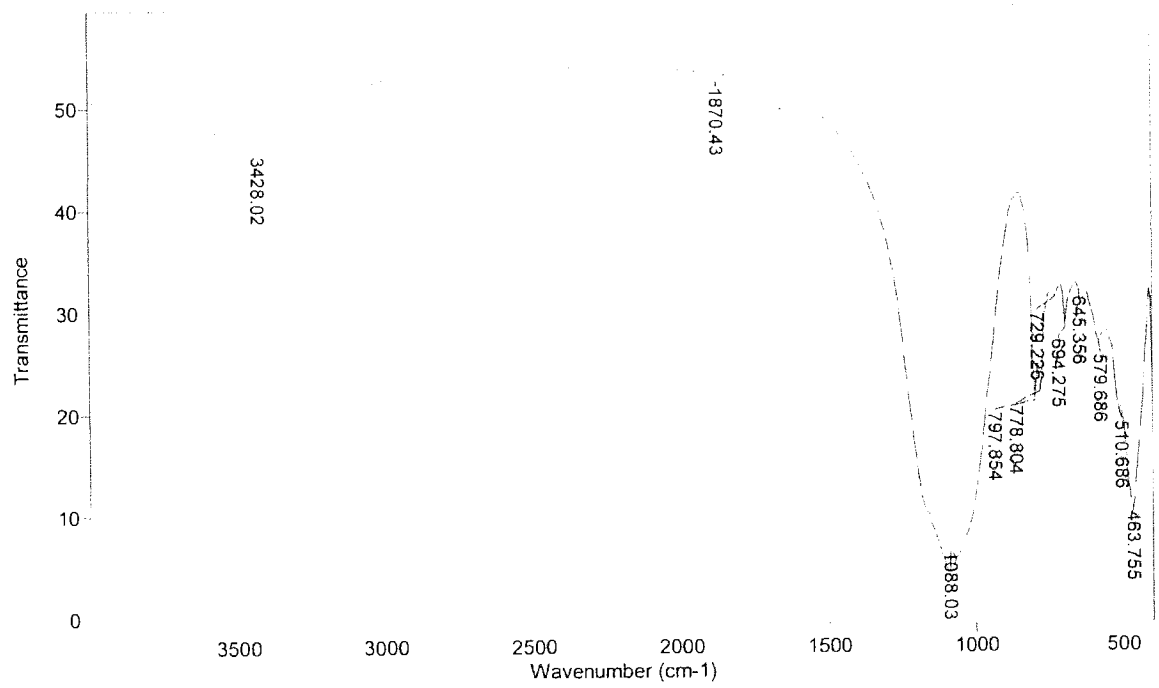

[45] Theng, B.K.G., *The Chemistry of Clay Organic Reactions,* **1974**, Halstead Press.
[46] Farmer, V.C. and Russell, J.D., *Spectrochimica Acta,* **1964**, 20, 1149 – 1173.
[47] Miller, J.G., *J.Phys.Chem,* **1961**, 65, 800 – 804.
[48] *CLAY MINERALOGY, Spectroscopic and chemical determinative methods,* CHAPMAN AND HALL, **1994.**
[49] Nakamoto,K., *Infra red and Raman Spectra of Inorganic and Co-ordination compounds,* Fourth Editon, John Wiley and Sons, **1986**.

Table 8 : Interpretation of Infra red spectrum recorded for fired Whichford Original clay

Absorption (cm^{-1})	Assignment	Comment
3428	OH	OH bonded to oxygen on the silicate layer. Heating would lead to the formation of metakaolin.[46]
1088	Si-O	Si-O stretching vibration and possible Al-OH bonds in the octahedral sheets.[46]
797 778 729	OH	OH bending. Possibly due to the presence of quartz.[47] Peak at 796cm^{-1} is linked with kaolin.[47]
694 645	Si-O/OH	Si-O vibration and OH bending.[45] Linked to kaolin type minerals.[47]
579 510 463	Si-O	Bending vibrations of Si-O.[45]

The infra red spectrum shown in figure 36 shows the existence of silicon and aluminium in the tetrahedral and octahedral layers as would be anticipated for a clay material. The lack of peaks at ~3700cm^{-1} and ~3600cm^{-1} in the spectrum shows dehydroxylation to have occurred, thus consistent with it this being a fired sample.

The infra red spectrum suggests kaolin to be the predominant clay mineral, which is consistent with the data obtained from XRD (table 6). Under heating kaolin is expected to undergo phase change to metakaolin at ~820°C, the extent of the calcination process on Whichford original clay is discussed in detail later. The appearance of weak band at ~3428cm^{-1} on figure 36 is associated with loosely bound –OH, nearly free of all hydrogen bonding. The appearance of this peak in this spectrum suggests that some –OH groups remain attached to aluminium cations after the breakdown of the octahedral structure.

Further to these investigations MAS NMR spectroscopy has been useful in evaluating the environments in which the silicon and aluminium atoms are situated. Distortions present in the spectra, as spinning side bands and resonant broadening, provide additional information regarding the presence of paramagnetic iron oxide impurities within the samples.

The spectra shown in figures 37 and 38 are those recorded from ^{27}Al and ^{29}Si MAS NMR of fired Whichford original clay, respectively.

Figure 37 : ^{27}Al MAS NMR spectrum of fired Whichford Original clay.

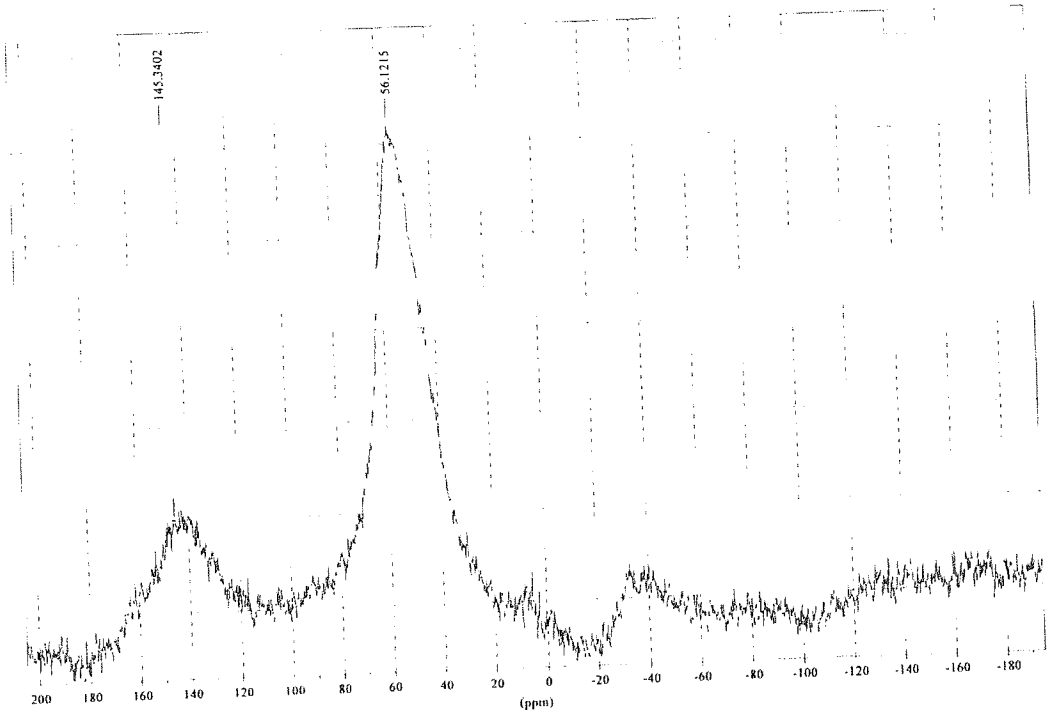

Figure 38 : ^{29}Si MAS NMR spectrum of fired Whichford Original clay.

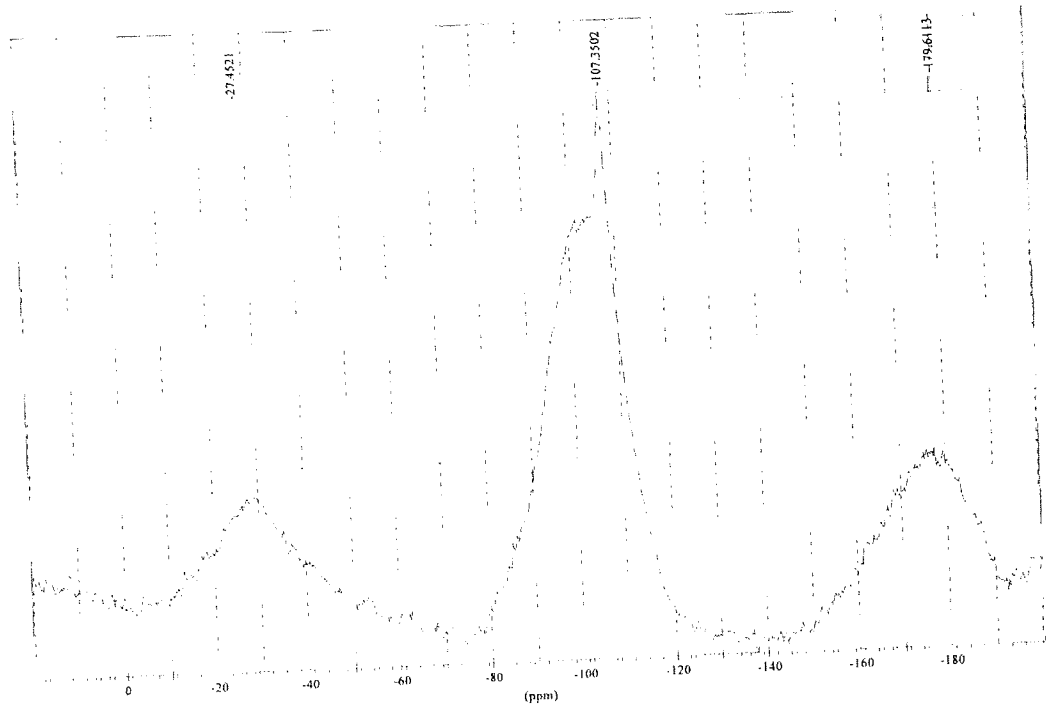

The ^{27}Al MAS NMR spectrum (figure 37) of fired Whichford original clay shows ^{27}Al to be occupying a tetrahedral environment[47]. The line broadening shown is a result of the presence of paramagnetic iron impurities. The deconvolution of the spectrum does not offer any additional information.

The spectrum did not show the appearance of five-co-ordinate aluminium, which formation is thought to be dependent upon the type and magnitude of the charge balancing cation.[50,51,52]

The ^{29}Si spectrum (figure 38) provides information to suggest that the silicon is in a Q_4 co-ordination environment[47], i.e. with four silicon atoms bonded to a SiO_4 tetrahedron. The broadness of the resonant peak suggests the presence of paramagnetic impurities close to the ^{29}Si active nuclei. Deconvolution of the spectrum shows the dominant peak at ~-107ppm with smaller side peaks at ~-104ppm and ~-102ppm, these are also indicative of Si in a Q_4 co-ordination environment. These additional peaks suggest the

---

[50] Roch, G, E., *PhD Thesis,* University of Kent in centerbury, **Jan 1999**.
[51] Woessner, D, E., *American Mineralogist,* 74, **1989,** 203 – 215.

distortion of silicon in the planes. Distortions occur when several SiO_4 tetrahedra have slightly differing bond angles thus giving rise to the slightly different resonant positions of the peaks. When deconvolution is not applied this leads to one broad resonant peak situated at a central position, as is observed in figure 38.

The presence of paramagnetic iron oxides within the fired Whichford original samples plays an important role as seen by the interference it causes in MAS NMR spectra. ^{57}Fe Mössbauer spectroscopy will provide additional information regards the nature of the iron within the fired Whichford original sample (figure 39).

^{57}Fe Mössbauer spectra were recorded using a microprocessor-controlled Mössbauer spectrometer using a 25mCi $^{57}Co/Rh$ source and a natural iron absorber. Spectra were computer-fitted and data are quoted relative to metallic Fe.

Figure 39 : ^{57}Fe Mössbauer spectrum of fired Whichford Original clay.

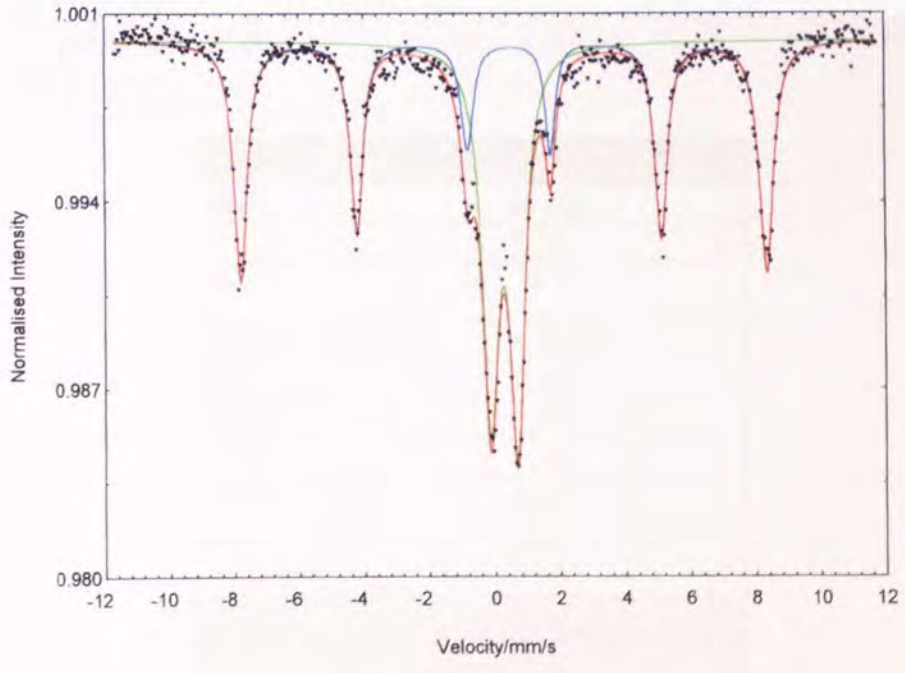

[52] Fitzgerald, J, J., Dec, S, F., and Hamza, A, I., *American Mineralogist,* **1989**, 74, 1405 – 1408.

Table 9 : Interpretation of Mössbauer spectrum recorded from fired Whichford Original clay.

δ/mms^{-1}	Δ/mms^{-1}	Assignment
0.29	0.82	α-Fe_2O_3
0.38	-0.09	Fe^{3+}

The spectrum shown in figure 39 exhibits a sextet typical of large particle α-Fe_2O_3 (hematite).[53] It is anticipated that removal *via* acid washing with HCl would be possible. The dominance of the doublet in the pattern further suggests the presence of paramagnetic Fe^{3+} species. Therefore Fe is occupying two different environments. It is also assumed that some Fe^{3+} will have structurally replaced Al^{3+} in the octahedral layer and will therefore not be removable.

Further information regarding bulk composition of the fired Whichford original clay was obtained from X-Ray Fluorescence (XRF). XRF identifies elemental composition.

Table 10 : Results from XRF.

Oxide	Whichford Original (fired)
SiO_2	64.53
TiO_2	0.98
Al_2O_3	18.5
Fe_2O_3	6.42
MnO	0.04
MgO	1.97
CaO	1.38
Na_2O	0.61
K_2O	2.87
P_2O_5	0.16
LOI	1.37
TOTAL	98.82

- LOI = Loss on Ignition.
- Values as percentages

[53] Berry, F.J., Eadon, D., Holloway, J., and Smart, L.E., *J. Mater. Chem.*, **1996**, 6, 221 – 225.

The above data for fired Whichford original clay shows a ratio between SiO_2 : Al_2O_3 of approximately 3.5 : 1. It is anticipated that a correlation would be seen between the amount of SiO_2/Al_2O_3 with the amount of Fe_2O_3 as often Fe^{3+} will replace Al^{3+}, however, there does not seem to be an obvious correlation. ^{57}Fe Mössbauer spectroscopy has previously confirmed the presence of Fe^{3+} and α-Fe_2O_3, which by washing with HCl can be removed. The strong golden colour of the residual washing liquor suggests that the majority of the iron is not structural and therefore can be removed. It is assumed that it is the large particle α-Fe_2O_3 that is removed as this will not take part in isomorphous substitution. The data also shows SiO_2 and Al_2O_3 make up the biggest proportion of oxides in the material, with Fe_2O_3 being the next.

Additional oxides of calcium, sodium and potassium were also observed by XRF for the fired Whichford original clay. Calcium may originate as a result of the presence of $CaSO_4$ in the form of gypsum, an impurity that can be removed by the addition of barium salts.

XRF further identified inclusions of MgO, MnO, P_2O_5 and TiO_2. MgO can be attributed to $Mg(OH)_2$ of the brucite layers whilst the others do not attribute to any particular type of mineral.

The use of XPS in conjunction with XRF is useful as XPS provides a surface analysis of the clay components and often similarities are observed between the two techniques.

The spectra shown in figure 40 are those recorded from the analysis of fired Whichford original clay.

Figure 40 : XPS spectra for fired Whichford Original clay.

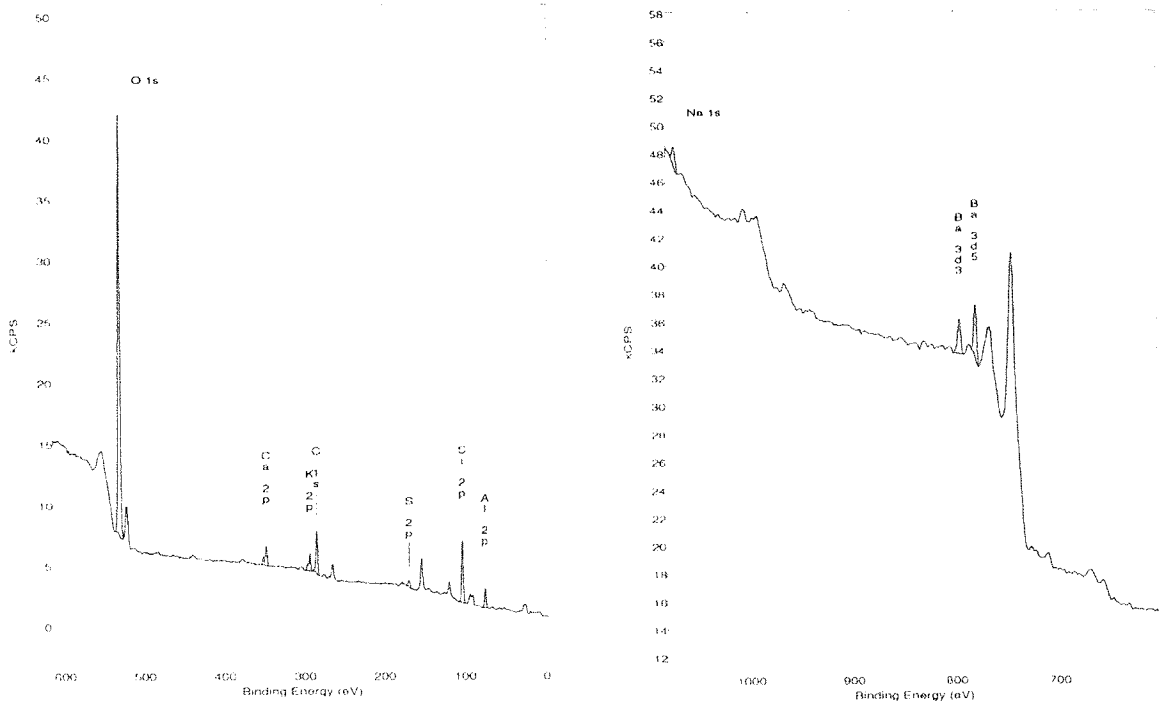

Table 11 : Interpretation of XPS recorded for fired Whichford Original clay.

Peak	Shell	Percent	Comment
Oxygen	1s	51.3	Si-O-Si or Al-O bonds or as a result of interstitial OH/H_2O.
Silicon	2p	20.3	Si atoms in the silica or tetrahedral layer.
Aluminum	2p	9.2	As a result of Al - O atoms in the octahedral layer.
Barium	$3d^3$	0.8	Additive to reduce froth formation during processing.
Fe	$2p^3$	0.8	Small amounts of Iron impurites are present at the surface.
Pottasium	2p	1.4	An impurity.
Sodium	1s	1.1	Consistent with the appearance of montmorillonite.
Calcium	2p	1.5	May be an impurity, however, also suggests the the presence of either Ca mica or montmorillonite.
Carbon	1s	12.2	It is reasonable to assume the presence of carbon. it could be as a result of standard.
Sulfur	2p	1.3	Most likely an impurity in the form of SO_4^{2-}.

The XPS data for fired Whichford original clay has provided information consistent with that already discussed. As anticipated for a clay sample XPS has identified silicon and aluminium, these occupy the tetrahedral and octahedral layers respectively. The appearance of oxygen further links with silicon and aluminium as Si-O and Al-O, oxygen is also attributable to hydroxyl and water molecules.

The presence of iron at the surface suggests a structural moiety. ^{57}Fe Mössbauer spectroscopy has shown this to be Fe^{3+} with the large particle α-Fe_2O_3 moiety being removable *via* washing with concentrated HCl.

XPS provides data consistent with XRF showing the presence of sodium and potassium that may suggest a member of the montmorillonite family. Again the detection of calcium suggests a gypsum ($CaSO_4$) impurity that is removable by treatment with barium salts.

Data so far has provided information regards the chemical composition of the fired Whichford original clay further analysis of the unfired Whichford original clay yielded further interesting results.

4.2 ANALYSIS OF NON-FIRED WHICHFORD ORIGINAL CLAY.

As anticipated the non-fired sample of Whichford original clay showed a more detailed XRD pattern than its fired counterpart, however the peaks identified correspond to literature data.[41,42,43.]

Figure 41 : XRD pattern for non-fired Whichford Original clay.

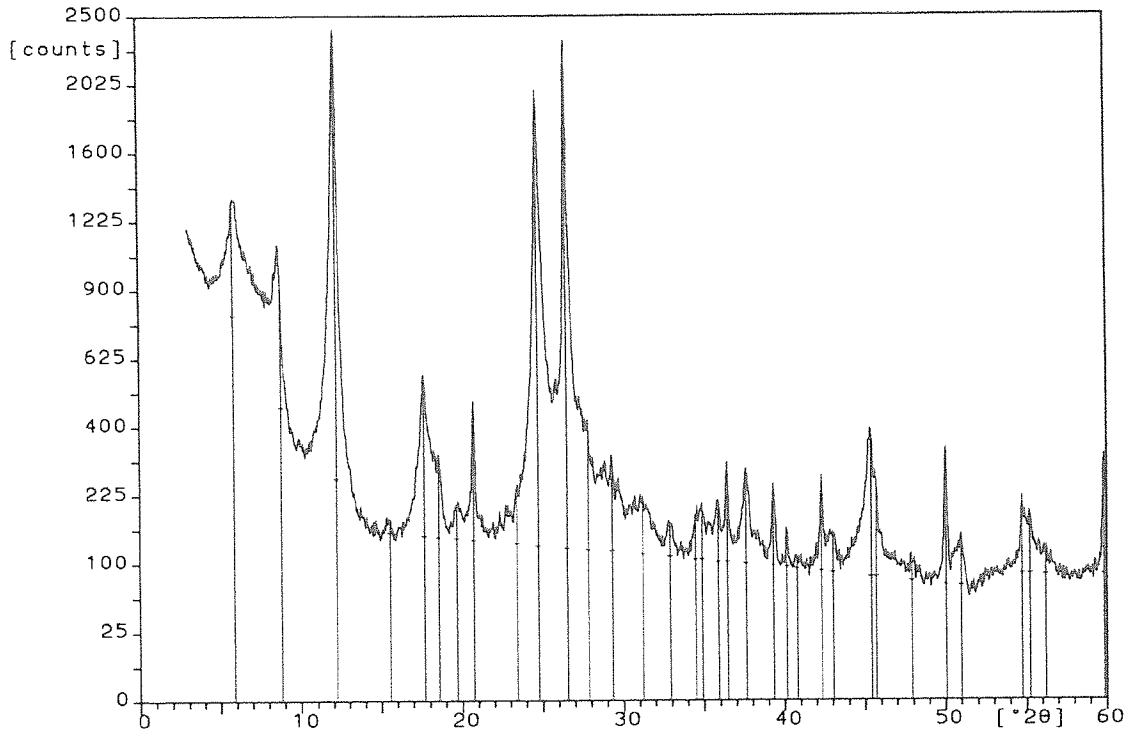

Table 12 : Interpretation of XRD pattern of non-fired Whichford Original clay.

2θ	d values (Å)	Assignment	Comment
5.86 17.64 23.42	15.07 5.02 3.79	Montmorillonite	Broad peaks suggests low crystallinity The appearance of this set of peaks is Indicative of the presence of montmorillonite
8.77 26.50	10.08 3.36	Illite	Suggests the presence of illite
12.18 24.74	7.26 3.60	Kaolinite	Large sharp peaks of equal intensity provide evidence to suggest the presence of kaolinite.
20.71 26.50	4.29 3.36	SiO_2	Two very sharp peaks attributable to quartz.

The results obtained correspond closely to those stated in the literature although d(measured) is dependent upon experimental conditions and so a small margin of error exists.

Like the fired sample the non-fired specimen of Whichford original clay is shown to be a mix of both clay and non-clay minerals. In addition to the kaolin and silica minerals observed for the fired version, the non-fired Whichford original also shows illite and

montmorillonite. It is therefore apparent that the heating process is detrimental to these particular minerals and hence they are not detected in the fired version. The presence of iron containing materials is not detected although both ^{57}Fe Mössbauer and MAS NMR previously indicated its presence. This may suggest it is present as small particle moieties that cannot be detected *via* XRD as it would not then contribute to a significant basal spacing.

The analyses of the non-fired Whichford original clay *via* infra red (figure 42) provided information to support the presence of both quartz (~796cm^{-1} and ~778cm^{-1}) and kaolinite (~3697cm^{-1} and ~3620cm^{-1}), although neither montmorillonite nor illite were detected (see figure 42). These were identified by XRD for this sample. The presence of kaolinite is further supported by peaks at ~912cm^{-1}, 796cm^{-1} and ~694cm^{-1}. A slight broadening of the peak at ~3620cm^{-1} suggests that the clay mineral type may be halloysite.

Figure 42 : Infra red spectrum of non-fired Whichford Original clay.

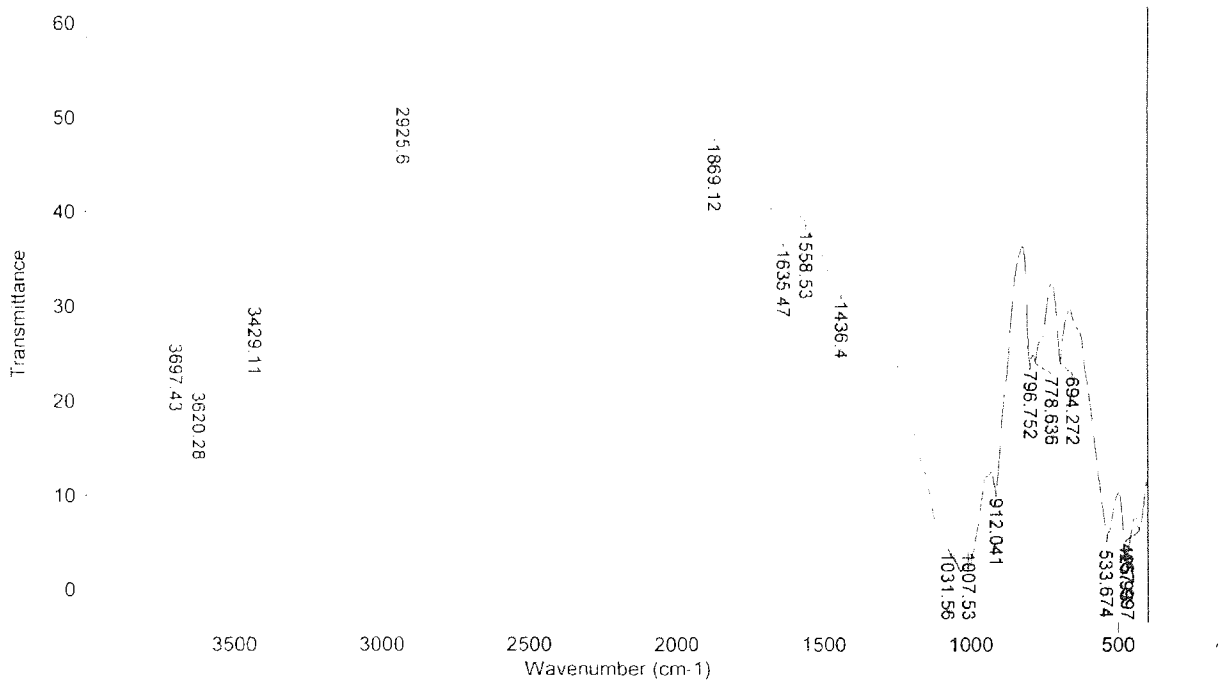

Table 13 : Interpretation of Infra red spectrum recorded for Whichford Original clay.

Absorption cm^{-1}	Assignment	Comment B
3697	H_2O	As a result of type 1 water. OH groups bonded to oxygens on the silicate layer.[44] Typical kaolin band.[47]
3620	OH	Type 1 OH directly related to the cation.[44] Kaolin type band, slight broadening may suggest halloysite.[47]
3429	OH	Indicative of type II, loosely associated water.[44]
2925	CO_3^-	Possibly due to adventitious carbonate
1635	H_2O	Adsorbed water H-O-H bending maxima.[47]
1436	Overtone	Overtone from 2925cm^{-1} band for carbonate.[44]
1031 1007	Si-O	Si-O in plane stretching vibrations.[45]
912	Al-OH	Vibrations of Al-OH, in the octahedral sheet.[45] OH deformation typical of kaolin.[47]
796 778	OH	May be due to quartz or OH bending maxima.[47] Peak at 796cm^{-1} arises due to kaolinite.[47]
694	Si-O	Si-O vibration and OH bending.[45] Linked to kaolin.[47]
533	Si-O	Bending vibrations.[45]

The lack of montmorillonite and illite in the infra red spectrum does not suggest they are not present. It may be that the bands are very weak and therefore are not being observed. Or it may be that bands associated with all of the minerals identified *via* XRD appear at similar infra red wavelengths and therefore are difficult to differentiate.

The spectrum is consistent with that of a non-fired clay, with the existence of bands at ~3700cm^{-1}, ~3600cm^{-1} and 3420cm^{-1} indicative of the presence of both type I and type II water. The peaks at ~3700cm^{-1} and ~3600cm^{-1} were absent in the fired version of Whichford original clay.

The interpretation of ^{29}Si and ^{27}Al MAS NMR data provided some information regards the environment of the silicon and aluminium in the octahedral and tetrahedral layers respectively,(figures 43 and 44).

Figure 43 : ^{29}Si MAS NMR spectrum of non-fired Whichford Original clay.

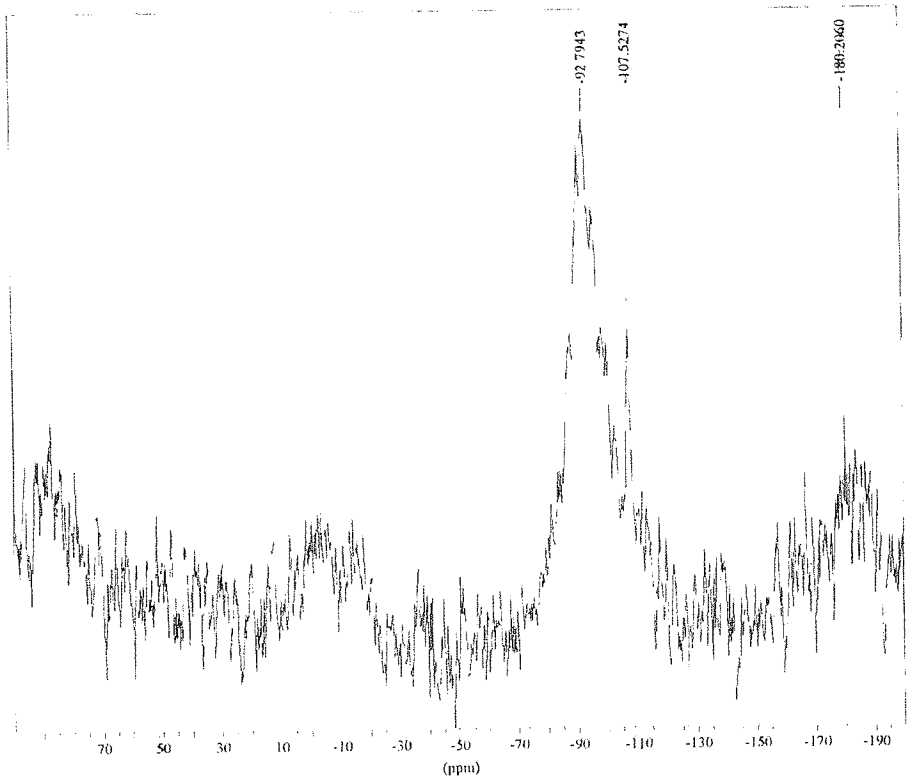

Figure 44 : ^{27}Al MAS NMR spectrum of non-fired Whichford Original clay.

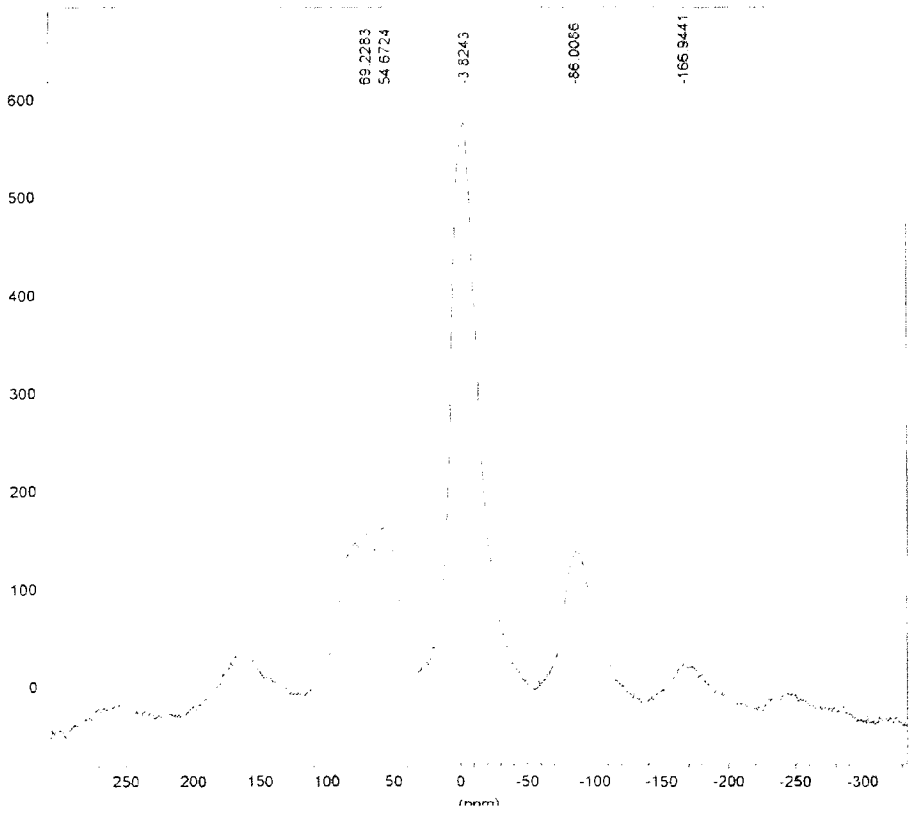

The spectrum shown in figure 43 with a large resonant peak at ~-97ppm is consistent with the majority of the silicon occupying a Q_3 co-ordination environment,[47] therefore not fully polymerised. The line broadening and loss of intensity exhibited by this peak suggests the active nuclei are situated close to paramagenetic iron impurities. The appearance of a low intensity sharp resonance at ~-107ppm is indicative of some silicon in a Q_4 environment.[47] The appearance of tetrahedral Al (~55ppm) in the ^{27}Al MAS NMR spectrum (figure 44) is consistent with the occurrence of Q_3 silicon which, as octahedral aluminium (5ppm) is still found, not all the aluminium is in the framework.

Both spectra show large amounts of background noise and loss of intensity of resonant peaks due to the presence of paramagnetic iron impurities close to active nuclei.

^{57}Fe Mössbauer spectroscopy was used to identify the nature of the iron within the non-fired Whichford clay. The spectrum shown in figure 45 demonstrates that the non-fired clay consists of two different iron moieties.

Figure 45 : ^{57}Fe Mössbauer spectrum of non-fired Whichford Original clay.

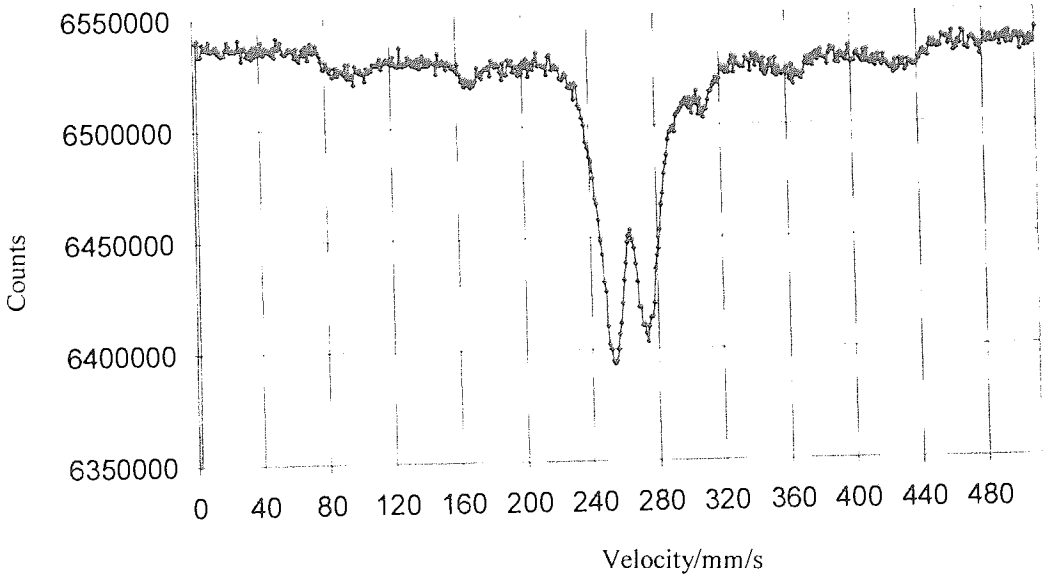

Table 14 : ^{57}Fe Mössbauer chemical shift data.

δ/mms^{-1}	Δ/mms^{-1}	Assignment.
0.29	-0.15	Fe^{3+}
0.35	0.96	Fe^{2+}

The presence of a strong doublet is consistent with the appearance of Fe^{3+}. The weaker peak along side the doublet is indicative of the presence of Fe^{2+}. Although it is not clear the general shape of the spectrum suggests a typical sextet pattern characteristic of α-Fe_2O_3. This was shown clearly in the fired spectrum of Whichford original clay and so suggests that upon firing a transformation of the oxides may be occurring. The small Fe^{3+} particles are sintering to form the larger α-Fe_2O_3 particles being observed.

A surface analysis of the non-fired Whichford original clay *via* XPS provided information to further support the presence of iron whilst presenting additional data to suggest the presence of montmorillonite and other clay minerals. (figure 46).

Figure 46 : XPS spectra for non-fired Whichford Original clay.

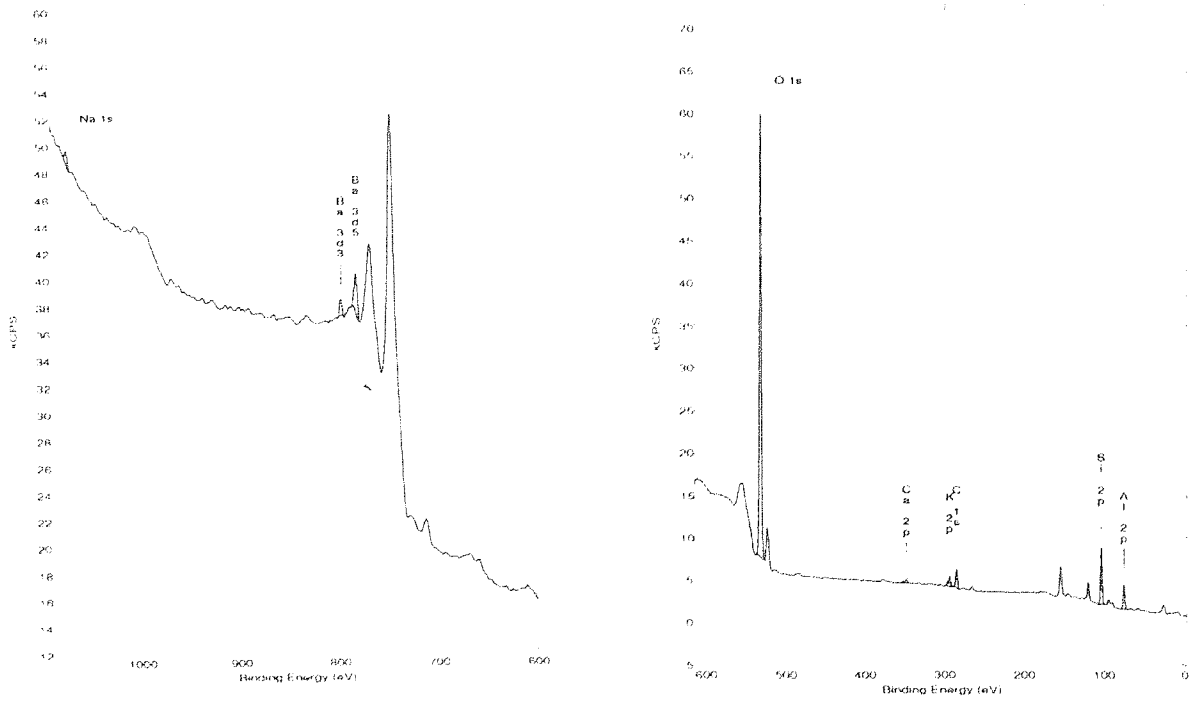

Table : 15 Interpretation of XPS spectra for non-fired Whichford Original clay.

Peak	Shell	Percent	Comment
Silicon	2p	20.3	A result of silica atoms in the tetrahedral layer
Aluminum	2p	12.7	Al atoms in the octahedral layer.
Barium	$3d^3$	0.3	Used as an additive during processing.
Sodium	1s	0.6	Suggests the presence of montmorillonite.
Iron	$2p^3$	1.8	Suggests small amounts of iron at the surface
Oxygen	1s	55.4	Present as Si-O and Al-O in the tetrahedral and octahedral layers respectively. Also due to OH/H_20.
Calcium	2p	0.5	May be an impurity or Ca mica or montmorillonite.
Potassium	2p	1.0	Possible impurity.
Carbon	1s	7.4	Reasonable to assume its presence, however may be due to pump oil standard.

The information provided by XPS has aided in supporting the conclusions and assumptions made previously. As anticipated for clay minerals silicon and aluminium were observed. The appearance of oxygen links with the silicon and aluminium as Si-O and Al-O, oxygen is also attributable to water and hydroxyl molecules within the clay structure.

The appearance of iron at the surface suggests a structural moiety and so corresponds with ^{57}Fe Mössbauer spectroscopy that has shown the presence of Fe^{2+} and Fe^{3+} that can replace silicon and aluminium in the tetrahedral and octahedral layers, respectively.

The appearance of sodium and potassium would indicate the presence of montmorillonite thus linking with earlier infra red data. The detection of Ca, initially suggested to be Ca mica/montmorillonite was through later analysis found to be an impurity of $CaSO_4$, in the form of gypsum. Barium and sulfur as SO_4^{2-} impurities were also noted, barium is utilised during processing to remove $CaSO_4$.

The lack of a correlation, as shown by XRF, (table 16) between the amounts of SiO_2/Al_2O_3 with the amount of Fe_2O_3 suggests that there is very little isomorphous substitution of Al^{3+} by Fe^{3+} although ^{57}Fe Mössbauer spectroscopy has shown the presence of iron that is not removable *via* acid washing.

Table 16 : Results from XRF.

Oxide	Whichford Original (non-fired)
SiO_2	59.15
TiO_2	0.91
Al_2O_3	17.73
Fe_2O_3	6.2
MnO	0.04
MgO	1.5
CaO	1.3
Na_2O	0.54
K_2O	2.73
P_2O_5	0.15
LOI	7.57
TOTAL	97.83

It can be seen from the data in table 16 that SiO_2 and Al_2O_3 make up the biggest proportion of oxides in the material. Fe_2O_3 makes up the next biggest proportion of the total amount of oxides, ^{57}Fe Mössbauer spectroscopy has shown this to be present as Fe^{2+} and Fe^{3+}.

Calcium, sodium and potassium, which were also observed *via* XPS were additionally identified in the bulk, thus providing further evidence to suggest micas or montmorillonites.

TGA/DTA were used to determine the changes that occur as a result of the heating process and ultimately to provide information on thermal stability. The changes that occur as a result of heating also provide further indication of the mineral type present.

Interpretation of the data is consistent with that found in the literature.[54,55] The results obtained from analysis of the non-fired Whichford original clay (figure 47) are consistent with those expected.

---

[54] Ed. Miller, B., *Thermal Analysis,* Wiley, **1982,** 1.
[55] Ed. Mackenzie, R, C., *Differential Thermal Analysis,* Academic Press, London and New York, **1970,** 1.

Figure 47 :DTA/TGA trace of non-fired Whichford Original clay.

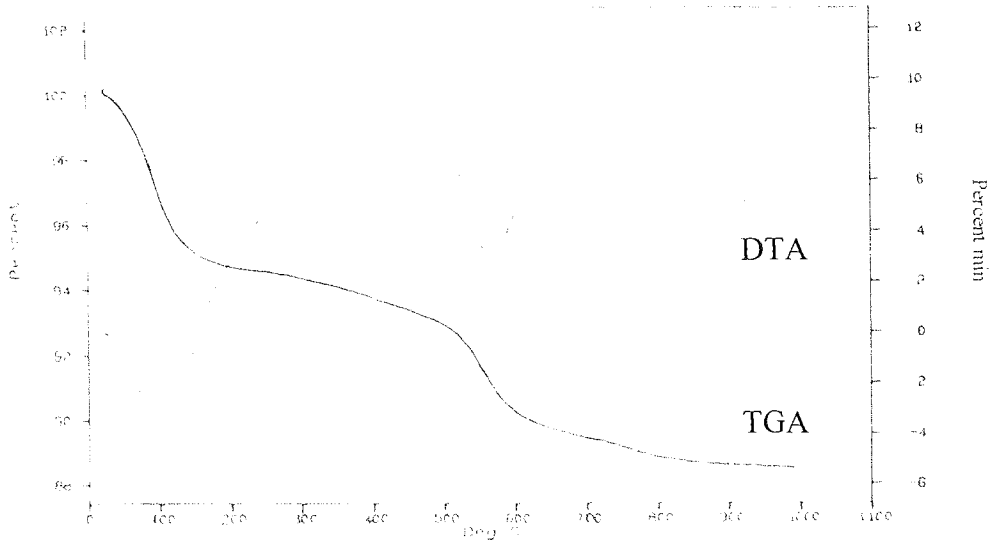

Table 17 : Interpretation of DTA curve for non-fired Whichford Original clay.

Temp °C	Comment
~100°C	Endotherm indicative of the loss due to loosely bound water.[53]
~400°C	Endotherm corresponding to loss of hydroxyl groups from $Mg(OH)_2$ in the brucite layer.[53]
~570°C	Attributed to a phase change of α-quartz to β quartz. Small shoulder may suggest the presence of two quartz structures. Typical inversion occurs around 573 +/-1°C this is affected by performing the experiment in air.[54]

Table 18 : Interpretation of TGA curve for non-fired Whichford Original clay.

Temp °C	Comment
~100°C	Loss probably due to loosely bound or sorbed water.[53]
~500-700°C	Dehydroxylation occurring as a result of the loss of interstitial water.[53]

The transitions observed on both the DTA and TGA curves for non-fired Whichford original clay correspond with literature data.[53,54] One at approximately 100°C corresponding to the loss of interlayer water and one between 500 – 700°C due to dehydroxylation due and the loss of interstitial water. These are supported by small broad endotherms on the DTA, at 100°C and 400°C with a suggestion of change of composition at ~900°C. It is thought that this final endothermic peak is due to the

breakdown of the anhydrous montmorillonite to an amorphous material from which new phases crystallise.

4.3 THE ANALYSIS OF NON-FIRED WHICHFORD T2.C CLAY.

The XRD data as shown in figure 48 for non-fired Whichford T2.C clay is representative of the other Whichford samples examined. From the data presented it can be seen that Whichford T2.C is a mix of clay and non-clay minerals. These like the original clay are predominantly montmorillonite, illite, kaolinite and quartz, respectively.

Figure 48 : XRD pattern of non-fired Whichford T2.C clay.

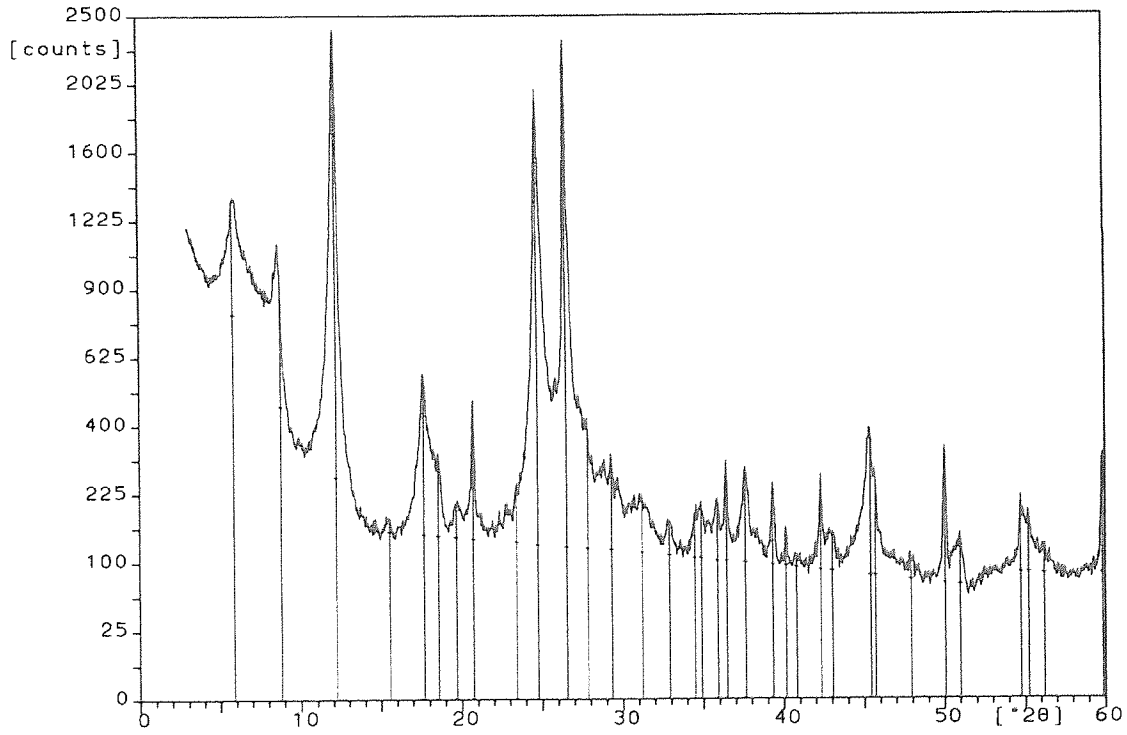

Table 19 : Interpretation of XRD pattern for non-fired Whichford T2.C clay.

2θ	d values (Å)	Assignment	Comment
6.12 17.86 23.55	14.43 4.96 3.78	Montmorillonite	Provide further evidence to support the presence of montmorillonite
8.92 26.68	9.91 3.34	Illite	Set of characteristic peaks corresponding to Illite.
12.36 24.74	7.16 3.60	Kaolinite	Medium intensity broad band suggests presence of kaolinite.
26.68 20.91	3.34 4.24	SiO_2	Very sharp peaks indicative of quartz.

The data do not show any further polymorphs of silica nor does it indicate at the present of iron although ^{29}Si and ^{27}Al MAS NMR spectra and ^{57}Fe Mössbauer spectroscopy later cited provide evidence for its existence. The lack of detection of iron *via* XRD may suggest that it is present as small particles.

The data obtained from the infra red analysis of non-fired Whichford T2.C clay (figure 49) is consistent with that obtained from non-fired Whichford original clay as shown in figure 42.

Figure 49 : Infra red spectrum of non-fired Whichford T2.C clay.

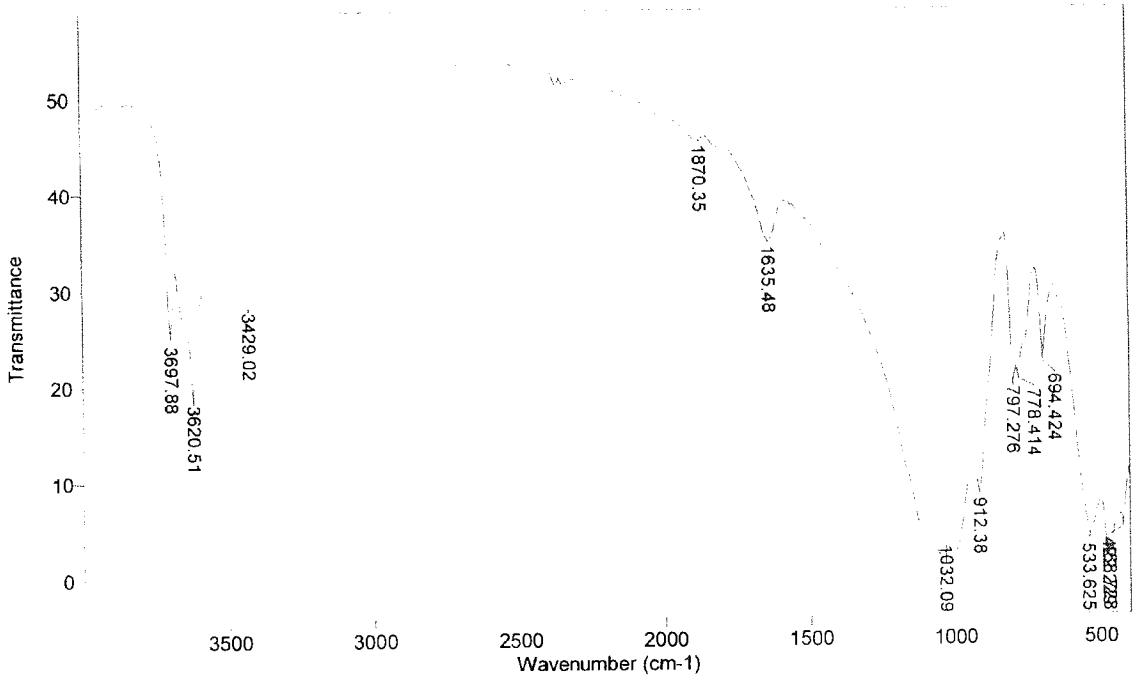

Table 20 : Interpretation of the Infra red spectrum of non-fired Whichford T2.C clay.

Absorption (cm^{-1})	Assignment	Comment
3697	H_2O	Type 1 water.[44] Doublet at 3697cm^{-1} and 3620cm^{-1} are indicative of a kaolin type mineral.[47]
3620	OH	Type 1 OH groups directly co-ordinated to the cation.[44] Broadness may suggest halloysite.[47]
3429	H_2O	Type II labile water as a result of weak intermolecular hydrogen bonds.[44]
1635	H_2O	Adsorbed water H-O-H bending maxima.[47]
1032	Si-O	In plane stretching vibration.[45]
912	Al-OH	Vibrations of Al-OH bonds in octahedral sheets.[45]
797 778	OH	Bending frequencies of OH.[45] Peak at 797cm^{-1} Associated with kaolin. May also suggest quartz.[47]
694	Si-O	Vibrations of Si-O.[45]
533	Si-O	Bending vibration.[45]

Again, infra red has shown the existence of silicon and aluminium in the tetrahedral and octahedral layers for the non-fired Whichford T2.C clay. The appearance of bands at ~3700cm^{-1}, ~3620cm^{-1} and ~3420cm^{-1} are indicative of type I and type II water thus the data are consistent with this being a non-fired clay. The predominant clay mineral appears to be kaolin as dictated by the nature of the peak at ~3700cm^{-1}. The broadness

of the peak at ~3620cm^{-1} suggests that this might be another member of the kaolin family, halloysite.

^{29}Si and ^{27}Al MAS NMR spectra as showed in figures 50 and 51 illustrate the environments in which silicon and aluminium are situated.

Figure 50 : ^{29}Si MAS NMR spectrum of non-fired Whichford T2.clay.

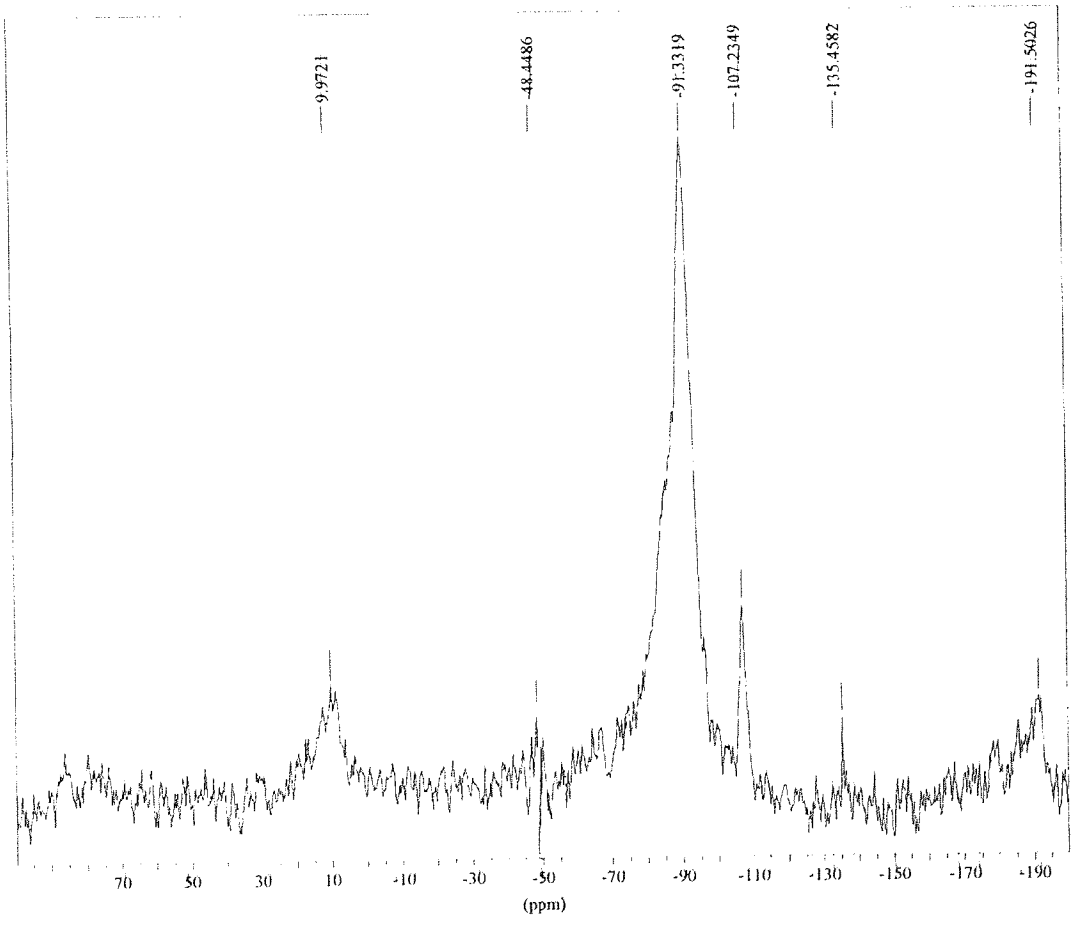

Figure 51 : ^{27}Al MAS NMR spectrum of non-fired Whichford T2.C clay.

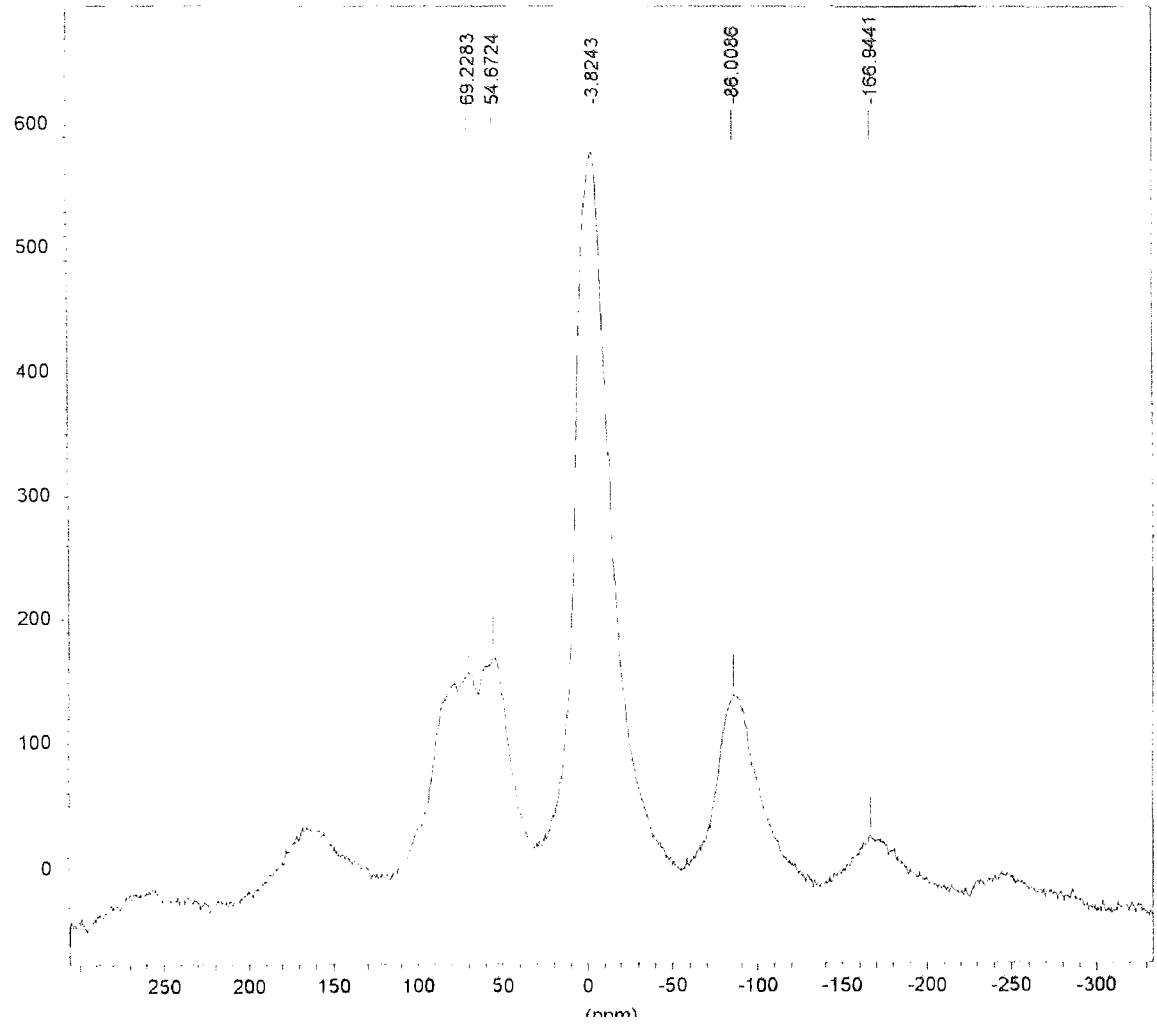

The strong sharp resonance at ~-91ppm shown on figure 50, is consistent with the appearance of silicon in a Q_3 co-ordination environment. The sharpness of the peak suggests silicon occupies an ordered environment that experiences little effect as a result of paramagnetic impurities. A much weaker resonance at ~-107ppm shows that some silicon also occupies a Q_4 environment. The nature of the spectrum suggests that paramagnetic impurities do not occupy sites close to active nuclei although their appearance is suggested by the presence of spinning side bands.

The ^{27}Al MAS NMR spectrum shows aluminium to be both tetrahedrally and octahedrally co-ordinated by resonances at ~-3ppm and ~54ppm, respectively. This corresponds with the information obtained from interpretation of the ^{29}Si MAS NMR spectrum. The positions of the spinning side bands are consistent with the appearance

of two resonant peaks. Paramagnetic impurities are not thought to be close to these active nuclei due to lack of distortion of resonant peaks.

^{57}Fe Mössbauer spectroscopy has shown there to be two iron species within the fired Whichford T2.C clay, as shown in figure 52.

Figure 52 : ^{57}Fe Mössbauer spectrum of non-fired Whichford T2.C clay.

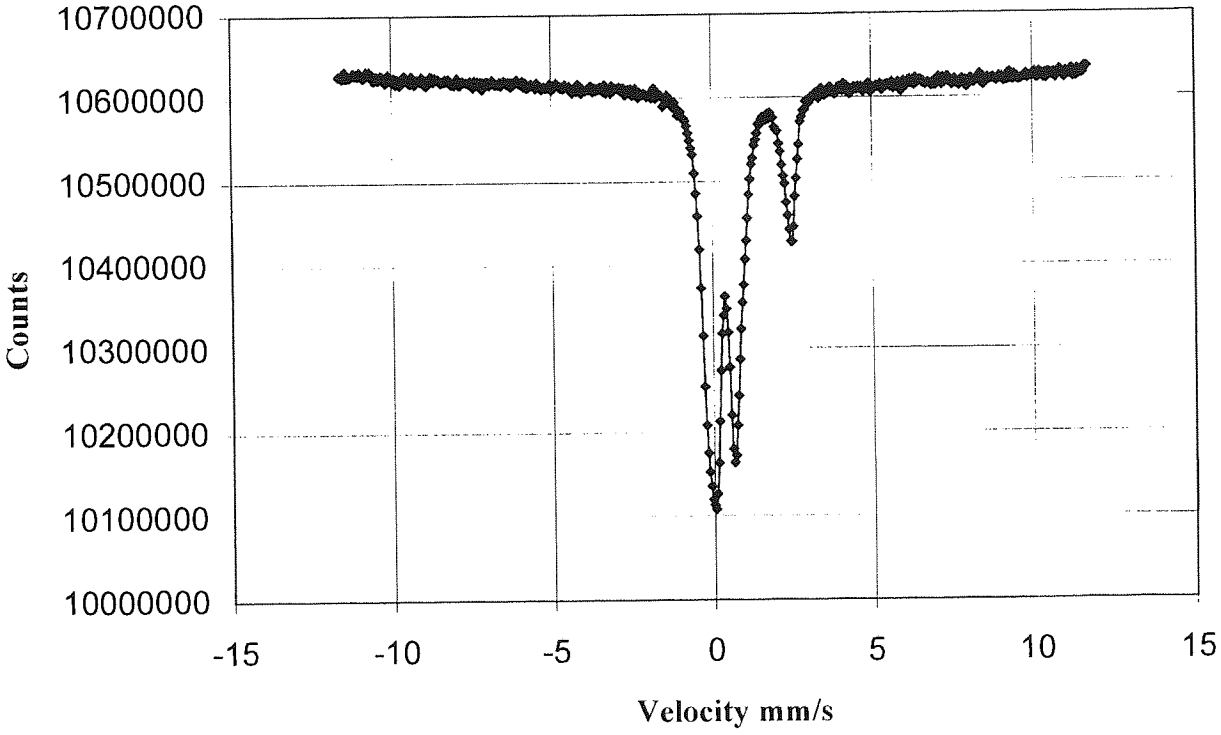

Table 21 : ^{57}Fe Mössbauer chemical shift data.

δ/mms^{-1}	Δ/mms^{-1}	Assignment
0.25	0.50	Fe^{3+}
1.23	2.52	Fe^{2+}

The spectrum shows the presence of both Fe^{3+} and Fe^{2+}.[56] The dominant doublet at 0mms^{-1} is consistent with the appearance of Fe^{3+} possibly as small particle

[56] Cranshaw, T, E., Dale, B.W., Longworth, G, O., and Johnson, C, E., *Mössbauer Spectroscopy and its applications,* Cambridge University Press, **1985.**

superparamagnetic α-Fe_2O_3. The weaker component of the spectrum at ~2mms^{-1} is indicative of the presence of Fe^{2+} although it is difficult to assign its form.

The surface analysis of fired Whichford T2.C clay by XPS has provided information to support the other conclusions and assumptions previously made. (figure 53) The data found is in agreement with that from other samples previously discussed.

Figure 53 : XPS spectra for non-fired Whichford T2.C clay.

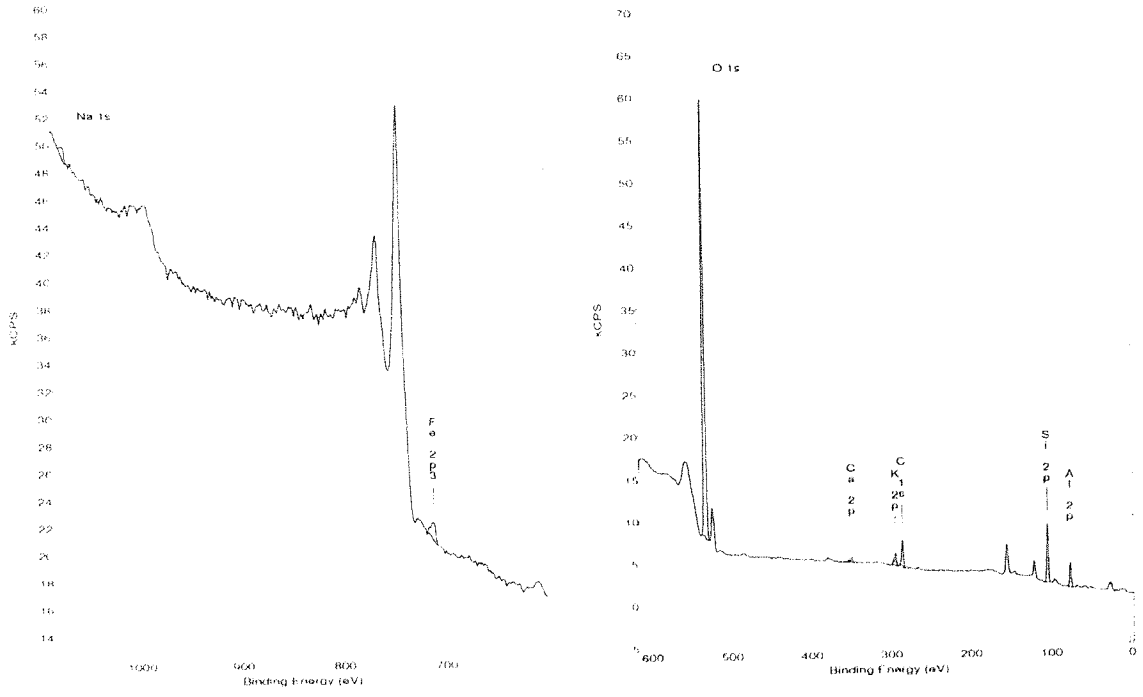

Table 22 : Interpretation of XPS spectra for non-fired Whichford T2.C clay.

Peak	Shell	Percent	Comment
Silicon	2p	20.2	As a result of silicon atoms in the tetrahedral layer.
Aluminum	2p	13.5	Due to Al in the octahedral layer.
Sodium	1s	0.6	Possibly an impurity however does suggest the presence of montmorillonite in the sample.
Potassium	2p	1.2	May be an impurity.
Oxygen	1s	53.8	As a result of Si-O and Al-O in the tetrahedral and octahedral layers respectively. Also due to OH/H_2O.
Calcium	2p	0.6	Suggests the presence of Ca mica/montmorillonite but may be an impurity.
Iron	$2p^3$	1.3	May be a structural moiety of Fe_2O_3.
Carbon	1s	8.8	Resonable to assume its presence, however may be a result of pump oil standard.

In conjunction with XPS, bulk analysis *via* XRF of the non-fired Whichford T2.C clay was performed, the data obtained from this is shown in table 23.

Table 23 : Results from XRF.

Oxide	Whichford New (non-fired)
SiO_2	63.16
TiO_2	0.99
Al_2O_3	18.37
Fe_2O_3	6.14
MnO	0.04
MgO	1.12
CaO	0.52
Na_2O	0.38
K_2O	2.87
P_2O_5	0.09
LOI	5.88
TOTAL	99.58

In addition to those elements identified *via* XPS, XRF has further identified inclusions of MgO, MnO, P_2O_5 and TiO_2. MgO can be attributed to $Mg(OH)_2$ of the brucite layers whilst the others do not attribute to any particular type of mineral.

TGA/ DTA are run simultaneously and used to determine the changes that occur as a result of the heating process and ultimately thermal stability. Changes that occur as a result of heating also provide further indication of the mineral types present.

The trace shown in figure 54 for non-fired Whichford T2.C clay shows similar patterns to that for the non-fired Whichford original clay, (figure 47).

Figure 54 : TGA/DTA trace of non-fired Whichford T2.C clay.

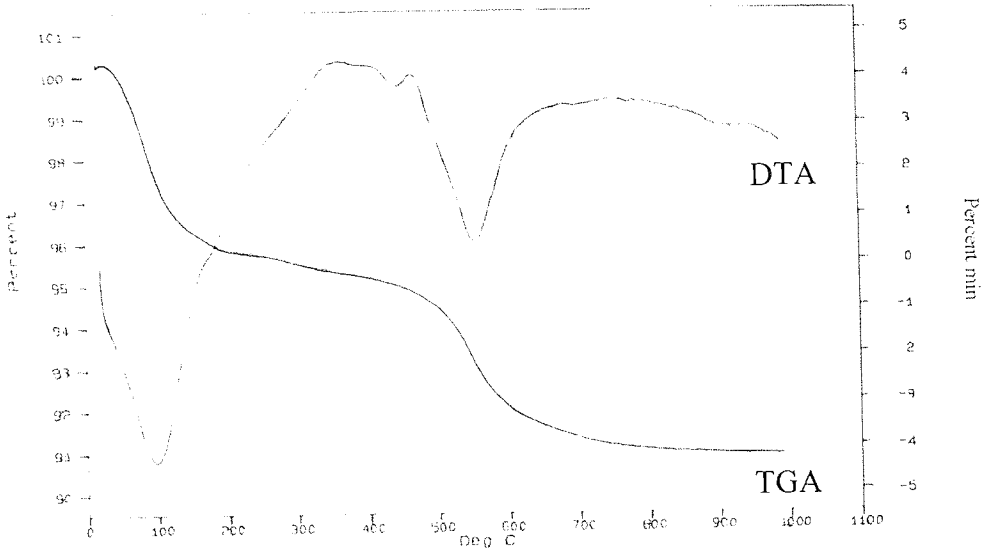

Table : 24 Interpretation of DTA curve for Whichford T2.C clay.

Temp °C	Comment
~100°C	Broad endotherm resulting from the loss of sorbed water. The endotherm is broader than that observed for Whichford Original clay this often signifies the presence of varying caions.[53,54]
~450°C	Small endothermic peak suggests the presence of Fe^{3+} substituting for Al^{3+}. The depression of the low temperature temperature dehydroxylation endotherm in relation to Whichford Original suggests the presence of more Fe^{3+} [54]
~570°C	Large broad endotherm represents the phase change from α-quartz to β quartz which exhibits greater stability.[54]
~850 – 900°C	Suggestion of a very small endotherm indicative of the Breakdown of anhydrous material to amorphous material.[54]

Table 25 : Interpretation of TGA curve for Whichford T2.C clay.

Temp°C	Comment
~100°C	Loss of sorbed, loosely bound water.[53]
~500-700°C	Dehydroxylation as a result of the loss of interlayer water.[53]

Whichford New clay exhibits defined transitions on its TGA. One at approximately 100°C and one at ~450°C corresponding to loss of interlayer water and dehydroxylation

due to loss of interstitial water, respectively. These are supported by small broad endotherms on the DTA, predominantly at 100°C.

DTA provides further data to suggest the presence of iron as Fe^{3+} substituting for Al^{3+} in the octahedral sites as dictated by the depression of the low temperature dehydroxylation endotherm at ~450°C.

Weight loss observed at ~570°C on DTA spectra is indicative of phase change of α-quartz to β-quartz which is more stable at higher temperatures. Typically inversion is observed at 573+/-1°C, however, performing the experiment in air will affect this.

DTA spectra for Whichford New clay presented a small further weight loss at ~850-900°C characteristic of the breakdown of anhydrous material to more amorphous material from which new phases crystallize. Overall weight loss as shown by TGA spectra was identical.

4.4 INFRA RED SPECTRA RECORDED FROM CALCINED WHICHFORD CLAYS.

The non-fired Whichford clays show identical mineral compositions when examined by infra red and only one set of results from the calcination experiments are therefore reported here, shown in figure 55.

Figure 55 : Infra red spectra of the calcined non-fired Whichford Original clay.

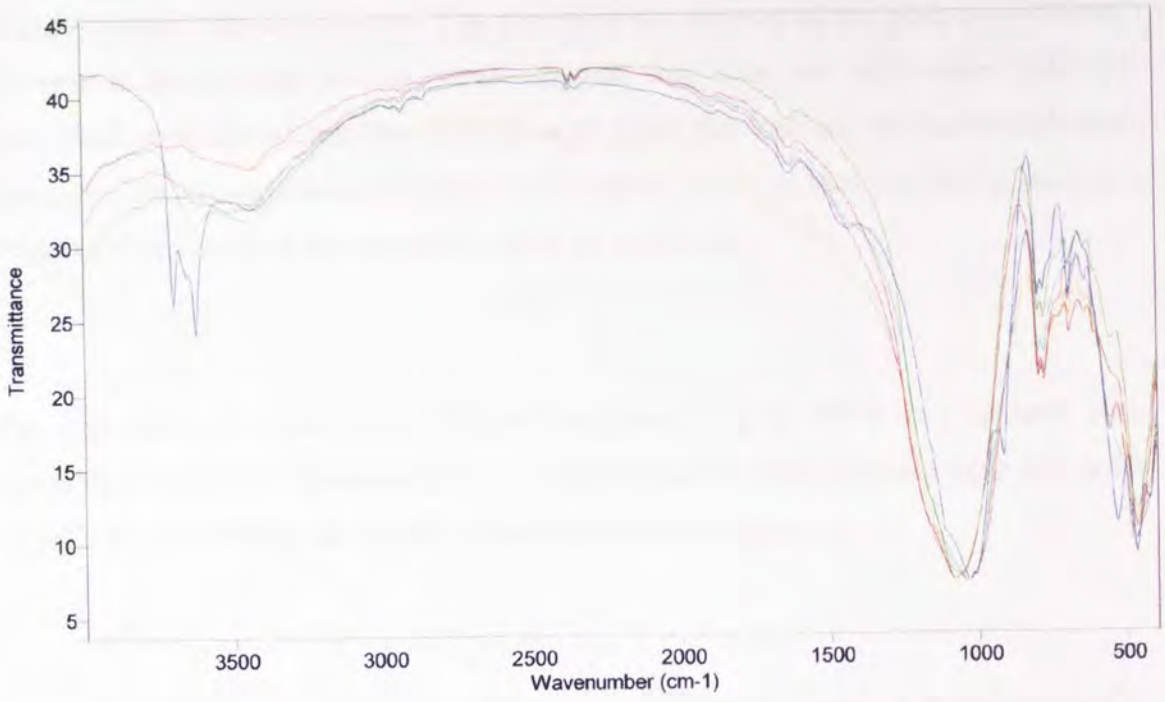

Blue line heated to 500°C

Turquoise line heated to 600°C

Yellow line heated to 700°C

Purple line heated to 800°C

Green line heated to 900°C

Red line heated to 1000°C

The spectra show the changes that occur as a result of the heating process. These changes imitate those that would occur during the firing process, since Whichford Potteries currently employ a heating process up to ~1020°C. The initial changes occurring up to 600°C are consistent with those that occur in kaolinite upon its dehydroxylation to metakaolinite.[46] The rate of loss of –OH associated with the cation as indicated by the band at ~3600cm^{-1} is decidedly rapid after 500°C. The bands at ~3600cm^{-1} and ~3400cm^{-1} consistent with the appearance of type I and type II water are of fairly equal intensity initially. The onset of dehydroxylation show these bands merging together to form a new broad band showing that some of the –OH groups are

taking on a different function, involving more hydrogen bonding. In conjunction with the disappearance of bands in this region, the band at ~1630cm^{-1} further consistent with absorbed water also disappears. The persistent appearance of the peak at ~3400cm^{-1} throughout the heating process would suggest that there are still some hydroxyls associated with the aluminium cations even after the loss of the octahedral sheet structure. The disappearance of bands in the region 912 – 913cm^{-1} by 600°C suggest a complete destruction of the octahedral sheet by this stage.

The appearance of a band at ~1850cm^{-1} on spectra up to 800°C is consistent with appearance of a small amount of $CaCO_3$ polymorph, its disappearance after this point suggests further heating has a detrimental effect upon its structure.

The band at ~790cm^{-1} appearing on all spectra is difficult to assign. It is possibly due to –OH bending frequencies perpendicular to the plane, however the position of the peak also suggests the presence of tridymite a further polymorph of silica. Bands in the region ~640cm^{-1} are attributed to Si-O vibrations, changes occurring at 800°C can be attributed transformations in phase through to quartz and/or cristoballite, XRD and NMR have already provided further information with regards to this.

By 1000°C all spectra show that complete loss of the clay structure has occurred with hydroxyl and Si-O peaks being the only ones observable. The appearance of two peaks at ~680cm^{-1}, by 1000°C suggests that further deformations may have occurred in the silicate framework

All spectra exhibit small bands in the range of ~2600 – 2900cm^{-1} indicative of adventitious carbonate.

4.5 CONCLUSIONS ON WHICHFORD CLAY ANALYSIS.

Characterisation of clay bodies has led to the identification of similarities and differences between Whichford original clay body and Whichford T2.C clay. Samples have been assessed in their raw and fired forms by the utilisation of a number of analytical techniques. Of particular interest has been the role of paramagnetic iron species within the clay structures as this is an important feature in obtaining adequate MAS NMR spectra.

Magnetic susceptibility measurements for all clay samples have shown a high susceptibility therefore confirming the presence of large amounts of iron to be present. Although this finding is useful it is purely qualitative.

^{57}Fe Mössbauer Spectroscopy has afforded far more significant data. The characteristic sextet pattern attributable to the presence of α-Fe_2O_3 is observed in the spectrum of fired Whichford original clay. This is indicative of large particle hematite whose removal *via* acid washing would be possible. It is unclear as to its appearance in the spectrum of non-fired Whichford original clay although a sextet pattern is suggested. In addition to this, spectra for all samples have shown characteristic peaks at ~0mms^{-1} and ~2mms^{-1} indicative of Fe^{3+} and Fe^{2+} respectively. Fe^{3+} will exist predominantly as small particle Fe_2O_3 that at elevated temperatures may exhibit superparamagnetism. In addition to this it is feasible to suggest some Fe^{3+} will be structural replacing Al^{3+} in the octahedral layer, in this instance it is not removable. Fe^{2+} is a more difficult moiety to assign although it could be attributable to an iron silicate. X-ray diffraction data have not afforded data to confirm the presence of iron it is therefore summarised that the majority of iron exists as small particle Fe_2O_3 that does not contribute to a significant basal spacing. XPS has highlighted iron as surface component , which is reflected in XRF that further supports the presence of hematite, forming ~6% of the total oxide composition of the clay samples. There is no obvious correlation between the amount of SiO_2/Al_2O_3 and the amount of Fe_2O_3. Differential thermal analysis exhibits an endotherm consistent with the replacement of Al^{3+} by Fe^{3+} in Whichford T2.C clay.

Further to the identification of iron as both a structural and loosely bound moiety analysis has provided a large amount of data regarding clay composition. ^{27}Al MAS

NMR has shown how the firing process increases the amount of aluminium present in the silicate framework. Infra red spectroscopy has also identified aluminium as Al-OH with absorptions at ~912cm^{-1} indicative of vibrations in the octahedral sheet. ^{29}Si MAS NMR spectra of non-fired clays have shown silicon to exist predominantly in a Q_3 co-ordination environment, with a smaller amount in the Q_4 region. Conversely spectra for fired samples show silicon in the Q_4 region to predominant although a small number still occupy Q_3 positions. The differences between the two sets of spectra indicate the transitions that occur in silicon environments during the firing process.

Infra red has been a valuable tool in tracking the changes that occur as a result of the calcinations process, it is assumed that these changes imitate those that occur as a result of the natural firing process. Whichford potteries currently employ a staged firing process up to ~1020°C.

The initial changes occurring up to 600°C are consistent with those that occur in kaolinite upon its dehydroxylation to metakaolinite.[46] XRD has confirmed the presence of kaolinite in the clay bodies. Within these early stages, the loss of loosely bound water is primarily observed, by ~700°C data suggests that all interlayer water has been removed. It is not until 800°C that changes in silicon environments are observed. TGA data present information to suggest that the transformation is from α-quartz to β-quartz the more stable form at elevated temperatures. Upon heating through to 1000°C further change in the silica environment is observed and now only a broad peak exists to suggest the presence of structurally bound hydroxyl groups. Infra red analysis of the basic raw clays provides data to support the typical clay structures with the presence of Si, Al, OH and H_2O predominating.

X-ray powder diffraction has provided most information regarding the nature of mineral inclusions within the clay bodies. Both Whichford clays provided very similar results, indicating a mix of both clay and non-clay minerals. High intensity sharp peaks at 20.97(2θ) and 26.74(2θ) are indicative of highly crystalline quartz. The mixture of broader bands on the spectra are more typical of the less ordered clay minerals of illite, montmorillonite and kaolinite.

XPS results suggest that montmorillonite may be present in both the calcium and sodium forms. Further analysis *via* XPS confirmed calcium to also be present in the form of gypsum ($CaSO_4$) which is eliminated by the addition of barium; this was further identified by XPS. Sulphur as SO_4^{2-} has been highlighted and identified as an impurity. The appearance of potassium in XPS spectra suggests micas to be present, however its lack in other spectra suggests that it is present on this occasion as an impurity. In addition to those elements identified by XPS and XRD, XRF has detected inclusions of MgO, MnO, P_2O_5 and TiO_2. MgO is attributable to $Mg(OH)_2$ of the brucite layers whilst the others do not correspond to any particular type of mineral.

In summary all clays appear to be a mix of both clay and non-clay minerals these being illite, kaolinite, montmorillonite and quartz respectively. Iron has been shown to be present as large particle α-Fe_2O_3, Fe^{2+} and Fe^{3+}. XRD leads to the belief that most is present as small particle Fe_2O_3 that does not contribute to a significant basal spacing and hence is not detected.

CHAPTER FIVE

5.0 INVESTIGATIONS INTO THE FIRING PROCESS.

5.1 INTRODUCTION.

The firing process used by Whichford Potteries involves gas firing, under slight positive pressure, of ¼ mm as measured by a water pressure gauge, although both 'pure' gas fired kilns with no pressure and electric kilns are sometimes used. The entire firing process takes up to 1-2 days depending upon the size of the vessels being fire; the final temperature of ~1020°C is achieved over a ten hour period and the vessels are then fired at this temperature for the remainder of the desired time. The use of pyrometric cones allows temperature to be monitored. Pyrometric cones, or pyroscopes as they are often termed, are clay bodies of standard shape and composition that when fired with the wares undergo sagging, the extent of which is indicative of the amount of heat work done on the vessels, although ultimately the whole process is controlled mechanically by use of a thermocouple. Whichford Potteries aim for an entirely oxidative environment as reduction leads to unwanted colour changes occurring within the clay. A strongly oxidising atmosphere in the kiln also enables the oxidation of carbon to carbon dioxide, so that all carbon can be burnt off before the surface of the ware vitrifies. Such unburnt carbon could later lead to undesirable reactions between carbon and iron within the mix.

In recent times Whichford Potteries have questioned the firing processes in use and have observed a number of problems to which solutions are required. One of the most important has concerned the fumes that are given off from the clays, as a result of the firing process. Of particular importance has been the identification of fluorine within the systems due to the formation of HF and its acidic nature. The interest therefore lies in the identification of cleaner clay systems. This involves the analysis of the raw material components that go into making Whichford original clay and the Whichford T2.C clay. The clay blends currently in use by Whichford potteries are;

- Whichford Original clay
  - ~50% Blockley Black clay
  - ~50% Naptan Yellow
  - ~ 3% Silver sand

- Whichford T2.C clay ~60% Blockley Yellow
  ~20% Reading
  ~20% Brosley P2
  ~ 4% Silver sand.

In addition to this Whichford have also noticed a phenomenon known as black hearting occurring within their products upon firing. This generally occurs within the clay bodies during firing in the range of 300 – 700°C and is a result of unburnt carbon in the mix reacting with iron present in the body. Unburnt carbon results in the reduction of iron to the ferrous form thus causing black hearting. Black hearts, which have undergone oxidation too late for the ferric iron to be bleached out result in red hearts. It is desirable that iron compounds should be oxidised to the ferric state, the colour of which can be bleached by oxides present in the body such as calcium oxide and alumina. To ensure the removal of carbon at low temperatures the kiln atmosphere must be strongly oxidising and the rate of heating slow. Although Whichford Potteries feel that they are fulfilling this criterion black hearting is still being observed and therefore there is a need to investigate this phenomenon further.

5.2 THE SEARCH FOR A CLEANER CLAY SYSTEM.

It is known that the range 300 – 700°C is particularly problematic as this is where a number of changes occur including the decompositions of carbonates and sulfides, which may be present as impurities, giving carbon dioxide and various oxides of sulfur. It is also the region in which inversion of α-quartz to β-quartz is observed. Of particular importance to Whichford Potteries has been the presence of fluorine and the acidic HF which when emitted as a gas is detrimental to the products and the environment. Whichford Potteries feel this is of particular relevance to their original formulation although both Whichford original and T2.C have been considered. The objective is to confirm its presence or absence. Gas analysis *via* the microwave pyrolysis of clay raw materials has been used as a means of determining the basic gases emitted. This has led to the determination of organic matter (see later). Fluorine was determined by ^{19}F MAS NMR.

5.2.1 AN INTRODUCTION TO ^{19}F MAS NMR IN CLAY SYSTEMS.

Fluorine is incorporated into the clay structure either during its formation or by hydrothermal alteration. The similarity of the F^- ion and OH^- ion in both ionic radii, 1.40 and 1.36Å, respectively, and electronegativity means that the substitution of OH^- for F^- is possible. It is suggested that F^- substitution for OH^- is linked to the Mg^{2+} ions of the octahedral layer.[57] The thermal stability of fluoride in clays provides further evidence for this.[56] The thermal testing of a variety of clays has shown that F^- is not lost until ~700 - 750°C. This coincides with the loss of clay structure due to dehydroxylation, suggesting that F^- is in the interior of the structure and at this temperature is eliminated as HF in conjunction with H_2O molecules formed by the condensation of –OH linked to Mg^{2+}.

There are only a few reports of the use of ^{19}F MAS NMR spectroscopy to gain structural information on clay systems. *Sanz and Santaren, 1990*[56] used relatively low resolution MAS NMR to obtain information regarding the location of fluorine in micas and sepiolite $[(Mg_{8-y-z}R^{3+}_y\square_z)(Si_{12-x}R^{3+}_x)O_{30}(OH)_4(OH)_2.R^{2+}_{(x-y+22)/2}(H_2O)_8]$ where □ represents a vacant site. *Huve et al*[58] have demonstrated the use of ^{19}F NMR in the structural determination of a variety of natural and synthetic 2:1 layer silicates.

^{19}Fluorine is an ideal nucleus for nuclear magnetic resonance as its 100% natural abundance and spin ½ make it identical to the proton, however the signal response for a given number of nuclei is 20% weaker.[59] The determination of fluorine in solution is easily characterized by the large chemical shift range of over 1000ppm. However, the elucidation of fluorine in a solid-state system such as clay is often problematic. There are a number of reasons for this. The resonances in ^{19}F MAS NMR spectra are intrinsically broad due to large gyromagnetic ratios resulting in strong dipole-dipole couplings. Fluorinated systems with large concentrations of protons must be proton decoupled. The proximity of ^{19}F and ^{1}H resonance frequencies makes this very difficult. In addition fluorine has large chemical shift anisotropies that produce strong

---

[57] Santaren, J., Sanz, J., and Ruiz-Hitzky, E., *Clays and Clay Minerals*, **1990**, 1, 63-68.
[58] Huve, L., Delmotte, L., Martin, P., Le Dred, R., Baron, J., and Saehr, D., *Clays and Clay Minerals*, **1992**, 2, 186 – 191.
[59] Mooney, E. F., *An Introduction to ^{19}F NMR Spectroscopy*, Heyden and Son LTD, **1970**.

spinning side bands under MAS conditions. These combine to make ^{19}F high resolution NMR spectroscopy generally problematic. Despite these problems there are literature reports[56,57,60,61,62] that demonstrate how solid state ^{19}F NMR is possible and the technical requirements needed to overcome such troubles. Clays generally only contain a few percent of fluorine and so are generally magnetically dilute. The high sensitivity of the nuclei means that adequate spectra are obtained from levels of only a few ppm. Although clays contain both H_2O and OH- groups in abundance the density of protons is not high enough to require proton decoupling. Therefore only the large ^{19}F chemical shift anisotropy is a problem.

Recent reports [57,58,59,63] of fast spinning techniques have shown how the effects of large chemical shift anisotropies can be reduced by spinning at speeds in the range of 12 – 16kHz. This is said to average out the homonuclear dipolar interactions between fluorines atoms with a consequent 10 – 20 fold reduction in line width being observed.[58]

The NMR spectra were obtained at room temperature on a Bruker AC-300 spectrometer at the carrier frequency of 282.4MHz. A zirconia MAS probe was used with a 7mm outside diameter. The spinning rate used was 5kHz with a pulse angle of 15°T. This was implemented so that the ^{19}F nucleus recovers its magnetisation and so can be pulsed faster. A relaxation delay of 0.5s was used. Chemical shifts were measured relative to an aqueous concentrated sodium fluoride solution accumulated over 360 scans. Corrections were made relative to trichlorofluoromethane ($CFCl_3$) in order to allow assignment of peaks comparative to those quoted in the literature. The first experiments used samples that had been ground into a paste with DMSO. It was anticipated that this would provide better spectral resolution. Later experiments used clays in their dry states and adequate spectra were obtained. The predominant peak seen in all spectra arises from the fluorinated components of the Kel-F (poly-(chlorotrifluoroethane)) spacers used during acquisition. A ^{19}F MAS NMR spectrum was obtained of Kel-F (figure 56) thus allowing satisfactory elimination of its peaks from subsequent spectra

---

[60] Harris, R, K., and Jackson, P., *Chemical Reviews,* **1991**, 91, 1427 - 1440
[61] Kreinbreck, A, T., Sazavsky, C, D., Pyrz, J, W., Nelson, D, G, A., and Honkonen, R, S., *Journal of Magnetic Resonance,* **1990**, 88, 267 - 276
[62] Labouriau, A., Kim, Y-W., Chipera, S., Bish, D, L., and Earl, W, L., *Clays and Clay Minerals,* **1995**, 43, 697 - 704

and also confirmation that the technique being used is satisfactory for the identification of fluorine.

Figure 56 : ^{19}F MAS NMR spectrum of Kel-F spacer component, relative to $CFCl_3$.

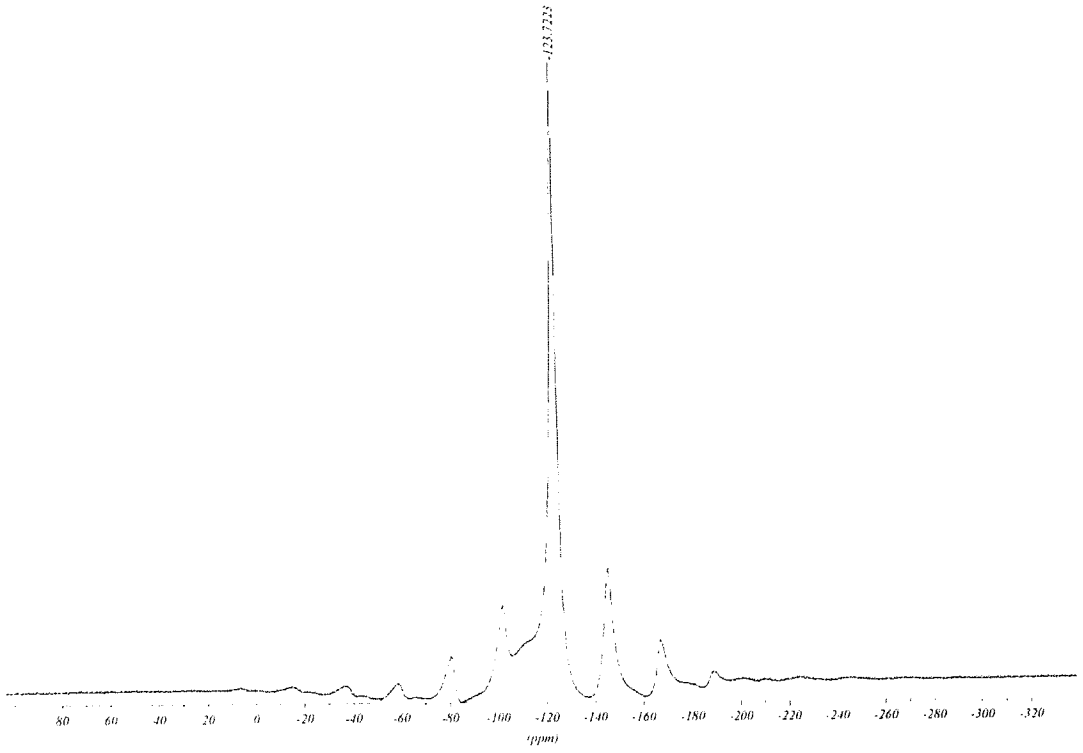

^{19}F MAS NMR analysis were performed on all of the raw materials used in the formulation of Whichford blends, these being,

Blockley Black
Naptan Yellow
Blockley Yellow
Reading
Brosley P2

In addition to the above, the raw clay blends of Whichford original and Whichford T2.C were examined.

---

[63] Clark, J, H., Goodman, E, M., Smith, D, K, Brown, S, J., and Miller, J, M., *Journal of the Chemical Society, Chemical Communications*, **1986**, 657 – 658.

5.2.2 GAS ANALYSIS *VIA* MICROWAVE PYROLYSIS OF WHICHFORD CLAYS.

Further to the identification of fluorine within the clay bodies additional analyses were performed to recognize the other gases emitted as a result of the firing process. This was studied by gas chromatography. Microwave heating was chosen as the method for pyrolysis of the clay samples as it allows similar temperatures to those used in the firing process to be obtained, but over a much shorter time period. The samples used for study were identical to those used in fluorine analysis and gases emitted were measured against standards using gas chromatography. The carrier gas used was helium with a flow rate of 30 m/s min^{-1} and a sample size of 1ml. The detector method was thermal conductivity, with a 5Å molecular sieve as the stationary phase. The detector is highly insensitive to the detection of hydrogen as its thermal conductivity is very similar to that of helium, although its presence can still be suggested. Any tar collected in the condenser after microwave pyrolysis was tested for organic content by washing with organic solvents such as dichloromethane, methanol and acetone. The solvent is allowed to evaporate off leaving any organic residue for analysis *via* infra red and NMR.

5.2.3 STANDARDS USED FOR THE IDENTIFCATION OF GASES EMITTED.

- N-Butane (100ppm), Ethane (99.8ppm), N-Hexane (96.1ppm), Methane (101ppm), N-Pentane (107ppm) and Propane (100ppm) in Nitrogen.
- 1% Methane, Ethane, Propane and N-Butane in Nitrogen.
- 1.27% Methane, 1.27% Ethylene, 100% Propylene and 1.04% N-Butylene in Nitrogen.
- 10% Carbon dioxide in Nitrogen.
- 0.992% Methane in Nitrogen.
- 1.00% Carbon dioxide, 1.00% Carbon monoxide, 1.00% Hydrogen and 1.00% Methane in Nitrogen.

- 5.99% Oxygen in Nitrogen

- 10% Carbon monoxide in Nitrogen.

- 15.00% Carbon dioxide, 7.03% Carbon Monoxide, 4.50% Methane and 7.06% Oxygen in Nitrogen.

The results obtained from these analyses will be presented as percentage concentration of the gases emitted, (see later) where one hundred percent is the total amount of gas analysed by the gas chromatograph.

The final stage of the investigations into the processes that occur during the firing of Whichford clays was the search for black hearts.

Black hearts are formed by the oxidation of iron to the ferrous state. This is detrimental to the appearance of Whichford Pottery wares as well as producing inferior products. Whichford Potteries currently employ two staggered firing processes one for the existing clay products and one for the new T2.C formula. The work performed has involved mimicking the processes used and observing black heart phenomenon.

The method used involved the firing of clay discs of uniform dimensions overnight in a furnace. The clay discs were evenly stacked using spacers and all discs were examined after firing for any signs of the black heart phenomenon.

The firing processes imitated are as follows:

Process one.

0°C – 300°C over 17 hours, 300 – 800°C over 5 hours and 800°C – 1000°C over 5 hours.

Process two.

0°C – 350°C over 17 hours, 350°C – 900°C over 4¼ hours and 900°C – 1000°C over 6¾ hours.

The results obtained (see later) aid in providing an overall view of the nature of Whichford Potteries clays during the heating process.

5.3 RESULTS FROM INVESTIGATIONS INTO THE FIRING PROCESS.

The investigations performed involved the analysis of all of the raw materials used to formulate the Whichford blends these being,

Blockley Black
Naptan Yellow
Blockley Yellow
Reading
Brosley P2.

In addition raw blends of Whichford original and Whichford T2.C were examined.

The ^{19}F MAS NMR spectra obtained for the above samples produced very similar spectra with resonance peaks in the range –110ppm to –116ppm. The spectrum shown in figure 57 is typical of those obtained from analysis of Whichford clays.

Figure 57 : Typical ^{19}F MAS NMR spectrum obtained from Blockley Black clay. (relative to NaF)

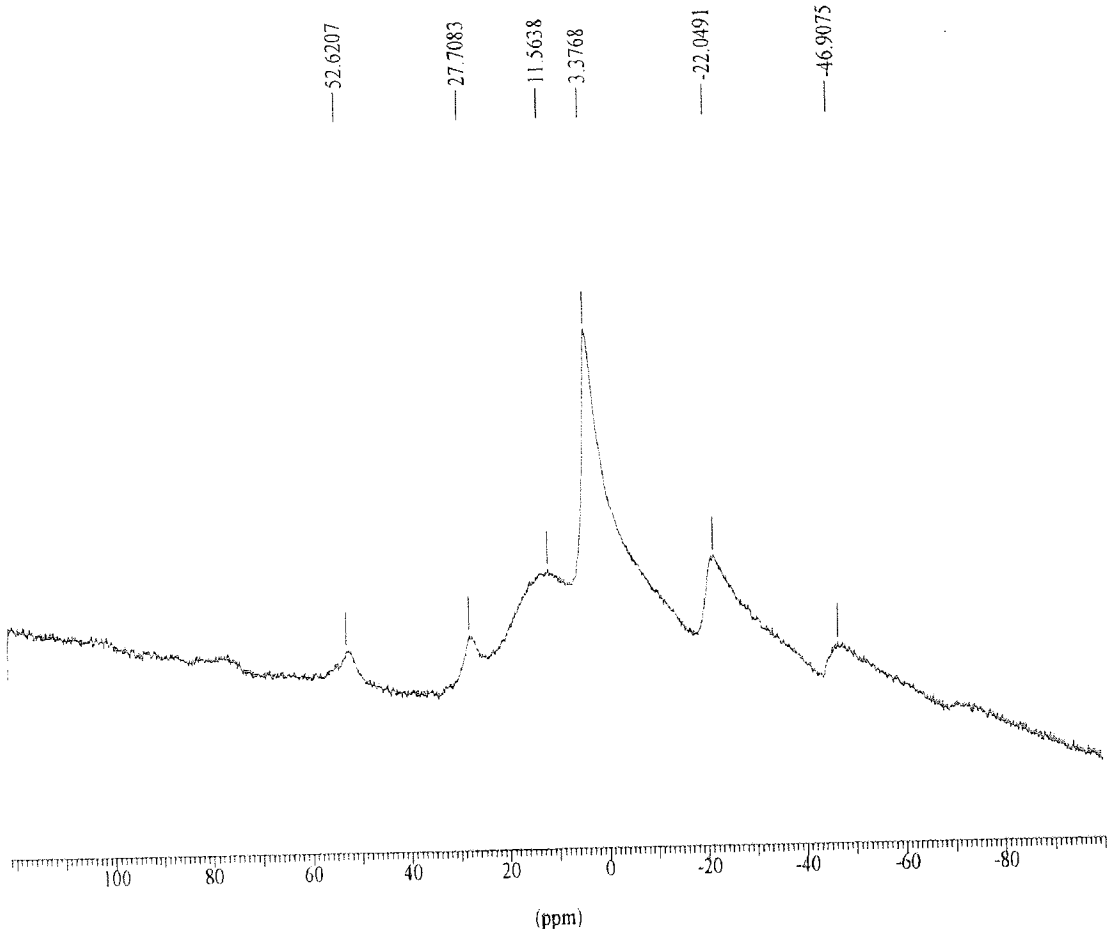

The sharp resonance observed at ~3ppm in figure 57 is attributed to the presence of fluorine from the Kel-F rotor used during acquisition of the spectrum. The small peak alongside this at ~11ppm is indicative of the presence of fluorine within the clay systems. The additional peaks at -22ppm, -46ppm, 27ppm and 52ppm are spinning side bands resulting from both the clay fluorine and Kel-F chemical shifts. The broadness of the fluorine peak is a result of large chemical shift anisotropies (CSA) attributable to the ^{19}F nucleus. A better resolution could be achieved by spinning at speeds greater than the CSA of fluorine, however this was not possible with the equipment available. All spectral peaks were adjusted relative to $CFCl_3$ so that comparisons could be made with literature reports where $CFCl_3$ is used as a standard. The adjustments were made by measuring the position of NaF (120ppm) peak relative to a standard $CFCl_3$ (0ppm) solution and numbers subtracted accordingly. This provided ^{19}F resonant peak positions for the Whichford clays in the range of -110ppm to -116ppm. It has not been possible

to quantify the amount of fluorine present. All Whichford clays examined produced silimar spectral patterns.

Table 26 : ^{19}F chemical shifts of Whichford clays relative to $CFCl_3$.

SAMPLE	^{19}F CHEMICAL SHIFT (ppm)
Whichford original	-110
Whichford T2.C	-115
Blockley Black	-115
Naptan Yellow	-116
Blockley Yellow	-116
Reading	-111
Brosley P2	NONE DETECTED

Interpretation of these data on their own is difficult as fluorine chemical shifts are dependent upon their environment and these will vary for different types of clays. In order to aid the interpretation of the fluorine chemical shifts, data from X-ray powder diffraction and infra-red analyses previously performed are discussed further (figures 41 and 42, tables 12 and 13, respectively). These provided an indication of the main clay component and hence the environments that may be surrounding the F^- ions.

Both the XRD pattern (figure 41, table 12) and the infra red spectrum (figure 42, table 13) provide an indication as to the main clay mineral components of the Whichford raw materials. The spectra obtained for all Whichford clays examined produced similar spectral patterns, therefore the interpretation is consistent throughout. Both sets of data have clearly identified the presence of the kaolin mineral, whilst the X-ray powder diffraction pattern has also shown montmorillonite to be present. The discrepancy between these sets of data may be the result of montmorillonites, being only present in small quantities and hence not enough to be detected *via* infra red analysis; hence kaolin must be the major component. This may also account for the presence of only one peak in ^{19}F MAS NMR spectra and not the two that would be anticipated for a mix of 1:1 and 2:1 layer silicates. The observed shift in the position of the resonance peak for the different Whichford clays may therefore be a result of differences in the Al_2O_3/MgO

ratio of the montmorillonite mineral present. This phenomenon was also observed by *Labouriau,A, 1995*[59].

It is therefore assumed that the ^{19}F resonance being observed is a result of the 1:1 type kaolin mineral that appears to predominate as the main clay component of Whichford clays. Kaolin minerals contain two types of hydroxyl site in a ratio of 1:3; these are the inner and the interlayer (inner surface) hydroxyls. Both sets of hydroxyls will undergo substituition by fluorine although the extent to which substitution occurs on the inner hydroxyls is less, as they are less willing to undergo exchange. Literature reports[59] have shown that both the inner and interlayer fluoride ions give rise to similar chemical shifts and therefore 1:1 layer silicates only give rise to one resonant peak as observed in Whichford clay spectra.

Although a separate resonance is not observed for the substitution of fluorine into the montmorillonite component of the clay, montmorillonite is still seen to be present within Whichford clays and therefore must be discussed. There are again two possible sites into which the fluorine could substitute. These are hydroxyls attached to {Al-Al-□} and {Al-Mg-□}, where □ represents a vacant site. Observations made by *Huve et al*[55] show that fluorine in montmorillonite is not evenly distributed within these sites but is ordered preferentially into {Al-Mg-□} sites over {Al-Al-□} sites. It is therefore concluded that fluorine, if present within the montmorillonite component of the clay, is substituting for hydroxyls directly bonded to {Al-Mg-□} sites.

It is therefore concluded that the single resonance observed in the ^{19}F spectra of Whichford clays is indicative of fluorine as a component of the 1:1 layer silicate kaolin.

The results shown in table 27 from gas chromatography provide an indication of the other gases that are emitted from Whichford clays during the firing process.

Table 27 : Gas analysis data.

	% CONCENTRATION OF GASES EMITTED						
SAMPLE	H_2	O_2	N_2	CO_2	CO	SO_2	$C_1 - C_5$
Whichford Original	0.050	0.24	99.30	0.41	Neg	×	Neg
Whichford T2.C	0.035	Neg	98.77	0.74	0.36	×	Neg
Blockley Black	0.027	0.21	98.73	0.86	0.17	Neg	Neg
Naptan Yellow	0.017	0.40	98.30	0.92	0.37	×	Neg
Blockley Yellow	0.036	0.61	98.41	0.74	0.21	×	Neg
Reading	Neg	0.34	99.04	0.62	Neg	Neg	Neg
Brosley P2	Neg	0.22	98.80	0.99	Neg	Neg	Neg

The percentages indicated are out of one hundred percent, where this is the total amount of gas analysed by the gas chromatograph.

Neg : Indicates where only negligible amounts of that component were detected. The amounts of these cannot be quantified suffice it is to say they are present.

× : Indicates that this component was not detected.

Nitrogen is observed as the major gas component of each sample. This is a result of nitrogen's being used to create an inert atmosphere within the microwave cavity during experimentation. Care was taken during sampling to restrict the amount of nitrogen allowed into the gas-bag, however this is difficult to regulate.

Although the experiment was carried out under an inert nitrogen atmosphere it is seen that some oxygen was still present and resulted in the oxidation of carbon to carbon monoxide, whilst carbonates and sulfides present as impurities generate the corresponding dioxides, thus explaining the presence of both CO_2 and SO_2. Both of these in significant quantities give rise to atmospheric contamination. It is unlikely that at the level identified these will present a problem. Build up of sulfur dioxide within the kiln during firing may be harmful to the ceramic wares, a problem of which Whichford Potteries must be aware. From an environmental point of view it is also necessary to mention that oxides of nitrogen and sulfur from high temperature combustion are

readily dissolved in water droplets. On a grand scale this is important in terms of acid rain and atmospheric contamination. On the small scale the acids formed will be detrimental to ceramic the wares.

The width of the base of the peak on some of the gas chromatograph peaks indicates the presence of methane. Analysis has shown the presence of $C_1 - C_5$ alkanes and alkenes such as butane, propane, ethylene and N-butylene. It is not possible to quantify the amount present but they appear to be small.

Data have shown that the gases coming directly from Whichford clay blends and the raw materials during processing are of relatively low concentration and although potentially harmful, the amounts are not significant enough to be problematic. This analysis has therefore shown that overall Whichford blends and raw materials can be considered as relatively innocuous.

The attempts at extraction of pyrolysis tar with the solvents dichloromethane, acetone and methane showed that the organic content of the clays is negligible. None of the clays tested produced any useable residue after evaporation of the washing solvent.

The final investigation into Whichford clays was the search for black hearting. The processes imitated have been described earlier in section 5.2.1. The results obtained were not as anticipated, as the visual analysis of the fired tiles never showed any signs of blackheart phenomenon, nor were any deformations seen. The overall shape of the discs did not change whilst the colour turned to that typical of a fired ceramic product.

The lack of the blackheart phenomenon in the clays fired in the small kiln suggests that there is nothing fundamentally wrong with the process being used. It is possible that the much larger kilns used by Whichford Potteries may be the cause of the problem. It has been suggested that Whichford might consider employing a longer initial heating to 300°C. The current 17 hour period may not be long enough for a kiln of considerable size to heat fully. A full 24 hour period is suggested. The most important region of the heating process is that between 300°C and 750°C as this is when carbonaceous material is removed and when the transformation of iron oxides to their ferric state occurs. It is suggested that this process could also be lengthened to accommodate the full removal of

all impurities. It is also imperative that wares within the kiln are adequately spaced to allow the circulation of oxygen and full oxidation to occur. The final stage of the process might well be of equal length to the second stage to allow the complete removal of fluorine as HF. Again adequate spacing of vessels will allow its free flow from the kiln and prevent it being trapped and hence spoiling of products.

5.4 CONCLUSIONS

The ^{19}F MAS NMR spectra of Whichford clays have confirmed the presence of fluorine in the Whichford raw materials by the appearance of a weak resonance in the –110 to –116 ppm region. It has not been possible to quantify the amount present, however it is possible, with the help of XRD and infra red spectroscopy, to provide an idea of the environment of the fluorine ions.

XRD and infra red analysis provided data that show the Whichford clays to be a mix of predominantly 1:1 and 2:1 layer silicates, namely kaolinite and montmorillonite. It is assumed that kaolinite is the major component as it is identified by both techniques The lack of detectable montmorillonite peaks in the XRD pattern suggests it to be only present in small quantities.

Kaolin as a 1:1 layer silicate has two hydroxyl sites available for substitution by fluorine ions, these are inner and interlayer –OH. Both sets are directly bonded to two cations of the octahedral sheet, in addition to this the interlayer –OH have associated with them a vacant site. The inner and interlayer hydroxyls are able to undergo exchange with fluorine, however the interlayer -OH is often less willing to undergo exchange. Literature reports[59] state that substitutions in both positions lead to similar chemical shift patterns therefore explaining the appearance of a single resonance on the Whichford spectra.

It has been assumed that montmorillonite is present in much smaller quantities than the kaolinite component. This explains why only one resonance was observed in the MAS NMR spectra and why its presence is only identified *via* infra red spectroscopy.

Montmorillonite is a 2:1 layer silicate and is therefore a more complex material than the 1:1 layer silicates. Again there are two sites available for substitution by the fluorine ion, these are –OH attached to {Al-Mg-□} and {Al-Mg-□}. Literature reports[55] have shown that fluorine within these clays is not statistically distributed and there is a greater affinity by F for –OH groups attached to {Al-Mg-□}. It can therefore be supposed that fluorine present in Whichford clays in the montmorillonite component are substitutes for –OH directly bonded to {Al-Mg-□} sites.

Fluorine is present in the Whichford clay samples. It is located structurally in the interior of the clay minerals and, upon heating, is eliminated as HF in the region of 700 – 750°C, in conjunction with H_2O formed by the condensation of –OH linked to Mg^{2+}.

Although it has not been possible to quantitatively determine the amount of fluorine present the small size of peaks on the MAS NMR spectra is noted. This is also reported elsewhere in literature[54,55,56,57,58,59] with F- only usually present in ppm quantities.

Further analyse of gases by the microwave pyrolysis of Whichford clays led to the identification of a number of gases, dihydrogen, dioxygen, dinitrogen, carbon dioxide, carbon monoxide, sulfur dioxide and C_1-C_5 alkanes/alkenes. The presence of dioxygen may result in the oxidation of some of the carbon to carbon monoxide. The carbonates and sulfides present as impurities will give the corresponding dioxides, hence the presence of SO_2 and CO_2. In large quantities these would give rise to atmospheric pollution but it is unlikely to be problematic in the quantities present. SO_2 can be harmful to ceramic wares if allowed to build up in the kiln. The production of both NO_2 and SO_2 from high temperature combustion is common. These are readily dissolved in water droplets which lead to acid rain and further atmospheric contamination. On the small scale involved here this is unlikely although the resultant acids formed are detrimental to ceramic wares. The presence of C_1 – C_5 alkanes and alkenes was observed but only on a very small scale.

It is fair to say that the low concentration of gases as a result of the pyrolysis of Whichford clays is environmentally insignificant, however allowing them to build up in

the kiln could be detrimental to the ceramic wares being fired. Analysis of pyrolysis tar by treatment with solvents revealed a negligible organic content in all clays examined.

Black heart in Whichford ceramic wares was not observed. This led to the conclusion that the size of the kiln plays an important role. It is therefore suggested that Whichford employ longer heating times through the period 300 – 700°C to ensure the removal of carbon which if left will lead to the formation of black hearting.

CHAPTER SIX

6.0 CATION EXCHANGE AND THE INFLUENCE ON THE PHYSICAL PROPERTIES OF CLAYS.

6.1 INTRODUCTION

The exchange of cations into smectite clays is well known[32,64,65] (see section 1.4.1). It is the cations outside the silicate lattice existing mainly in the interlayer region that undergo exchange. This is usually performed by treatment with an aqueous solution of the desired cation, for example if Na^+ were the desired cation to be exchanged into the clay then an aqueous solution of NaCl would be used.

The nature of the cation within the interlayer region does not affect the silicate structure of the clay but it will influence the properties of the clay, therefore in changing the interlayer cation through the cation exchange process it is inevitably altering the physical properties of the clay.

There are a number of reports in the literature describing how the nature of the interlayer cation affects the dehydroxylation process upon heating and furthermore how the cation is thought to be linked to the appearance of five co-ordinate aluminium, a transient form of aluminium occasionally observed during the heating process where the change from octahedrally co-ordinated aluminium in the non-fired state to tetrahedral aluminium in the fully fired state, occurs. Both facets are discussed within this chapter.

The majority of the exchange reactions discussed herein have been carried out using microwave methodology with reactants in an aqueous environment. The benefits of microwave methodology have already been extensively discussed in section 1.7. All the exchange reactions discussed have been performed on an Na^+ intercalated Wyoming Bentonite species with subsequent exchanged cations being Cu^{2+}, Li^+ and K^+. The successive calcination reactions used to observe the dehydroxylation/dehydration process and the appearance of five co-ordinate aluminium were performed in a programmable oven using 0.5g of sample at 300°C – 1000°C. The temperature ramp

---

[64] Bond, S.P., PhD Thesis, CEAC Department, Aston University, **1991.**
[65] Grimshaw, R.W., and Harland, C.E., *Ion-Exchange : Introduction to theory and practice,* The Chemical Society Monographs for Teachers No. 29, **1975.**

was 4°C min^{-1} and each temperature was held for one hour before the removal of the sample from the oven.

6.1.1 CATION EXCHANGE AND FIVE CO-ORDINATE ALUMINIUM.

The ^{27}Al quadropolar nucleus is probably the most studied nucleus in solid state NMR spectroscopy. Its applications in clay chemistry have been extensively explored[47,66,67,68] especially in the identification of octahedrally and tetrahedrally co-ordinated aluminium. It has been shown how octahedral Al yields isotropic chemical shifts in the region –10 – 20ppm, whilst four co-ordinate aluminium is observed between 50 – 80ppm. The transition from octahedrally bound aluminium to tetrahedrally co-ordinated aluminium occurs during the heating process and is a result of dehydroxylation.

More recent reports have shown peaks in the range of 31 – 37ppm which have been assigned to 5-coordinate aluminium.[49,50.] The difficulties found in detecting 5 co-ordinate aluminium have been associated with the overall instability of this co-ordination environment combined with a ~90% loss in intensity of ^{27}Al NMR signal intensity upon dehydroxylation.

The formation of five-coordinate aluminium during dehydroxylation could occur in two ways,

- Hydroxyl groups could join in such a way that columns of 5 co-ordinate aluminium are formed interspersed with 4- and 6- co-ordinate aluminium.

- The elimination of all hydroxyl groups leading to the formation of 5 co-ordinate aluminium only.

---

[66] Plee, D., Borg, F., Gatineau, L., and Fripiat, J.J., *J.Am.Chem.Soc.* 107, 2362 – 2369, **1985.**
[67] Kinsey, R.A., Kirkpatrick, R.J., Hower, J., Smith, K.A., and Oldfield, E., *American Mineralogist,* 70, 537 – 548, **1985.**
[68] Schroeder, P.A., Pruett, R.J., and Hurst, V.J., *Clays and clay Minerals,* 46, 429 – 435, **1998.**

Therefore if 6-, 5- and 4- coordinate aluminium are all observed then either the first pathway is being followed, or the second pathway is occurring but is incomplete.

It has further been reported[49] that in those clays that do not contain any charge balancing cations, 5 co-ordinate aluminium is more readily observed, as it is generally present at a higher concentration. It is suggested that the charge balancing cation plays an important role in determining the pathway of dehydroxylation from 6-5-4 co-ordinated aluminium.

The work to assess the effect of the interlayer cation on the appearance of 5 co-ordinated Al has been carried out using Wyoming Bentonite clay exchanged firstly with Na^+, to produce a mono-ionic species from which other exchange reactions can take place. Subsequent reactions exchanged the Na^+ for Cu^{2+}, Li^+ and K^+

Further studies looking at the effect of interlayer cation upon dehydroxylation using TGA/DTA analysis have also been performed.

6.1.2 CATION EXHANGE AND THE DEHYDROXYLATION PROCESS.

The replacement of the natural inorganic cations that are found in the interlayer region, usually Na^+ of Ca^{2+}, by other inorganic cations will act to modify the properties of clay and hence the process that is observed *via* dehydroxylation/dehydration.

The dehydration of a clay mineral occurs in the range of 100°C – 300°C and is due to the loss of physisorbed water and some of the water molecules surrounding the cation. Dehydroxylation occurs in the range of 500°C – 1000°C. During this heating period the residual water molecules bound to the interlayer cation will be removed, with breakdown of the structure beginning to occur. This may eventually lead to some recrystallisation.

It has been demonstrated in many literature reports[69,70,71,72,73] that Thermal Gravimetric (TGA) and Differential Thermal (DTA) Analysis are useful tools for the study of the

---

[69] Koster Van Groos, A.F., and Guggenheim, S., *American Mineralogist,* 74, 627 – 636, **1989**.

dehydration/dehydroxylation of cation exchanged clay materials. In addition evidence from infra red analysis[69,74] has also been found to support the trends observed *via* TGA and DTA. Interpretation of data follows a similar pattern to that already adopted here and described in chapter three.

The specification of the temperatures on a DTA pattern is subject to discussion in the thermal analysis literature.[56] For the purpose of the results presented herein, the specfic temperature is taken as the midpoint of the peak from where the curve starts to its rapid return to the baseline, since at this point the thermal event or reaction is considered nearly complete. If more than one thermal reaction occurs at approximately the same temperature then the signals of both reactions will be additive so the temperature of each separate peak is difficult to determine.

Because all cation exchange reactions were performed under ambient conditions from the mono-ionic Na^+ form of Wyoming Bentonite, it is reasonable to assume that any observed differences between DTA traces are related to the interlayer chemistry, i.e. cation size, type and charge.

---

[70] Koster Van Groos, A.F., and Guggenheim, S., *American Mineralogist,* 72, 1170 – 175, **1987**.
[71] Koster Van Groos, A.F., and Guggenheim, S., *American Mineralogist,* 69, 872 – 879, **1984**.
[72] Koster Van Groos, A.F., and Guggenheim, S., Clays and Clay Minerals, 34, 281 – 286, **1986.**
[73] Mosser, C., Michot, L.J., Villieras, F., and Romeo, M., *Clays and Clay Minerals,* 45, 789 – 802, **1997**.
[74] Tettenhorst, R., *The American Mineralogist,* 47, 769 – 772, **1962**.

6.2 Na^+ EXCHANGED WYOMING BENTONITE.

When forming the fully exchanged Na^+ species it was important to ensure that Na^+ was in a large excess to ensure the full removal of Ca^{2+} ions that are often tenaciously held. The ^{29}Si MAS NMR spectra shown in figures 58, 59 and 60 are representative of the structural changes that occur as a result of the heating of Na^+ intercalated Wyoming Bentonite.

Following heating the initially white sample had become a grey powder. The colour change is thought to be related to a change in the oxidation state of the contaminant iron oxide.

Figure 58 : ^{29}Si MAS NMR Na^+ Wyoming Bentonite not heated.

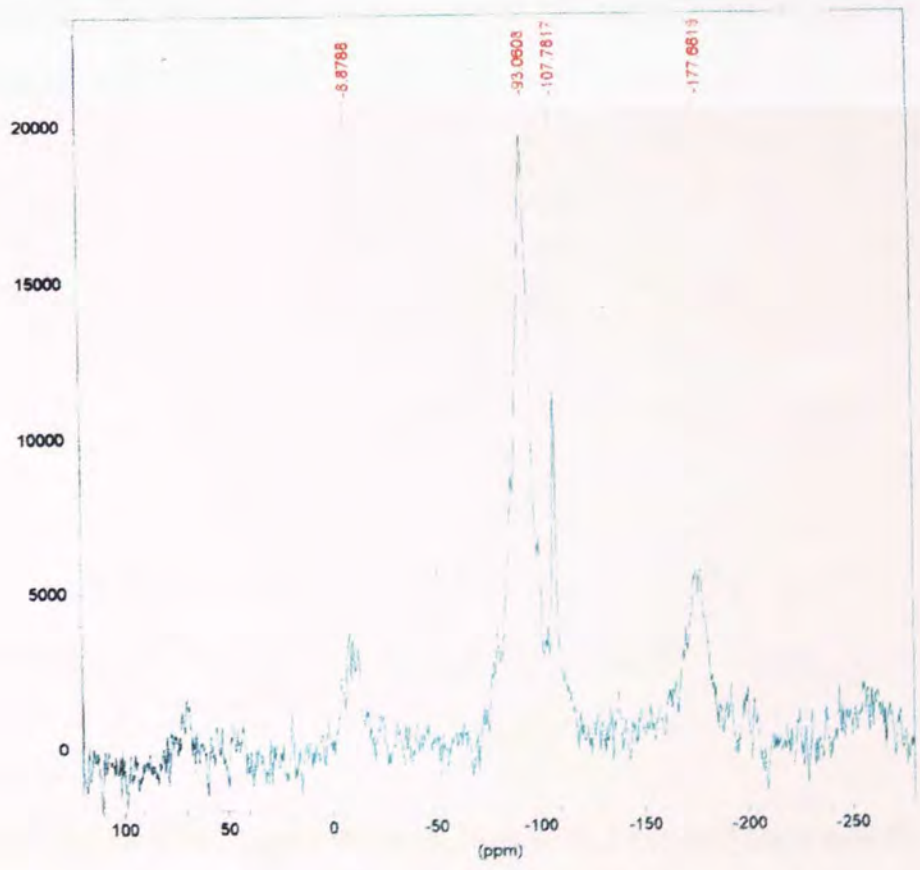

Figure 59 : ^{29}Si MAS NMR spectrum of Na^+ Wyoming Bentonite heated to 500°C.

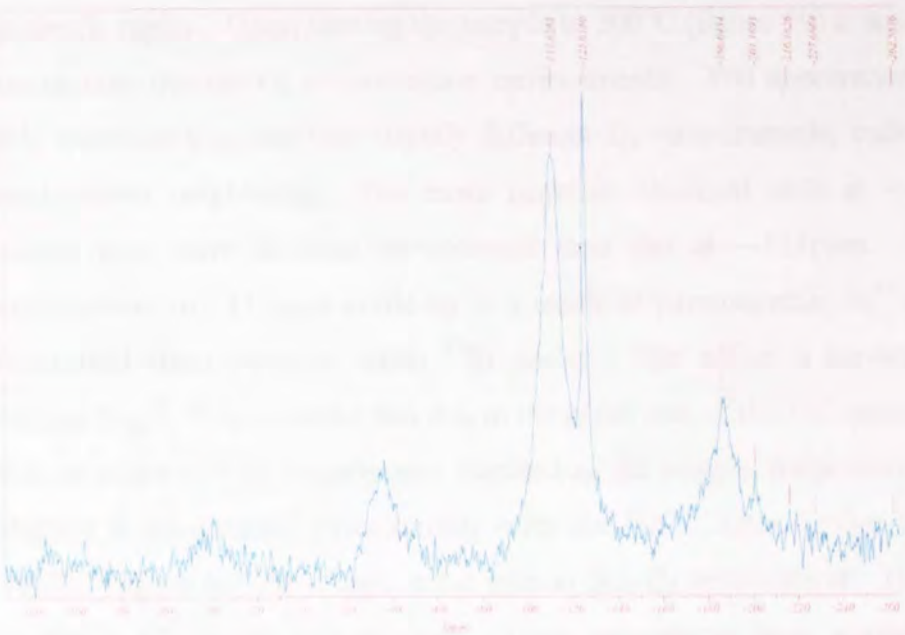

Figure 60 : ^{29}Si MAS NMR spectrum of Na^+ Wyoming Bentonite heated to 1000°C.

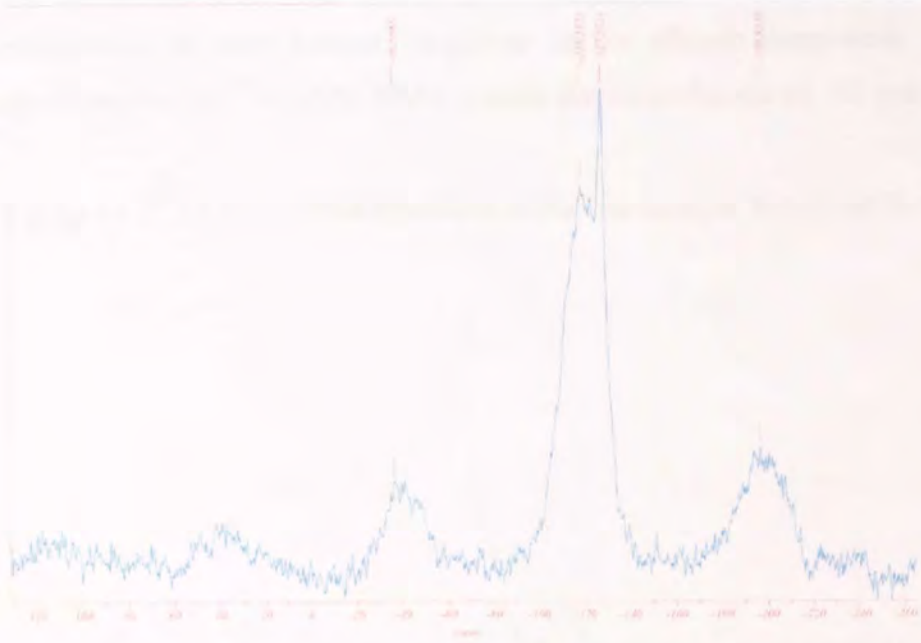

The ^{29}Si MAS NMR spectra shown in figures 58, 59 and 60 show how the co-ordination environment of silicon is affected as a result of the heating process. It is seen from figure 58 how prior to heating silicon occupies two environments Q_3 and Q_4 as indicated by the resonant peaks at ~-93ppm and ~–107ppm, respectively. The strength

of the peak at ~-93ppm suggests that this is the dominant co-ordination environment, however the width of the peak suggests the silicon groupings are less ordered than those in the Q_4 region. Upon heating the sample to 500°C (figure 59) it is seen that all silicon atoms now occupy Q_4 co-ordination environments. The appearance of two peaks on this spectrum suggests two slightly different Q_4 environments, indicative of different next-nearest neighbours. The more negative chemical shift at ~-125ppm suggests silicon in a more shielded environment than that at ~-111ppm. The less shielded environment of ~111ppm could be as a result of paramagnetic Fe^{3+} substituting in the octahedral sheet close to active ^{29}Si nuclei. This effect is known as paramagnetic deshielding[75] It is assumed that due to the small size of the Na^+ cation, all the silicon in this structure will be slightly less shielded as the oxygen framework will have rotated slightly to co-ordinate more closely with the Na^+. After further heating through to 1000°C (figure 60) the silicon atoms remain in a Q_4 environment. The spectrum shown in figure 60 shows that the two silicon resonances have moved closer together, suggesting that dehydroxylation, the removal of inner hydroxyls, results in re-arrangement of the silicon within the clay structure. Thus the heating process has had the effect of increasing the polymerisation of the silicon in the framework by eliminating Al next nearest neighbour in the silicate framework. This change is confirmed by the ^{27}Al MAS NMR spectra shown in figures 61, 62 and 63.

Figure 61 : ^{27}Al MAS NMR spectrum of Na^+ exchanged Wyoming Bentonite, 500°C.

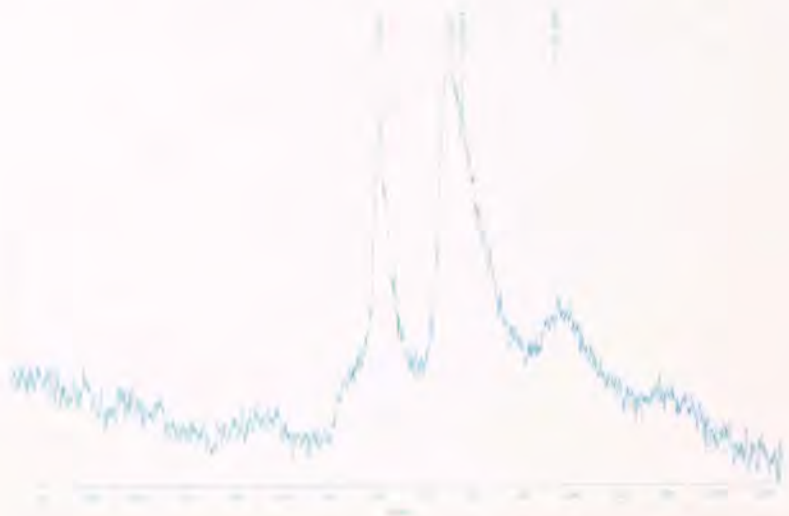

[75] Weiss, C.A., Jr., Altaner, S.P., and Kirkpatrick, R.J., *American Mineralogist,* 72, 935 – 942, **1987**.

Figure 62 : ^{27}Al MAS NMR spectrum of Na^+ Wyoming Bentonite heated to 600°C.

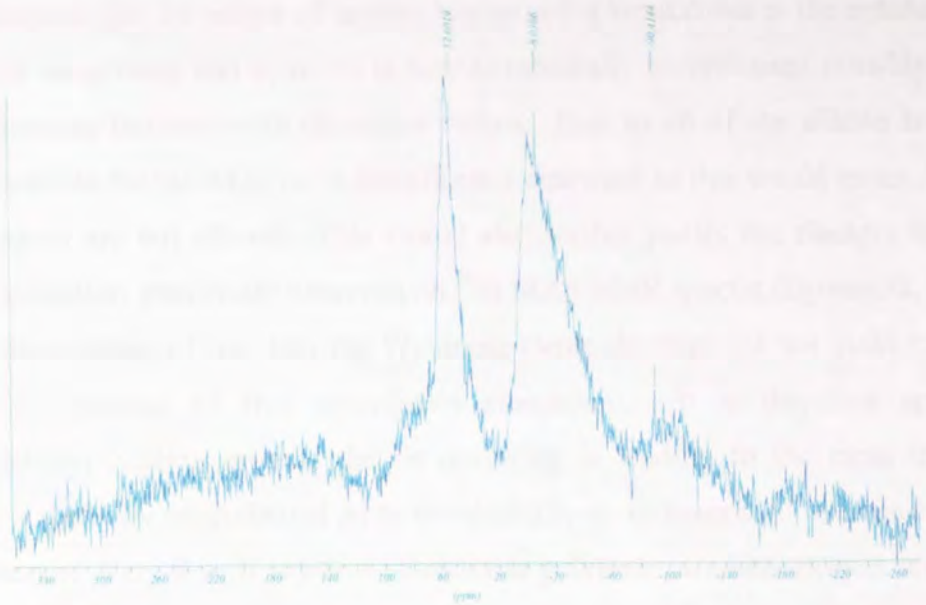

Figure 63 : ^{27}Al MAS NMR spectrum of Na^+ Wyoming Bentonite heated to 700°C.

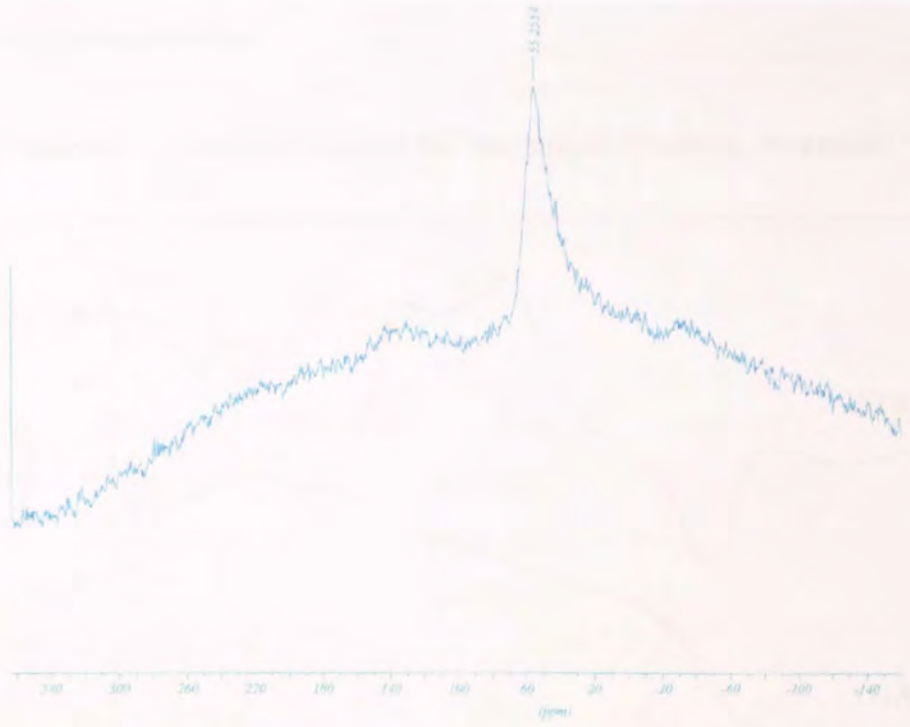

During the initial stages of heating up to 600°C (figures 61 and 62) Na^+ exchanged Wyoming Bentonite consists of a mixture of both six co-ordinate (~3ppm and ~8ppm) and four co-ordinate (~55ppm and ~52ppm) aluminium atoms within the clay. It is not

until after being heated to 700°C (figure 63) that a significant change is observed, with all aluminium now occupying a tetrahedral co-ordination environment. This would suggest that the action of heating has caused a breakdown in the octahedral structure of the aluminium and some Al is now tetrahedrally co-ordinated possibly as a result of it forming linkages with the metal cation. Due to all of the silicon being Q_4 it is not possible for the Al to be in the silicate framework as this would mean Al-O-Al linkages which are not allowed. This would also further justify the changes in the silicon co-ordination, previously observed on ^{29}Si MAS NMR spectra (figures 58, 59 and 60). The intercalation of Na^+ into the Wyoming Bentonite clay did not yield spectra to suggest the presence of five co-ordinate aluminium. It is therefore apparent that the dehydroxylation process that is occurring is leading to the rapid transformation of octahedrally co-ordinated Al to tetrahedrally co-ordinated Al, the result of weak Al-OH bonds. Very few, if any five co-ordinate polyhedra are interspersed between the six co-ordinate and four co-ordinate aluminium.

The data obtained from DTA/TGA (figure 64, tables 28 and 29) provides evidence to support the changes that are seen to be occurring within the clay structure as a result of the heating process.

Figure 64 : TGA/DTA trace for Na^+ exchanged Wyoming Bentonite.

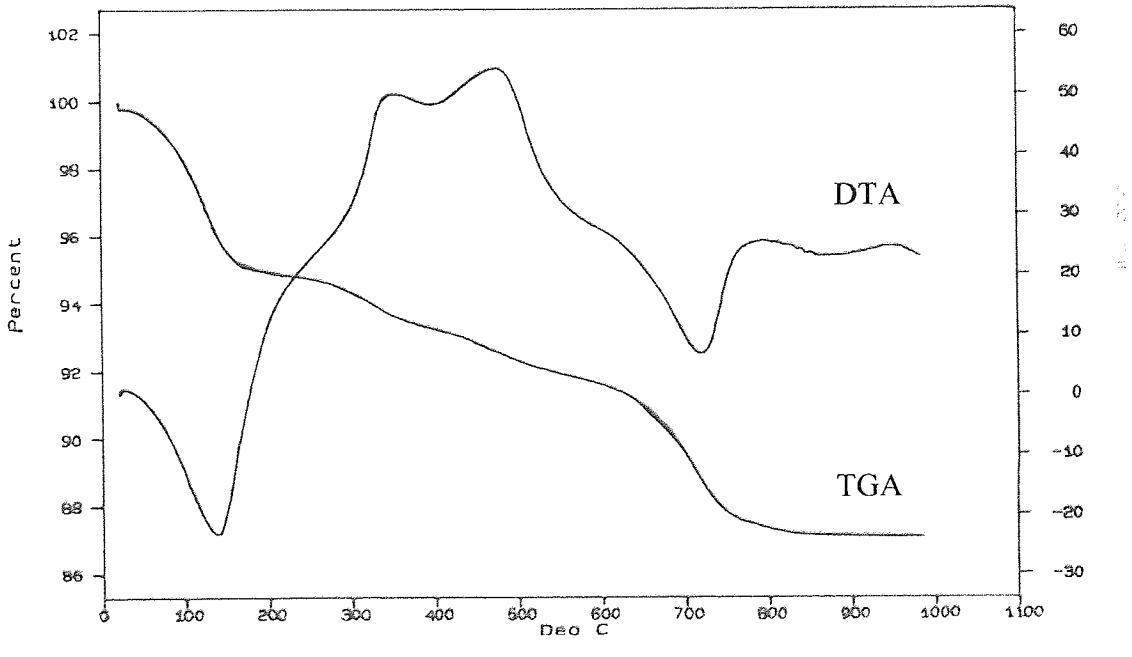

Table :28 Interpretation of TGA trace for Na^+ Wyoming Bentonite

TEMP°C	COMMENT
~0 - 150	Dehydration of the clay sample[51]. Loss of physisorbed water and the first water molecules surrounding the cation.[68]
~150 - 600	The last water molecules bound to the Na^+ cation.[68] Dehydroxylation of the structure may begin.
>600	A sharp weight loss corresponding to the dehydroxylation of the Structure.[51,52,68.]

Table 29 : Interpretation of DTA trace for Na^+ Wyoming Bentonite.

TEMP°C	COMMENT
~100	A large exotherm indicative of sample dehydroxylation. The magnitude of this peak suggests an additionally hydrated species where the bonding energy of the water being relatively high.[52] .
~400	A second dehydration peak resulting from the removal of the remaining more strongly bonded water.[68]
~700 - 800	Exotherm indicative of dehydroxylation in smectite type minerals.[52]
~800-900	Very small endotherm indicative of the breakdown of the sample to a more amorphous material.[52] The low intensity of the peak suggests low Mg^{2+} content and the delayed exothermic peak that follows suggests quartz like formations.[51,52.]

It is thought that the size of the Na^+ cation allows it to occupy a position in the centre of the interlayer region.

The appearance of two dehydration peaks below 400°C is indicative of sorbed water loss. The magnitude of the DTA peaks is of particular interest; their large size suggests a relatively heavily hydrated sample with the water in the interlayer region having a relatively high average bonding energy.

Up to 400°C rehydration of the clay mineral is still possible, the effects of heating do not become irreversible until above ~490°C, with the onset of dehydroxylation.

The broadness and asymmetry of the peaks seen above 600°C suggests at least a two-step dehydroxylation mechanism, with intermediate structures with differing amounts of six-coordinate and five-coordinate polyhedra.

The major onset of dehydroxylation is not observed until ~700°C when a large endotherm occurs as shown in the trace of figure 64. This is characteristic of this type of mineral, while for most other clay minerals dehydroxylation starts at ~500°C.[52]

The occurrence of the final endothermic peak at ~900°C, which is only prominent in some samples, is followed by a small exothermic reaction. This is related to chemical composition with a small endotherm being indicative of a species low in Mg^{2+}. This peak also indicates breakdown to a more amorphous material from which new crystalline phases form. This is consistent with the changes observed on ^{27}Al MAS NMR spectrum for Na^{+} Wyoming Bentonite heated to 700°C (figure 63).

The calcination of Na^{+} exchanged Wyoming Bentonite by furnace treatment over the range 500°C – 1000°C, in 100°C increments, yielded orange/brown coloured powders, a colour change caused by a change in the oxidation state of iron impurities. Note, the presence of iron oxides within the samples does not affect the position of the peaks.

6.2.1 Cu^{2+} EXCHANGED WYOMING BENTONITE.

The Cu^{2+} exchange was performed on the Na^{+} form of Wyoming Bentonite using an aqueous copper chloride solution in excess. This yielded a green powder when ground and dried.

The exchange of Cu^{2+} into the mono-ionic Na^{+} species produced some very interesting MAS NMR results. The Cu^{2+} ion being d^9 paramagnetic added further to the problems of background noise and thus some loss of intensity has been observed. This may also have led to some contact or pseudo-contact shifting of resonant peaks with ^{29}Si MAS NMR spectrum (figure 65) which shows that by 500°C silicon is in two distinct Q_0 environments (-69ppm and -57ppm). The transition from Q_4 to Q_0 in such a short heating period suggests that some remarkable structural re-arrangement has occurred.

Figure 65 : ^{29}Si MAS NMR spectrum of Cu^{2+} Wyoming Bentonite heated to 500°C.

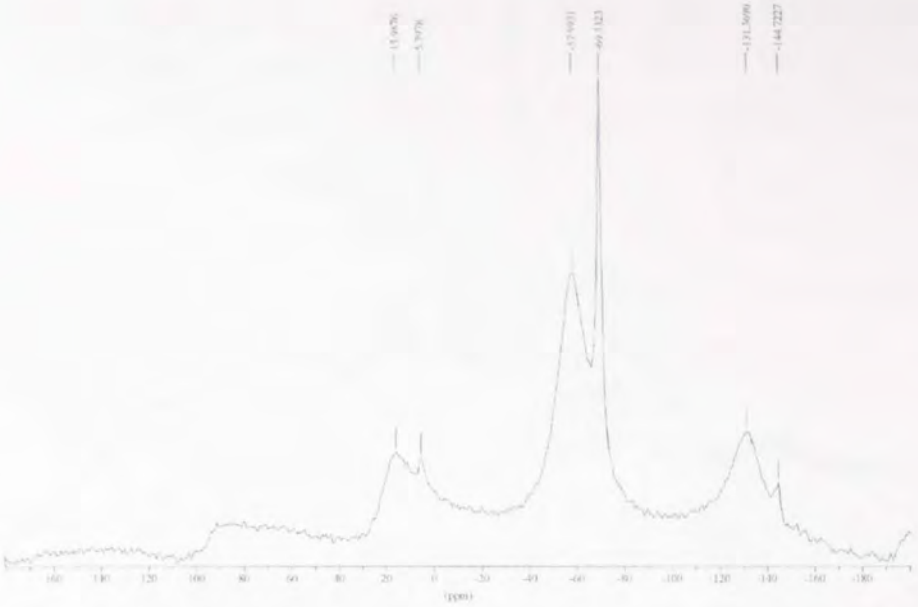

The initial suggestion for such a notable change in structure was that the Cu^{2+} ion was migrating into the hexagonal cavities of the Si-O network and thus what was being observed was a result of an interaction of the silicon with the Cu^{2+} ions, to achieve Cu-O-Si linkages. Literature[72] supported this by suggesting that migration of this nature can occur at temperatures as low as 200°C. However, if this were occurring it would be reflected by dramatic changes in the ^{27}Al MAS NMR spectra, whereas figure 66 shows that no such variations were observed.

Figure 66 : ^{27}Al MAS NMR spectrum for Cu^{2+} Wyoming Bentonite heated to 500°C.

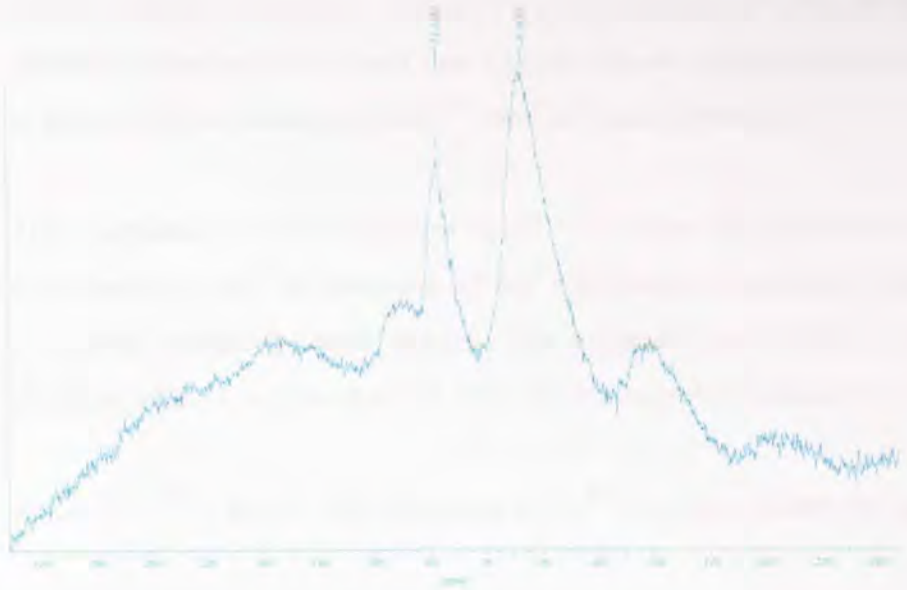

It is seen from figure 66 that during the initial heating stages, the Cu^{2+} intercalated Wyoming Bentonite does not show any significant differences from the Na^{+} type, (figure 62) with aluminium occupying both octahedral and tetrahedral co-ordination environments, shown by the resonant peaks at ~-6ppm and ~-54ppm respectively. The width of the peaks and associated spinning side bands are partly a result of quadropolar interactions but more significantly of the presence of the higher level of paramagnetic impurities within the sample. It is therefore concluded from this data that the dramatic changes observed in the ^{29}Si MAS NMR spectrum (figure 65) are a result of the increasing aluminium content within the silicate framework. As the amount of tetrahedral aluminium surrounding the silicon increases this leads to a decreasing bond strength sum and hence less negative ^{29}Si resonances. This also explains why both octahedral and tetrahedral aluminium are being observed. Because this phenomenon was not observed for the Na^{+} intercalated species it is assumed that the Cu^{2+} is acting in some manner to accelerate the formation of Q_0 silicate, however how this happens is not known.

Unlike the case for the Na^{+} intercalated Wyoming Bentonite,(figure 63) the spectrum of the Cu^{2+} form does not show all the aluminium to be occupying tetrahedral sites until 900°C, when only one very small broad peak is observed at ~46ppm. (figure 67). The

shift of the peak down-field and the large shoulder on the peak suggest that a small amount of aluminium is still octahedrally co-ordinated but its presence is obscured beneath a larger resonance. It is clear from the amount of noise on the spectrum and the apparent distortion of the peak that a large amount of interference is being experienced as a result of the paramagnetic Fe^{3+} and Cu^{2+} species present.

The completion of the transition to all ^{27}Al being in tetrahedral sites by 1000°C is confirmed on the ^{29}Si spectrum of Cu^{2+} Wyoming Bentonite (figure 68) by all ^{29}Si occupying a single Q_0 environment. This suggests that all silicon is experiencing equal shielding effects as a result of the next-nearest neighbour aluminium atoms.

Figure 67 : ^{27}Al MAS NMR spectrum of Cu^{2+} Wyoming Bentonite heated to 900°C.

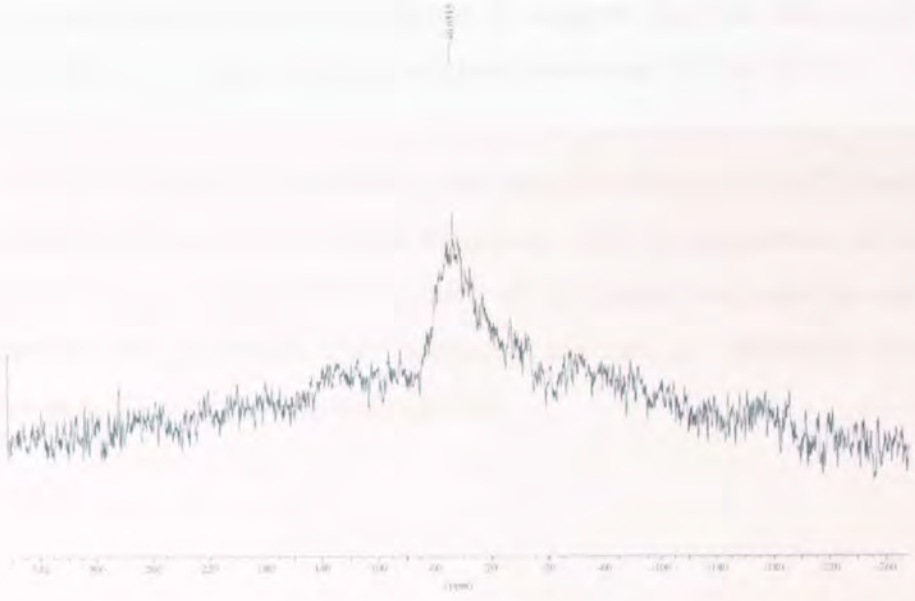

Figure 68 : ^{29}Si MAS NMR spectrum of Cu^{2+} Wyoming Bentonite heated to 1000°C.

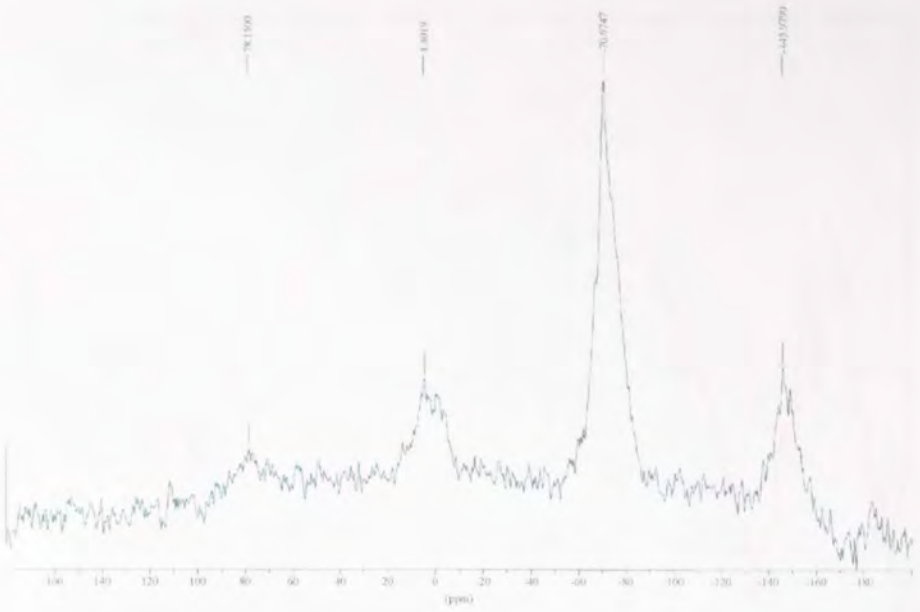

The sharpness of the peak in figure 68 suggests that the silicon is having very little interaction with its next-nearest neighbours whether Fe^{3+} or Cu^{2+}.

The lack of a band at ~820cm^{-1} on the infra red spectrum of Cu^{2+} intercalated Wyoming Bentonite (figure 69), which is consistent with the appearance of Cu-O-Si linkages, further suggests that Cu^{2+} migration of the nature suggested is not occurring; this supports the conclusion that increasing amounts of tetrahedral aluminium and the change to Q_0 silicon are linked together.

Figure 69 : Infra red spectrum of Cu^{2+} Wyoming Bentonite heated to 500°C.

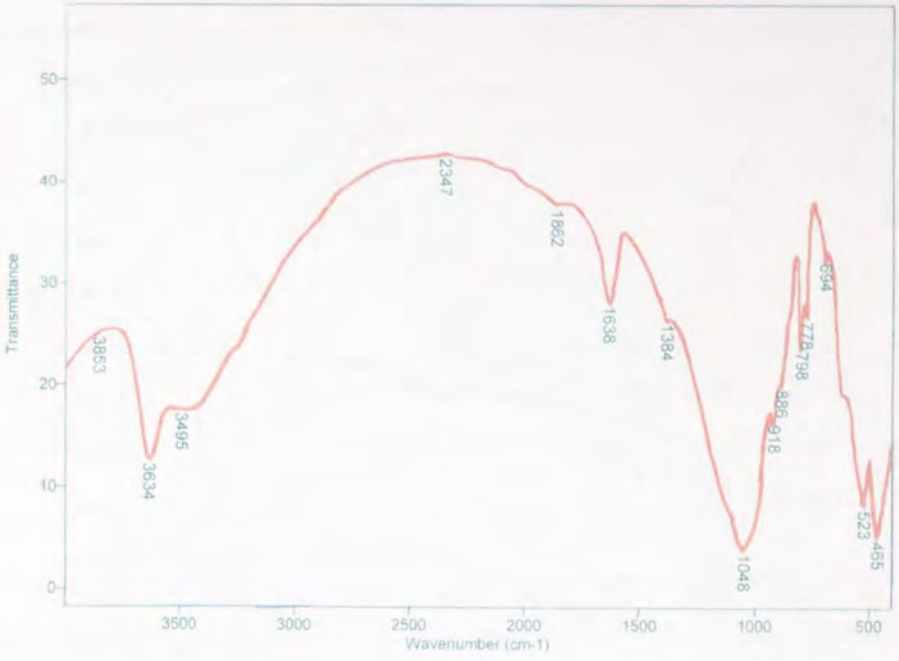

The search for five co-ordinate aluminium in the calcined samples of Cu^{2+} Wyoming Bentonite did not yield the results expected. Five co-ordinate aluminium was not observed in any of the spectra obtained for Cu^{2+} Wyoming Bentonite. Thus it is sufficient to say that the intercalation of Cu^{2+} into the sample did not affect the appearance of five co-ordinate aluminium. However, it may have played a role in the acceleration of the appearance of Q_0 silicon.

The analysis of Cu^{2+} Wyoming Bentonite *via* TGA/DTA provided results consistent with the dehydration/dehydroxylation of a clay material.

Figure 70 : TGA/DTA trace of Cu^{2+} intercalated Wyoming Bentonite.

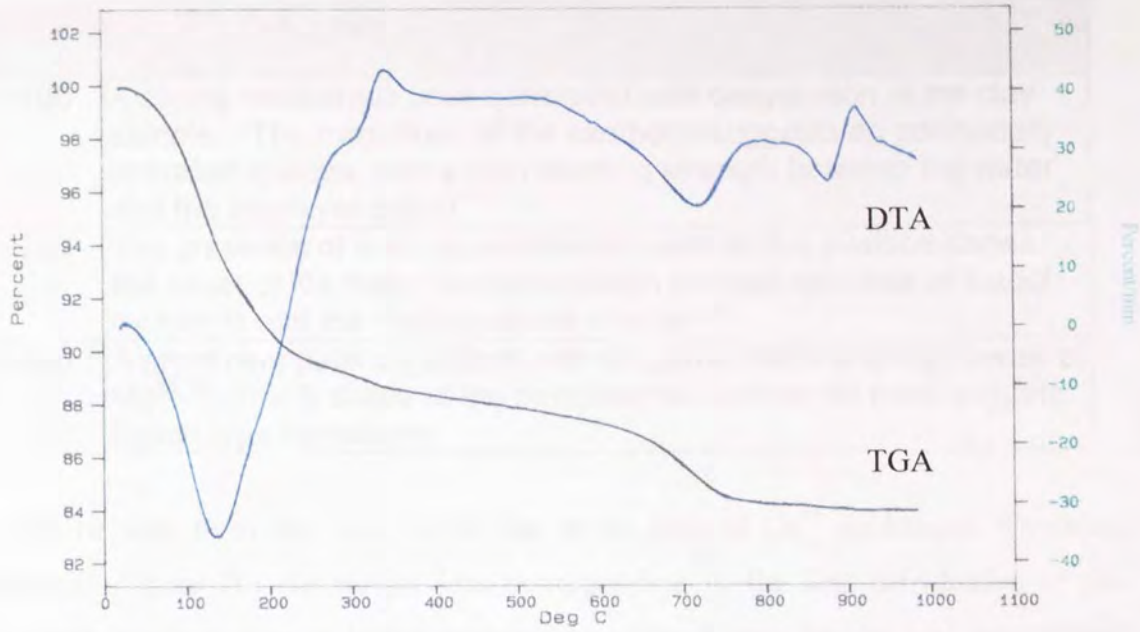

The green powder obtained from Cu^{2+} exchange on the Na^{+} Wyoming Bentonite, when subjected to heating for TGA/DTA analysis, produced a grey/white powder. The results from this are shown above in figure 70.

Table 30 : Interpretation of TGA trace for Cu^{2+} Wyoming Bentonite.

TEMP^{O}C	COMMENT
~100 - 200	Large initial loss of water due the first dehydration of the Interlayer cation.[72] Also shows the loss of sorbed water.
~200 - 600	Further dehydration as the remaining water from around the cation is removed.[68,72] The first stages of dehydroxylation begin at ~500°C.[51,52,68]
>600	Dehydroxylation with structural changes begin to occur.[51,52,72.]

Table 31 : Interpretation of DTA curve for Cu^{2+} Wyoming Bentonite.

TEMP°C	COMMENT
~100	A strong exothermic peak consistent with dehydration of the clay sample. The magnitude of the exotherm suggests an additionally hydrated species, with a high bonding strength between the water and the interlayer cation.[52]
~700	The presence of a strong exothermic peak at this position shows the onset of the major dehydroxylation process with loss of bound hydroxyls and the start structural change.[52]
~900	A prominent peak consistent with dehydroxylation and high levels of Mg^{2+}.[52] The S shape of the endothermic/exothermic peak suggets Spinel type formations

In can be seen from the TGA curve that in the case of Cu^{2+} exchanged Wyoming Bentonite (figure 70) the weight loss corresponding to the first dehydration of the interlayer cation occurs at higher temperatures than it was for the Na^{+} intercalated species (figure 64). This reveals a stronger interaction between the Cu^{2+} cation and the water molecules, which is also shown by the magnitude of the first dehydration peak on the DTA. There is a bigger percentage weight loss than was observed for the Na^{+} cation. The Cu^{2+} Wyoming Bentonite is more heavily hydrated than the Na^{+} form and the Cu^{2+}-water bonds are stronger than the Na^{+}-water bonds.

The larger size of the endothermic peak at ~900°C on the Cu^{2+} (figure 70) when compared to the Na^{+} trace (figure 64) cannot be because the Cu^{2+} Wyoming Bentonite has a larger Mg^{2+} content as the one came from the other. It is documented[52] that the nature of the interlayer cation can have a marked effect on the size of the high temperature peaks, and it most probably this phenomenon that is being observed here. The S shape of this final curve is indicative of the final stages of heating in a montmorillonite type mineral, thus showing the formation of spinel (γ-Al_2O_3).

The study of Cu^{2+} intercalated Wyoming Bentonite has shown that a change in the interlayer cation does act to change the dehydration/dehydroxylation process of clay minerals.

6.2.2 K^+ EXCHANGED WYOMING BENTONITE.

The exchange of K^+ into the Na^+ Wyoming Bentonite was performed using an aqueous solution of KCl. This yielded a white powder when ground and dried.

The ^{29} Si MAS NMR spectrum for K^+ exchanged Wyoming Bentonite (figure 71) shows two resonances indicative of silicon occupying two separate chemical environments.

Figure 71 : ^{29}Si MAS NMR of K^+ Wyoming Bentonite heated to 500°C.

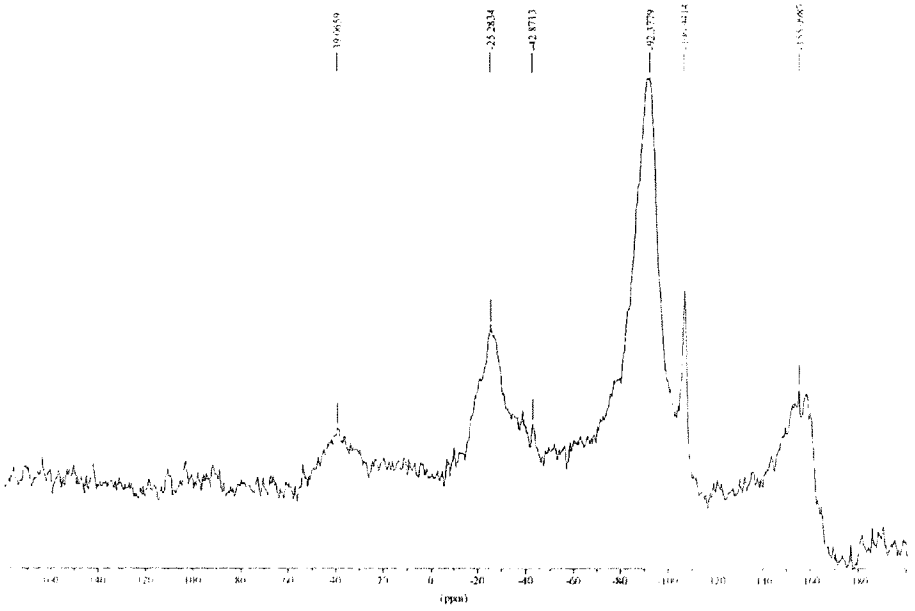

The size of the peak at ~-116ppm suggests that there is very little silicon in a Q_4 environment, however, whatever is present is in a fully polymerised state with no tetrahedral ^{27}Al next-nearest neighbours. The peak at ~-92ppm is indicative of a greater quantity of silicon in a Q_3 co-ordination environment. The lower peak position and obvious broadening is as a result of silicon nuclei being closer to paramagnetic Fe^{3+} species. The lower resonance position of this peak is the result of paramagnetic shielding. The spectrum shown in figure 72, ^{27}Al of K^+ Wyoming Bentonite heated to 500°C, provides information to support what is shown in the ^{29}Si MAS NMR spectrum (figure 71).

Figure 72 : ^{27}Al MAS NMR spectrum of K^+ Wyoming Bentonite heated to 500°C.

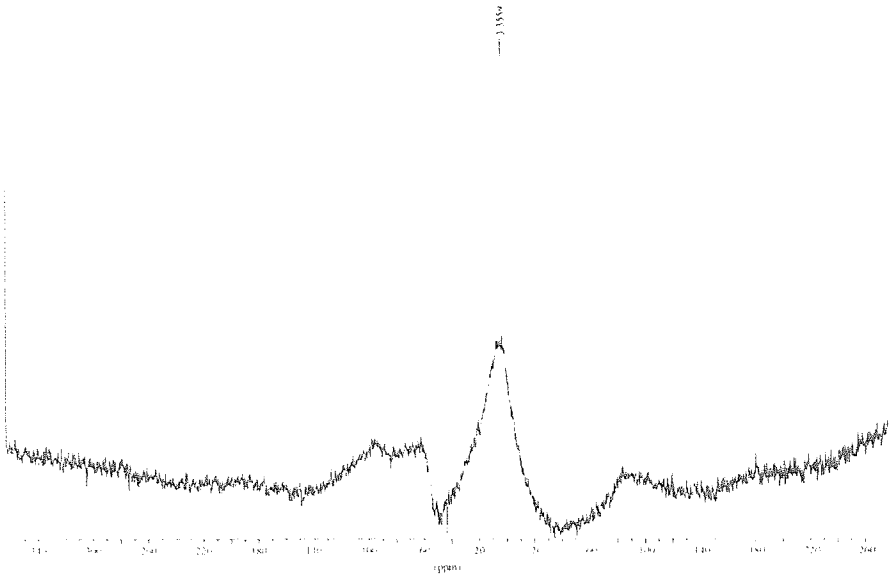

The single large resonance at ~3ppm on the spectrum is indicative of a large amount of ^{27}Al in an octahedral co-ordination. The shape of the peak on this spectrum also suggests the formation of a small amount of tetrahedrally co-ordinated aluminium as is expected from analysis of the ^{29}Si spectrum. The noise on the spectrum and broadness of the peak is again as a result of paramagnetic impurities being close to active nuclei.

The further heating of the sample to 600°C provides results very similar to those obtained from the Cu^{2+} exchanged Wyoming Bentonite, with the appearance of Q_0 silicate and an apparent increase in the amount of tetrahedrally co-ordinated aluminium (figures 73 and 74).

Figure 73 : ^{29}Si MAS NMR spectrum of K^+ Wyoming Bentonite heated to 600°C

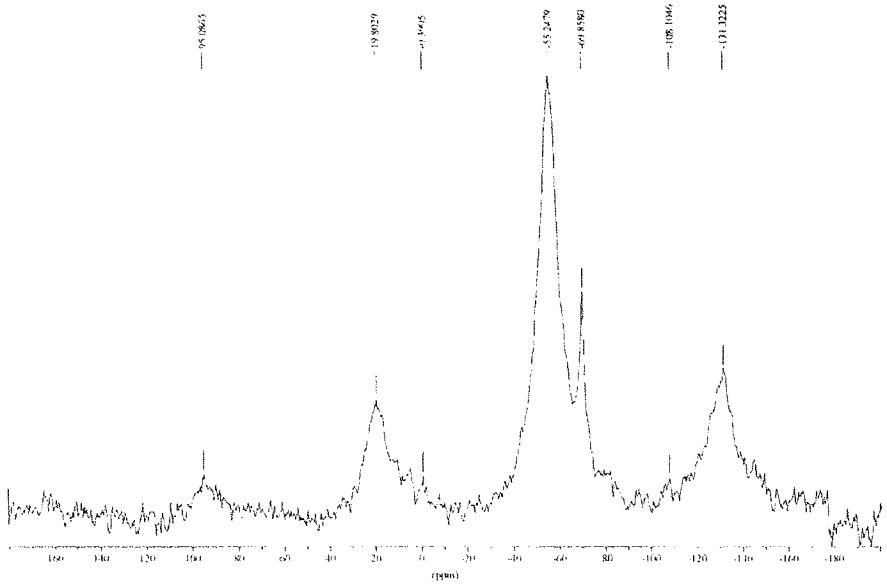

Figure 74 : ^{27}Al MAS NMR spectrum of K^+ Wyoming Bentonite heated to 600°C.

The spectrum shown in figure 73 again exhibits two ^{29}Si environments both of Q_0 co-ordination. It does not follow that this is a result of migration of K^+ into the hexagonal cavities of the silicate layer as there is no direct evidence for this and the migration of K^+ ions is not supported by the literature.[68] The corresponding increase in the amount of tetrahedrally co-ordinated aluminium, as shown in figure 74, suggests that Q_0 silicate is being formed as a result of the deshielding effect caused by increasing

aluminium content in the silicate framework. An increase in the amount of tetrahedral aluminium leads to decreasing bond strength sums and hence less negative ^{29}Si chemical shifts.

It is apparent from the ^{29}Si spectrum (figure 73) that there are two distinct environments of silicon with different concentrations, and different degrees of shielding of the silicon nucleus. This is again reflected in the ^{27}Al spectrum (figure 74) which also exhibits a resonant peak at ~58ppm indicative of a large amount of ^{27}Al still occupying an octahedral environment. Further heating did not lead to the complete disappearance of octahedral aluminium until ~800°C when a single sharp resonance was observed. The subsequent heating up to 1000°C showed the magnitude of this resonance to increase indicative of all ^{27}Al in a tetrahedral environment. It was also by this stage that ^{29}Si showed all silicon to be in a single environment with a resonance of ~-71ppm as shown in figure 75.

Figure 75 : ^{29}Si MAS NMR spectrum of K^+ Wyoming Bentonite heated to 1000°C.

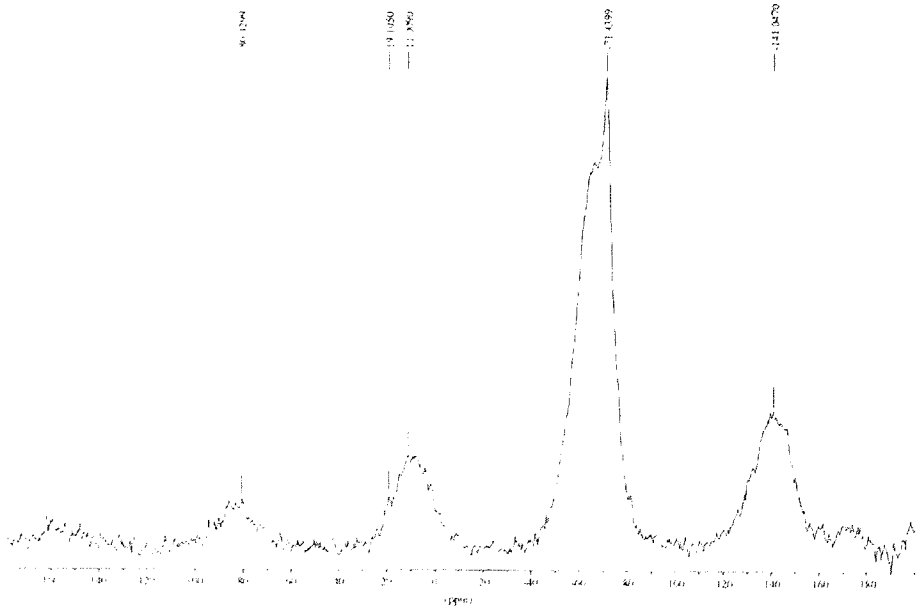

It is apparent from the data presented thus far that the thermal processes of the K^+ intercalated Wyoming Bentonite appear intermediate between the Na^+ and the Cu^{2+} forms, with these showing transformations to solely tetrahedral aluminium at 700°C and 900°C respectively, and the transformation to Q_0 silicon occurring between 500°C and

600°C for the K^+ form. Further investigation of this narrowed the window to between 500°C and 525°C. This information suggests that there may be a kinetic factor affecting the appearance of Q_o silicon, which could have been investigated by repetition of the experiment using different timing scales. Due to the nature of this work, this has not been carried out but is certainly an item for further work.

There was no evidence to suggest that the intercalation of the K^+ ion into the mono-ionic Wyoming Bentonite species affects the appearance of five co-ordinate aluminium.

The TGA/DTA traces obtained as a result of the analysis of the dehydration/dehydroxylation processes involved in the K^+ Wyoming Bentonite can be seen in figure 76.

Figure 76 : TGA/DTA trace of K^+ Wyoming Bentonite.

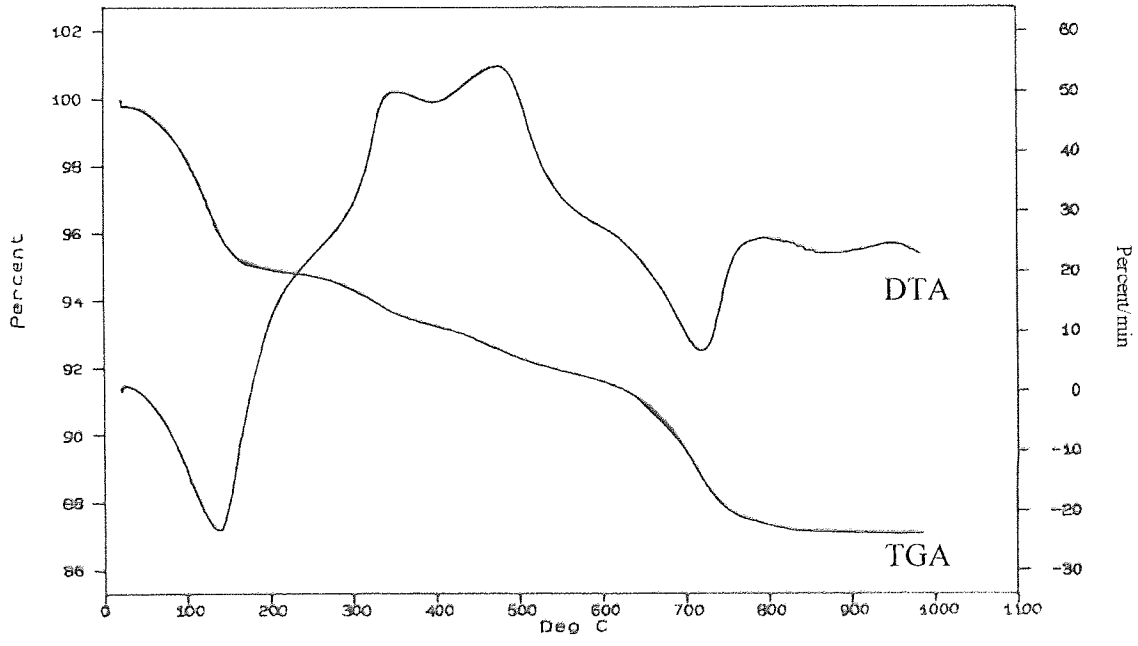

Table 32 : Interpretation of TGA trace of K^+ Wyoming Bentonite.

TEMP°C	COMMENT
~100 - 200	Small weight loss. Peak is indicative of dehydration of the cation.[72] also loss of sorbed water.
~200 - 500	The loss of the last water from the cation and the start of dehydroxylation.[68]
~500 - 700	The main onset of dehydroxylation

Table 33 : Interpretation of DTA trace of K^+ Wyoming Bentonite.

TEMP°C	COMMENT
~100	Small endotherm indicative of dehydration, the size of the peak Suggests a sample of lower hydration.[52]
~400	Further dehydration due to the loss of the last water from the Interlayer cation.[68]
~700	Medium intensity endotherm indicative of the onset of dehydroxylation within the clay sample.[52]
~900	Small endotherm suggesting a low Mg^{2+} content.[52] Also indicative of the breakdown of anhydrous material to an amorphous material from which new phases crystallize.[68]

The thermal analysis trace of K^+ exchanged Wyoming Bentonite as shown in figure 76 shows initial endothermic peaks (~100°C) on the DTA trace of significantly smaller size than those observed on both the Na^+ and Cu^{2+} traces. This suggests that the amount of water sorbed by K^+ saturated samples is less than other cation intercalated samples. This will be primarily due to the lower hydration energy of the K^+ ion and hence the lower average bonding energy of the interlayer water in the K^+ sample. Thus much steeper and rapid dehydration process is observed. Due to its size K^+ does not usually undergo cation migration and occupies an interlayer position although not quite centrally.[68]

The asymmetric peak observed on the DTA trace at ~700°C at the onset of dehydroxylation is the result of the K^+ ion causing a change in the bond strength of Al....O,OH. Initial dehydroxylation is delayed and so an asymmetric peak is formed.

The final endotherm at ~900°C, indicative of phase changes, is intermediate in magnitude, between those for Na^+ and Cu^{2+}.

6.2.3 Li^+ EXCHANGED WYOMING BENTONITE.

Li^+ intercalated Wyoming Bentonite was prepared from the Na^+ form using an excess of aqueous LiCl solution.

The ^{29}Si and ^{27}Al MAS NMR spectra obtained from heating the Li^+ intercalated Wyoming Bentonite to 500°C (figures 77 and 78) exhibit similar trends to those seen for both the K^+ and Cu^{2+} samples.

Figure 77 : ^{29}Si MAS NMR spectrum of Li^+ Wyoming Bentonite heated to 500°C.

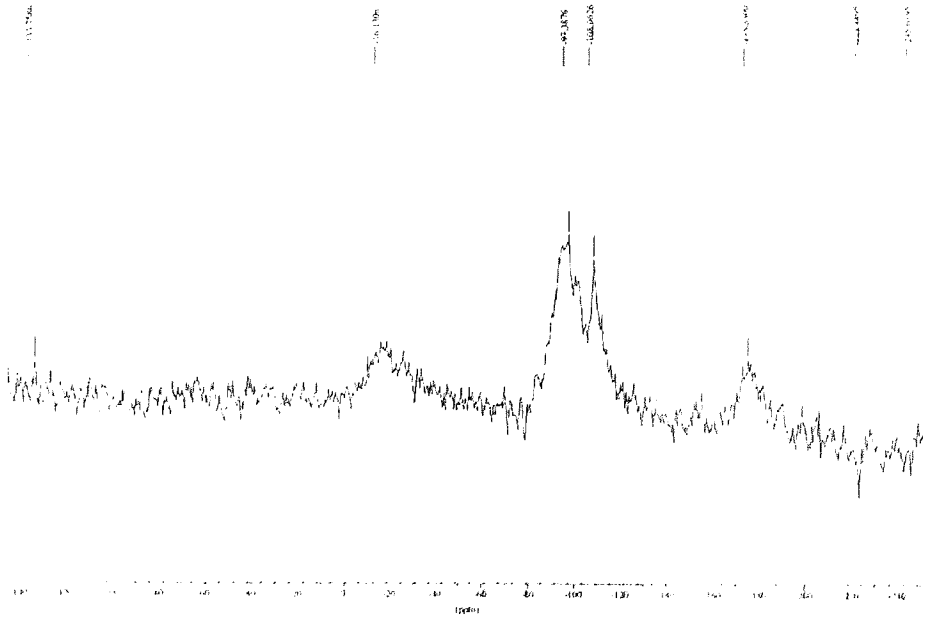

Figure 78 : ^{27}Al MAS NMR spectrum of Li^+ Wyoming Bentonite heated to 500°C.

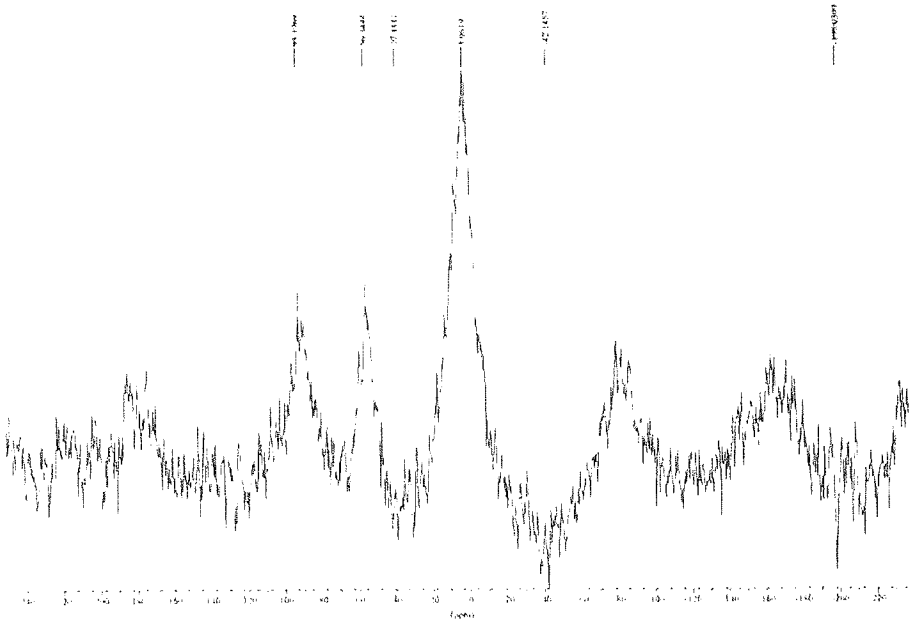

The two resonant peaks shown on ^{29}Si MAS NMR spectrum, at ~-108ppm and ~-97ppm are indicative of silicon in two separate Q_0 environments, with the silicons at ~-108ppm experiencing more shielding. These differences can also be related to the electronegativity of the other cations to which the oxygen atoms of the ^{29}Si tetrahedron are co-ordinated. Although the formation of lithium silicate phases is highly probable, as there are many literature reports to support the migration of lithium.[33,75,76,77.] There is no evidence at this stage to support its appearance here and it is thought that the formation of Q_0 is a result of the deshielding effect observed when the amount of aluminium in the silicate framework increases. The ^{27}Al MAS NMR spectrum (figure 78) provides evidence to support this by showing the appearance of tetrahedrally co-ordinated aluminium (~3ppm) as well as some in an octahedral environment (~56ppm).

Further heating of Li^+ Wyoming Bentonite to 1000°C did not significantly change the environment of the silicon or aluminium. The silicon remained in two Q_0 environments at ~-107ppm and ~-97ppm with a much higher concentration in the former position. The ^{27}Al MAS NMR spectrum exhibited two aluminium resonances one at ~0ppm indicative of octahedrally co-ordinated ^{27}Al and one at ~55ppm consistent with ^{27}Al in a tetrahedral environment. Since not all the ^{27}Al are tetrahedrally co-ordinated, there is

another factor involved in the deshielding of the silicon nucleus. Evidence for this is found by looking at the ^{6}Li MAS NMR spectrum obtained.(Figure 79, see later)

The large amount of noise on all the spectra results from the effect of paramagnetic impurities in conjunction with the large quadrupole moment of ^{7}Li ($-4.5 \times 10^{-30} em^2$) and the nuclear spin of ^{7}Li being $^{3}/_{2}$. Both of these factors combined with the structural changes that occur as a result of the heating process result in very untidy spectra that are difficult to interpret.

In addition to those nuclei discussed previously ^{6}Li has also been investigated. This nucleus was chosen over ^{7}Li, which is conventionally examined, as it has a much lower quadrupole moment (-8×10^{-32} e m^2 and -4.5×10^{-30} e m^2, respectively) and so will give rise to much narrower spectral lines.

The narrow lines achieved from the ^{6}Li MAS NMR study of Li^{+} Wyoming Bentonite indicate that the second order quadrupole interaction is small. The resonances obtained in the spectra of heated Li^{+} Wyoming Bentonite all exhibit a chemical shift in the range of $-0.7 - 0.1$ppm (figure 79) which in heated Li^{+} samples is indicative of Li^{+} occupying sites of low symmetry.

Figure 79 : ^{6}Li MAS NMR spectrum of Li^{+} Wyoming Bentonite heated to 500°C.

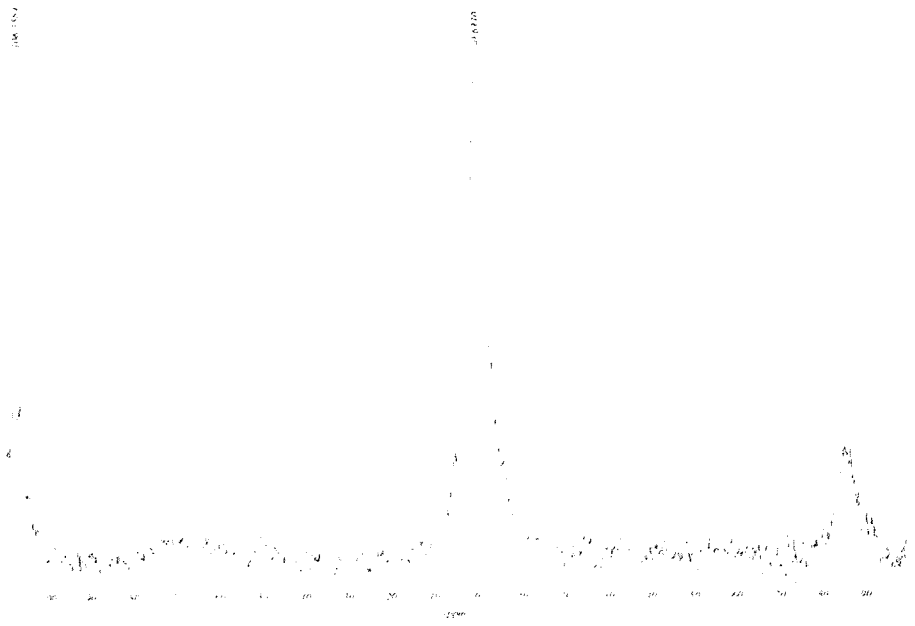

The spectrum shown in figure 79 is typical of all the ^{6}Li spectrum obtained from heated Li^{+} exchanged Wyoming Bentonite from 500°C through to 1000°C in 100°C increments. It has been determined[75] that Li^{+} ions migrate from their interlayer sites into vacancies in the octahedral sheet or hexagonal cavities in the silicate layer as a result of mild heating, as low as 150°C – 250°C. It is therefore assumed that the Li^{+} being observed *via* ^{6}Li MAS NMR is situated in either of these places. The position and shape of the resonance is consistent with Li^{+} in a low symmetry environment; this would not be consistent with the octahedral sites so it is reasonable to assume that Li^{+} ions have migrated from the interlayer region into the hexagonal cavities within the tetrahedral sheet. This would result in cation-cation repulsions in the tetrahedral sheet increasing thus leading to a further distortion of the six membered oxygen rings.

Figure 80 : TGA/DTA trace for Li^{+} Wyoming Bentonite.

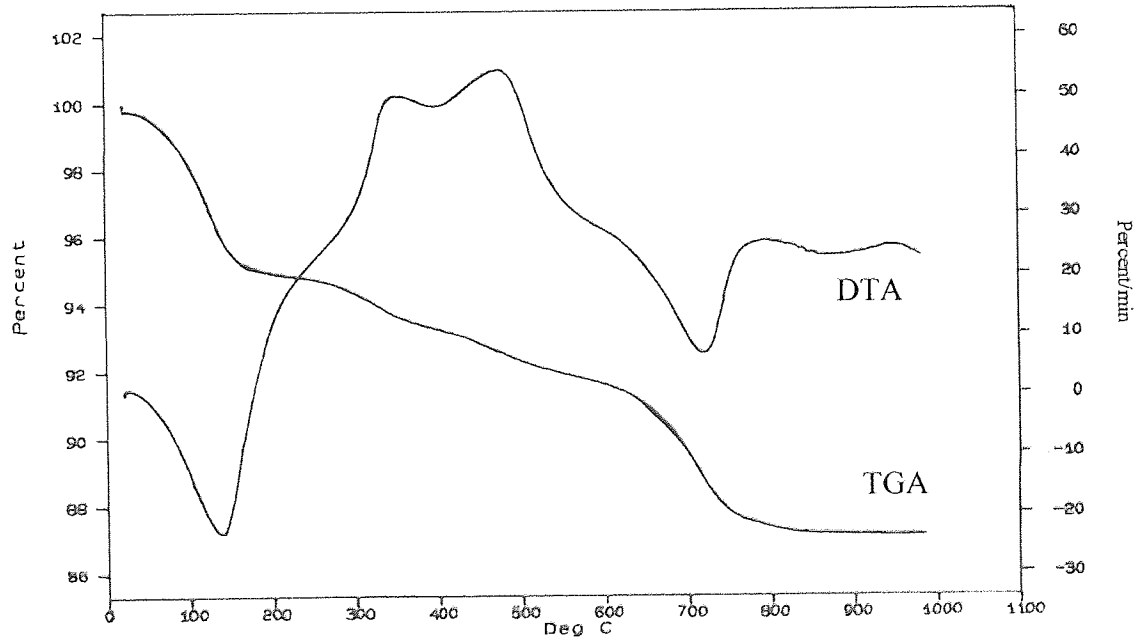

Table 34 : Interpretation of TGA trace of Li^+ Wyoming Bentonite.

TEMP°C	COMMENT
~100 - 150	Weight loss consistent with the loss of sorbed water and the Loss of water from the cation.[72]
~150 - 650	Loss of the last water by dehydration from around the Interlayer cation.[68] Some dehydroxylation may also occur.
~650 – 900	The onset of the main dehydroxylation.

Table 35 : Interpretation of DTA trace of Li^+ Wyoming Bentonite.

TEMP°C	COMMENT
~100	Endotherm consistent with dehydration of the sample. The small size of this endotherm suggests a sample of low water content.[68]
~400	Further dehydration due to loss of water from the interlayer cation.[68]
~700	A small endothermic peak consistent with the onset of the dehydroxylation of the sample.
~900oC	Very small endothermic peak followed by a delayed exothermic peak, suggests very low Mg^{2+} content.[52] Indicative of further dehydroxylation.

The TGA/DTA trace of Li^+ exchanged Wyoming Bentonite appears very similar to that obtained from K^+ intercalation of the sample. The small size of the initial dehydration peak at ~100°C on the DTA trace suggests a sample of low water content possibly due to a high hydration energy of the interlayer cation. The following peaks at ~400°C and ~700°C are consistent with further dehydration and dehydroxylation respectively. The small peak at ~900°C is consistent with a sample of low Mg^{2+} content and is indicative of some further dehydroxylation.

The analysis of Li^+ Wyoming Bentonite *via* ^{27}Al MAS NMR has not yielded data to suggest the appearance of five fold ^{27}Al.

6.3 CONCLUSIONS ON ION EXCHANGE REACTIONS OF WYOMING BENTONITE.

The objectives of the work discussed within this chapter were to investigate the effect of the interlayer cation upon the dehydration/dehydroxylation process of Wyoming Bentonite clay and to assess the nature of the cation on the appearance of five co-ordinate aluminium during the heating process. In addition to this ^{29}Si MAS NMR of the exchanged samples have also been investigated.

The initial cation exchanged was Na^+ to form a mono-ionic Na^+ species from which subsequent exchange reactions could be carried out.

It has been shown by the examination of all of the ^{27}Al MAS NMR spectra that five co-ordinate aluminium was not observed. All spectra showed that upon heating to 500°C aluminium exists in both tetrahedral and octahedral environments regardless of the type of cation inserted. Cation type does however appear to affect the rate at which all aluminium is converted from an octahedral environment to a tetrahedral co-ordination. For the Wyoming Bentonite samples intercalated with Li^+, Na^+ and K^+ this can be explained in simple terms of cationic radii. As the cationic radii varies regularly through these cations the heating effects change in consequence. The sample intercalated with copper is a slightly more complex situation, due to the additional chrge on the cation. The effects of this are again reflected in MAS NMR results.

The lack of five co-ordinate aluminium in all of the spectra suggests that weak Al-OH bonds are allowing rapid transformation of octahedrally co-ordinated ^{27}Al to tetrahedrally co-ordinated ^{27}Al. The Al-OH bonds are therefore the weakest when there is very little five co-ordinate aluminium being formed and so dehydroxylation continues unhindered.

The analysis of exchanged Wyoming Bentonite clays by ^{29}Si MAS NMR yielded some very interesting results, with the appearance of Q_0 silicate. The initial suggestion for its appearance was that of cations migrating into hexagonal cavities in the silicate layer, however, with the exception of Li^+ there was no evidence for this. The corresponding changes observed in the ^{27}Al spectra provided data to suggest that Q_0 silicate was

appearing as a result of increasing amounts of tetrahedral aluminium in the silicate framework. The increase in tetrahedral aluminium content leads to decreasing bond strength sums and therefore less negative ^{29}Si chemical shifts, as were observed. The appearance of a resonant peak at ~0.1ppm on ^{6}Li MAS NMR spectrum (figure 79) is indicative of Li^+ occupying sites of low symmetry which is consistent with Li^+ occupying the hexagonal cavities within the tetrahedral sheet. This therefore suggests for the Li^+ sample the appearance of Q_0 is a combination of two factors, increasing tetrahedral ^{27}Al content and migration of Li^+.

Thermal gravimetric and differential thermal analysis was used to monitor the changes that occur as a result of the heating process. The TGA traces for all samples examined exhibited the basic dehydration/dehydroxylation patterns as would be expected. These were shown by weight losses at ~0°C-150°C, 150°C – 600°C and >600°C respectively (figures 64,70,76 and 80). Interpretation of the DTA traces (figures 64,70,76 and 80) highlighted observable differences in patterns for the different cations examined. It is assumed that because all cation exchange reactions were performed on a mono-ionic Na^+ Wyoming Bentonite species under ambient conditions that the differences observed are related to the interlayer chemistry i.e. cation size, type and charge.

The work presented herein has to some extent explained the effects of changing the interlayer cation within smectite clays upon the their properties. In this case particularly the effect cation exchange has upon the dehydration/dehydroxylation process, the appearance of five co-ordinate aluminium and the effect on ^{29}Si phases.

CHAPTER SEVEN

7.0 PHYSICAL AND CHEMICAL INVESTIGATIONS OF CHINESE CLAYS.

7.1 INTRODUCTION.

This is a study of the chemical and physical characteristics of two Chinese clay bodies and two Chinese clay raw materials used in the manufacture of Chinese porcelain and pottery. The materials in question originate from a variety of areas, these being, Yixing, Wuxi, and Jingdezhen, respectively. The lack of literature on Yixing and Wuxi porcelain bodies indicates they are relatively unknown to the western ceramicist. Conversely, there appears to have been extensive research into porcelain originating from Jingdezhen and in particular the porcelain stone used in the production of porcelain bodies.

Jingdezhen in south China is one of the oldest and most famous areas known for the production of porcelain bodies; it has been the raw materials used there that have determined the development of this Chinese porcelain through the dynasties. It is believed that porcelain stone has been used in the making of Jingdezhen porcelain for many hundreds of years. It is often found with a mixture of clay and non-clay minerals, predominantly kaolin, although actual composition has varied over the dynasties. Kaolin is rarely used alone; due to a high alumina level and too little flux, vitrification below 1400°C is difficult and such high temperatures are often problematic. The high quantity of fusible materials in porcelain stone combined with the plasticity of kaolin makes it an ideal mix and hence raw material. Increasing the quantity of kaolin within the mix will act to further enhance the strength and quality of ceramic wares; the literature reports[76] compositions of this type appearing from the time of the Yuan Dynasty (1280 – 1368).

Porcelain stone has been reported[77] as belonging to a specific group of hydrothermally altered rocks whose chemical compositions appear close to standard ceramics. Its composition is highlighted as including products of hydrothermal transformation of acids (kaolinization, sericization, pyrophyillization or chlorisation) and is thought to be favourable for use in the porcelain industry due to its low level of colouring oxides and

---

[76] Yap, C.T., and Hua, Y., *Applied Spectroscopy*, **1992**, 46, 1488 – 1494.
[77] Anderson, J.L., *Journal of the Australian ceramic Society*, **1982**, 18

favourable mineral composition. Additional features of porcelain stone are its ability to exhibit 'rubbery' properties when ground, and a low plasticity and high mechanical strength upon drying. The high mica content of porcelain stone imparts plasticity to the ground stone, therefore the sum of the estimated mica and kaolin content could be used to provide an indication of overall plasticity.[78]

The weathering of porcelain stone plays an important role in properties imparted on the final porcelain body. In general highly weathered porcelain stone is used during production when the sericite ($KAl_2Si_3AlO_{10}(OH)_2$) component, formed during the aging process, acts as a flux. This also combines well with other components to produce translucent porcelain.[79]

Much work outside China has been on studying of porcelain stone, predominantly for the purpose of comparison to 'home grown' porcelain raw materials of similar composition, with the aim of widening the current raw material base. Such work has been particularly prevalent in both Australia[76] and Russia[80] where reports of deposits of raw materials suitable to replace traditional raw materials have been made. This availability enhances the development of modern ceramic materials and ultimately their service life.

The data presented in this chapter provide a detailed analysis of two samples of Chinese clays from Yixing and Wuxi districts of China and of two samples of raw material from the Jingdezhen area, (Jingdezhen porcelain stone and 'Jingdezhen porcelain stone with kaolin'). The literature[81] has highlighted compositions typical of traditional ceramic bodies, characteristically an complex mix of clay minerals.

The materials have been examined using a range of techniques including ^{27}Al and ^{29}Si MAS NMR Spectroscopy, Fourier Transform Infra-Red (FTIR) Spectroscopy, X-ray Diffraction, ^{57}Fe Mössbauer spectroscopy, particle size analysis and thermal gravimetric and differential thermal analysis.

---

[78] Tite, M.S., Freestone, I.C., and Bimson, M., *Archaeometry*, **1984**, 26, 139 – 154.
[79] Yanyi, G., *Archaeometry*, **1987**, 27, 3 – 19.
[80] Maslennikova, G.N., Platov, Y.T., and Zhekisheva, S.Z., *Glass and Ceramics*, **1993**, 50, 472 – 475.
[81] Adylov, G.T., and Gornostaeva, S.A., *Glass and ceramics*, **1995**, 52, 158 - 159.

7.2 STUDY OF CHINESE CLAY RAW MATERIALS.

The Chinese clay raw materials examined originate from the Jingdezhen area of china and are Jingdezhen porcelain stone and Jingdezhen porcelain stone and kaolin. Literature[75,76,78] has reported how porcelain stone from the Jingdezhen area has been used in the production of Chinese porcelain wares over hundreds of years.

7.2.1 : ANALYSIS OF JINGDEZHEN PORCELAIN STONE.

The XRD pattern for Jingdezhen porcelain stone shows the appearance of peaks indicative of the presence of both illite and quartz (figure 81), therefore showing this sample to be a mix of both clay and non-clay minerals. No further polymorphs of quartz were identified.

Figure 81 : XRD pattern of Jingdezhen porcelain stone.

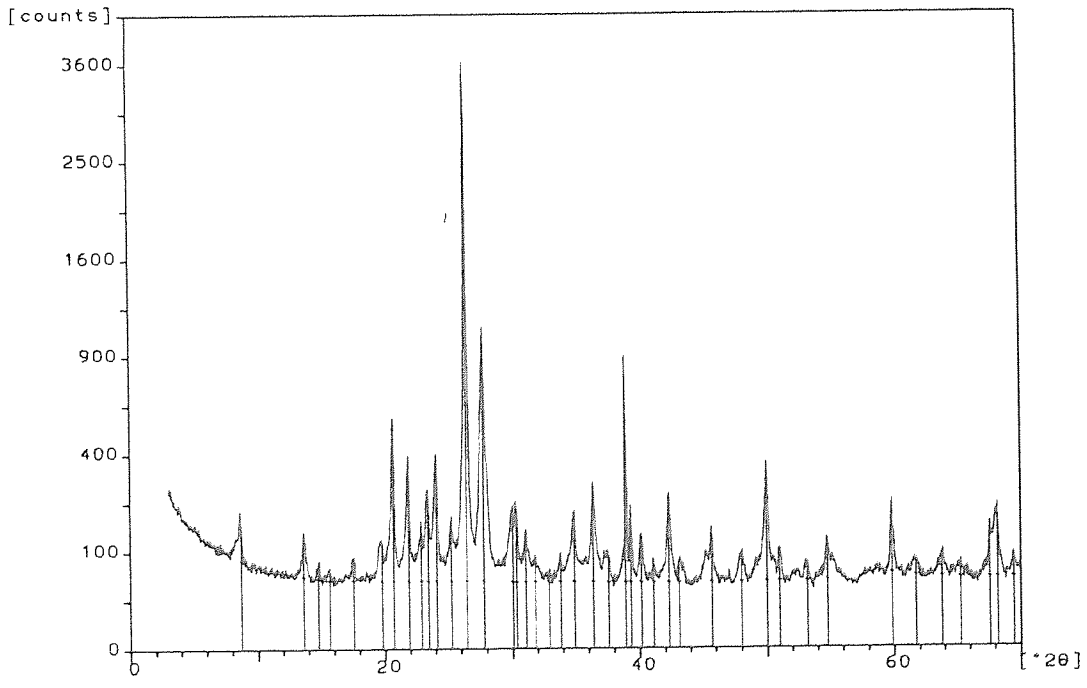

Table 36 : Interpretation of Jingdezhen Porcelain stone XRD pattern.

2θ°	d(values) Å	Intensity	Comment
8.68 17.50 26.41	10.18 5.07 3.37	Weak Weak Strong	Characteristic set of peaks consistent with the appearance of illite. The reflection at 26.41(2θ) is a mixture of illite and quartz. Other peaks suggest disordered illite.
20.66 26.41	4.30 3.37	Strong Strong	Consistent with the appearance of quartz. Intensity of reflection shows high crystallinity. No other polymorphs were identified.

Bands observed on the infra red spectra at ~3627cm^{-1} and 788cm^{-1} (figure 82) are further indicative of the presence of illite and quartz, respectively thus corresponding with the XRD data presented.

Figure 82 : Infra red spectrum of Jingdezhen porcelain stone.

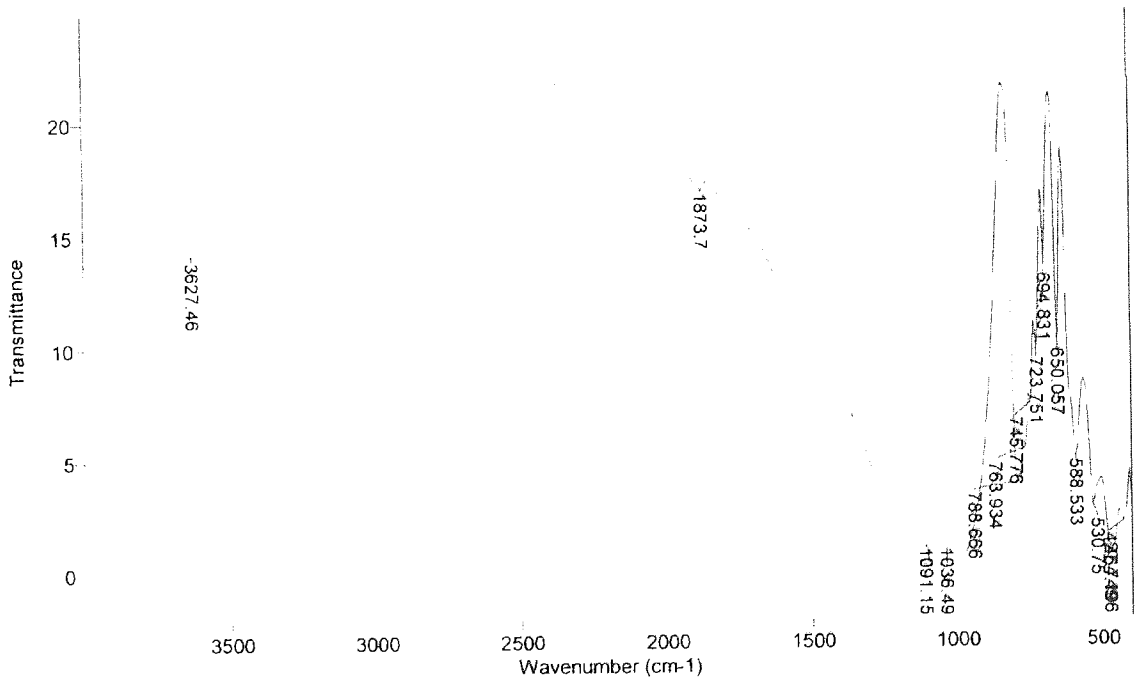

Table 37 : Interpretation of infra red spectrum Jingdezhen porcelain stone.

Absorption cm^{-1}	Assignment	Comment
3627	OH	Type I OH[44] bonded directly to the silicate layer, related to the cation. The broad OH peak close to $3625cm^{-1}$ and with large range is indicative of an an illite type mineral.[47] Broadness of the band may also suggest substitution of Al/Mg by Fe.
1091 1036	SiO	Principal stretching vibrations.[45]
788	OH/Quartz	May be due to OH bending maxima or the appearance of quartz.[47]
694	SiO/OH	SiO vibrations and bending of OH.[45]
530 426	SiO/SiOMg SiOMg	Bending vibrations.[45]

Very few infra red data exist in the literature regarding the composition of Chinese clays. These data are consistent with literature findings on the typical clay compositions of other materials.

The infra red data for Jingdezhen porcelain stone verify the presence of silicon and aluminium in the tetrahedral and octahedral layers. The presence of water molecules shows this to be a non-fired raw material. The Infra red data for the Jingdezhen porcelain stone are consistent with that from XRD showing this to be a clearly complex ceramic raw material.

The broadness of the band at ~$3627cm^{-1}$ suggests the isomorphous substitution of Al/Mg by Fe^{3+}.

The appearance of iron within the sample is confirmed by the ^{29}Si MAS NMR spectrum of Jingdezhen porcelain stone, (figure 82) note the large number of spinning side bands and the degree of background noise which prove that the sample contains high quantities of paramagnetic iron impurities close to active sites.

Figure 83 : ^{29}Si MAS NMR spectrum of Jingdezhen porcelain stone.

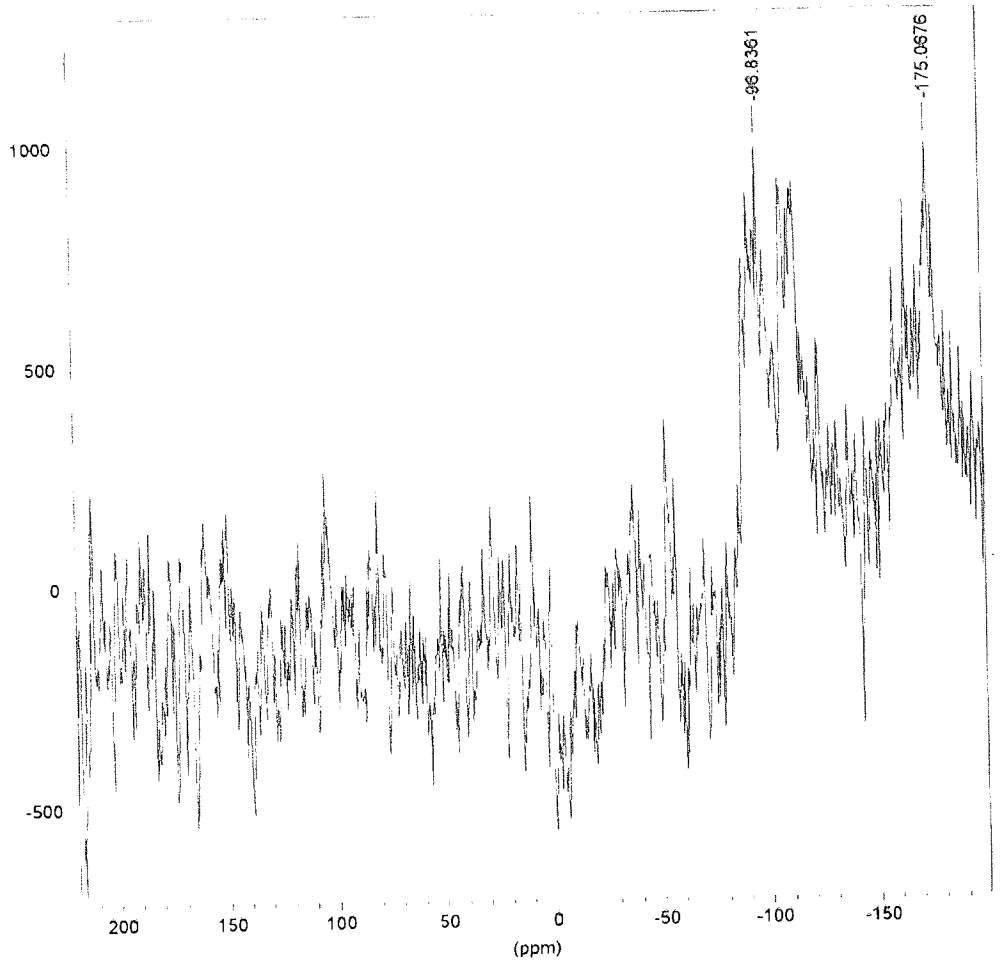

The high degree of distortions shown on the spectrum makes it difficult to interpret, however, the peak at ~-96ppm suggests that some silicon may be occupying a Q_3 co-ordination environment.[47] Thus the silicon is sharing one of its vertices with another atom, this being aluminium that arises through substitution. This is reflected in the ^{27}Al MAS NMR spectrum (figure 84) with the appearance of both tetrahedrally (~50ppm) and octahedrally (~3ppm) bound aluminium

Figure 84 : ^{27}Al MAS NMR spectrum of Jingdezhen porcelain stone.

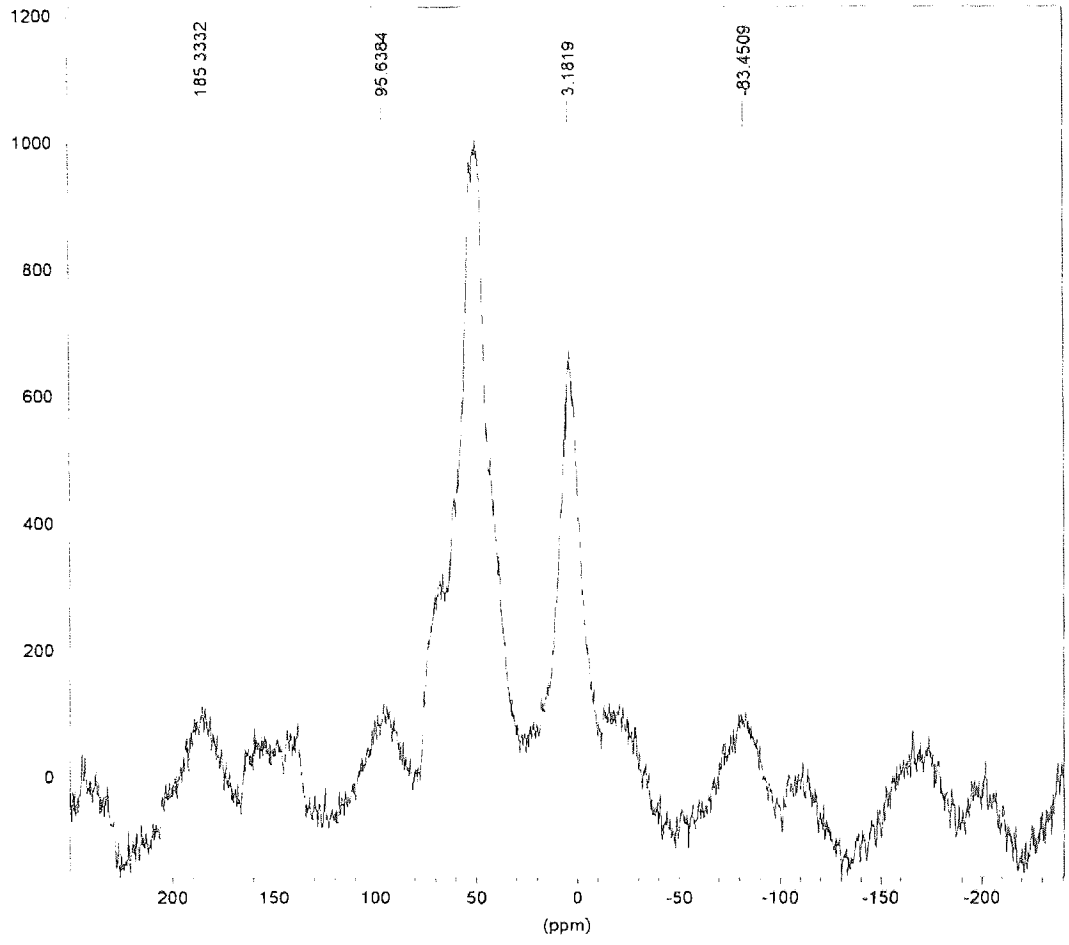

The slight distortion of the resonance at ~50ppm as shown on figure 84 suggests non-uniformity in the layers and this is also suggests the appearance of Al-O-Si.

The large quantity of noise on both the ^{29}Si and ^{27}Al MAS NMR spectra of Jingdezhen porcelain stone suggests that the iron impurities present will be so as structural moieties. ^{57}Fe Mössbauer spectroscopy has not been performed to verify this although washing with concentrated HCl does not produce a coloured solution, suggesting that iron cannot easily be removed.

The dehydration/dehydroxylation trace obtained from the TGA/DTA analysis of Jingdezhen porcelain stone was slightly unusual, as shown in figure 85.

Figure 85 : DTA/TGA trace of Jingdezhen porcelain stone.

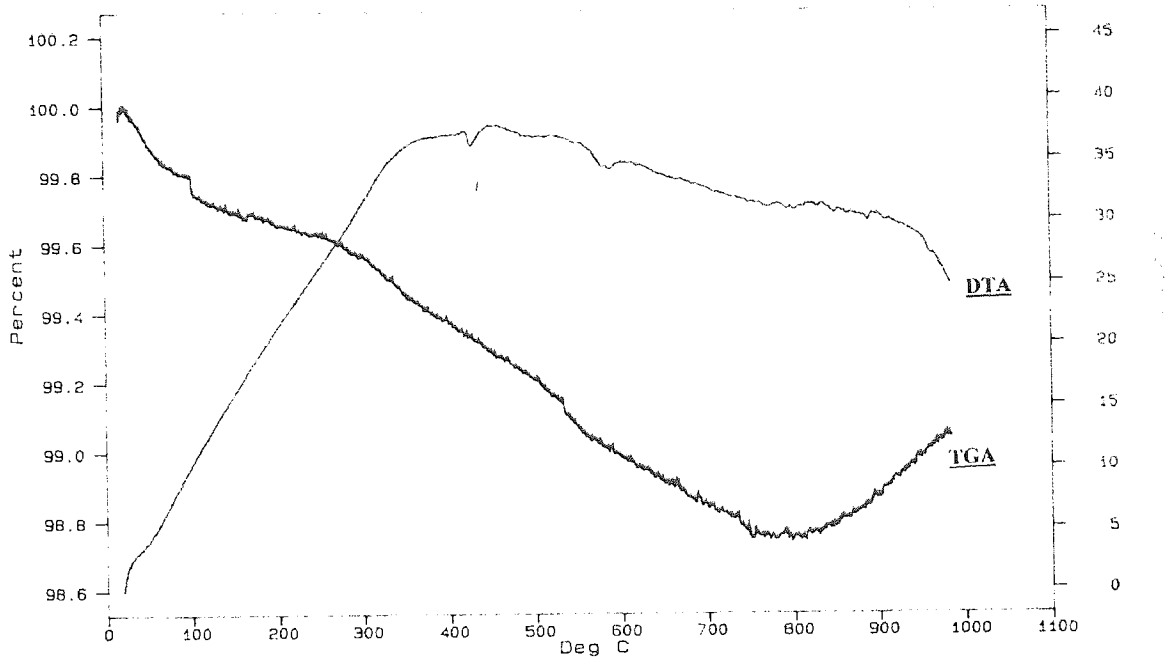

The TGA analysis of Jingdezhen porcelain stone shows a weight loss due to dehydroxylation of approximately 2%. The water loss is not as staged as is usually observed, with only a small step existing at ~100°C. This therefore suggests that the majority of the water is trapped and is not being driven off very quickly.

Table 38 : DTA analysis of Jingdezhen porcelain stone.

Temp°C	Comment
~400-450	Very small endotherm indicative of loss of hydroxyl from the brucite ($Mg(OH)_2$) layer. Also substitution of Al^{3+} by Fe^{3+}.
~570	Small endothermic peak corresponding to the transformation of α quartz to β quartz.[53]

Neither the DTA or TGA analysis provide much information regarding the dehydration/dehydroxylation pattern of the Jingdezhen porcelain stone. The slope of the TGA shows approximately 2% water loss although the DTA trace does show transitions consistent with dehydration/dehydroxylation.

The small endotherm at ~570°C on the DTA trace, highlights the phase transition from α to β quartz, the more stable moiety at higher temperatures. The characteristic weight

loss at ~450°C is also indicative of the substitution of Fe^{3+} for Al^{3+} in the octahedral layers, as shown earlier by infra red (figure 82) and suggested by MAS NMR spectra.(figures 83 and 84)

The particle sizing was used to identify the particle size distribution of the aqueous clay suspensions. Samples were observed using a suspension in filtered distilled water over the range 1μm - 100μm using a Malvern SB-20 particle sizer. Jingdezhen porcelain stone exhibited a particle size distribution in the range 2μm - 100μm, as shown in figure 86.

Figure 86 : Particle size distribution for Jingdezhen porcelain stone.

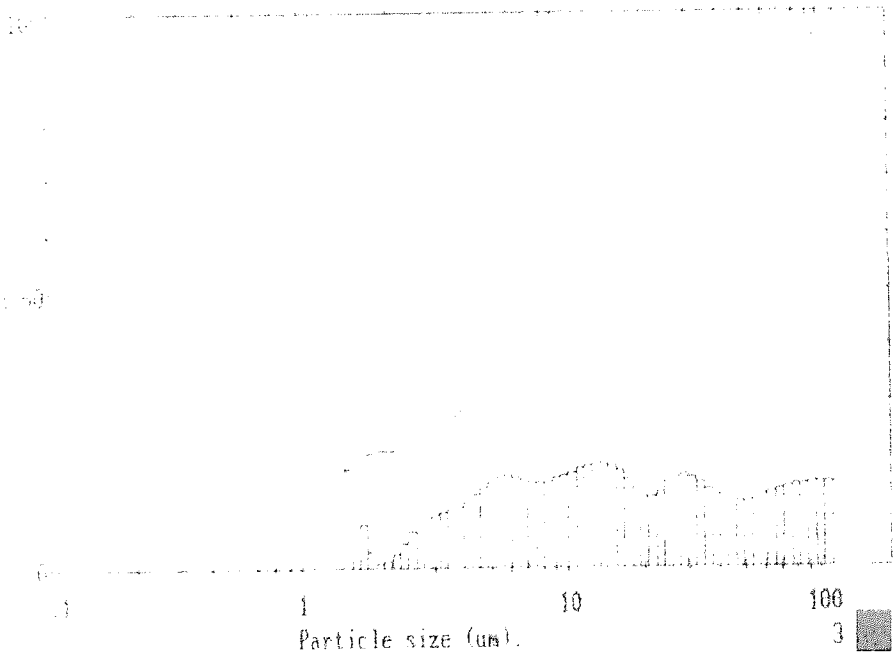

7.2.2 ANALYSIS OF 'JINGDEZHEN PORCELAIN STONE AND KAOLIN'.

The second Chinese raw material analysed was 'Jingdezhen porcelain stone and kaolin'. The XRD pattern obtained (figure 87) gave results consistent with those obtained from the original Jingdezhen and porcelain stone sample (figure 82)

Figure 87 : XRD pattern of Jingdezhen porcelain stone and kaolin.

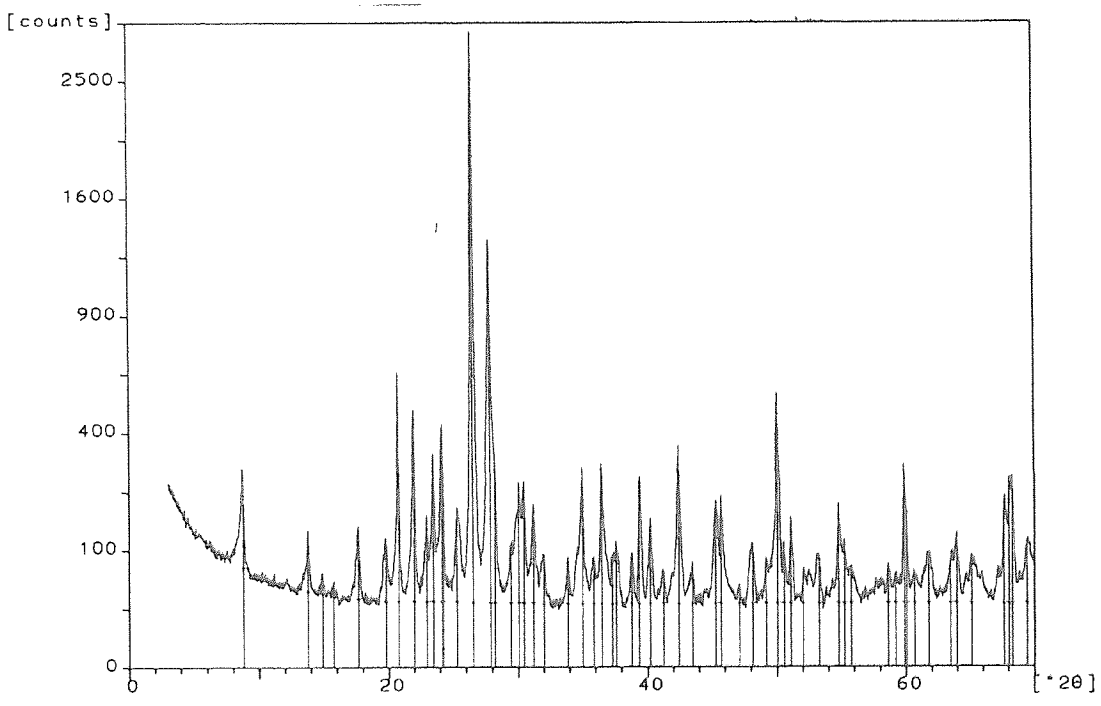

Table 39 : Interpretation of XRD pattern 'Jingdezhen Porcelain stone and Kaolin'.

2θ°	d(values) Å	Intensity	Comment
8.76 17.62 26.52	10.09 5.03 3.36	Medium Medium Strong	Characteristic set of peaks indicative of the presence of illite.
20.75 26.54	4.28 3.36	Strong	Peaks suggest highly crystalline mineral quartz.
20.75 53.25	4.28 1.72	Strong Weak	Indicative of the presence of Goethite (αFeOOH). Reflection at 20.75 (2θ) shared with quartz.

In addition to those peaks observed for illite and quartz, the spectrum of the sample of 'Jingdezhen porcelain stone and kaolin' has peaks indicative of the iron impurity,

Geothite (α-FeOOH). It is assumed that a peak for kaolin should be clearly visible on the XRD pattern, however this has not been evident. The lack of kaolin in the 'Jingdezhen porcelain stone and kaolin' sample was further supported by data gained from infra red analysis, as shown in figure 88.

Figure 88 : Infra red spectrum of 'Jingdezhen porcelain stone and kaolin'.

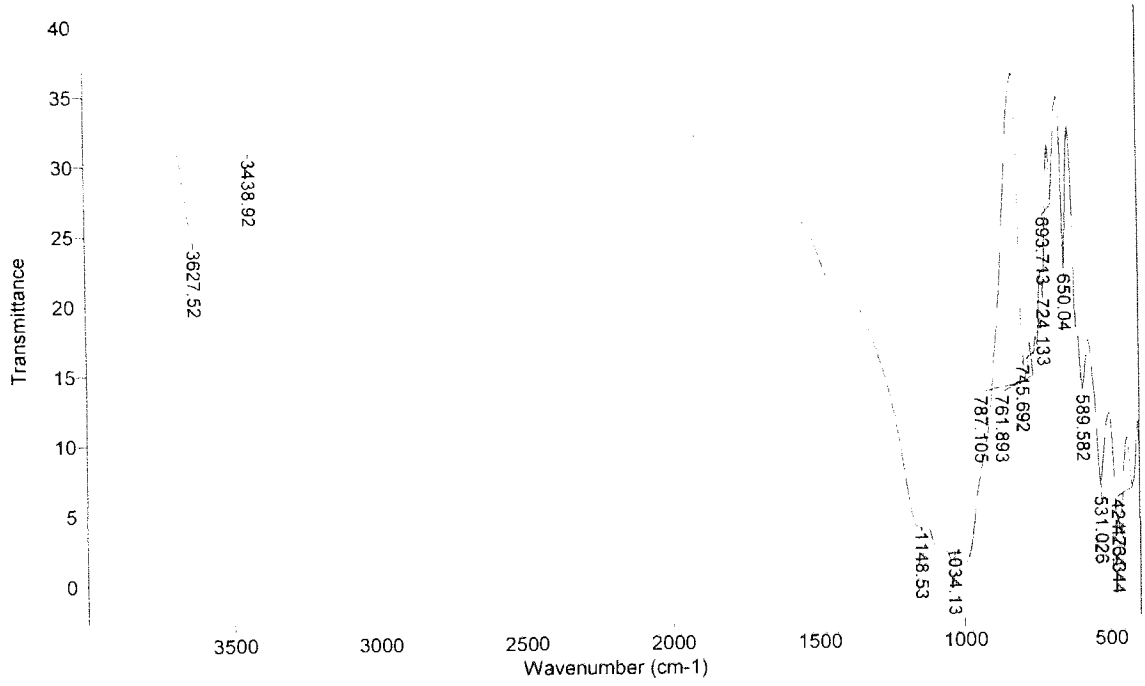

Table 40 : Interpretation of Infra red spectrum 'Jingdezhen porcelain stone and kaolin'.

Absorption cm^{-1}	Assignment	Comment
3627.52	OH	Type I OH bonded directly to the cation.[44] The broad large range absorption is indicative of an illite type mineral.[47] There is some suggestion of Al/Mg by Fe substitution.
3437.92	OH/H_2O	Absorption indicative of the more labile H_2O/OH.[44]
1148.53 1034.13	SiO	Principal SiO stretching mode.[45] The appearance of two distinct peaks may suggest structural distortion.[47]
787.11	OH/Quartz	OH bending maxima or due to the appearance of quartz.[47]
693.71	SiO	SiO vibrations and bending of OH.[45]
531.03 424.43	SiO/SiOMg SiOMg	Bending vibrations.[45]

The lack of kaolin in both the XRD pattern and infra red spectrum suggests that it is not present in the raw material as anticipated. It would appear from both the XRD and Infra red data that the predominant clay mineral in this sample is illite, with bands consistent with its appearance observed in both

Like the previous Jingdezhen sample this appears to be a non-fired sample as indicated by bands at ~3620cm^{-1} and 3400cm^{-1} attributed to type I and type II water, respectively.[44] The results obtained for both of the porcelain stone samples are not consistent with those cited within literature studies, since the observation of a greater quantity of kaolin and feldspar was anticipated.

The broadness of the peak at ~3620cm^{-1} suggests that there may be some substitution of Al/Mg by Fe^{3+} in the octahedral layer. Both ^{29}Si MAS NMR (figure 89) and ^{27}Al MAS NMR exhibited large spinning side bands, combined with loss of resonance and background noise. This was particularly prevalent for the ^{27}Al spectrum where a resonance could not be identified.

Figure 89 : ^{29}Si MAS NMR spectrum of 'Jingdezhen porcelain stone and kaolin'.

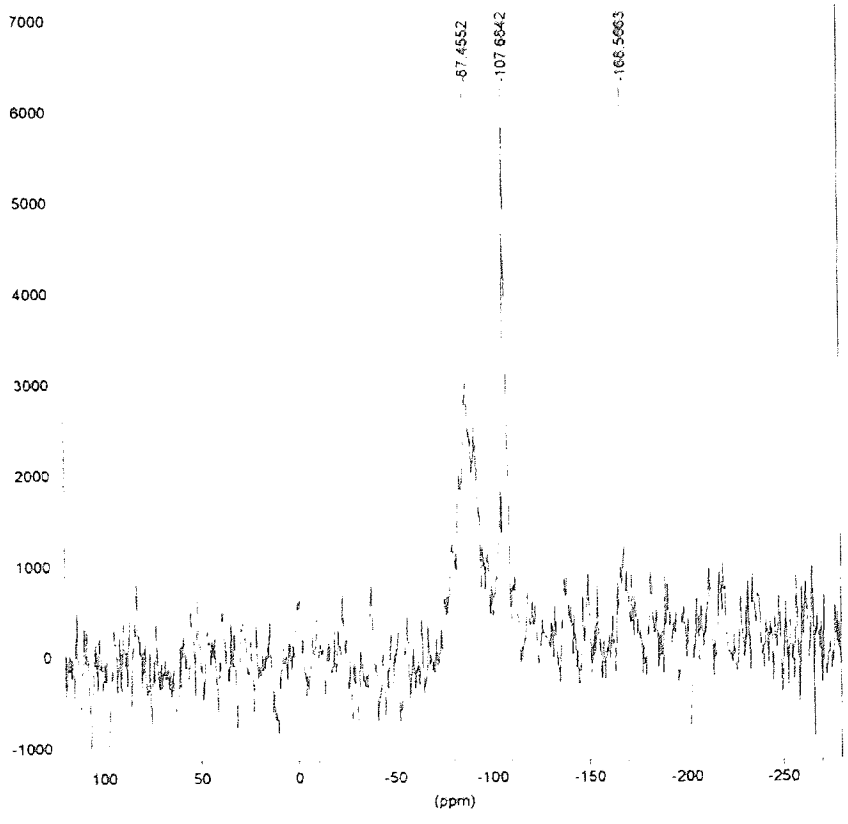

The ^{29}Si MAS NMR spectrum shows a strong sharp resonance at ~-107ppm that indicates that many of the silicon occupies a Q_4 co-ordination environment. A smaller broad resonance at ~-87ppm shows silicon in a Q_3 environment possibly situated closer to paramagnetic impurities as indicated by the greater distortion.[47] Had it been possible to obtain a ^{27}Al MAS NMR spectrum then both octahedrally and tetrahedrally co-ordinated aluminium would therefore have been observed.

The pattern of dehydration/dehydroxylation, as determined by TGA/DTA, showed very similar results to those obtained from the original Jingdezhen and porcelain stone sample. The trace obtained for 'Jingdezhen porcelain stone and kaolin' as shown in figure 90, exhibits a slightly more staged dehydration/dehydroxylation TGA trace, with transitions appearing at ~100°C and ~500°C associated with the loss of sorbed and bound water, respectively.

Figure 90 : DTA/TGA trace of Jingdezhen porcelain stone and kaolin.

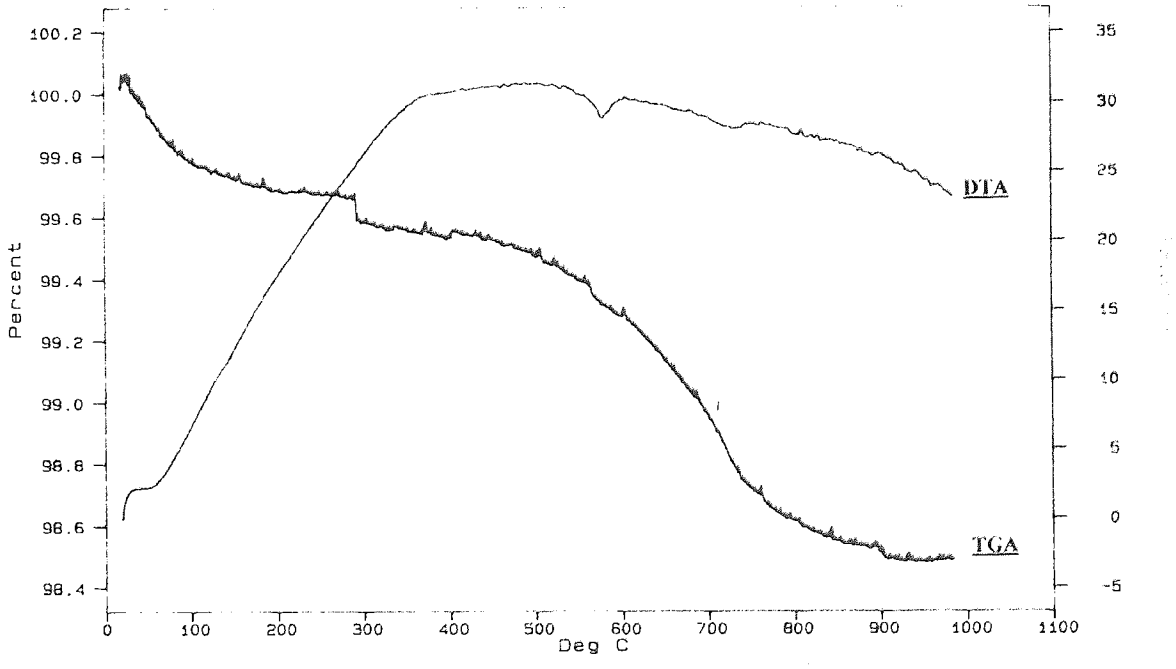

Table 41 : Interpretation of the TGA trace of 'Jingdezhen porcelain stone and kaolin'.

Temp°C	Comment
~100 - 300	Loss of sorbed or loosely bound water.
~500 - 700	Further weight loss indicative of the removal of structural OH as water.

Table 42 : Interpretation of the DTA trace of 'Jingdezhen porcelain stone and kaolin'.

Temp°C	Comment
~100	Very small endotherm indicative of the loss of loosely bound hydroxyls.
~570	Endotherm corresponding to the inversion of α quartz to β quartz. As well as further dehydroxylation.
~750 - 800	Indicative of dehydroxylation due to the removal of structural OH.

The loss of the loosely bound water is supported by transitions on the DTA at ~100°C and ~570°C. The small endotherm at ~570°C is further indicative of the phase change of α quartz to β quartz the more stable moiety at higher temperatures. Unlike the original Jingdezhen porcelain stone a further transition on the DTA is observed here representative of further dehydroxylation, suggesting that the water is more tenaciously held.

Particle sizing was used to identify particle size distribution in the clay suspensions. The distribution for 'Jingdezhen porcelain stone and kaolin' showed approximately 50% of the particles to fall into the 300μm - 100μm region.(figure 91) It would appear upon comparison of this data to the original Jingdezhen porcelain stone that the apparent addition of kaolin to the sample causes the particles to agglomerate to give much larger particles.

Figure 91 : Particle size distribution for Jingdezhen porcelain stone and kaolin.

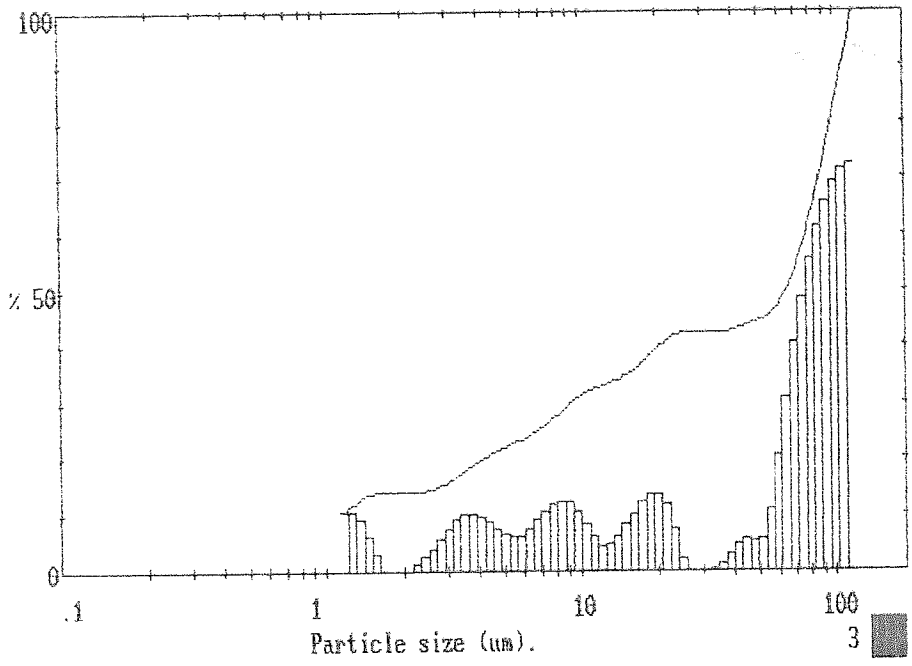

7.3 SUMMARY OF JINGDEZHEN PORCELAN STONE AND JINGDEZHEN PORCELAIN STONE AND KAOLIN.

Characterisation of the Chinese raw materials has afforded some interesting data allowing a better understanding of sample composition to be gained and which can later be used to determine if there is a connection between Chinese raw materials and Chinese clay bodies.

Infra red has proved an invaluable tool in determining functionality within the samples. Data has shown both the Jingdezhen samples to be of typical clay composition, with a predominance of silicon and aluminium in the tetrahedral and octahedral layers. Data has shown both samples to be hydrous and non-fired. Literature [75,76,77,78] provides information to suggest that kaolin plays a significant role in the composition of porcelain stone. Infra red data for the Jingdezhen samples are not consistent with this observation, with illite being the only clay mineral observed, formed as a result of the aging process. Broadness of the illite peaks suggests possible substitution of aluminium or magnesium by iron. Further examination of the infra red spectra showed he presence of quartz in both samples, XRD also provides evidence to support its presence.

XRD data have afforded the most information regarding clay mineral composition. Both samples were shown to be a mix of clay and non-clay minerals. Geothite was observed in the pattern of 'Jingdezhen porcelain stone and kaolin'. Findings are consistent with data obtained from infra red spectra.

^{29}Si MAS NMR spectra for both the Jingdezhen samples show silicon to be in a Q_3 environment, whilst for the 'Jingdezhen porcelain stone and kaolin' some silicon is also observed as Q_4. Consequently, ^{27}Al MAS NMR spectra show both octahedrally and tetrahedrally co-ordinated aluminium. The amount of noise on the spectra is a result of interactions of the spin I = ½ nuclei with paramagnetic species.

TGA traces show water loss as a result of the heating process. An unusual trace is observed for the original Jingdezhen porcelain stone with TGA appearing to indicate a phase change rather than normal patterns of water loss. DTA exhibits transitions consistent with those observed on TGA. Both Jingdezhen samples exhibit transitions

consistent with the phase change of α quartz - β quartz and endotherms indicative of the substitution of some Al^{3+} by Fe^{3+} in the octahedral sites.

Analysis of the particle size of the Jingdezhen samples in suspension led to the conclusion that particles exist in the range 1μm - 100μm. The addition of kaolin to the Jingdezhen porcelain stone causes a predominance of particles in the 30μm - 100μm region, whereas Jingdezhen porcelain stone shows an even spread over the whole particle range.

7.4 ANALYSIS OF CHINESE CLAYS.

The two Chinese clays originate from the Wuxi and Yixing areas of China. A lack of literature on these clays suggests that they are relatively unknown to the western ceramicist. The data presented herein provides a detailed analysis of these two clay materials and aims to identify similarities between those Jingdezhen raw materials previously examined.

7.4.1 ANALYSIS OF WUXI CLAY.

As for the raw material samples XRD shows Wuxi clay (figure 92) to be a mix of both clay and non-clay minerals; in this instance these are predominantly quartz and kaolinite. Unexpectedly kaolinite was not observed in the Jingdezhen samples while illite was found to be the dominant clay mineral.

Figure 92 : XRD pattern of Wuxi Clay.

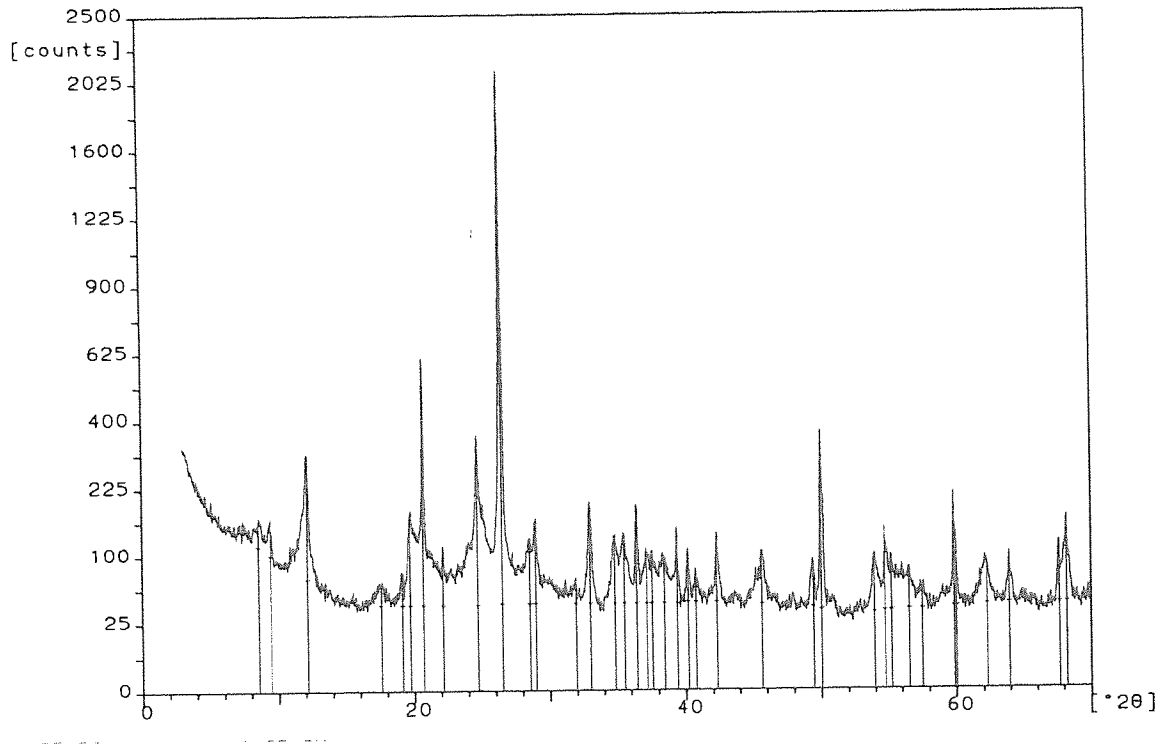

Table 43 : Interpretation of the XRD pattern of Wuxi clay.

2θ°	d(values) Å	Intensity	Comment
20.67	4.29	Strong	Two peaks consistent with the appearance of quartz. Sharpness of the peak is indicative of a high crystallinity. There is no indication of any other polymorphs of silica.
26.48	3.36	Strong	
12.15	7.28	Medium	Suggest the appearance of kaolinite. Peak at 24.71 (2θ°) is characteristic of 002 reflection of kaolinite.
24.71	3.60	Medium	
37.15	2.42	Weak	

No further polymorphs of quartz were observed, whilst the sharpness of the peaks indicate a sample of highly crystalline quartz. Infra red provides data to support that from XRD, as shown in figure 93. The Bands at 3699cm^{-1} and 3622cm^{-1} are indicative of kaolin whilst the peak at 694cm^{-1} are most probably linked with the appearance of quartz.

Figure 93 : Infra red spectrum of Wuxi clay.

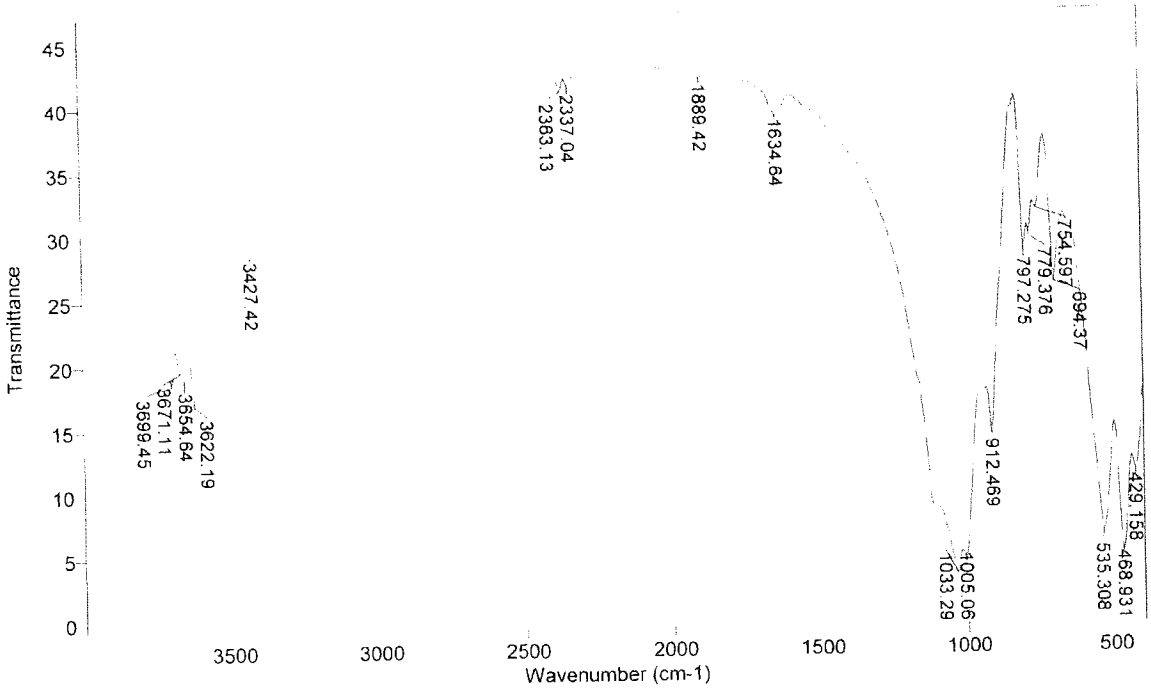

Table 44 : Interpretation of Infra red spectrum of Wuxi clay.

Absorption cm^{-1}	Assignment	Comment
3699 3671 3654 3622	OH	All type I OH bands.[44] Absorptions at $3699cm^{-1}$ and $3622cm^{-1}$ are indicative of a kaolin type structure. The central bands at $3671cm^{-1}$ and $3654cm^{-1}$ suggest relative order in structure. Disordered kaolin would give a single band.[47]
3427	OH/H_2O	Type II usually more labile water.[44]
1634	OH/H_2O	H-O-H bending maxima.[44]
1033 1005	SiO	Indicative of the principal SiO stretching mode.[45]
912	OH	OH deformation band also a characteristic of the kaolin group.[47]
797 779 754	Silica Mineral or OH or Kaolin	1)OH bending maxima 2) Slightly downshifted quartz absorptions 3) $797cm^{-1}$ characteristic of Tridymite (SiO_2 polymorph)[47] 4) Possible well ordered kaolin.[47] Most probably quartz as linked with absorption at $694cm^{-1}$.
694	SiO/OH	SiO vibrations and bending of OH.[45]
535 468	SiO/SiOMg SiOMg	Bending vibrations.[45]

The fact that kaolin appears in the spectra recorded from Wuxi clay suggests that in this instance kaolin is a component of the overall mix and not just porcelain stone.

The appearance of peaks at ~3699cm^{-1} and ~3670cm^{-1} are consistent with this being a hydrated sample and hence non-fired. The infra red data for Wuxi clay has also identified the presence of tridymite, a polymorph of silica formed as a result of the aging process, therefore supporting the deduction that highly weathered porcelain stone is used during production.[78]

Infra red data further verifies the presence of silicon and aluminium in the tetrahedral layers.

The ^{29}Si MAS NMR spectrum of Wuxi clays exhibits a strong broad resonance at ~-92ppm.consistent with silicon in a Q_3 co-ordination environment, as shown in figure 94.

Figure 94 : ^{29}Si MAS NMR spectrum of Wuxi clay.

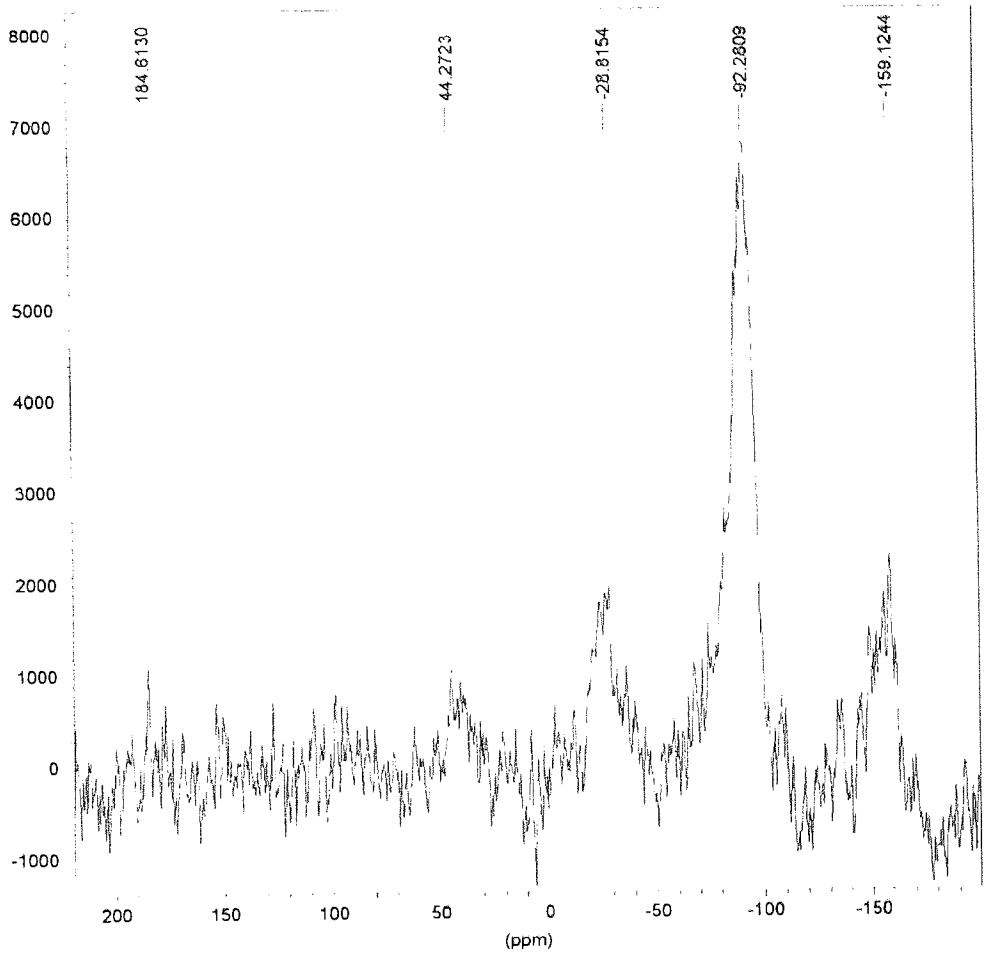

The broadness of the peak at ~-92ppm as shown in figure 94 suggests paramagnetic species occupying sites close to active centres. The resonances at ~-159ppm and ~-28ppm are spinning side bands and so artefacts of the experiment. The appearance of Q_3 silicon shows that the silicon is not fully polymerised and is therefore sharing one vertix with another atom, probably Al. This is not strongly reflected in the ^{27}Al MAS NMR spectrum of Wuxi clay (figure 95) as only one sharp resonance is observed at ~1ppm consistent of Al in an [AlO_6] co-ordination. However, the ^{27}Al spectrum of Wuxi clay also suggests the appearance of some tetrahedrally co-ordinated Al, as indicated by the shoulder on the SSB at ~93ppm. The information obtained thus far for Wuxi clay exhibits little similarity between Wuxi clay and Jingdezhen raw materials.

Figure 95 : ^{27}Al MAS NMR spectrum of Wuxi Clay.

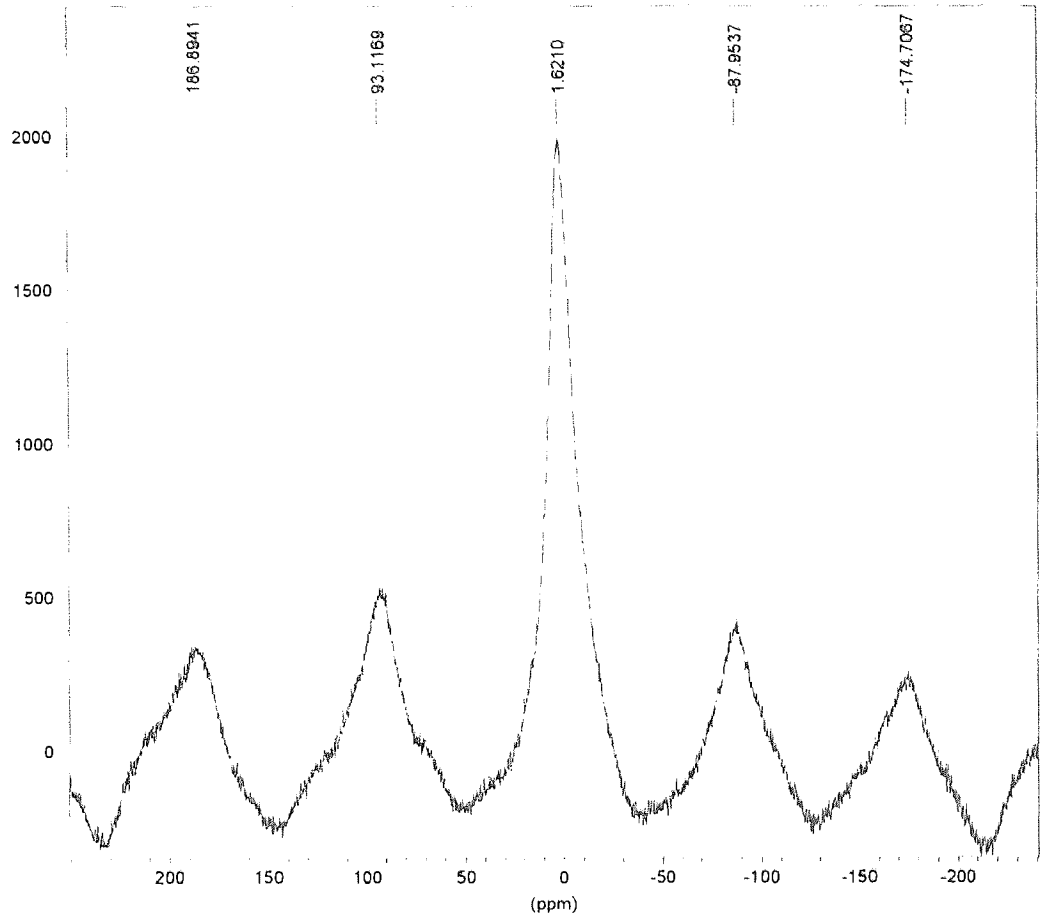

Both the ^{29}Si and ^{27}Al MAS NMR spectra for Wuxi clay, reported above have highlighted the adverse effect that iron has upon them. ^{57}Fe Mössbauer spectroscopy performed on Wuxi clay has provided further information regarding the nature and environment of iron with the sample.

^{57}Fe Mössbauer spectra were recorded using a microprocessor-controlled Mössbauer spectrometer using a 25mCi ^{57}Co/Rh source and natural iron absorber. Spectra are computer fitted and chemical isomer shift data quoted relative to metallic iron.

The spectra shown in figure 96 of Wuxi clay shows the presence of two iron species.

Figure 96 : ^{57}Fe Mössbauer spectrum of Wuxi clay.

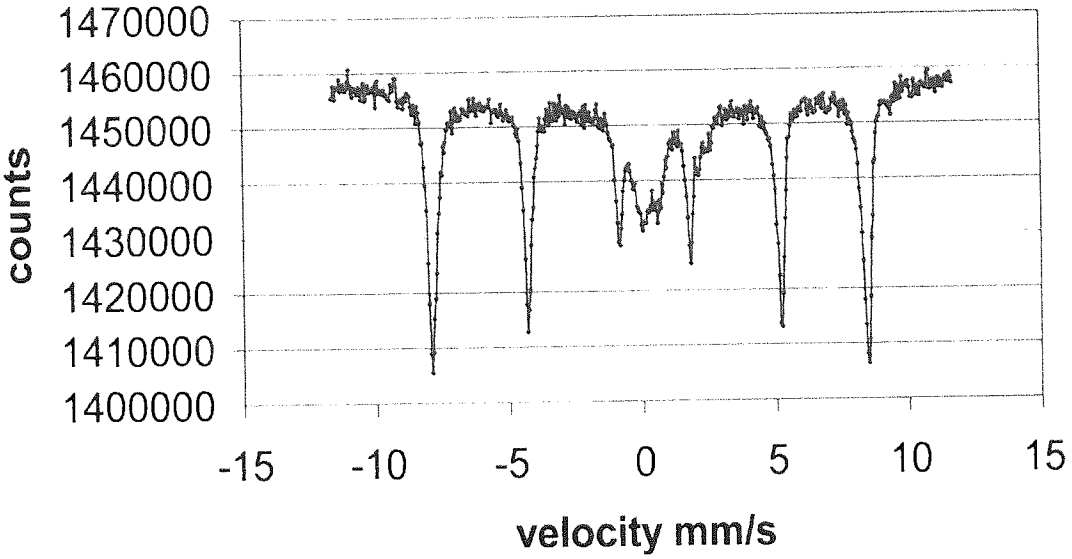

The spectrum shows a sextet typical of large particle α-Fe_2O_3[52] that should be removable *via* acid washing with HCl. The extent of this has been observed in the MAS NMR spectra. The spectrum also shows Fe^{2+} to be present; it is possible this is as small particleFe_2SiO_4.

TGA/DTA data obtained for Wuxi clay (figure 97) provided a much clearer trace than those shown for the Jingdezhen samples (figures 85 and 90)

Figure 97 : DTA/TGA trace of Wuxi clay.

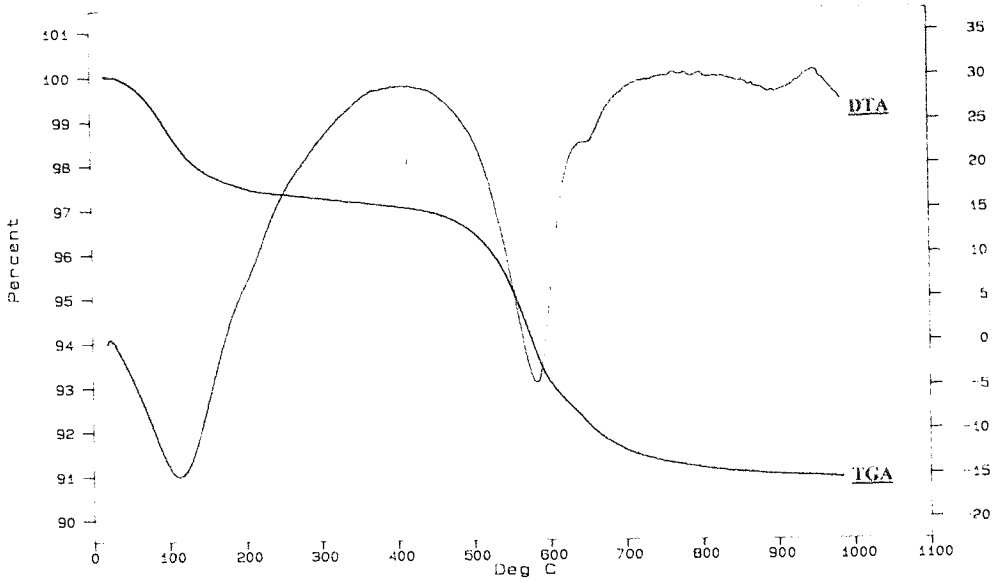

Table 45 : Interpretation of the DTA trace of Wuxi clay.

Temp°C	Comment
~100	Endotherm due to loosely bound hydroxyl groups.
~575	Endothermic peak corresponding to the transformation of α quartz to β quartz.[53] Followed by a small shoulder indicative of some recrystallisation. Start of dehydroxylation.
850-900	Suggestion of a small endotherm indicative of further dehydroxylation of interstitial water.

Table 46 : Interpretation of the TGA trace of Wuxi clay.

Temp°C	Comment
~100	Loss of loosely bound or sorbed water.
~500-700	Dehydroxylation occurring as a result of the loss of interstitial water.

The clearly observed transitions, at ~100°C and ~575°C shown on the TGA trace in figure 97 are consistent with loss of loosely bound and interstitial water respectively. These are supported by transitions on the DTA at ~100°C and ~400°C. The additional endotherm at ~850 – 900°C on DTA trace is indicative of further dehydroxylation.

The appearance of a small shoulder at ~570°C is indication of further phase change beginning to occur in the Wuxi clay after the characteristic transition of α quartz - β quartz.

The particle size distribution for Wuxi clay as shown in figure 98, exhibits particles to cover the full range from 1μm - 100μm, with a predominance of particles in the 10μm - 100μm region.

Figure 98 : Particle size distribution Wuxi clay.

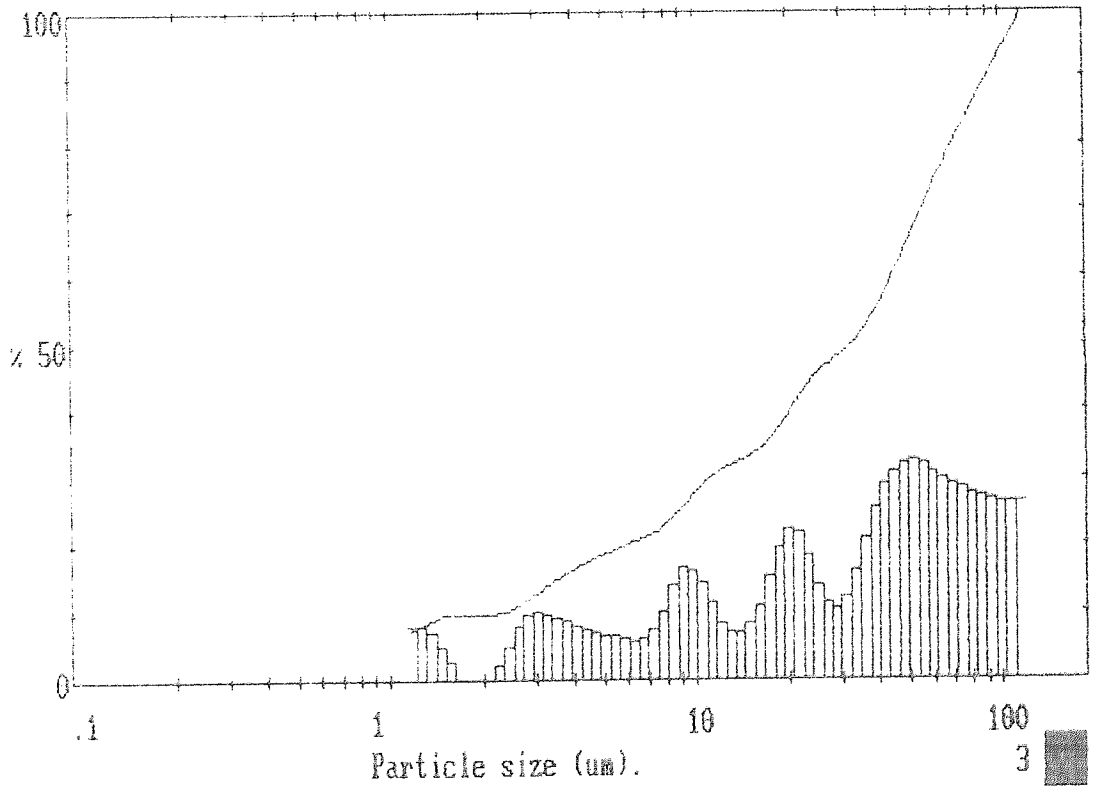

The distribution shown above is not unlike that observed for Jingdezhen porcelain stone (figure 86) with the latter showing a more even spread of particle size.

7.4.2 ANALYSIS OF YIXING CLAY

The XRD data for Yixing clay as presented in table 47 and shown in figure 99 is consistent with that from Wuxi clay and the Jingdezhen raw materials exhibiting peaks consistent with the appearance of illite, kaolinite and highly crystalline quartz.

Figure 99 : XRD pattern of Yixing clay.

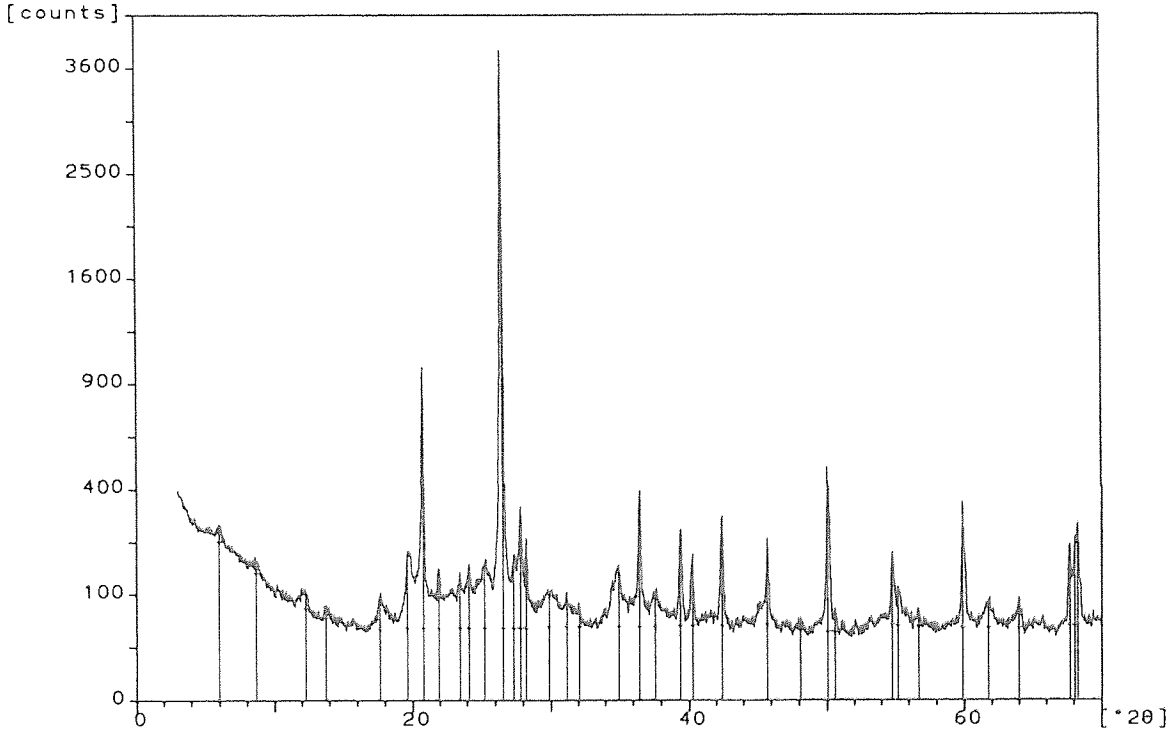

Table 47 : Interpretation of XRD pattern for Yixing clay.

2θ°	d(values) Å	Intensity	Comment
5.96 17.59 23.45	14.83 5.04 3.79	Weak	Reflections suggest some montmorillonite to be present.
12.28 24.11	7.20 3.69	Weak	Suggests the appearance of kaolinite.
8.60 17.59 26.54	10.27 5.04 3.36	Weak Strong	A trio of peaks consistent with the appearance of illite. Reflection at 26.54 (2θ) shared with quartz.
20.75 26.54	4.28 3.36	Sharp	Indicative of the quartz in a highly crystalline state.

In addition to these, Yixing clay also exhibits small reflections consistent with the appearance of montmorillonite, a clay mineral not observed in any of the other samples.

Infra red data on Yixing clay (figure 100) confirm what is already known regarding clay constitution and is consistent with the information gained from XRD (figure 99)

Figure 100 : Infra-Red spectrum of Yixing clay.

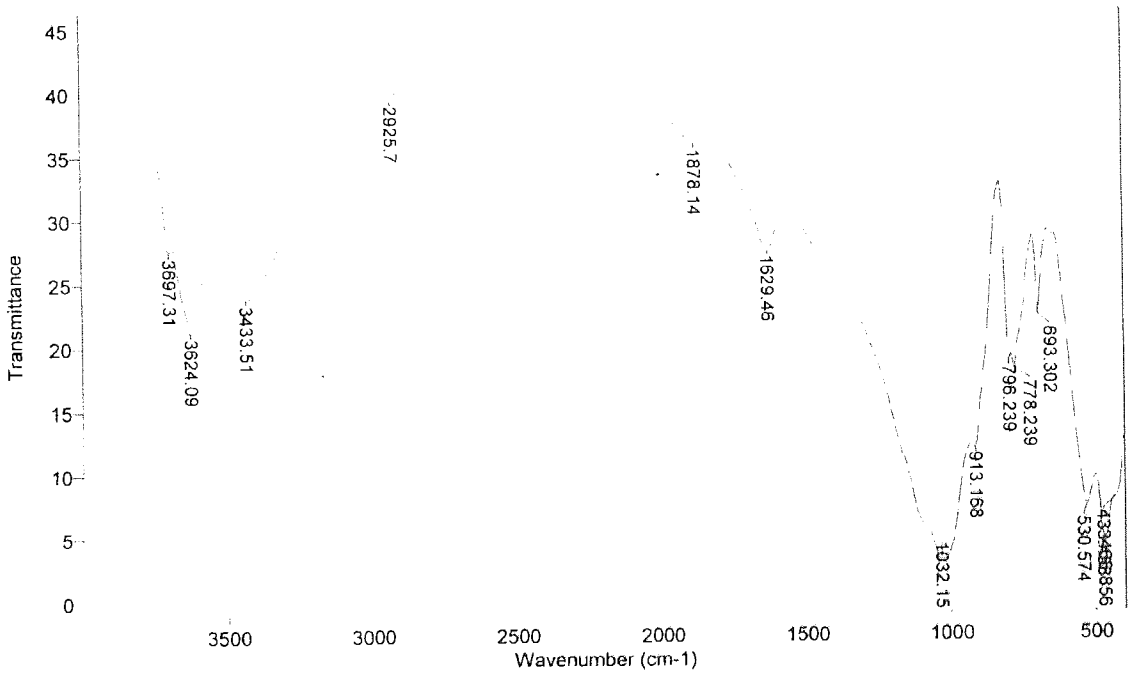

Table 48 : Interpretation of Infra-Red spectrum of Yixing clay.

Absorption cm^{-1}	Assignment	Comment
3697	OH	Kaolin type absorption.[47]
3624	OH	Type I OH[44] . Kaolin type absorption.[47] Absence of a peak at ~3620cm^{-1} suggests mineral may be halloysite.[47]
3624	OH	OH stretch indicative of low Fe montmorillonite.[47]
3433	OH	Type II OH/H_2O, more labile.[44] Kaolin type peak[47]
1629	OH	H-O-H bending maxima, type II OH/H^2O.[39]
1032	SiO	Principal stretching mode.[45]
913	OH	OH bending absorption typical of a dioctahedral mineral such as kaolin.
796 778 639	Quartz	This trio of bands are characteristic of quartz the weakness of the band at 796cm^{-1} compared to band at 778cm^{-1} is indicative of halloysite as well as kaolinite.[47]
530 433	SiO/SiOMg SiOMg	Bending vibrations.[45]

The appearance of bands at ~3697cm^{-1}, in the spectrum recorded from Yixing clay is indicative of the appearance of kaolinite whilst the absence of a peak at ~3620cm^{-1} may suggest that this actually exists as the additionally hydrated member of the kaolinite family, halloysite. The appearance of kaolin within the Yixing clay and not the Jingdezhen raw materials suggests that kaolin is a component of the overall mix.

The presence of water molecules as shown by bands at ~3697cm^{-1} and ~3624cm^{-1}, show this to be a non-fired clay. Whilst the appearance of an OH stretch at ~3624cm^{-1} is consistent with low Fe-content montmorillonite. This interpretation is consistent with that of the XRD reflections previously observed.

The infra red results obtained for all samples examined show them to be clearly complex materials.

As shown previously for the other samples examined, the ^{29}Si and ^{27}Al MAS NMR spectra for Yixing clay exhibit much background noise resulting from paramagnetic impurities close to active nuclei, see figures 101 and 102, respectively.

Figure 101 : ^{29}Si MAS NMR spectrum of Yixing clay.

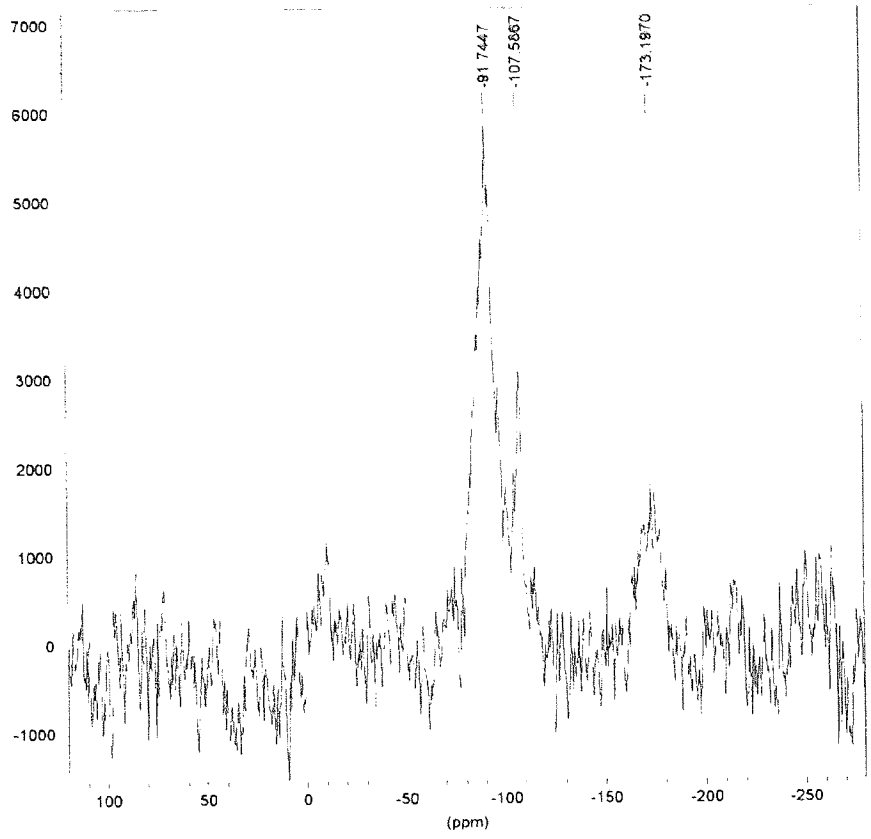

Figure 102 : ^{27}Al MAS NMR spectrum of Yixing clay.

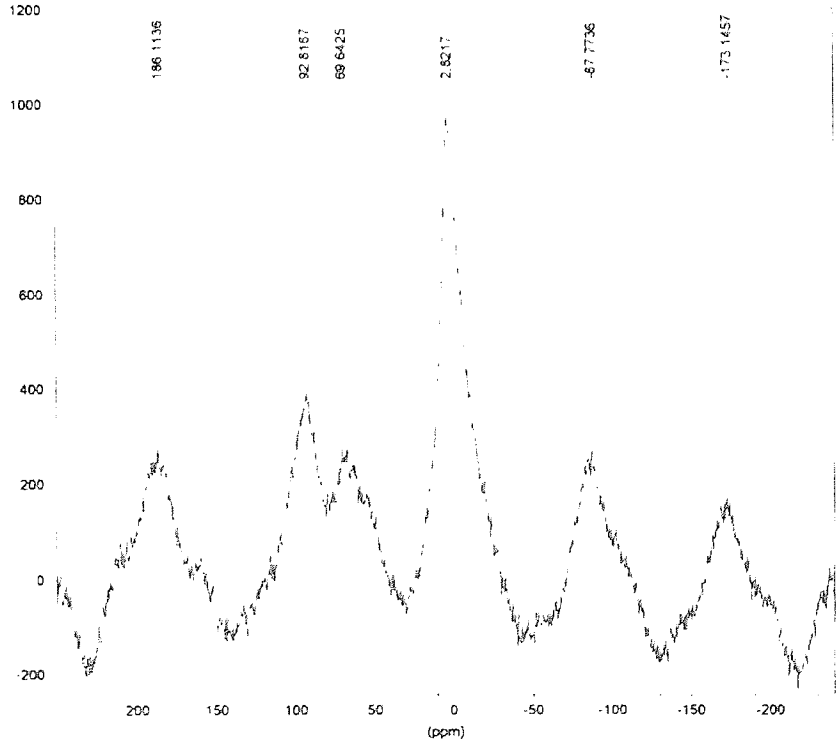

Yixing clay exhibits similar ^{29}Si MAS NMR spectra to the Jingdezhen porcelain stone and kaolin sample (figure 89) with silicon atoms occupying both Q_4 and Q_3 co-ordination environments, as shown by resonances at ~-107ppm and ~-91ppm, respectively.[47] The strength of the peak at ~-91ppm shows the majority of the silicon to be Q_3 co-ordinated whilst the broadness shows it to be situated close to paramagnetic iron. ^{27}Al MAS NMR spectrum (figure 102) confirming the presence of both octahedrally and tetrahedrally co-ordinated aluminium, with resonances at ~2ppm and ~69ppm, respectively. This is as anticipated. Again these results are similar to those obtained from 'Jingdezhen porcelain stone and kaolin',(figure 89) where both octahedral and tetrahedral aluminium are observed, tetrahedral Al is predominant in the Jingdezhen and kaolin spectrum.

XRD data have previously provided information to suggest that Yixing clay has montmorillonite character. Literature reports[82] montmorillonite to possess two types of octahedral aluminium based on geometrical differences. This may also partially account for the magnitude of the resonance observed in Yixing spectra.

The presence of paramagnetic iron within Yixing clay is further supported by results from ^{57}Fe Mössbauer spectroscopy. The spectrum shown in figure 103 shows Yixing clay to contain two iron moieties.

Figure 103 : ^{57}Fe Mössbauer Spectrum of Yixing clay.

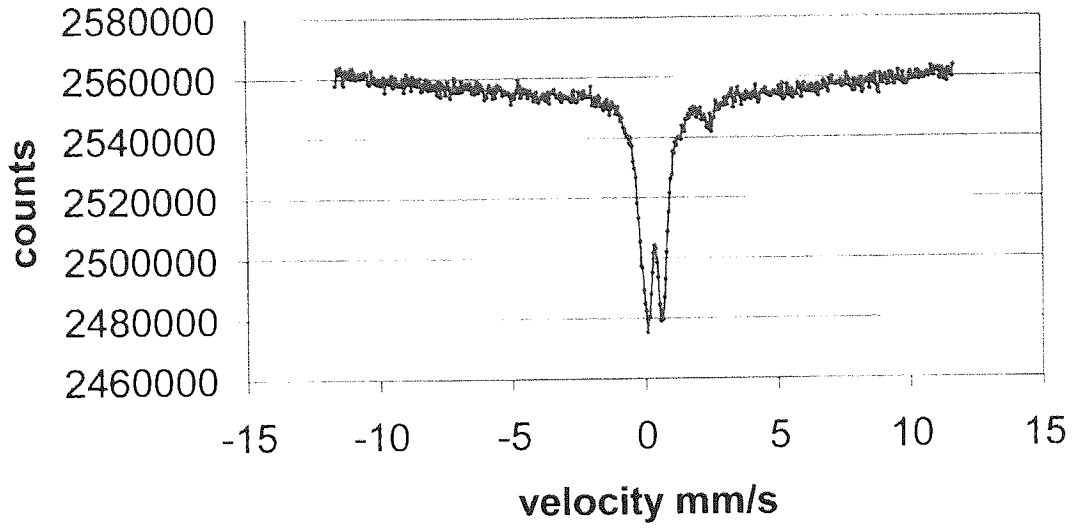

The spectrum shows the presence of both Fe^{2+} and Fe^{3+}. The Fe^{3+} moiety may be associated with small-particle α-Fe_2O_3. The much weaker component is more difficult to assign with certainty but could relate to a little small-particle Fe_2SiO_4, as shown in Wuxi clay.

The dehydration/dehydroxylation pattern obtained from TGA/DTA analysis of Yixing clay (figure 104) provided very similar results to those Chinese clay and raw materials examined previously.

[82] Chatterjee, H., Iwasaki, T., Hayashi, H., Ebina, T., and Torii, K., *Journal of Molecular Catalysis,* **!988,** 136, 195 – 202.

Figure 104 : DTA/TGA trace of Yixing clay.

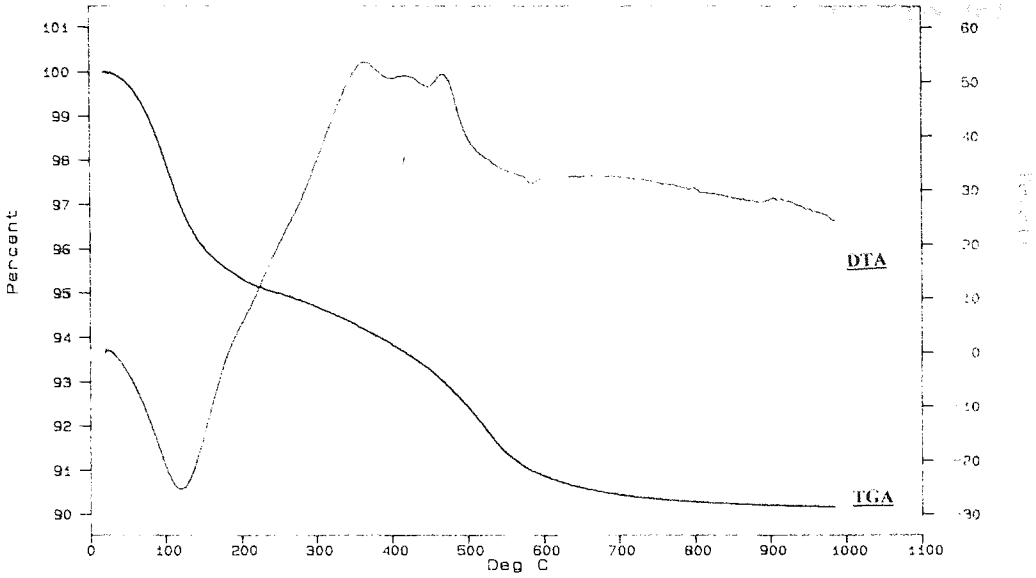

Table 49 : Interpretation of the TGA trace of Yixing clay.

Temp°C	Comment
~100	Indicative of the loss of loosely bound water
~500 - 600	Small weight loss due to dehydroxylation through the removal of structural OH groups.

Table 50 : Interpretation of the DTA trace of Yixing clay.

Temp°C	Comment
~100	Endotherm. Loss of loosley bound OH groups.
~400	Very small endotherm indicative of loss of hydroxyl from brucite ($Mg(OH)_2$ layer.
~450	Very small endotherm suggesting substitution of Al^{3+} by Fe^{3+}.
~570	Very small endotherm showing the transition from α quartz to β quartz. Typical inversion occurs at 573°C +/- 1°C this is affected by performing the experiment in air.

The TGA trace of Yixing clay shows defined transitions, at ~100°C and 500 – 600°C consistent with the loss of both loosely bound and interstitial water. Positions of the transitions correspond closely with literature data.[53,54] These are supported by small DTA transitions at ~100°C and ~400°C. AS for the other samples examined the phase change of α quartz to β quartz is observed, with a DTA transition at ~ 570°C.

The characteristic weight loss at ~450°C for Yixing clay is indicative of the substitution of Fe^{3+} for Al^{3+} in the octahedral sites.

Particle size analysis of the samples shows Yixing clay (figure 105) to exhibit particles across the whole range of 1μm - 100μm, with predominance in the 80μm - 100μm region. This is consistent with the data obtained from 'Jingdezhen porcelain stone and kaolin' (figure 91) where a predominance of particles in the top end of the range is also observed.

Figure 105 : Particle size distribution Yixing clay.

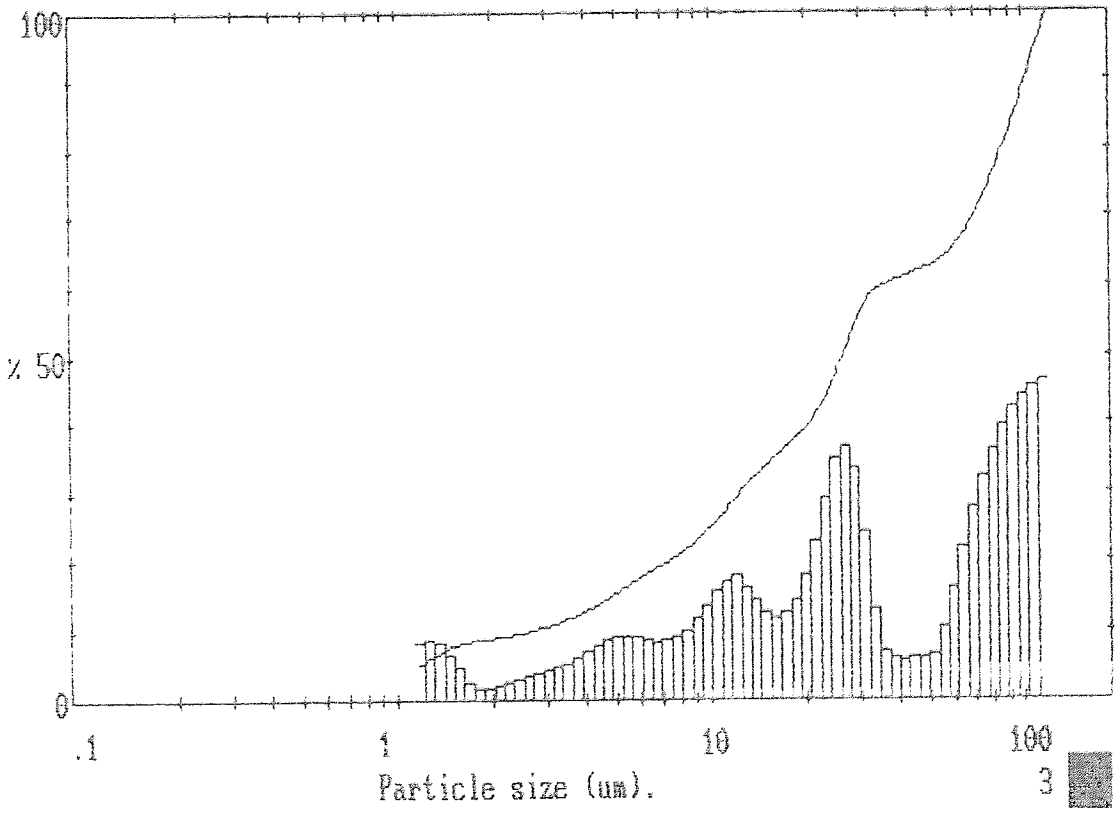

7.5 SUMMARY OF WUXI AND YIXING CLAY.

The infra red data for both Wuxi and Yixing clay samples have shown them to be of typical clay composition, with a predominance of silicon and aluminium in the tetrahedral and octahedral layers, respectively. Data also show the samples to be hydrous and thus non-fired. Spectra for both Wuxi and Yixing clay have shown the appearance of kaolin as well as the additionally hydrated halloysite in addition to those observed for the Jingdezhen samples. A peak at ~3624cm^{-1}on the Yixing spectrum is indicative of low-Fe montmorillonite. Further to this the presence of quartz was also identified in both samples. XRD has afforded data consistent with that from infra red analysis, showing both samples to be a complex mix of both clay and non-clay minerals.

^{29}Si MAS NMR spectra for both of the Chinese clays show silicon to predominantly occupy a Q_3 environment. In addition to this Yixing clay shows some silicon in a Q_4 environment, consistent with information obtained from Jingdezhen porcelain stone and kaolin sample. ^{27}Al MAS NMR spectrum reflects the observations made on ^{29}Si MAS NMR spectra, by showing the appearance of both octahedrally and tetrahedrally bound aluminium. This is clearly observed in the Yixing spectrum although for the Wuxi clay the less intense tetrahedral resonance appears hidden beneath spinning side bands. Again, data from Yixing clay appears consistent with that obtained from Jingdezhen porcelain stone and clay.

Large spinning side bands and noisy spectra are an artefact of the MAS NMR experiment, resulting from paramagnetic iron oxide impurities within the sample. ^{57}Fe Mössbauer spectroscopy on Yixing and Wuxi clay has shown the presence of both Fe^{2+} and Fe^{3+}. It is possible that the Fe^{3+} moiety in the Yixing spectrum is associated with small particle α-Fe_2O_3, whilst the spectrum for Wuxi clay shows a sextet indicative of large particle α-Fe_2O_3. Both sets of data show Fe^{2+} possibly present as Fe_2SiO_4. None of the iron containing materials are thought to be structural.

TGA traces show water loss as a result of the heating process. Wuxi clay exhibits an additional isotherm at ~850 – 900°C indicative of further dehydroxylation.

A further strong endotherm at ~450°C on Yixing clay traces suggests the substitution of Al^{3+} by Fe^{3+} in the octahedral sites. This was also observed for Jingdezhen porcelain stone.

Particle size distributions for Yixing clay and Wuxi clay, show particle size distributions covering the whole range of 1μm - 100μm, with Yixing clay showing a predominance towards the larger end of the spectrum as observed for Jingdezhen porcelain stone and kaolin.

7.6 CONCLUSION

Analysis has highlighted similarities between Yixing clay and the Jingdezhen porcelain stone, with these samples exhibiting similar ^{27}Al and ^{29}Si MAS NMR, infra red, TGA/DTA and particle size distributions. All of the Chinese samples have been shown to be hydrous and non-fired with typical clay composition of silicon and aluminium in the tetrahedral and octahedral layers, respectively.

In conclusion the data presented leads to the suggestion that Jingdezhen raw materials could be a significant component of Yixing clay, whereas no such evidence was observed for Wuxi clay.

CHAPTER EIGHT

8.0 MICROWAVE ASSISTED FORMATION OF LAYERED DOUBLE HYDROXIDES.

8.1 INTRODUCTION.

Layered double hydroxides (LDHs) are known as the 'anti-type' of naturally occurring clays due to the presence of exchangeable anions between the layers as opposed to exchangeable cations in natural clays. Layered double hydroxides therefore have the opposite structure and polarity to that of naturally occurring clays and it is their intrinsic basicity combined with their ability to swell in aqueous media and undergo exchange with large anions that allows them to find applications as adsorbents and catalysts.[36]

Structurally LDHs consist of brucite-like (hydrotalcite-like, $Mg_6Al_2(OH)_{16}(CO)_3.4H_2O$ derived from magnesium hydroxide) layers, in which some of the divalent metal cations have been replaced by trivalent metal cations to give overall positively charged sheets which is compensated for by the presence of anionic species in the interlayer region. Water and carbonate also exist in the interlayer region.

LDHs have the general formula $[M^{II}_{(1-x)}M^{III}_x(OH)_2][A^{n-}]_{x/n} . 2H_2O$ where;

M^{II} = Divalent cation = Mg^{2+}, Ni^{2+}, Cu^{2+}

M^{III} = Trivalent cation = Al^{3+}, Cr^{3+}, Ni^{3+}

A^{n-} = Gallery anion.

The metal cations occupy the centres of octahedra where the vertices contain hydroxide ions, the octahedra are connected by edge sharing to form a sheet.(further discussion on LDH structure and properties can be found in section 1.6.1).

The conventional methods for the synthesis of LDHs are well documented.[36,83,84,85,86] The straightforward synthesis of LDHs is difficult due to the fact that LDH hosts are essentially basic and the layering species usually acidic, which results in a disordered LDH. The conventional synthesis takes approximately 24 hours and involves a coprecipitation technique wherein metal nitrates and precipitants are added slowly and simultaneously at a fixed pH under stirring followed by aging and/or hydrothermal treatment for crystallinity improvement.

More recent reports[17,18] have discussed the synthesis of LDHs *via* microwave methodology. In this method, both metal nitrates and precipitants are added in a very short time (<5-10sec), which is in contrast to the coprecipitation method, which takes a few hours (2-4hr). It is additionally reported how synthesis time is dramatically reduced from the usual ~25.5 hours to 12 min producing a well crystalline product of equal quality. It is further discussed as to how enhancement of crystallinity will depend upon the trivalent metal cation.

The work presented herein has investigated the use of microwave methodology to produce layered double hydroxides, and how the change of trivalent cation affects the crystallinity. The LDHs produced were MgAl(TA) LDH and MgCr(TA) LDH where TA = terephthalate (-$OOCC_6H_4COO$-) an inorganic anion which has little affinity for the layers and so will easily undergo exchange. In order to examine the difference between conventional and microwave methodology the MgAl(TA) LDH was also synthesised *via* conventional methods. In addition the MgAl(TA) LDH has been used in subsequent exchange reactions with HF in an attempt to exchange F- into the LDH. The extent of fluorine exchange was monitored by use of ^{19}F MAS NMR, a technique that was discussed in chapter five.

---

[83] Prévot, V., Casal, B., and Ruiz-Hitzy, E., *J.Mater.Chem.*, 11, 554 – 560, **2001**.
[84] Constantino, V.R.L., and Pinnavaia, T.J., *Inorg. Chem.*, 34, 883 – 892, **1995**.
[85] Dimotakis, E.D., and Pinnavaia, T.J., *Inorganic Chemistry*, 29, 2393 – 2394, **1990**.
[86] Vaccari, A., *Catalysis Today*, 41, 53 – 71, **1998**.

8.1.1 MgAl(TA) LDH SYNTHESISED BY MICROWAVE METHODOLOGY.

The synthesis of the MgAl(TA) LDH *via* microwave methodology did not follow the method cited in the literature[18]. In the literature method a carbonate intercalated layered double hydroxide is synthesised by the simultaneous addition of the nitrate solution (A) and precursor solution (B) into 100ml of water at room temperature. To produce a gel-like slurry that was stirred for 2min before microwave irradiation in a 1l conical flask. This method is not reproducible and therefore adjustments were made with reference to *Drezdon,*[36] whose work was consulted when preparing the MgAl(TA) LDH *via* conventional methods.

The LDHs were characterized by use of XRD, FT-IR and TGA/DTA. The extent of the subsequent fluorine exchange on this sample by use of aqueous solutions of HF was assessed *via* ^{19}F MAS NMR.

Figure 106 : XRD pattern of MgAl(TA) LDH microwave sample.

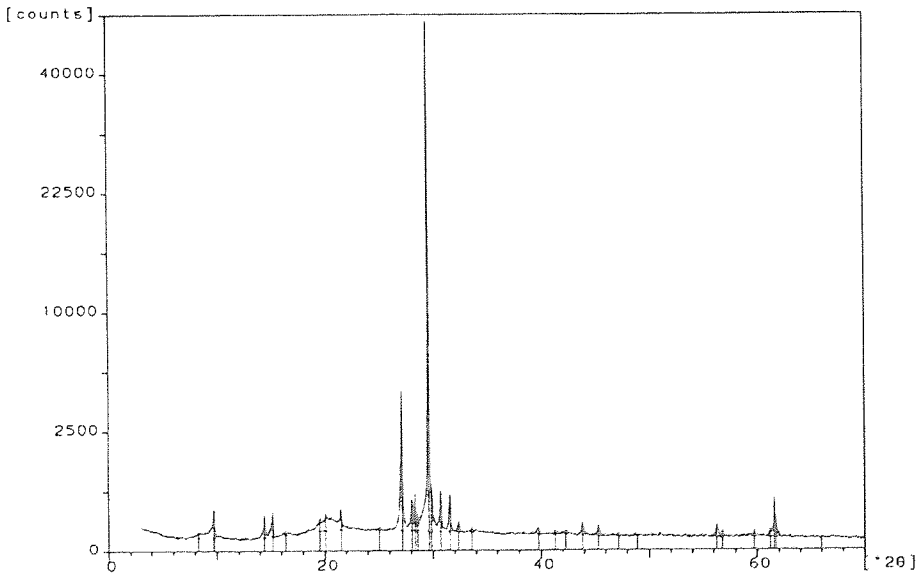

The peaks on the XRD pattern (figure 106) are difficult to assign for such a material as they do not follow typical clay-like characteristics. The pattern however, does reveal the interlayer distance (basal spacing, d(001)) and to some extent the quality of the product. The typical basal spacing (d(001) is quoted in the literature[36] for a terephthalate intercalated layered double hydroxide to be ~14.4Å. The X-ray powder diffraction results shown in figure 106 for MgAl(TA) LDH give a d(001) value of 10.7Å. This is lower than the anticipated value and may arise because both terephthalate and carbonate are partially occupying the interlayer space. The large difference between these two values implies that carbonate accounts for a lot of the space in the interlayer region. The presence of carbonate is feasible as the experiment was performed in air.

As carbonate is present in the interlayer region, it is important to verify that this peak is indeed due to terephthalate and not carbonate. Evidence for this is given by the fact that the basal spacing is also a reflection of the size of the sample housed between the layers (the bigger the species the bigger the d value). The d(001) value must therefore be due to terephthalate and not carbonate due to the relative size differences of the anions (carbonate is much smaller than terephthalate) also due to the strong affinity that carbonate has for the layers the spacing is smaller due to such strong attractive forces. A typical d(001) spacing for $Mg_4Al_2(OH)_{12}CO_3.3H_2O$ is 7.7Å

The sharpness of the peaks that do appear shows a sample of very high crystallinity, uniformity and order within the structure.

The characterization *via* TGA/DTA of the sample MgAl(TA) LDH by microwave methodology also provided evidence suggesting the intercalation of large amounts of carbonate (figure 107).

Figure 107 : TGA/DTA trace for MgAl(TA) LDH microwave methodology.

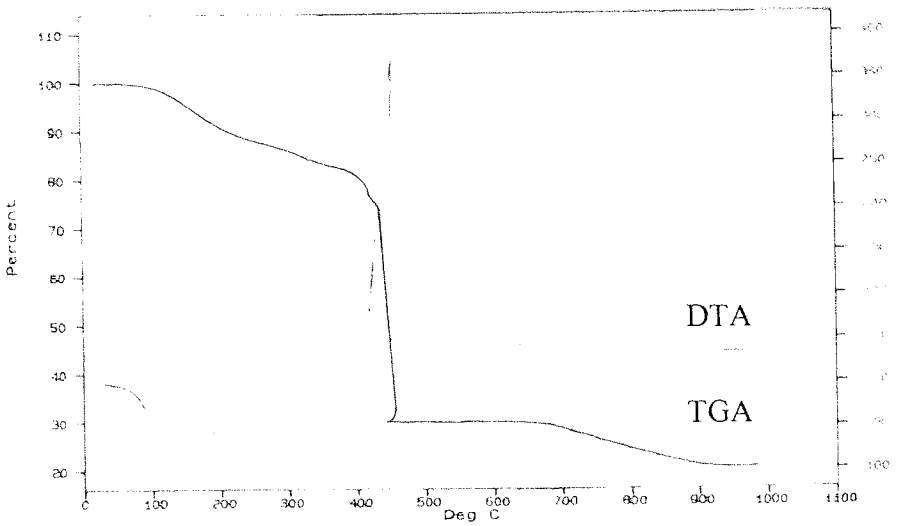

Figure 107 shows the thermal behaviour of MgAl(TA) LDH when heated from 0°C through to 1000°C in air. The DTA shows very small endothermic transitions consistent with limited dehydration/dehydroxylation processes occurring. The very small endotherm identified at ~100°C is consistent with desorption of interstitial water. This endotherm that follows at ~200°C is broader and corresponds to the desorption of any organic residues from the precursors. The appearance of two further small endotherms in the region 300°C – 400°C is indicative of the loss of OH groups present in the inlayed water. The corresponding weight loss over this period, (0°C – 400°C) as shown by TGA, is ~25% which is consistent with that expected for the loss of water from the structure. The intense exothermic spike as shown on the DTA, at ~450°C implies a rapid almost catastrophic structural change, corresponding to the loss of all interlayer material, terephthalate, carbonate and water. The loss of water on the TGA trace is usually seen as an endothermic transition, it is therefore determined that the predominant change occurring associated with the exotherm, is the loss of the organic terephthalate moiety and carbonate from the interlayer region. This in turn causes significant structural changes and so forces the water out of the structure. Therefore it can be said that the apparent cooling of the sample as shown by the TGA is due to the fact that a large amount of material has been made available at a temperature

significantly higher than its normal boiling point and higher than the operating temperature of the equipment. Therefore as the temperature of the material being heated exceeds the actual internal temperature of the equipment, heating ceases until normal conditions are resumed. The apparent cooling therefore is as a result of the equipment acting as a coolant and thus re-starting the heating process.

López[87] also provides data to suggest that this unusually shaped exotherm is indicative of the elimination of carbonate. This is typically lost between 445°C and 515°C. It is not an artefact of one experiment as the results were found to be reproducible. The final weight loss observed is consistent with the final stages of breakdown of the hydrotalcite like structure.

DTA/TGA analysis has shown that MgAl(TA) LDHs synthesised *via* microwave methodology are relatively thermally unstable. The characterisation of the sample by FT-IR provides information to determine the functionality of the MgAl(TA) LDH, as shown in figure 108.

[87] López, T., Bosch, P., Asomoza, M., Gómez, R., and Ramos, E., *Materials Letters,* 31, 311 – 316, **1997**.

Figure : 108 Infra red spectrum of MgAl(TA) LDH synthesised by microwave methodology.

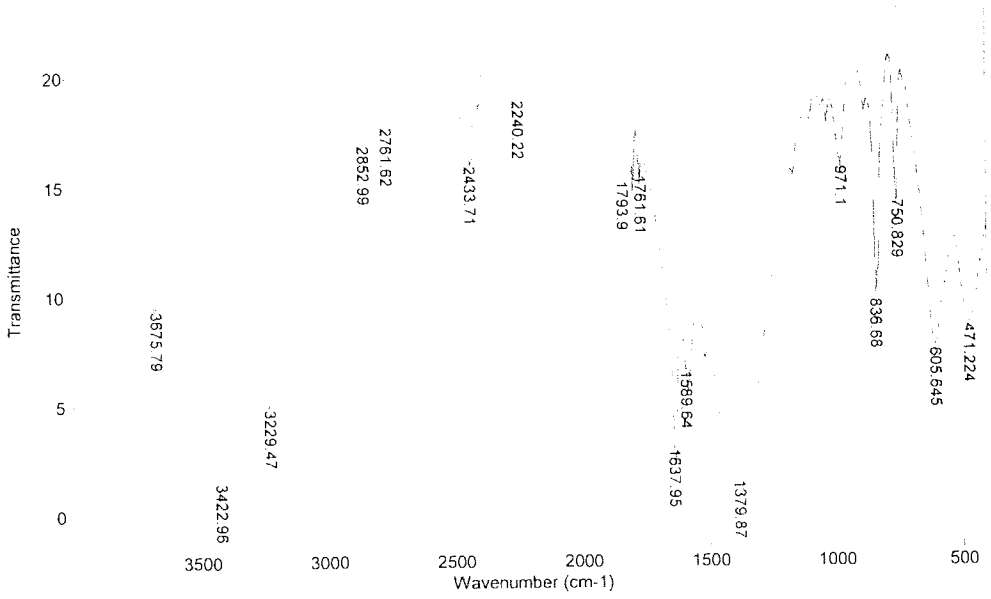

Table 51 : Interpretation of Infra red spectrum of MgAl(TA) LDH microwave.

Absorption cm^{-1}	Assignment	Comment
3675	OH (free)	Free hydroxyl. Peak is consistent with extensive hydrogen bonding between layer and interlayer[18,89]
3422 3229	OH	OH stretch of water molecules in the interlayer region.[18,89]
2852 2761	CO_3^{2-}	Small sharp peaks consistent with the appearance of carbonate. This is an overtone from the fundamental peak at ~1379cm^{-1} and combination overtone from 1589cm^{-1}.[36]
1637	OH	OH bending of water molecules in the interlayer.[89]
1589	Terephthalate CO_3^{2-}	Indicative of the presence of carbonate and proof of terephthalate in the interlayer region.[36] The lack of a peak at ~1700cm^{-1} characteristic of free acid shows that all terephthalate is in dianion form
1379	CO_3^{2-}	Strong band indicative of carbonate[36]
<900	Al-O Mg-O	Bands in this region arise as a result of M-(OH) stretching and M-(OH)-M bending vibrations. Where M = M(II) and/or M(III).[89]

The data presented in table 51 by interpretation of figure 108 shows that for the MgAl(TA) LDH both carbonate and terephthalate exist in the in the interlayer region and is so consistent with the information obtained from XRD and TGA/DTA analysis. The appearance of bands at ~3700cm^{-1}, ~3400cm^{-1} and ~1640cm^{-1} is consistent with hydrogen bonding between layer and interlayer water, OH stretching and OH bending vibrations, respectively. These are as expected for clay like structures of this type. Infra red analysis may prove important when compared to those for the other layered double hydroxide samples synthesised. The strength of the band at ~1379cm^{-1} compared to that at ~1589cm^{-1}, which are attributable to carbonate and terephthalate respectively, further provide evidence to suggest that carbonate is occupying the majority of the interlayer region with only a small amount of terephthalate being successfully intercalated.

An additional aspect of work performed on the MgAl(TA) LDH has been the exchange of the terephthalate anion for the fluorine anion using an aqueous solution of HF. It was assumed that by using solutions of HF at various concentrations the degree of anion exchange could be determined *via* the analysis by ^{19}F MAS NMR. This has not been the case although ^{19}F MAS NMR (figure 109) has shown the successful exchange of F- into the layered double hydroxide structure with the size of the peak suggesting that ^{19}F is present in significant quantities.

Figure 109 : ^{19}F MAS NMR spectrum of F- exchanged MgAL(TA) LDH.

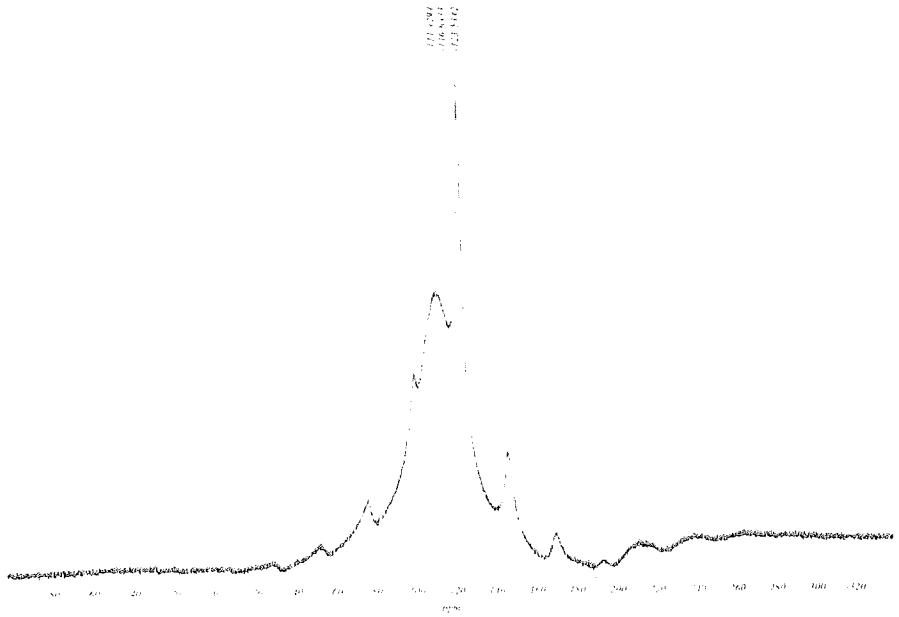

The peak observed at ~123ppm in figure 109, is a result of using a Kel-F rotor during the acquisition of the spectra. The resonant peak corresponding to the inclusion of F^- within the clay structure is that at ~-116ppm. The problems associated with obtaining ^{19}F MAS NMR spectra have been discussed previously in chapter five. It is not possible to perform quantitative analysis of this data but it can be used to demonstrate that F^- is present. In the layered double hydroxide structure fluoride can occupy the interlayer region and it can also undergo isomorphous substitution for oxygen atoms on the layers. If the latter is the case the F^- will occupy two possible sites for substitution,

1. {Al-Al-□}
2. {Al-Mg-□} where □ is a vacant site.

The actual positions of insertion of the F^- ion cannot at this stage be determined.

The data presented so far show how the synthesis of MgAl(TA) LDHs by use of microwave irradiation does produce a material of very high crystallinity. However, it

has also been shown how the synthesis of the LDH on the bench top under atmospheric conditions has led to the insertion of carbonate into the interlayer region resulting in a mixed cation LDH. It is the elimination of carbonate from the interlayer region at ~450°C that renders the LDH thermally unstable.

The anion exchange of these samples with fluoride appears to have been successful with clear resonances being observed on ^{19}F MAS NMR spectra. It cannot at this stage be said how or where the F^- ion is inserting or how much is present.

8.1.2 MgAl(TA) LDH SYNTHESISED BY BENCH TOP TECHNIQUES.

The synthesis was carried out using a Schlenk line for ~24 hours. Characterization has again been by XRD, TGA/DTA and FT-IR. The use of Schlenk line omits air from the reaction chamber and the experiment is therefore performed under an inert nitrogen atmosphere. Subsequent exchange reactions were not performed on this sample.

The XRD pattern shown in figure 113 reveals by the slightly broader width of the peaks that this sample is not quite as crystalline as the sample produced by microwave methodology (figure 108). Thus uniformity and order within the layered double hydroxide has been reduced. This does not mean that the conventional methodology yields inferior products, merely that synthesis by use of microwave irradiation enhances material properties. It is also important at this stage to consider the obvious differences in the two methodologies in particular the different heating processes and the very different degrees of exposure to ambient carbon dioxide. It is therefore reasonable to suggest that both of these factors will additionally affect the nature of the LDH formed.

Figure 110 : XRD pattern for MgAl(TA) LDH by conventional synthesis.

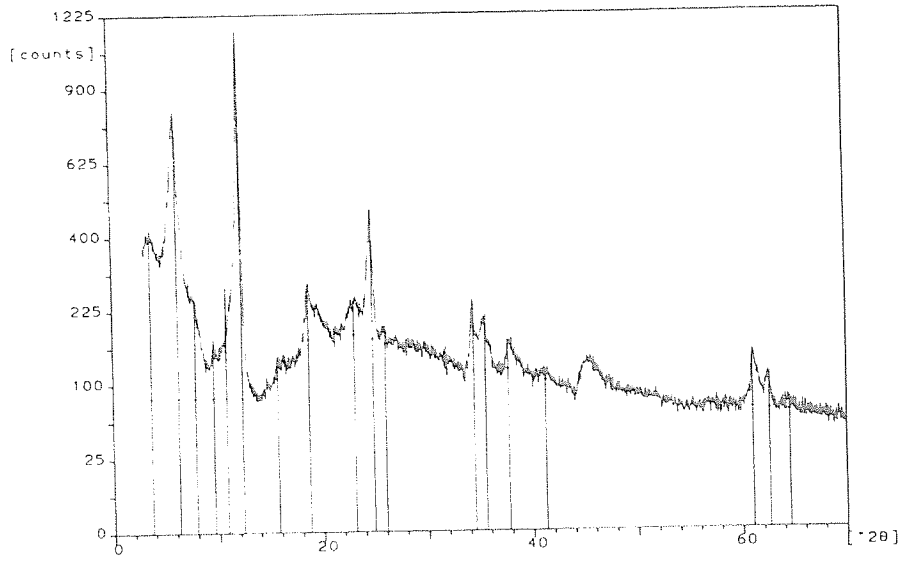

The XRD data presented in figure 110 also reveals the interlayer (basal) spacings of the material. The d(001) value obtained for this sample of MgAl(TA) LDH is ~14.1Å which when compared to the literature[36] value of ~14.4Å is very close. The close correlation of these values therefore shows the successful intercalation of the terephthalate dianion between the layers, with very little adventitious carbonate.

Comparison of the two sets of data presented so far show how although synthesis *via* microwave methodology appears to produce a more highly crystalline material, of order and uniformity, the prolonged conventional synthesis results in better intercalation of the organic anion and the exclusion of adventitious carbonate that it often tenaciously held and thus difficult to remove. The exclusion of carbonate is a direct consequence of performing the experiment in an inert nitrogen atmosphere. A further simple experiment in this area would involve the preparation of a MgAl(TA)LDH *via* microwave synthesis but in the absence of atmospheric CO_2. Due to time constraints this has not been possible however it is certainly a point for further work.

The interpretation of the data obtained from TGA/DTA analysis (figure 111) of the MgAl(TA)LDH also suggests a more stable material. The absence of an intense exothermal peak at ~445°C – 515°C, consistent with the elimination of carbonate suggest there to be very little CO_3^{2-} occupying the interlayer region. The exotherm starting at ~515°C through to ~600°C might be the removal of tenaciously held CO_3^{2-}, however the temperature is considerably higher than usually observed for such a process. The corresponding TGA weight loss is ~15% thus showing very little carbonate in the interlayer region. The approximate ratio of terephthalate to carbonate for the conventionally synthesised material is 4 : 1, respectively.

Figure 111 : TGA/DTA trace of MgAl(TA) LDH *via* conventional synthesis.

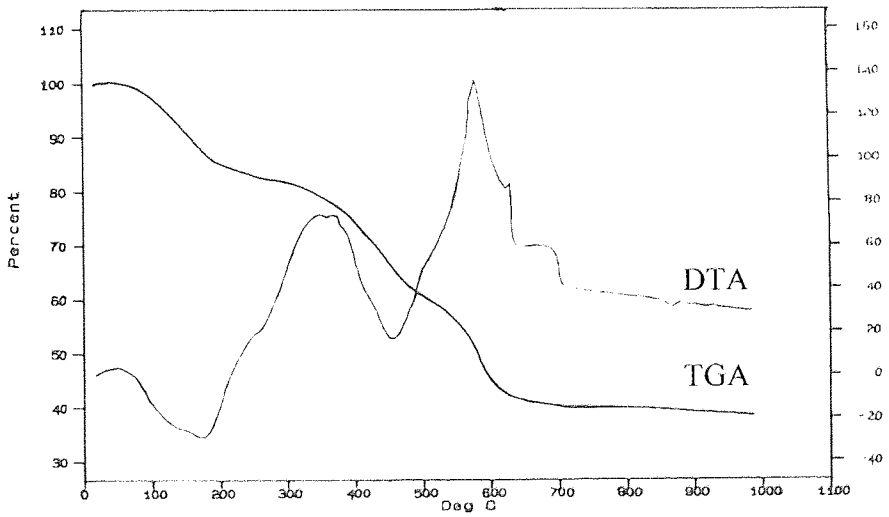

The TGA/DTA trace shown in figure 111 exhibits that basic dehydration/dehydroxylation patterns that would be expected from a clay-like material. The TGA curve exhibits three major weight loss regions at ~100°C, 100°C – 550°C and 550°C – 900°C consistent with the first stages of dehydration, loss of interlayer water and the onset of dehydroxylation and structural change. The weight loss regions observed on the TGA trace accompany the major endothermic peaks shown on the DTA. The DTA endotherm at ~100°C is consistent with loss of sorped water and first water from the cation. The following endothermic peak at ~450°C is consistent with further dehydration and loss of bound water and any further water associated with the cation. The final sets of small endothermic peaks in the 600°C – 900°C region are

consistent with the onset of dehydroxylation, structural change and the beginning of structural breakdown.

The analysis of this sample *via* TGA/DTA has shown this to be a more thermally stable layered double hydroxide than that produced by microwave methodology, one of the major reasons for this is lack of carbonate sharing the interlayer region with the terephthalate dianion.

Infra red analysis did not show any significant differences between the two MgAl(TA) LDH samples (microwave and conventional methodology). This is as would be expected as infra red provides information regards the functional groups present and therefore very small differences would not be identified.

Figure 112 : Infra red spectrum of MgAl(TA) LDH by conventional synthesis.

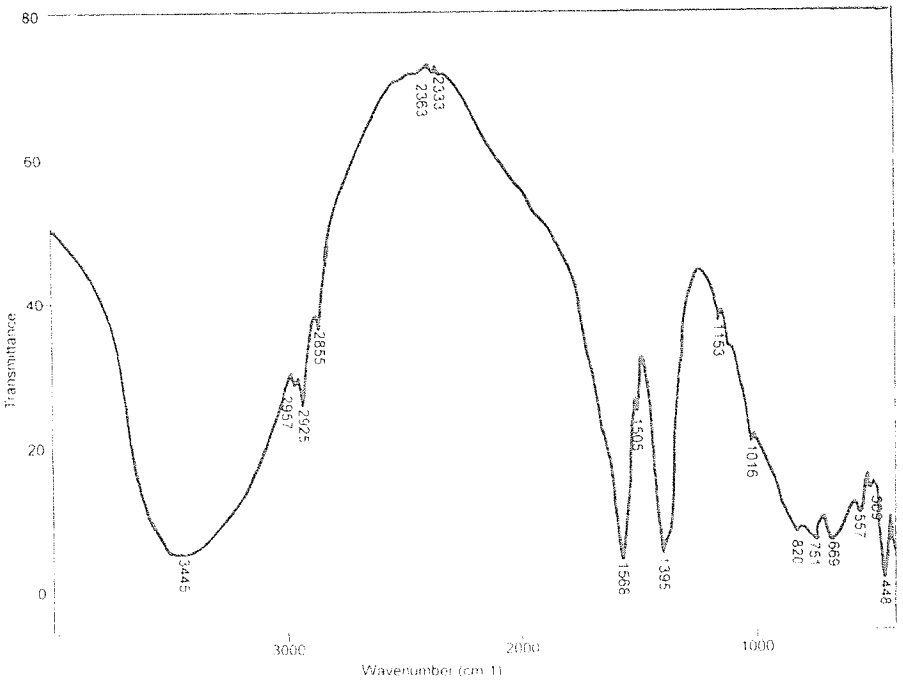

Table 52 : Infra red data for MgAl(TA) LDH by conventional synthesis.

Absorption cm^{-1}	Assignment	Comment
3445	OH	OH stretch of water molecules in the interlayer region.[18,89]
2957 2925	CO_3^{2-}	Small sharp peaks consistent with the appearance of carbonate. This is an overtone from the fundamental peak at ~1395cm^{-1} and combination overtone from 1568cm^{-1}.[36]
1568	Terephthalate CO_3^{2-}	Indicative of the presence of carbonate and proof of terephthalate in the interlayer region.[36] The lack of a peak at ~1700cm^{-1} characteristic of free acid shows that all terephthalate is in dianion form
1395	CO_3^{2-}	Strong band indicative of carbonate[36]
<1000	Al-O Mg-O	Bands in this region arise as a result of M-(OH) stretching and M-(OH)-M bending vibrations. Where M = M(II) and/or M(III).[89]

The infra red analysis of the conventionally synthesised MgAl(TA) LDH (figure 112, table 52) exhibits a characteristic peak at ~3445cm^{-1} indicative of OH/H_2O moieties, the absence of a peak at ~1640 – 1670 cm^{-1} suggests that it is OH rather than H_2O. Therefore the conventionally synthesised sample has less free water than the microwave

formed product. The appearance of a peak at ~1568cm^{-1} confirms the successful intercalation of the dianion terephthalate between the layers, the lack of a peak at ~1700cm^{-1} which is characteristic of free acid confirms that it is the dianion form. Carbonate has also been identified as existing in the layers as determined by peaks at ~2957 cm^{-1}, ~2925 cm^{-1} and ~1395 cm $^{-1}$. The strength of the peak at ~1395cm^{-1} suggests carbonate to be present in significant quantities, however it is reasonable to suggest that this is atmospheric CO_2 being detected by the infra red apparatus and not CO_3^{2-} in the interlayer region. However, it is known from both XRD and TGA/DTA analysis that carbonate is present in significant quantities in the interlayer region.

In summary it can be said that although synthesis of the MgAl(TA) LDH by ambient conditions microwave methodology is quicker and produces a different material with enhanced properties, they are less thermally stable than their conventionally synthesised counterparts. The inclusion of terephthalate into the interlayer region is not as successful by microwave methodology with more carbonate occupying the interlayer region than in the conventionally synthesised material. The additional carbonate in the microwave-produced material is a direct result of the synthesis being performed under ambient conditions. Therefore the differences observed cannot solely attributed to the use of microwave irradiation and the more likely cause is the differing concentrations of CO_3^{2-}.

8.1.3 MgCr(TA) LDH SYNTHESISED BY MICROWAVE METHODOLOGY.

In the literature[18] it is also reported how the nature of the trivalent cation affects the crystallinity of the layered double hydroxide produced by microwave irradiation. The investigation of this carried out by the synthesis of a MgCr(TA) layered double hydroxide, i.e. replacing Al^{3+} for Cr^{3+}. The characterization was performed as previously by application of XRD, TGA/DTA and FT-IR.

The XRD pattern obtained (figure 113) showed a highly crystalline material, well ordered and exhibiting uniformity, although it does not appear to exhibit improved properties over the MgAl(TA) version.

Figure 113 : XRD pattern of MgCr(TA) LDH by microwave methodology.

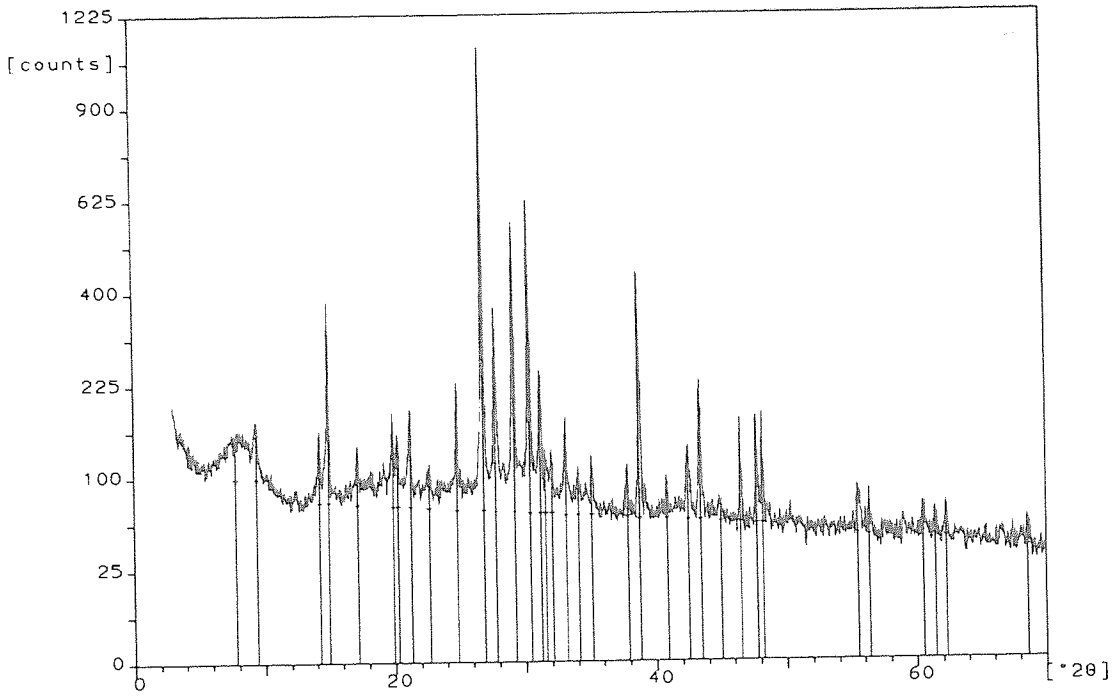

The XRD pattern shown in figure 113 reveals a d(001) spacing of ~11.4Å which compared to the literature value of ~14.4Å for terephthalate intercalated LDH is significantly lower. This again indicates that carbonate occupies the interlayer region along with the terephthalate dianion. This is reasonable as performing the synthesis in air can easily lead to the incorporation of adventitious carbonate.

The interpretation of TGA/DTA traces (figure 114) provided further evidence supporting the inclusion of a large amount of carbonate within the interlayer region. Again there is an intense and complex exothermic process occurring at 500°C indicative of a rapid and intense structural change.

Figure 114 : TGA/DTA trace of MgCr(TA) LDH by microwave methodology.

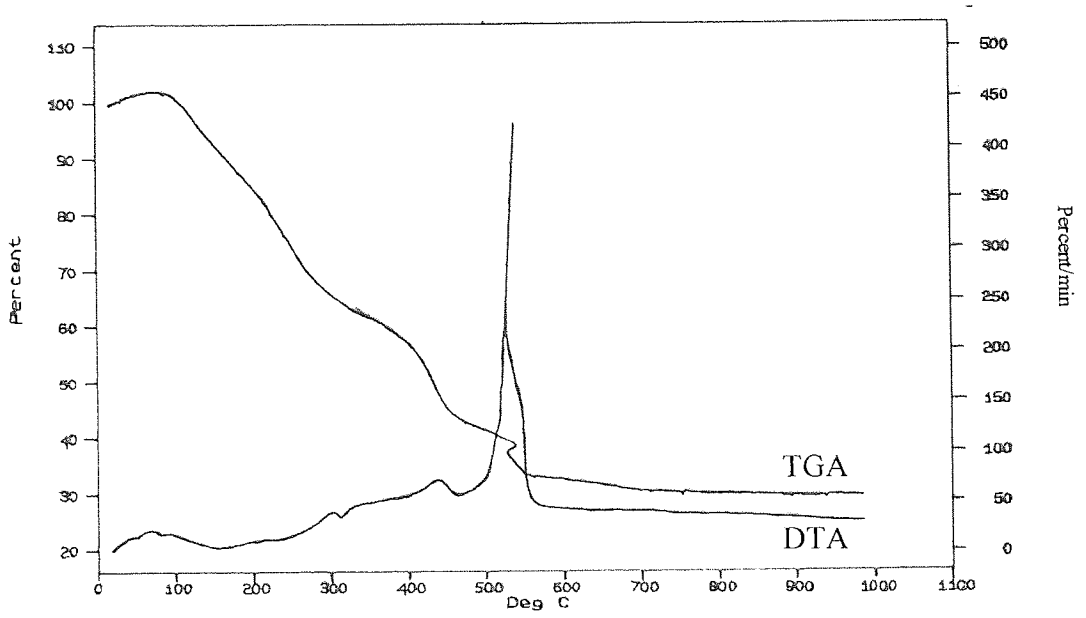

Figure 114 shows the thermal behaviour of MgCr(TA) LDH when heated from 0°C – 1000°C in air. The very small endotherms exhibited by the DTA peak at ~100°C, ~250°C and 450°C are consistent with the dehydration of water from the interlayer region, further dehydration from the interlayer anion and the loss of OH groups from inlayed water, respectively. The corresponding weight loss exhibited by the TGA curve over this region (0°C – 450°C) is ~60%, much larger than the corresponding MgAl(TA) version. The intense exothermic peak observed in the DTA curve at ~500°C is consistent with the elimination of predominantly terephthalate in conjunction with carbonate and water from the interlayer region. The intensity of the peak would suggest a significant amount of material has been expelled. The trace also suggests some cooling of the sample has occurred. The explanation given earlier (page 230) suggests that the phenomenon being observed is due to the equipment acting as a coolant due to the temperature of the material exceeding that of the actual equipment internal temperature. It is assumed that the major weight loss is due to the expulsion of terephthalate and carbonate from the interlayer region, this causes extensive structural change, so forcing water out of the structure. There is not any literature existing to provide a further explanation for the phenomenon being observed. The weight loss over this final period as determined by the TGA curve is ~20%.

Infra red analysis did not show any significant differences between this LDH and the others examined, as shown in figure 115.

Figure 115 : Infra red spectrum of MgCr(TA) LDH by microwave methodology.

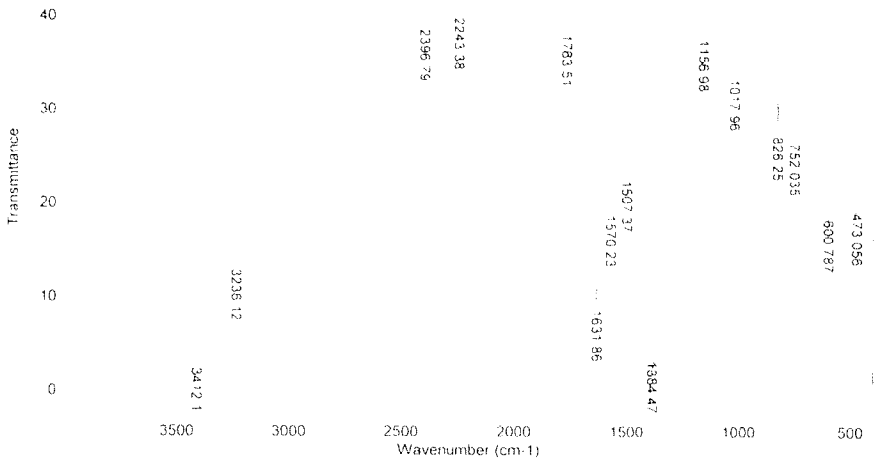

Table 53 : Interpretation of Infra red spectrum of MgCr(TA) LDH microwave.

Absorption cm^{-1}	Assignment	Comment
3412 3236	OH	OH stretch of water molecules in the interlayer region.[18,89]
1631	OH	OH bending vibration of water molecules in the interlayer region.[89]
1570	Terephthalate CO_3^{2-}	Indicative of the presence of carbonate and proof of terephthalate in the interlayer region.[36] The lack of a peak at ~1700cm^{-1} characteristic of free acid shows that all terephthalate is in dianion form
1384	CO_3^{2-}	A strong band indicative of carbonate[36]
<1000	Al-O Mg-O	Bands in this region arise as a result of M-(OH) stretching and M-(OH)-M bending vibrations. Where M = M(II) and/or M(III).[89]

The characteristic peaks observed on figure 115 at ~3400cm^{-1} and 1600cm^{-1} are consistent with OH stretching and bending vibrations of water molecules in the interlayer region. The appearance of the peak at ~1600cm^{-1} suggests this is H_2O and not OH. The information obtained from FT-IR is consistent with that obtained from XRD and TGA/DTA showing the presence of both terephthalate and carbonate in the

interlayer region. The strength of the fundamental peak at 1384cm^{-1} suggests carbonate to be present in significant quantities.

8.2 CONCLUSIONS

The objectives were to see if the synthesis of layered double hydroxides by using microwave irradiation produced a material with enhanced properties. In addition to this it was anticipated that changing the nature of the M^{3+} cation would enhance crystallinity of the sample. The anion exchange of fluorine into the MgAl(TA) LDH was also considered.

The data presented have shown that the synthesis of layered double hydroxides *via* microwave methodology does appear to enhance the crystallinity of the material as shown by the narrow peaks observed on XRD patterns for MgAl(TA) microwave and MgCr(TA) microwave (figures 106 and 113) when compared to that of MgAL(TA) conventional (figure 110). XRD also reveals the interlayer distance (basal spacing) for the materials synthesised. The typical literature value for a terephthalate intercalated LDH is ~14.4Å. Any differences in the basal spacing of the materials synthesised would suggest the inclusion of another anion as well as terephthalate, in this case carbonate. It has been shown how for the microwave synthesised samples carbonate occupies a significant proportion of the interlayer region whilst the conventional synthesis is predominantly just terephthalate intercalated.

The addition of carbonate into the interlayer region occurs as a result of performing the experiments in air, carbonate is tenaciously held and therefore difficult to remove. TGA/DTA traces show how for the microwave synthesised samples all of the interlayer material is being expelled at ~450°C – 500°C. Conversely, TGA/DTA data for the conventionally synthesised material show a more thermally stable material (figure 111).

Infra red spectra (figures 108, 112 and 115) provide information relating to the functionality of the layered double hydroxides. They confirm the inclusion of terephthalate within the layers in addition to the inclusion of carbonate. There are not any pronounced differences between the infra red spectra of the samples examined.

In conclusion it has been shown how microwave irradiation will act to enhance the crystallinity of layered double hydroxides, however it does not lead to the straight forward inclusion of the precursor into the layers due to being performed in air large amounts of carbonate also reside in the interlayer region. The work described in the literature[18] examined the synthesis of carbonate intercalated layered double hydroxides therefore explaining why they did not observe this phenonomen. The synthesis *via* conventional methodology restricts the insertion of adventitious carbonate into the interlayer region as it is performed under an inert atmosphere.

At this stage it cannot be said that enhanced properties observed are solely attributable to the use of microwave heating and at present it appears that the main differences observed are as a result of different concentrations of carbonate which result due to different experimental conditions. Further investigation would require the microwave synthesis of a layered double hydroxide under inert conditions. This has not been performed due to time constraints.

Examination of the nature of the M^{3+} cation did not appear to significantly affect the crystallinity of the material, with very few differences being observed between XRD patterns of the MgAl(TA) microwave material (figure 106) and the MgCr(TA) microwave material (figure 115).

^{19}F MAS NMR of the anion exchange of MgAl(TA) microwave synthesised layered double hydroxide showed the successful exchange of fluorine into the clay samples by the appearance of a resonant peak at ~-116ppm. The large sharp resonance at ~-123ppm is as a result of the Kel-F rotor used during acquisition of the spectrum. It was not possible to quantify the amount of F^- present it is sufficient to say that it is there and that the exchange has been successful.

CHAPTER NINE

9.0 FURTHER WORK.

It is clear from the work presented herein that there is much scope for further work in all of the areas investigated.

9.1 DETERMINATION OF FREEZE-THAW THRESHOLD LIMITS.

The analysis of freeze-thaw treated tiles by ultrasonic and three-point flexural testing provided information to suggest that a threshold region exists. Up to this point up the action of freeze thaw will be to compound the clay and make it stronger, but passing this threshold leads to weakening of the clay body. The data presented have suggested that this threshold lies in the range of 35 to 75 cycles.

The determination of the exact threshold region would be valuable. Future development work in this area would require the production of more freeze-thaw treated tiles across a range of cycles between the predetermined limits. The continued analysis of these tiles *via* ultrasonic and three-point flexural testing should yield the desired answer. The identification of this threshold limit could be particularly important to the ceramics industry.

9.2 QUANTIFICATION OF FLUORINE LEVELS IN WHICHFORD CLAYS.

The success thus far has been the identification of fluorine in the solid state clay systems. Although only negligible amounts have been shown to be present, ideally quantifying these amounts is desirable.

Future investigation of this *via* ^{19}F MAS NMR would require the calibration of the MAS NMR system against a standard compound of known concentration. It is important that the fluorine standard utilised is in the same system as the samples to be examined. The removal of fluorine from the Kel-F rotor used during acquisition of the spectrum is essential, so as to avoid unwanted errors.

9.3 DETERMINATION OF KINETIC FACTORS ASSOCIATED WITH CATION EXCHANGE.

The appearance of Q_0 silicate as a result of heating cation intercalated Wyoming Bentonite was surprising. The data obtained suggested this phenomenon arose due to an increase in tetrahedrally bound ^{27}Al in the silicate framework. This was reflected in both ^{29}Si and ^{27}Al MAS NMR spectra.

It was observed that for different cations the formation of Q_0 silicate occurred at differing temperature. This has been related, in simple terms to variations in the cationic radii causing changes in the heating process.

Further development in this area would focus on the kinetic factors involved with Na^+, K^+, Li^+ and Cu^{2+} exchange and the observations of Q_0 silicate. Thus using different reaction times and temperatures to monitor closely the reaction taking place.

9.4 LAYERED DOUBLE HYDROXIDES.

Development of the work commenced on layered double hydroxides would focus primarily on the microwave preparation of layered double hydroxides under inert conditions. With the present data it is difficult to associate any enhanced properties solely to the use of microwave heating. It is anticipated that this further work will allow an enhanced comparison of the bench top and microwave formed materials.

Further to this additional experiments evaluating the effect of changing the M^{III} should be performed in order to gain a set of comprehensive results between which comparisons can be made.

REFERENCES.

1 Grim, R.E., *Clay Mineralogy*, McGraw-Hill, New York, **1953** The Royal Society, *Clay Minerals: Their Structure Behaviour and use.* University Press, Cambridge, **1984.**

2 Grimshaw, R.W., *The Chemistry and physics of clays and allied ceramic materials,* Fourth Edition, **1971.**

3 Grimshaw, R.W., and Harland, C.E., *Ion-Exchange: Introduction to theory and practice,* The Royal Society, Mongraphs for Teachers No.29, **1975.**

4 Millot. G.; *Geology of Clay;* Chapman and Hall, **1970.**

7 Michael. P., *Studies of Clay Minerals and their decomposition products,* PhD Thesis, Aston University, **1989.**

8 Brindley, G.W., and Brown, G., *Crystal structures of clay minerals and their X-ray identification*, Mineralogical Society of London, **1984.**

9 http://www.neutron.anl.gov/ceramics.htm

10 http://www.ceaspub.eas.asu.edu/concrete/hardened-concrete/img001.jpg

11 http://digitalfire.com/education/clay/outdoor.htm

12 Maciulaitis Romuldas, *Zi Int.*, **1994,** 47, 313 – 322.

13 http://www.ceramres.co.uk/ptp/1997_projects/molearyp.htm

14 Ulibarri, M.A., Labajos, F.M., Rives, V., Trujillano, R., Kagunya, W., and Jones, W., *Inorg. Chem.* **1994,** 33, 2592.

15 Taehyun, K., Tsigdinos, G.A., and Pinnavaia, T.J., *J. Am. Chem. Soc.*, **1988,** 110, 3653.

16 Carlino, S., "Chemistry between the sheets", *Chemistry in Britian,* **Sept 1997,** 59 .

17 Prévot.V., Casal, B., and Ruiz-Hitzky.E., *"Intracrystalline alkylation of Benzoate ions into layered double hydroxides"*,. In press.

18 Kannan, S., and Jasra.R.V., *"Microwave assisted rapid crystallization of Mg-M(III) hydrotalcite where M(III) = Al, Fe and Cr."*, In press.

19 Whittaker, A.G., and Mingos, D.M.P., *Journal of Microwave Power and Electromagnetic Energy,* **1994,** 29, 195 – 219.

20 Ferguson, D.R., *"The basics of microwave heating for organic synthesis"*, **Oct 2000,** 69.

21 Gabriel, C., Gabriel, S., Grant, E.H., Halstead, B.S.J. and Mingos, M.P., *Chemical Society Reviews,* **1998**, 27, 213 – 223.

22 Laurent, R., Laporterie, A., Dubac, J., Berlan, J., Lefeuvre, S. and Audhuy, M., *Journal of Organic Chemistry,* **1992**, 56, 7099 –7102.

23 Whittaker, G., *The New Scientist,* **Feb 1998**, 34 –37.

24 Baghurst, D.R. and Mingos, M.P., *Journal of the Chemical Society., Chemical Communications,* **1992**, 674 – 677.

25 Varma, R.S. and Kumar, D., *Tetrahedron Letters,* **1999**, 40, 7665 – 7669.

26 Galema, S.A., *Chemical Society Reviews,* **1997**, 26, 233 – 238.

27 Thostenson, E.T. and Chou, T.W., *Composites part A: Applied Science and Manufacturing,* **1999,** 30, 1055 – 1071.

28 Gedye, R.N., Smith, F.E. and Westaway, K.C., *Canadian Journal of Chemistry,* **1988**, 66, 17 –26.

29 Gedye, R.N., Rank, W. and Westaway, K., *Canadian Journal of Chemistry,* **1991**, 69, 706 – 711.

30 Ashcroft, R.C., Bond, S.P., Beever, M.S., Lawrence, M.A.M., Gelder, A., McWhinnie, W.R. and Berry, F.J., *Polyhedron,* **1992**, 11, 1001 – 1006.

31 Pelesko, J.A., *IMA Journal of Applied Mathematics,* **2000**, 64, 39 – 50.

32 Monsef-Mirazi, P., Kavanagh,D.M., Bodman, S., Lange, S and McWhinnie, W.R., *Journal of Microwave Power and Electromagnetic Energy,* **1999**, 34, 216 – 220.

33 Bond,S.P., Gelder, A., Homer, J., McWhinnie, W.R. and Perry, M.C., *Journal of Materials Chemistry,* **1991**, 1, 327 – 330.

34 Posner, A.N. and Quirk, J.P., *Proceedings of the Royal Society of London Seris A,* **1964**, 278, 35 – 56.

35 Zapata, B., Bosch, P., Fetter. G., Valenzuela, M.A., Navarrete, J. and Lara, V.H., *International Journal of Inorganic Materials,* **2001**, 3, 23 – 29.

36 Drezdon, M, A., *Inorganic Chemistry,* **1988**, 27, 4628 – 4632.

37 Maksoud, T.M.A., Mokbel, A.A. and Morgan, J.E., *Journal of Materials Processing Technology*

38 Ed. Setzer, M.J. and Auberg, R. *Frost Resistance of Concrete, Proceedings of the International Rilem Workshop 34,* Chapman and Hall, **1997.**

39 Allen, T., *Particle size measurement, Volume 2, Fifth Edition,* Chapman and Hall, **1997.**

40 Gregg, S. J., and Sing, K. S. W., *Adsorption surface area and porosity,* ACADEMIC PRESS London and New York, **1967**.

41 Moore, D.M., and Reynolds, R.C., *X-Ray Diffraction and the identification and analysis of clay minerals,* Oxford University Press, **1989**.

42 Ed. Van Olphen, H., and Fripiat, J.J., *Data handbook for clay and other non-metallic minerals,* Pergamon Press, **1979**.

43 Berry, L.G., and Thompson, R.M., *X-Ray powder data for ore minerals,* The Geological Society of America, Memoir 85, **1962**.

44 Theng, B.K.G., *The Chemistry of Clay Organic Reactions,* **1974**, Halstead Press.

45 Farmer, V.C. and Russell, J.D., *Spectrochimica Acta,* **1964**, 20, 1149 – 1173.

46 Miller, J.G., *J.Phys.Chem,* **1961**, 65, 800 – 804.

47 *CLAY MINERALOGY, Spectroscopic and chemical determinative methods,* CHAPMAN AND HALL, **1994.**

48 Nakamoto,K., *Infra red and Raman Spectra of Inorganic and Co-ordination compounds,* Fourth Editon, John Wiley and Sons, **1986**.

49 Roch, G, E., *PhD Thesis,* University of Kent in centerbury, **Jan 1999**.

50 Woessner, D, E., *American Mineralogist,* 74, **1989,** 203 – 215.

51 Fitzgerald, J, J., Dec, S, F., and Hamza, A, I., *American Mineralogist,* **1989**, 74, 1405 – 1408.

52 Berry, F.J., Eadon, D., Holloway, J., and Smart, L.E., *J. Mater. Chem.,* **1996**, 6, 221 – 225.

53 Ed. Miller, B., *Thermal Analysis,* Wiley, **1982,** 1.

54 Ed. Mackenzie, R, C., *Differential Thermal Analysis,* Academic Press, London and New York, **1970,** 1.

55 Cranshaw, T, E., Dale, B.W., Longworth, G, O., and Johnson, C, E., *Mössbauer Spectroscopy and its applications,* Cambridge University Press, **1985.**

56 Santaren, J., Sanz, J., and Ruiz-Hitzky, E., *Clays and Clay Minerals*, **1990**, 1, 63-68.

57 Huve, L., Delmotte, L., Martin, P., Le Dred, R., Baron, J., and Saehr, D., *Clays and Clay Minerals,* **1992**, 2, 186 – 191.

58 Mooney, E. F., *An Introduction to ^{19}F NMR Spectroscopy,* Heyden and Son LTD, **1970**.

59 Harris, R, K., and Jackson, P., *Chemical Reviews,* **1991**, 91, 1427 – 1440.

60 Kreinbreck, A, T., Sazavsky, C, D., Pyrz, J, W., Nelson, D, G, A., and Honkonen, R, S., *Journal of Magnetic Resonance,* **1990**, 88, 267 – 276

61 Labouriau, A., Kim, Y-W., Chipera, S., Bish, D, L., and Earl, W, L., *Clays and Clay Minerals,* **1995**, 43, 697 – 704

62 Clark, J, H., Goodman, E, M., Smith, D, K, Brown, S, J., and Miller, J, M., *Journal of the Chemical Society, Chemical Communications*, **1986**, 657 – 658.

63 Bond, S.P., PhD Thesis, CEAC Department, Aston University, **1991.**

64 Grimshaw, R.W., and Harland, C.E., *Ion-Exchange : Introduction to theory and practice,* The Chemical Society Monographs for Teachers No. 29, **1975**.

65 Plee, D., Borg, F., Gatineau, L., and Fripiat, J.J., *J.Am.Chem.Soc.* 107, 2362 – 2369, **1985.**

66 Kinsey, R.A., Kirkpatrick, R.J., Hower, J., Smith, K.A., and Oldfield, E., *American Mineralogist,* 70, 537 – 548, **1985**.

67 Schroeder, P.A., Pruett, R.J., and Hurst, V.J., *Clays and clay Minerals,* 46, 429 – 435, **1998**.

68 Koster Van Groos, A.F., and Guggenheim, S., *American Mineralogist,* 74, 627 – 636, **1989**.

69 Koster Van Groos, A.F., and Guggenheim, S., *American Mineralogist,* 72, 1170 – 175, **1987**.

70 Koster Van Groos, A.F., and Guggenheim, S., *American Mineralogist,* 69, 872 – 879, **1984**.

71 Koster Van Groos, A.F., and Guggenheim, S., Clays and Clay Minerals, 34, 281 – 286, **1986.**

72 Mosser, C., Michot, L.J., Villieras, F., and Romeo, M., *Clays and Clay Minerals,* 45, 789 – 802, **1997**.

73 Tettenhorst, R., *The American Mineralogist,* 47, 769 – 772, **1962**.

74 Weiss, C.A., Jr., Altaner, S.P., and Kirkpatrick, R.J., *American Mineralogist,* 72, 935 – 942, **1987**.

75 Yap, C.T., and Hua, Y., *Applied Spectroscopy,* **1992**, 46, 1488 – 1494.

76 Anderson, J.L., *Journal of the Australian ceramic Society,* **1982**, 18.

77 Tite, M.S., Freestone, I.C., and Bimson, M., *Archaeometry* , **1984**, 26, 139 – 154.

78 Yanyi, G., *Archaeometry*, **1987**, 27, 3 – 19.

79 Maslennikova, G.N., Platov, Y.T., and Zhekisheva, S.Z., *Glass and Ceramics,* **1993**, 50, 472 – 475.

80 Adylov, G.T., and Gornostaeva, S.A., *Glass and ceramics*, **1995**, 52, 158 - 159.

81 Chatterjee, H., Iwasaki, T., Hayashi, H., Ebina, T., and Torii, K., *Journal of Molecular Catalysis,* **1988**, 136, 195 – 202.

82 Prévot, V., Casal, B., and Ruiz-Hitzy, E., *J.Mater.Chem.*, 11, 554 – 560, **2001**.

83 Constantino, V.R.L., and Pinnavaia, T.J., *Inorg. Chem.*, 34, 883 – 892, **1995**.

84 Dimotakis, E.D., and Pinnavaia, T.J., *Inorganic Chemistry,* 29, 2393 – 2394, **1990**.

85 Vaccari, A., *Catalysis Today,* 41, 53 – 71, **1998.**

86 López, T., Bosch, P., Asomoza, M., Gómez, R., and Ramos, E., *Materials Letters,* 31, 311 – 316, **1997**.